

# Importance of geotechnical cross-section unsaturated zone for landslide occurrence in flysch deposits

---

**Peranić, Josip**

**Doctoral thesis / Disertacija**

**2019**

*Degree Grantor / Ustanova koja je dodijelila akademski / stručni stupanj:* **University of Rijeka, Faculty of Civil Engineering in Rijeka / Sveučilište u Rijeci, Građevinski fakultet u Rijeci**

*Permanent link / Trajna poveznica:* <https://urn.nsk.hr/urn:nbn:hr:157:773572>

*Rights / Prava:* [Attribution-NonCommercial-NoDerivatives 4.0 International/Imenovanje-Nekomercijalno-Bez prerada 4.0 međunarodna](#)

*Download date / Datum preuzimanja:* **2024-04-27**



*Repository / Repozitorij:*

[Repository of the University of Rijeka, Faculty of Civil Engineering - FCERI Repository](#)



UNIVERSITY OF RIJEKA  
FACULTY OF CIVIL ENGINEERING

Josip Peranić

**IMPORTANCE OF GEOTECHNICAL  
CROSS-SECTION UNSATURATED ZONE  
FOR LANDSLIDE OCCURRENCE IN  
FLYSCH DEPOSITS**

DOCTORAL THESIS

Supervisor: Prof. Željko Arbanas, PhD

Rijeka, 2019



Supervisor: Professor Željko Arbanas, PhD

The doctoral thesis was defended on \_\_\_\_\_  
at the University of Rijeka, Faculty of Civil Engineering, in front of the  
committee members:

1. Assistant Professor Vedran Jagodnik, PhD (committee chair)
2. Assistant Professor Martina Vivoda Prodan, PhD (member)
3. Associate Professor Sabatino Cuomo, PhD (external member)





*To my parents. For your endless love and support.*



# Acknowledgements

Without the guidance and enthusiasm of many great people who I came across during my research, this dissertation might have never seen the light of day. This whole experience would have been much harder without the help and support of my colleagues. There would have been little joy in this adventure without the encouragement and understanding of my family and friends.

I owe the greatest gratitude for this achievement to my supervisor. Željko, thank you for the opportunity to learn from you and for guiding me toward such a challenging and interesting field of research. I am grateful for you always having had the time and patience for my questions, always guiding me where to seek for the answers, and above all, for your inexhaustible enthusiasm, dedication, and compassion in your guidance. Thank you for that and many other things.

Sabatino, thank you for your friendly welcome at the University of Salerno and for accepting the supervision of my work. The period I spent at your institution was a valuable experience for my professional growth and also a wonderful experience. This I owe to you and your colleagues. Vito, thank you for all the tests conducted and for your devotion to sharing your knowledge with me. I learned a lot from you about soil testing in partially-saturated conditions. Mariagiovanna, for always finding the time for me, all the specimens prepared, tests performed, results analyzed, and above all, for your friendship, thank you. Matej, thank you for the knowledge shared and all of the tests performed. I always felt that I could turn to someone when I had doubts or felt lonely in my work. Thank you for that. It meant a lot to me.

I owe thanks to my dear colleagues. Sanja, thank you for your efforts during the defense of the research topic and suggestions on how to improve this research. Martina, thank you for carefully reading this manuscript and endeavoring to improve it. Thank you both for all of your help and knowledge shared during my study. Above all, thank you for your friendship, laughter, and encouragement during my research. Vedran, you helped me in many ways during my study and have guided me during my first steps in our laboratory. I am grateful for your help and suggestions during field and laboratory measurements, especially with the permeability tests. You handed me the first book about unsaturated soil mechanics several years ago and today you are the chair of my thesis defense committee. Thank you for being a part of my story.

Juraj and Sara, thank you for being there for me when I needed it the most. Juraj, the number of tests and field measurements that you helped me with is countless. Thank you for taking care of my measurements and equipment when I did not have the time for it. Sara, thank you for all of the exams and tasks that you took care of for me, without needing to ask.

Elvis, thank you for sharing the meteorological data you are collecting devotionally. I am grateful for all of the data comparisons and the discussions we shared. Igor and Duje, thank you for helping me with the groundwater level measurements. The expertise and efficiency of your work saved me a lot of time.

To my students who have helped me with the laboratory measurements at the University of Salerno and Rijeka: Sandi and Domagoj, thank you.

To my dear friends and family who I often had to put aside: thank you for always having understanding and patience. Toni, thank you for caring and always being there for me when I needed you. Mom and dad, thank you for this wonderful adventure. You have always been my strongest support. From your shoulders, no obstacle seems too high and no goal seems unattainable. For all your love and support, thank you.

Una, I hoped that the right words would come - I doubt I will ever find them. For your infinite patience, for always waiting for me with the hug and smile, for all your love and encouragement, for going through it all together with me... thank you. This was a wonderful adventure because of you.

-----

I would like to thank the following organizations and companies that have supported my research in different ways:

GEO-SLOPE International, Ltd. for providing the GeoStudio 2018 for my research purposes; Meteorological and Hydrological Service of Croatia for providing the rainfall data; The Erasmus+ programme for supporting a part of my stay at the University of Salerno.

This work has been supported in part by Ministry of Science, Education and Sports of the Republic of Croatia under the project Research Infrastructure for Campus-based Laboratories at the University of Rijeka. The project has been co-funded from the European Fund for Regional Development (ERDF).

Support has also been provided in part by the Ministry of Science, Education and Sports of the Republic of Croatia under the bilateral Croatian-Slovenian research project “Laboratory investigations and numerical modeling of landslides in flysch deposits in Croatia and Slovenia” and the bilateral Croatian-Japanese research project “Risk Identification and Land-Use Planning for Disaster Mitigation of Landslides and Floods in Croatia”.

## Abstract

Factors primary controlling rainfall-induced slope failures are both rainfall characteristics and soil properties. Rainfall causes a transient infiltration process through the unsaturated part of the slope which affects sloping material by increasing the moisture content and pore-water pressure, changing the effective stress and hydro-mechanical properties of the soil. To study the physical process of rainfall infiltration and how it affects the slope stability state, the dependency between water retention properties, hydraulic permeability, shear strength properties and the water content or negative pore-water pressures existing above the phreatic surface have to be known. Unlike for the shallow-type landslides, very few studies were performed for the case of deep-seated landslides built of material with relatively low hydraulic conductivity. This kind of studies were never performed for landslides occurring in flysch deposits.

This study presents the results of different field investigations, laboratory tests, and numerical activities that were performed to build up a numerical model capable to determine the influence of rainfall infiltration process on slope stability state through time. Undisturbed samples of the residual soil from a flysch rock mass were used to perform different laboratory tests in saturated and unsaturated conditions, aimed to provide an advanced hydro-mechanical characterization of the soil behavior under negative pore-water pressure. For the first time, the water retention curves, hydraulic conductivity functions, and unsaturated shear strength characteristics of the investigated soil were determined. Simulation results showed that rainfall duration, instead of intensity, is the crucial factor causing the landslide instability. Results suggest that only about 8 mm of rainfall can infiltrate into the slope during a day. The shear strength component associated with the negative pore-water pressure was found to have a negligible influence on the slope stability at the time of failure since positive pore-water pressure exists along the entire sliding surface. However, it is the unsaturated zone with specific hydraulic features that delay the landslide triggering event. Reduced hydraulic permeability and retention capacity of the soil between the phreatic line and slope surface are factors that postpone build-up of positive pore-water pressure along the sliding surface and enable the slope to remain stable during a long-lasting heavy precipitation.

**Keywords:** *flysch, unsaturated residual soil, rainfall-induced landslides, water retention curve, hydraulic conductivity function, unsaturated shear strength, numerical analysis.*



## Prošireni sažetak

Klizišta uzrokovana oborinama učestalo se događaju diljem svijeta u različitim klimatskim, geološkim i topografskim uvjetima. Rastući broj studija provedenih unazad dva desetljeća ukazuje kako promjene značajki oborina, vezano uz moguće globalne klimatske promjene, mogu dodatno povećati učestalost nastanka klizišta. Uz značajke oborina, karakteristike tla drugi su faktor od ključne važnosti za nastanak klizišta uzrokovanih oborinama. Ovisno o odnosu intenziteta kiše i hidrauličkih značajki materijala koji sačinjavaju površinski dio padine, infiltracija oborine u kosinu tijekom vremena odvija se kao nestacionarni proces pri kojem dolazi do promjene vlažnosti tla i preraspodjele pornih pritisaka unutar nesaturirane zone geotehničkog presjeka. Pritom najvažniji utjecaj na količinu i brzinu infiltracije, promjenu efektivnih napreznja i mogući pad čvrstoće materijala imaju hidrauličke i mehaničke značajke tla. Kako bi se riješila jednačina koja opisuje tečenje vode kroz nesaturirano tlo u vremenu i kvantificirao utjecaj oborine na stanje stabilnosti kosine, potrebno je poznavati funkcije značajki tla u nesaturiranim uvjetima: retencijsku krivulju, funkciju hidrauličke propusnosti te odnos između značajki čvrstoće i vlažnosti tla ili negativnih pornih pritisaka. Matrična sukcija je termin koji se u mehanici nesaturiranih tala najčešće koristi za negativni porni pritisak. Za razliku od plitkih klizišta u materijalima veće propusnosti, studije u kojima se proučava utjecaj nestacionarnog procesa infiltracije oborina na stabilnost dubokih klizišta izgrađenih od materijala relativno niske propusnosti vrlo su rijetke. Prethodna istraživanja klizišta u naslagama fliša u dolini Rječine bavila su se prvenstveno porastom pozitivnih pornih pritisaka uslijed dugotrajnih oborina i utjecajem procesa trošenja flišne stijenske mase na fizičko-mehaničke značajke tla. Pritom je utjecaj dugotrajnih oborina uzet u obzir u analizama stabilnosti jednostavnim podizanje razine podzemne vode (vrlo često i do površine terena), čime se smanjuju efektivna napreznja i reducira posmična čvrstoća materijala duž klizne plohe. Budući da u ovoj vrsti analiza vrijeme nije jedna od varijabli, distribuciju pornih pritisaka i stabilnost kosine nije moguće analizirati u vremenu. Također, pretpostavlja se da je materijal ispod razine podzemne vode potpuno saturiran, odnosno potpuno suh iznad te razine. Utjecaj matrične sukcije unutar nesaturirane zone geotehničkog presjeka se zanemaruje, kao i svi efekti na hidro-mehaničke značajke tla.

Kako bi se, po prvi puta u slučaju istraživanih materijala i predmetnog područja, aplicirali principi nesaturirane mehanike tla na nastanak klizišta uzrokovanih oborinama,



provedene su brojne terenske i laboratorijske aktivnosti. Dva osnovna razloga zbog kojih je klizište Valići odabrano kao pilot područje za provedbu istraživanja su prisutnost rezidualnog tla u površinsko dijelu padine za koje je primijećeno značajno isušivanje tijekom sušnih ljetnih mjeseci, te činjenica da su reaktivaciji klizišta u veljači 2014. godine prethodile višemjesečne intenzivne oborine. Neporemećeni uzorci tla uzeti s površinskog dijela klizišta korišteni su za određivanje hidro-mehaničkih značajki tla u nesaturiranim uvjetima. Različitim tehnikama mjerenja i korištenjem ukupno šest laboratorijskih uređaja, određene su retencijske krivulje za proces adsorpcije i desorpcije pri različitim vertikalnim naprezanjima. Metodom nelinearne regresije određeni su parametri najčešće korištenih jednadžbi za opis retencijskih funkcija. Mjerenja hidrauličke propusnosti u saturiranim i nesaturiranim uvjetima, u kombinaciji s retencijskim krivuljama omogućili su definiranje funkcije propusnosti tla u nesaturiranim uvjetima. Time je definirana zavisnost hidrauličke propusnosti materijala od matrične sukcije ili vlažnosti tla. Korištenjem modificiranih uređaja za direktno smicanje tla baziranih na principu transliranih osi, određen je utjecaj matrične sukcije na značajke čvrstoće tla. Definirane funkcije značajki tla u nesaturiranim uvjetima i rezultati terenskih mjerenja iskorišteni su za definiranje dvodimenzionalnog numeričkog modela kojim je moguće simulirati nestacionarni proces infiltracije oborina u kosinu, te odrediti utjecaj ovog procesa na stanje stabilnosti kosine u vremenu. Kako se parcijalna diferencijalna jednadžba tečenja vode kroz nesaturirano tlo rješava u prostoru i vremenu, pri čemu nelinearnost jednadžbe proizlazi iz nelinearnog odnosa materijalnih značajki i matrične sukcije, rješavanje iste najčešće podrazumijeva iterativne postupke i upotrebu numeričkih metoda. Komercijalno dostupni program SEEP/W (GEO-SLOPE International, Ltd.) baziran na metodi konačnih elemenata korišten je za rješavanje problema infiltracije oborina u kosinu korištenjem realnih ili umjetno generiranih zapisa oborina. Distribucije pornih pritisaka izračunate za različite vremenske trenutke integrirane su u program koji implementira metodu analize granične ravnoteže SLOPE/W (GEO-SLOPE International, Ltd.) kako bi se za svaki od proračunatih profila raspodjele pornih pritisaka izračunao faktor sigurnosti kosine. Time je utvrđena vremenska promjena stanja stabilnosti kosine izgrađene u naslagama fliša, uzimanjem u obzir različitih inicijalnih i rubnih uvjeta. Rezultati analiza potvrdili su dugotrajnost oborina kao presudan faktor za nastanak nestabilnosti, dok ekstremne količine oborina u kraćem vremenskom periodu rezultiraju značajnim površinskim otjecanjem. Čak i kada su mjereni intenziteti u periodu od rujna do veljače 2014. godine reducirani za 50 posto, rezultati analiza ukazuju kako se na dan reaktivacije kosina nalazi u stanju marginalne stabilnosti. Iako komponenta posmične čvrstoće povezana s matričnom sukcijom u trenutku sloma nema utjecaja na stabilnost kosine, utvrđeno

je kako upravo nesaturirana zona geotehničkog presjeka, sa svojim specifičnim hidrauličkim značajkama, odgađa gubitak stabilnosti kosine pri ekstremnim oborinama. U tom smislu, smanjena hidraulička propusnost i retencijski kapacitet nestaturirane zone s negativnim pornim pritiscima, faktori su koji usporavaju porast pornih pritisaka duž klizne plohe i osiguravaju stabilnost kosine tijekom dugotrajnih oborina.

**Ključne riječi:** *fliš, nesaturirano rezidualno tlo, klizišta uzrokovana oborinama, retencijska krivulja, funkcija hidrauličke propusnosti, čvrstoća tla u nesaturiranim uvjetima, numeričke analize.*



# Contents

<b>CHAPTER 1 INTRODUCTION</b>	<b>1</b>
1.1. Research background	2
1.2. Hypotheses	9
1.3. Research objectives	9
1.4. Methodology	10
1.5. Outline	13
<b>CHAPTER 2 STUDY AREA AND GEOTECHNICAL PROPERTIES OF THE RESIDUAL SOIL FROM A FLYSCH ROCK MASS</b>	<b>17</b>
2.1. Investigation site	18
2.2. Physical properties of the soil	21
2.3. Grain-size distribution analysis and plasticity limits	22
2.4. Field investigations	25
2.5. Climate conditions and rainfall measurements	34
<b>CHAPTER 3 THE BASIC CONCEPTS OF THE UNSATURATED SOIL MECHANICS</b>	<b>45</b>
3.1. Phase properties of unsaturated soil	46
3.1.1. <i>Quantifying each phase</i>	47
3.2. Air-water interaction and implications in geotechnical engineering	49
3.3. Surface tension and capillary phenomena	51
3.4. Soil suction components	54
<b>CHAPTER 4 SOIL-WATER RETENTION CURVE</b>	<b>59</b>
4.1. Role of the SWRC in unsaturated soil mechanics	60
4.2. Literature overview	60
4.3. Testing program	62
4.3.1. <i>Standard and volumetric pressure plate extractor apparatus</i>	63
4.3.2. <i>Suction-controlled oedometer apparatus</i>	64

4.3.3.	<i>The HYPROP evaporation method device</i>	66
4.3.4.	<i>Dew-point potentiometer WP4-T</i>	67
4.4.	Test results	68
4.5.	Interpretation of the SWRC results	76
4.5.1.	<i>Interpretation for the drying branch of the SWRC</i>	77
4.5.2.	<i>Interpretation for the wetting branch of the SWRC</i>	78
4.6.	SWRC prediction models	79
<b>CHAPTER 5 PERMEABILITY FUNCTION</b>		<b>81</b>
5.1.	Determination of UHCF – literature overview	82
5.1.1.	<i>Direct measurement of water flow properties</i>	85
5.1.2.	<i>Estimation techniques for determination of UHCF</i>	90
5.2.	Testing program for determination of the UHCF	99
5.2.1.	<i>Measurements of the saturated coefficient of permeability</i>	99
5.2.2.	<i>Measurements of the unsaturated coefficient of permeability</i>	102
5.3.	Test results and estimation of the UHCF	104
<b>CHAPTER 6 UNSATURATED SHEAR STRENGTH</b>		<b>109</b>
6.1.	Literature overview	110
6.1.1.	<i>Unsaturated shear strength based on the effective stress approach</i>	112
6.1.2.	<i>Unsaturated shear strength based on the independent state variables approach</i>	115
6.1.3.	<i>The “suction stress” concept</i>	119
6.2.	Previous studies of shear strength properties of flysch material from the Rječina River Valley	133
6.3.	Conventional direct shear tests on undisturbed samples	135
6.3.1.	<i>Test results for undisturbed and remolded specimens</i>	139
6.3.2.	<i>Interpretation of conventional direct shear test result</i>	142
6.4.	Determination of shear strength characteristics of undisturbed samples in unsaturated conditions	144
6.4.1.	<i>Suction-controlled test results</i>	163
6.4.1.1.	<i>Interpretation of test results</i>	170

6.4.2. <i>Wetting test results</i>	177
6.4.2.1. <i>Interpretation of the wetting test results</i>	184
<b>CHAPTER 7 NUMERICAL SIMULATIONS</b>	<b>187</b>
7.1. Literature overview	188
7.2. Rainfall infiltration modeling	196
7.2.1. <i>Theoretical background</i>	196
7.2.2. <i>Key-in material properties</i>	197
7.2.3. <i>Initial and boundary conditions</i>	200
7.3. Slope stability modeling	206
7.3.1. <i>Theoretical background</i>	207
7.3.2. <i>Key-in material properties</i>	210
7.4. Results of numerical simulations	211
7.4.1. <i>Influence of the rainfall input data (10', 1h and daily rainfall)</i>	215
7.4.2. <i>Influence of material properties: shear strength and unit weight</i>	215
7.4.3. <i>Artificial rainfall data: influence of the rainfall intensity</i>	217
7.4.4. <i>Results for different values of constant flux boundary conditions</i>	217
7.4.5. <i>Results for different initial pore-water pressure distributions</i>	219
<b>CHAPTER 8 DISCUSSION AND CONCLUSION</b>	<b>221</b>
Bibliography	237
List of figures	269
List of tables	281
Curriculum vitae	283



## List of abbreviations

1D	One-dimensional
2D	Two-dimensional
3D	Three-dimensional
AEV	Air entry value
AExV	Air expulsion value
CH	Clay of high plasticity, fat clay
CL	Clay of low plasticity, lean clay
DTM	Digital terrain model
FEM	Finite element method
FoS	Factor of safety
GSD	Grain-size distribution
HAEPD/S	High air-entry value porous disc/stone
LEM	Limit equilibrium method
LiDAR	Light Detection and Ranging
REV	Representative elementary volume
RH	Relative humidity
SCDSA	Suction-Controlled Direct Shear Apparatus (Megaris s.a.s.)
SSCC	Suction stress characteristic curve
SWAC	Soil wet area curve
SWRC	Soil-water retention curve
UGDSBPS	Unsaturated GDS Back Pressured Shear Box (GDS Instruments Ltd.)
UHCF	Unsaturated hydraulic conductivity function
UniLJ	University of Ljubljana, Slovenia
UniRi	University of Rijeka, Croatia
UniSa	University of Salerno, Italy
USCS	Unified Soil Classification System
USPF	Unsaturated soil property function





## **1. INTRODUCTION**

This chapter provides an introduction to the research topic. The basic theory of rainfall-induced landslides is presented, with a review of the current state of research for landslides in flysch deposits caused by long-term heavy precipitation. Hypotheses and research objectives are stated, and the methodology is presented. The outline of the thesis is provided at the end of the chapter.

## 1.1. Research background

Landslides are one of the most widespread natural hazards that cause human casualties and enormous economic losses worldwide. According to the World Bank report (2005), 3.7 million km<sup>2</sup> of the land surface is prone to landslides worldwide (Haque et al. 2016), and nearly 300 million people live in areas of potential landslide risk (Dilley et al. 2005). Due to climate change and increasingly frequent extreme weather events, mass movements have become common natural phenomena, which cause considerable damage and economic losses in many European countries (e.g., Schuster 1996; Klose et al. 2015). According to Jaedicke et al. (2014), approximately 3.6 million Europeans live in landslide-prone areas, while 20,000 km of roads and railways are highly exposed to landslides. The International Disaster Database reported that, in the last century, Europe was the second highest in the world among all continents in fatalities and had the greatest economic losses (1.55 billion Euros) as a result of landslides (Sassa and Canuti 2009; Guha et al. 2015).

The failure of earth material existing on a slope can be triggered by a wide range of geologic and extreme weather conditions, including eruptions of volcanos, earthquakes, and heavy precipitation (Wieczorek 1996). Human activities may also initiate landslides. Growing urbanization, uncontrolled land-use, deforestation, and extreme weather conditions associated with global climate change are factors causing an increase in landslide disasters. In the last decades there has been a steadily increasing number of scientific papers dealing with impacts of climate change on landslides (Wu et al. 2015; Gariano and Guzzetti 2016), where temperature change and change of precipitation patterns are the key factors influencing slope stability (Crozier 2010; Coe 2016).

Many researchers try to link various phenomena occurring in nature due to the increase in mean land-surface air temperature, which causes increased landslide activity all around the globe. For example, increased landslide activity is related to processes, such as: i) glacial retreat in mountain regions, which increases landslide activity due to removal of ice support (e.g., Hürlimann et al. 2012; Haeberli 2013; Fischer et al. 2013); an increased quantity of available loose debris for debris flows and increased rainfall infiltration into loose debris material due to removal of snow and ice cover (e.g., Lancaster et al. 2012; Fischer et al. 2012; Legg et al. 2014); ii) degradation of permafrost in rock (e.g., Geertsema et al. 2006; Raveland and Deline 2011) and soil (e.g., Francani et al. 2011); iii) increased sea level (e.g., Collins et al. 2007; Lee 2011);

Brooks et al. 2012); and iv) changes in droughts and wildfires (e.g., Nott et al. 2001; Cannon and DeGraff 2009; De Graff 2018).

Precipitation, either rainfall or snowmelt, is the most common cause of landslides. Landslides are being triggered by precipitation in all parts of the world in a wide variety of climatic, geologic, and topographic settings (Lu and Godt 2013). The factors that primarily control rainfall-induced slope failures are both rainfall characteristics and soil properties (e.g., Rahardjo et al. 2007; 2016). In general, rainfall causes a transient infiltration process in the slope which affects slope material by changing the moisture content and pore water pressure distribution in the soil profile, thereby changing the effective stress which can cause changes in shear strength of the soil, and finally, can lead to movements of soil mass and slope failure. Depending on the type of analysis, quantities such as rainfall characteristics, potential and actual evaporation, evapotranspiration, net infiltration, initial water content or pore water pressure distribution, constant and time-changing boundary conditions, water retention curves, unsaturated hydraulic conductivity functions, and shear strength functions of materials involved in the study usually have to be quantified or known, and accounted for. The latter, known as the unsaturated soil property functions (USPFs), have to be known since they define hydro-mechanical properties of unsaturated soil and have a direct influence on both the water infiltration process and stability of the slope. Different types of landslides are more or less sensitive to varying rainfall characteristics (e.g., Alonso et al. 1995; Van Asch et al. 1999; Rahardjo et al. 2007). Extreme storms with high intensities will often cause shallow landslides and debris flow, while deep-seated landslides in a material with low hydraulic conductivity are usually influenced by long-term infiltration, rise of the groundwater table, and antecedent rainfall. Varied approaches are used to assess how changing precipitation patterns and migration due to climate change affect the stability of slopes. As outlined by Crozier (2010), existing hydrologic and slope-stability models are capable of predicting landslide response from climate change, but there are great margins of error in global- and downscaled-climate projections that make landslide predictions uncertain. While some studies account only for the impact of precipitation characteristics changes (e.g., Chiang and Chang 2011; Kristo et al. 2017; Robinson et al. 2017), other account for changes in characteristics of both evapotranspiration and precipitation on occurrence of deep-seated and shallow landslides (e.g., Buma and Dehn 2000; Coe 2012; Comegna et al. 2013).

According to many papers dealing with rainfall-induced landslides, two types of instabilities could be distinguished respective to the mechanism leading to failure of the slope due to rainfall infiltration. The above is usually reflected in landslide depth, dividing landslides

into deep-seated or shallow landslides, and pore-water pressures existing on a sliding surface when a failure occurs, which in general can be positive or negative. In the context of the unsaturated soil mechanics, term matric suction is commonly used to denote negative pore-water pressure existing in the soil. In the case of deep-seated landslides with the low hydraulic conductivity of the soil, pore-water pressure conditions existing on the failure surface are typically positive. Failure generally occurs due to the rise of groundwater table which generates an increase in positive pore-water pressure, causing a decrease of effective stress and finally reducing the shear strength of soil along the potential surface of rupture. Depending on the hydraulic conductivity and retention properties of soil existing between the slope surface and phreatic line, longer infiltration periods are required to initiate landslide of this type. The time of landslide occurrence greatly depends on antecedent rainfall, since it defines the position of initial groundwater level and moisture content along the soil cross-section which affects retention capabilities, soil permeability and thus infiltration rates. On the other hand, the stability of steep, shallow landslides very often relies on the shear strength component associated with the matric suction existing within the cross-section of a slope. In case of rainfall, water content increases through the transient process of rainfall infiltration, causing a decrease of matric suction and the decrease of available shear strength. High-intensity rainfall can cause the more rapid elimination of matric suction within the steep slope built of highly-permeable material, and can possibly cause instability in shallow layers under unsaturated or saturated conditions.

Many studies focus on the rainfall-induced shallow landslides. For example, shallow-type landslides triggered by rainfall in pyroclastic soils frequently occur in Italy (e.g., Pasuto and Silvano 1998; Crosta and Dal Negro 2003; Aleotti et al. 2004; Casagli et al. 2006; Cuomo 2006; Pagano et al. 2010; Cascini et al. 2010; 2011; 2013; 2014; Pirone et al. 2016, and Santo et al. 2018). High-intensity rainfall frequently causes shallow-type slope failures in steep residual slopes of Singapore (e.g., Toll et al. 1999; Toll 2001; Rahardjo et al. 2001; 2005; 2007; 2007b; 2010; Rahimi et al. 2011; Rahardjo et al. 2016; and Kristo et al. 2017). Lu and Godt (2008) performed a case study for the colluvial deposits that mantle many steep bluffs along the Puget Sound in the Seattle, Washington area, where extreme precipitation commonly induces shallow landslides. Cho and Lee (2001) and Kim et al. (2012) investigated the influence of rainfall infiltration on shallow landslides in Korea. Ng and Shi (1998), Ng and Pang (2000); Lan (2004), Zhang and Ng (2003), and Li et al. (2005) analyzed the influence of rainfall intensity and duration on stability of shallow slopes in Hong Kong, while Gofar and Lee (2008)

and Xue et al. (2016) completed similar studies of landslides in Malaysia and China, respectively.

There is a far smaller number of rainfall-induced deep-seated landslide studies in the literature, in which interaction between rainfall infiltration process, existing ground conditions and unsaturated soil properties of low-conductivity materials are analyzed. There could be several reasons for this. First, as already mentioned, the stability of deep-seated slope mostly depends on the groundwater level conditions. Except in the highest part, potential sliding surface is mostly completely saturated and exposed to positive pore-water pressure conditions. Since the failure occurs due to increased pore pressures, Terzaghi's effective stress approach and principles based on saturated soil mechanics are sufficient for performing the slope stability analysis. At the same time, to rely on the shear strength component associated with soil suction seems to be contradictory from the standpoint of common engineering practice, since the soil suction dissipates as the water content of the slope exposed to rainfall increases. The second thing is that to quantitatively analyze the rainfall infiltration process through the low-permeability soil above the phreatic line, USPFs have to be known. USPFs can be obtained either from direct measurements performed in the laboratory or in-situ, or estimated from some of the basic geotechnical properties of soil. The latter are usually determined through more simple laboratory tests for soil characterization. Many studies have shown that in case of high-plasticity, fine-grained soils which undergo significant volume changes when matric suction (or water content) is changed, estimation techniques used to predict, instead of directly measure dependency between matric suction and water retention properties, hydraulic permeability or shear strength characteristics, generally become unreliable and inaccurate. The latter implies direct measurements of unsaturated soil properties which, unlike for saturated conditions, cannot be considered material constants but, rather, usually have a non-linear relationship respective to matric suction. The non-linear feature implies a significant number of measuring points required to determine different USPFs. Desaturation of soil reduces the cross-section area of water in soil-pores, thereby, reducing the hydraulic conductivity of soil respective to the water phase. Measurements of material properties under varying negative pore-water pressure values usually imply modifications of standard laboratory testing equipment and procedures, resulting in higher operating costs and need of expensive equipment. As the laboratory procedures used to determine the shear strength, deformation and permeability characteristics of low-permeability soils are typically time-consuming by themselves, the effort required for experimental determination of the USPFs in case of fine-grained soils, which are the key-in input parameters governing the transient rainfall infiltration process and affecting the slope

stability state, could be another important reason for the limited number of studies performed. For example, Sun et al. (2009) developed a numerical model based on the finite element method (FEM) and the limit equilibrium method (LEM) to study the effects of rainfall infiltration on deep slope failure. They performed a case study of Nongji Jixiao landslide in Wanzhou District, Chongqing of China with an average thickness of landslide body of 14.2 m. However, compared with the permeability features and retention properties of residual soil from a flysch rock mass obtained in this study, the material under consideration is much more coarse, with an air entry value (AEV) below 1 kPa and around three orders of magnitude higher value of saturated coefficient of permeability ( $1.3\text{E-}05$  m/s). Zhao et al. (2017) published a paper in which the influence of the coupling effect of rainfall infiltration and reservoir water level fluctuations on the stability of the Baijiabao Landslide in China's Three Gorges Reservoir Area was investigated. They used the FEM to simulate the coupling effect of rainfall and reservoir water level decline on the Baijiabao landslide during the drawdown of reservoir water level from 1 December 2014 to 18 August 2015, a period for which the mutation of field monitoring displacements was most obvious. They showed that the model could achieve the dynamic response of the seepage field, stress field and displacement field in the landslide under complex dynamic hydraulic boundary conditions, and that rainfall and reservoir water level decline have varying effects on landslide deformation at different stages.

However, these type of studies are completely absent in the literature in case of rainfall infiltration process through flysch deposits. Landslides in flysch deposits frequently occur in European countries such as Italy, Slovenia, Austria, Czech Republic, and Poland and are mainly caused by heavy precipitation. Previous studies of landslides in flysch slopes have mainly focused on the increase in pore water pressure caused by long-term, heavy precipitation as a landslide triggering factor (Arbanas et al. 2014) and on the effects of the weathering process of flysch rock masses on physical and chemical changes of material.

For the first type of studies in flysch deposits, different researchers (e.g., Mišćević et al. 2009; Vivoda et al. 2013; Berisavljević et al. 2015; Berti et al. 2017; Arbanas et al. 2017b), utilized conventional slope stability analyses, which are still most frequently employed in geotechnical engineering practice. This type of slope stability analysis account for rainfall influence on slope stability by changing the groundwater flow conditions, where the rising of the groundwater table increases pore water pressures and reduces the slope stability. This type of analysis is based on simple LEM or FEM formulations without physics and governing equations required for solving the problem of transient rainfall infiltration through the unsaturated soil. Since time is not a variable in the governing equations, the analysis is typically

performed for specific scenarios, while coupling between the rainfall infiltration and change of slope stability state through time is not possible with this approach. This type of analysis assumes saturated, steady-state water flow, where in the worst-case scenario, the phreatic surface is often assumed to coincide with the soil surface (Collins and Znidarcic 2004). In this case, further infiltration is not possible, and further rainfall does not affect the stability of the slope (Collins and Znidarcic 2004).

For the second type of study in flysch deposits, the effects of the weathering process of flysch rock masses on strength, physical properties and/or mineralogical composition was investigated by, e.g., Vivoda Prodan and Arbanas (2016), Vivoda Prodan et al. (2017), and Vlastelica et al. (2018).

Berti and Simoni (2012) presented the results of monitoring activities carried out in two slopes prone to landslide occurrence, made of clay-shales in the Northern Apennines of Italy. Descriptive statistics and simple, physically-based theories for infiltration and groundwater flow were adopted to analyze and interpret the collected field data. Maček et al. (2016) investigated the Slano blato, one of the oldest and largest landslides in Slovenia, reactivated in the form of a large earthflow in November 2000. For a material classified as fat clay (CH), water retention properties and saturated coefficient of hydraulic permeability were determined for samples produced in the laboratory, by using only fine-grained portion of material. The results indicated high AEV (1300 kPa) and low saturated coefficient of permeability (around  $5.0\text{E-}10$  m/s). Simple conceptual rainfall infiltration models were used to compare rainfall infiltration results with in-situ measurements. The conclusion of conducted study was that material and climate features on the Slano blato landslide result in sliding mass to exist in always saturated state. The exception is only the top few centimeters of soil where desiccation can occur due to excessive evaporation in the dry season.

However, none of these studies analyses the influence of the rainfall infiltration process, rainfall pattern and antecedent rainfall, coupled with the USPFs that govern the complex infiltration processes between the soil surface and phreatic line, on the state of stability of flysch slopes. Due to direct exposure to the atmosphere, the weathering process of the flysch rock mass is the most pronounced in the near-surface part of the slope, where a specific type of residual soil is formed. The weathering impact typically fades as the depth increases from the soil surface, resulting in complex soil-profile with different physical and hydro-mechanical features of soil along the geotechnical cross-section. Previous studies of landslides in the Rječina River Valley indicate that infiltration in the unsaturated part, together with groundwater level rise, occurs relatively slowly, which influences the rate of increase in pore pressures and



a decrease in the shear strength of soil (e.g., Benac et al. 2011; Dugonjić Jovančević and Arbanas 2012). Long rainy periods have shown to be crucial for landslide initiation, and all landslide occurrences came after long periods of heavy rainfall (Benac et al. 2011). Good examples of recent landslides triggered after few months of heavy rainfall are the Grohovo Landslide, which occurred in December 1996, and the landslide reactivated above the Valići Lake in February 2014. With the residual soil present at the slope surface and directly exposed to the atmosphere, the Valići Landslide was chosen as an investigation site for a novel comprehensive study of rainfall-induced landslides in flysch deposits with consideration of unsaturated soil mechanics principles. A novelty of this study consists in consideration of hydro-mechanical properties governing the transient process of rainfall infiltration into the slope and affecting the slope stability state through time. Preliminary laboratory tests performed on samples obtained from a near-surface part of the landslide body indicated that the investigated material is a lean clay (CL) with prevailing silt-size particles (above 50 %). After the dry summer period, the superficial part of the slope was found to have low water contents, with a degree of saturation very often around 50 %. After a few rainstorms in September and October 2014, in-situ measurements showed that only the very superficial part of the material was saturated, while at 0.5 m of depth material remained partially saturated. The first insights from permeability measurements in saturated conditions indicated that hydraulic features were dramatically different for specimens obtained from undisturbed samples and specimens prepared in laboratory conditions with the remolding and consolidation technique. The latter suggested that, in case of direct measurements of USPFs, undisturbed specimens should be preferred. The complex nature of this material and long periods of heavy rainfall that precede instability phenomena on these slopes suggest that the negative pore water pressure and desaturation of residual soil in the superficial part of slope could play an important role on landslide occurrence in flysch deposits. To study dependency between the state of slope stability in time and change in water content and pore-water pressure distribution along the cross-section of the slope, the relationship between water content (or matric suction) and water retention, permeability, and shear strength properties of the investigated soil have to be determined first. Such procedures should account for all of the relevant processes that are known to affect the USPFs, such as the hysteresis effect for soils undergoing a drying and wetting process, and stress state, which are reflected in all of the above-mentioned USPFs.

## 1.2. Hypotheses

Considering the current state of research in the field of rainfall-induced landslides in flysch deposits, the following hypotheses are stated:

(i) *Unsaturated hydraulic properties and negative pore water pressures have a significant influence on the rainfall infiltration process in the unsaturated zone of a slope in flysch deposits;*

(ii) *Long-term rainfall infiltration causes a decrease of matric suction in the soil, resulting in a reduction of stiffness and shear strength of the residual soil. Antecedent rainfall and rainfall patterns have an important role when analyzing the slope stability in residual soil from a flysch rock mass.*

(iii) *Matric suction has an important role on the state of slope stability in the unsaturated part of a slope in flysch deposits.*

## 1.3. Research objectives

To verify the research hypotheses, extensive experimental work should be performed to define USPFs which are required when solving equations describing the rainfall infiltration process and assessing the state of slope stability over time. USPFs should account for hysteresis effects that soil exhibits when undergoing the drying and wetting process, with special accentuation on the wetting process, as it is relevant for the the rainfall infiltration process in the unsaturated part of the slope. Great care should be devoted to possible differences in engineering behavior of soil regarding the sample preparation technique and sample disturbance. Due to the complex process which residual soil from the flysch rock mass undergoes during the formation process, including physical and chemical changes of the original bedrock material, it is expected that hydro-mechanical properties of undisturbed samples and of those reproduced under laboratory conditions by using various techniques, could greatly differ. Thus, to reflect features of material present in-situ, the use of undisturbed samples should be preferred when conducting laboratory experiments for the determination of soil properties in unsaturated conditions. This particularly applies on measurements for determination of water-retention and permeability properties, where features and interconnectivity of voids are known to have a dominant effect. Finally, material features should be obtained considering the stress conditions and loading paths that material undergoes on a slope.

Considering the previously stated and research hypotheses, the following are considered as the main research objectives:

*(i) Determination of the soil-water retention curves, permeability functions and shear strength characteristics of the residual soil from the flysch rock mass during the wetting and drying process.*

*(ii) Determination of the importance of geotechnical cross-section unsaturated zone for the rainfall infiltration process and landslide occurrence in flysch deposits.*

## **1.4. Methodology**

To investigate the importance of geotechnical cross-section unsaturated zone for the rainfall infiltration process and landslide occurrence in flysch deposits, research activities included laboratory measurements, field surveys and investigation works, and conduction of numerical simulations. All activities could be divided into several interrelated steps, whose fulfillment ensured reaching the defined research objectives. The proposed research methodology is elaborated in the following part.

The collection of soil samples from the Valići Landslide was performed in the very early stage of research. One of the most important aims of this study was to define material properties on samples which are representative for in-situ conditions. In that sense, sampling techniques should ensure the preservation of soil structure, density and, when required, water content as close as possible to those existing in-situ in time of sampling. For example, in the initial stage of research, undisturbed samples were collected in a small sampling pit by using the steel cutters of various testing devices directly in-situ, or with hard plastic tubes which were statically inserted into the soil and excavated to minimize disturbance effects, avoiding the use of dynamic forces. The hand-equipment for undisturbed soil sampling (Eijkelkamp Soil&Water, Inc.) was used on several occasions to determine water content and density in the first few meters of soil. In the latter part of the research, during May and June 2018, two boreholes were drilled with machine rotary drilling. Inclinator casing was installed in borehole B1 up to the depth of 30 m, while the piezometer standpipe was installed in borehole B2, up to 20 m of depth. Periodical inclinometer surveys were performed using the portable inclinometer measuring system Digitilt Classic Inclinometer System (Durham Geo-Enterprises Inc.), while the Rugged TROLL 100 Data Logger and Rugged BaroTROLL Data Logger (In-Situ Inc.) were installed in piezometer for continuous measuring and logging of groundwater level. Disturbed

samples were used when soil structure did not affect the results of laboratory tests. For example, disturbed samples were used for classification tests and determination of basic geotechnical properties. The following basic geotechnical properties were determined: specific gravity of solid particles,  $G_s$ ; saturated,  $\rho_s$ , and dry density of soil,  $\rho_d$ ; granulometric composition (wet sieving tests combined with the hydrometer and SediGraph methods); and Atterberg's limits (liquid limit, plastic limit, and plasticity index). Classification of soil was performed according to the Unified Soil Classification System (USCS).

Undisturbed samples were used in experimental procedures aimed to provide advanced hydraulic and mechanical characterization of soil in both saturated and unsaturated conditions. Soil-water retention curve (SWRC) relates the water content of soil with the (matric) suction values. Differentiation of the SWRC presented in the volumetric water content form enables the determination of the water storage capabilities of soil as a function of matric suction. SWRC can be used to estimate different USPFs as well. The following hydraulic properties of soil were determined using the undisturbed samples, considering different stress conditions and wetting paths that the soil undergoes in-situ:

- (i) SWRC was defined by using the measurement results obtained with a variety of devices and measurement techniques in their optimum measuring range (suction-controlled oedometer-type devices; standard pressure plate and volumetric extractor devices; mini-tensiometers; and dew-point potentiometer WP4-T). Used procedures enabled to investigate the effect of overburden pressure on retention properties, hysteresis during the drying and wetting processes and the influence of the matric suction on effective stress.
- (ii) The coefficient of permeability was determined for saturated conditions (falling head method in conventional oedometer apparatus and constant head method in conventional triaxial apparatus) and under negative pore water pressures (HYPROP evaporation method device).

The following mechanical characteristics were obtained by using different testing procedures:

- (i) Consolidation properties (conventional oedometer apparatus).
- (ii) Saturated shear strength characteristics of soil (conventional direct shear apparatus).
- (iii) Unsaturated shear strength characteristics of soil (modified direct shear apparatuses).

A non-linear regression analysis was performed on the fragmented SWRC laboratory measurement results to obtain the best-fit parameters for some of the most commonly used SWRC equations. Due to the significant hysteresis observed during the wetting and drying process, SWRC parameters were obtained for both desorption and adsorption process. The obtained SWRC parameters and saturated coefficient of permeability values,  $k_s$ , were used to estimate the unsaturated hydraulic conductivity functions (UHCFs) for the soil undergoing the drying and the wetting process. The influence of sample disturbance on hydraulic conductivity was determined by measuring the saturated coefficient of permeability on both undisturbed and disturbed (completely remolded and consolidated) samples. To assess the possible influence of sample disturbance on shear strength and stiffness characteristics, standard direct shear tests were performed on both undisturbed and disturbed samples. Modified direct shear apparatuses implementing the axis translation technique to control or measure matric suction were used to perform strain-controlled tests under constant values of matric suction (herein, suction-controlled tests). Due to the long testing time (around one month per test), only two tests were performed as stress-controlled wetting tests to determine if an increase of water content due to the reduction of matric suction could induce failure of the specimen under imposed loading conditions (herein, wetting tests). In wetting tests, specimens were wetted at different rates until failure conditions were reached in terms of acceleration of shear displacement under constant stress conditions. The obtained results enabled quantification of the increase in shear strength of the investigated soil due to an increase of the matric suction. The unsaturated shear strength envelope was obtained in terms of  $\chi$  method (Bishop's effective stress correction approach) and  $\phi^b$  method (extended Mohr-Coulomb failure criteria). The above activities have determined how matric suction affects the retention properties, hydraulic conductivity and shear strength of residual soil from a flysch rock mass, and have ensured fulfillment of the first research objective. At the same time, all of the previously mentioned activities have provided necessary input data for conduction of numerical analysis of slope stability during a rainfall infiltration process.

The final part of the research was to assess the influence of the unsaturated zone between the phreatic line and soil surface on landslide occurrence due to rainfall. Numerical analysis were performed for the Valići Landslide case study. All of the in-situ investigation works and measurements, available digital terrain models (DTMs) obtained from different studies and determined USPFs (SWRC, UHCF, and unsaturated shear strength) were used to build a numerical model, define initial and boundary conditions, and define key-in material properties. Transient FEM seepage analysis was performed by using the SEEP/W (GEO-SLOPE

International, Ltd.) software to determine pore water pressure distribution during the rainfall infiltration. The generated model enables investigation of the influence of different USPFs, initial, and boundary (time-dependent) conditions on simulation results. Different rainfall patterns, with changing intensities and durations can be applied as the flux boundary conditions at the slope surface. The influence of different pore-water pressure distributions (or moisture conditions) on the rainfall infiltration process can be determined as well. Calculated pore-water pressure profiles were integrated into the SLOPE/W (GEO-SLOPE International, Ltd.) software, which uses the limit-equilibrium method (LEM) to determine the factor of safety (FoS) of the slope. In this way, the change of slope stability state over time due to the rainfall infiltration process can be analyzed. The obtained results ensured the fulfillment of the second research objective.

## 1.5. Outline

The investigated problem is elaborated through several interrelated chapters. Each chapter starts with a literature review, where the most important works and latest findings relevant to the field of research are presented. Research methodology is presented in the following part, where all of the employed experimental procedures, devices, measuring techniques, and performed analysis are described in detail. The obtained results are presented and interpreted in the closing part of chapter.

are presented and interpreted in the final part of the chapter. which is closed by underlying important results, findings and conclusions.

The introduction to the topic of research is provided in **Chapter 1**. Research background introduces the basic problems of rainfall-induced landslides and provides background and motivation for the research. A detailed review of the current state of research in the area of rainfall-induced landslides in flysch deposits is provided first. Research hypotheses are stated, and the main objectives of the research are defined next. Finally, the employed methods and workflow of the research are presented in more details. An outline of the thesis is provided at the end.

**Chapter 2** describes the study area and investigated materials. The main features of the flysch rock mass and previous researches dealing with landslides in the Rječina River Valley are described in the first part. Features of the case study Valići Landslide from February 2014,

sampling procedures, in-situ investigation works, and field surveys are described in the following part. The results of various laboratory tests for determination of basic geotechnical properties and soil classification are presented as well. Climate conditions relevant for the research topic are presented and the main features of precipitation characteristics, whose role is crucial for the landslide triggering in the investigated area, are elaborated. Precipitation measurements obtained from the nearby location, which were used to define the flux boundary condition in numerical analysis are presented in the final part of the chapter.

The basic concepts of the unsaturated soil mechanics are provided in **Chapter 3**. Basic properties of the air-water interface are described, and the four-phase soil model is introduced first. Relations used to quantify each phase and basic variables are defined. Surface tension and capillary phenomena with application in geotechnical engineering are presented, matric suction is defined, and Kelvin's capillary model is derived here. The chapter closes with a definition of soil suction components and their relevance in various engineering applications.

The importance of the SWRC in unsaturated soil mechanics and procedures and measuring techniques employed to obtain SWRCs of investigated soil are described in **Chapter 4**. Some definitions and features of water retention properties of soils with different textures are presented first. Development of measurement techniques and devices with an application on different types of soil are presented in the following part. Material properties that were found to control water retention properties of soil are discussed as well. The testing program, including different techniques and measuring devices used to define SWRC of investigated material, under different stress conditions and during the drying and wetting path are described in detail. The obtained results are presented in the following part, regarding soil suction vs. different forms of water content. The influence of matric suction change on volume changes and change of the effective stress are presented and discussed as well. A non-linear regression analysis procedure is performed on obtained SWRC results to obtain the best-fit parameters of some of the most frequently used SWRC equations. The interpreted SWRC results are compared with retention properties of materials found in the literature. Finally, two models used to predict SWRCs of fine-grained soils are tested and compared with the results obtained in the final part of the chapter.

**Chapter 5** is devoted to unsaturated hydraulic conductivity. Theoretical basics of water flow through the unsaturated porous medium is described first. A detailed overview of existing methods, which can be used to obtain permeability function is provided, including both direct and indirect measurement procedures which can be used in laboratory or in-situ. Some of the estimation techniques are introduced as well. Different set-ups of soil column tests, devices

based on the axis translation methods and methods that use centrifuge are described among direct measurement methods. Different regression-based approaches such as parameter estimation method, empirical models, and closed-form equations that utilize, for example, SWRC properties and  $k_s$ , are discussed among indirect methods for estimation of permeability function. The testing program for determination of hydraulic conductivity of investigated soil, both in saturated and unsaturated conditions is described in the following part. A falling head method in conventional oedometer apparatus and constant head method in conventional triaxial apparatus were utilized for measurements in saturated conditions. Measurements for determination of SWRC obtained with the HYPROP device were used to calculate the coefficient of permeability respective to water phase for matric suction values up to 130 kPa, according to the Darcy-Buckingham law and the Extended Evaporation Method (Schindler et al. 2015). Finally, the estimation procedure of the UHCF for the investigated soil is presented.

The influence of the matric suction on shear strength characteristics of investigated soil is elaborated through the **Chapter 6**. According to numerous experimental works performed on different soil textures and under different ranges of matric suction, some general observations on the shear strength characteristics are summarized first. Two basic approaches commonly used to determine the shear strength of unsaturated soils, namely the effective stress approach (Bishop 1959) and the independent state variables approach (Fredlund and Morgenstern 1977) are presented. Some of the more recently developed advanced concepts, such as the suction stress concept (Lu and Likos 2006), which consider different interparticle mechanisms that affect the effective stress of the unsaturated soil are presented. Limitations and advances of these approaches, along with modifications proposed by different authors are discussed as well. The next part of the chapter summarizes results from previous studies in which shear strength properties of flysch samples from the Rječina River Valley were investigated. These studies include laboratory tests performed on completely disturbed soil samples in saturated conditions, by using the conventional direct shear and ring shear apparatus. Methods used for determination of shear strength properties in saturated and unsaturated conditions in this study are described, and test results are shown in the following part of the chapter. Test results obtained on undisturbed and disturbed specimens are interpreted, and some general conclusions on the influence of the matric suction on the behavior of investigated material during shear are made. The chapter is concluded by summarizing and interpreting results obtained from the long-lasting wetting test.

All of the findings brought up through previous chapters are utilized to build a numerical model and perform numerical analysis described in **Chapter 7**. Various approaches which can



be used to determine the influence of rainfall on the landslide triggering are reviewed first. Basic concepts, theoretical framework and governing equations used to describe transient water flow through unsaturated soil are presented. The most important findings from previously performed numerical studies dealing with the influence of various factors on the stability of slope exposed to rainfall, such as rainfall intensity, duration and pattern, different initial moisture conditions and pore water pressure profiles, material properties of different soil textures, etc. are discussed in the following part. An overview of some of the most important studies where numerical simulations were employed to investigate the rainfall-induced landslides of shallow- and deep-seated type is provided as well. Finally, works found in the literature that investigate the influence of the rainfall on the stability of slopes built in flysch deposits are presented. The FEM model built in SEEP/W (GEO-SLOPE International, Ltd.) for modeling of the rainfall infiltration process and the procedure of coupling with the SLOPE/W (GEO-SLOPE International, Ltd.), which implements the LEM to perform stability analysis, are described afterwards. Geometrical conditions and domain discretization, initial and boundary conditions including various flux boundary conditions derived from collected rainfall data, key-in material properties, and calculation methods used in numerical simulations are described first. The obtained results are presented in the form of change of pore-water pressures and degree of saturation in slope during the rainfall infiltration through time, and change of the factor of safety for the analyzed sliding surface and calculated pore-water pressure distributions. The latter determine the influence of rainfall infiltration on the state of slope stability through time. Finally, results are presented and interpreted for various flux boundary conditions applied, representing rainfalls of different characteristics.

The final **Chapter 8** concludes the thesis by outlining the key scientific contributions and the most important findings of the conducted research. A possible application of findings is addressed, and some guidelines for possible further research are provided.

## **2. STUDY AREA AND GEOTECHNICAL PROPERTIES OF THE RESIDUAL SOIL FROM A FLYSCH ROCK MASS**

This chapter provides information about the study area and the investigated material in the context of research. Materials composing slopes of the Rječina River Valley are described first, with accentuation on the flysch rock mass, which is typically present at the lower parts of the valley. Being highly prone to the weathering process, especially its incompetent fine-grained members, landslides typically occur in these formations. Due to direct exposure to the atmosphere, the weathering process of the flysch rock mass is the most pronounced in the near-surface part of the slope, where residual soil is formed. The weathering impact typically vanes with the depth, resulting in a complex soil-profile with varied physical and hydro-mechanical features. A deep-seated landslide reactivated above the Valići Lake in the winter of 2014 was chosen as an investigation site for a comprehensive study of rainfall-induced landslides in flysch deposits. The results obtained from a series of laboratory tests performed to determine basic index and classification properties of soil are presented first. Field investigations, including the investigation drilling, water content, and density measurements, inclinometer and groundwater level surveying, and precipitation measurements are presented. Finally, basic climate and rainfall characteristics, which is considered to be the major landslide triggering factor in the investigated area, for the last few decades are analyzed and presented.

## 2.1. Investigation site

The Rječina River Valley, located in the outback of the City of Rijeka, Croatia, is well known to have experienced numerous historical and recent landslides on both slopes of the valley (Arbanas et al. 2014). The valley is composed of Cretaceous and Paleogene limestone at the top of the slopes and Paleogene siliciclastic rocks at the lower slopes and the valley bottom, where the sliding processes have primarily developed.

The term flysch was introduced in 1827 by the Swiss geologist Bernhard Studer and originates from the German word *fliessen*, which means flow. Actually, flysch is a sequence of alternations of various clastic sedimentary rocks that were deposited as deep marine facies during an early stage of orogenesis. Well-known flysch deposits are found in the forelands of the Pyrenees, Dinarides, northern Alps and Carpathians and tectonically similar regions in Italy, the Balkans and Cyprus. Flysch is characterized by rhythmic alternations of sandstone and fine-grained layers that contain siltstones, silty shales, and clayey shales. Flysch deposits may also include breccias, conglomerates and limestone beds. From a geotechnical point of view, a flysch rock mass could be described by the following characteristics (Marinos and Hoek 2001): i) heterogeneity due to alterations of competent and incompetent members; ii) the presence of clay minerals; iii) tectonic fatigue and sheared discontinuities, often resulting in a soil-like material; and iv) generally low permeability and significant weakening where free drainage does not occur due to the presence of clay minerals.

Numerous studies in the Rječina River Valley focused on the determination of basic physical and mechanical material properties, modeling and monitoring of landslides in flysch deposits. For example, the Grohovo Landslide is the largest active landslide in the Rječina River Valley which was studied in detail by many researchers. After a long period of heavy precipitation, the instability event occurred in the form of a complex retrogressive landslide in December 1996. The first monitoring, and field investigation works were performed in the period from 1999 to 2010. Topographical, geophysical surveyings, and engineering geological mapping, drilling of several boreholes, laboratory testing of obtained samples, and periodical inclinometer, groundwater level, and geodetic measurements of benchmark movements obtained in the following decade provided information for description of the landslide geometry, engineering geological cross-section of the landslide, and sliding mechanism, insight into displacement magnitudes and groundwater conditions. Obtained samples were used to

determine mineralogic composition, basic index properties and to perform classification of materials (e.g., Benac et al. 1999, 2005, 2011, 2014). The next part of the extensive research of the Grohovo Landslide was conducted in the framework of the Croatian-Japanese joint research project “Risk Identification and Land-Use Planning for Disaster Mitigation of Landslides and Floods in Croatia,” which was conducted from 2009 to 2014. Being chosen as one of three pilot areas, a comprehensive monitoring system was installed on the Grohovo Landslide which still operates, although in somewhat reduced volume. Advanced field and laboratory equipment, software for numerical simulations, and knowledge gained through this bilateral scientific project enabled investigation of shear strength properties of investigated materials under more complex loading conditions, performing advanced numerical slope stability analysis, including both landslide initiation and propagation process, and establishment of the advanced monitoring system with fully-automated continuous collection of in-situ data (e.g., Oštrić et al. 2012; Vivoda et al. 2013; Ljutić et al. 2013; Arbanas et al. 2014, 2014b; Vivoda Prodan et al. 2017). Dugonjić Jovančević et al. (2016) presented a research of the dormant landslide located on the south-western slope of the Valley, which was reactivated in 1885 due to intense and long-term rainfall. The same landslide was studied by Benac et al. (2009) regarding the origin of the instability phenomena along the karst-flysch contacts. Both of the above-mentioned landslides are indicated in Figure 1.

The Valići Landslide occurred on 13 February 2014 at the southwestern slope of the Rječina River Valley after a long period of heavy rain. High landslide risk due to potential damage to the reservoir and the Valići Dam, demanded urgent landslide mitigation measures in the form of lowering of the water level in the reservoir and surface drainage from the landslide body (Arbanas et al. 2017). Preliminary field investigations, including remote sensing-mapping, field mapping, and ground surveying are summarized in Mihalić Arbanas et al. (2017). Detailed field geomorphological mapping of the active landslide was performed the day after the landslide reactivation using the existing LiDAR (Light Detection and Ranging) DTM derived topographic map from 2012. Geodetic surveys with the purpose of deriving a detailed topographic map of the landslide were finished in November 2014 (Mihalić Arbanas et al. 2017). The obtained results indicated that the instability occurred as a reactivation inside the displaced mass of the larger historical landslide, which was developed more than 50 years ago and was partially stabilized by drainage at the time of the construction of the Valići Dam (Mihalić Arbanas et al. 2017). The landslide type was identified as a translational landslide, with the approximate length and width of the displaced mass of 230 m and 120 m, respectively. Due to the lack of detailed field investigations, slope stability analysis using the shear strength

reduction method was performed to investigate the possible position of the yielding zone and the approximate volume of displaced mass (Arbanas et al. 2017b). An approximate depth of the sliding surface was found to be about 20 m. Figure 2 shows the results of the preliminary investigation works summarized in Mihalić Arbanas et al. (2017) in the form of a) landslide map and b) defined engineering geological cross-section.

Features such as residual soil covering the landslide surface, observed desaturation of the superficial material during the dry summer periods, the fact that the landslide was triggered after few months of heavy precipitation and the risks posed by possible landslide reactivation (see Arbanas et al. 2017) have resulted in the Valići Landslide to be chosen as a pilot area for a new, comprehensive study of rainfall-induced landslides in flysch deposits. Unlike previous ones, this study focuses on applying the principles of unsaturated soil mechanics, where the crucial part is defining the hydro-mechanical properties of the material that directly affect the stability of the slope under the transient rainfall infiltration process. With this objective, field investigations were performed to define moisture and groundwater table conditions, while various laboratory tests that were performed defined required USPFs.

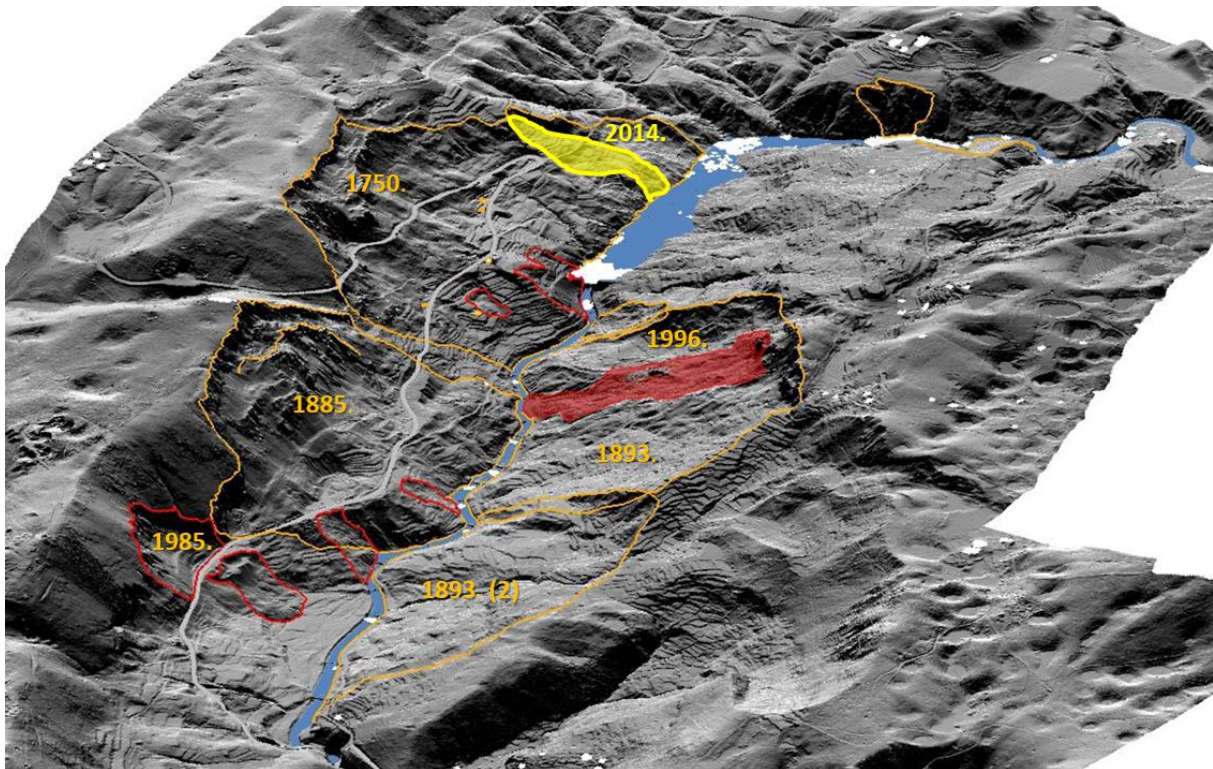


**Figure 1:** LIDAR-derived bare-earth DTM of the Rječina River Valley with contours of historical (yellow) and more recent (red) landslides. The zones colored in red and yellow represent the areas of the Grohovo Landslide from 1996, and the Valići Landslide reactivated on 13 February 2014, respectively (modified from Arbanas et al. 2017).

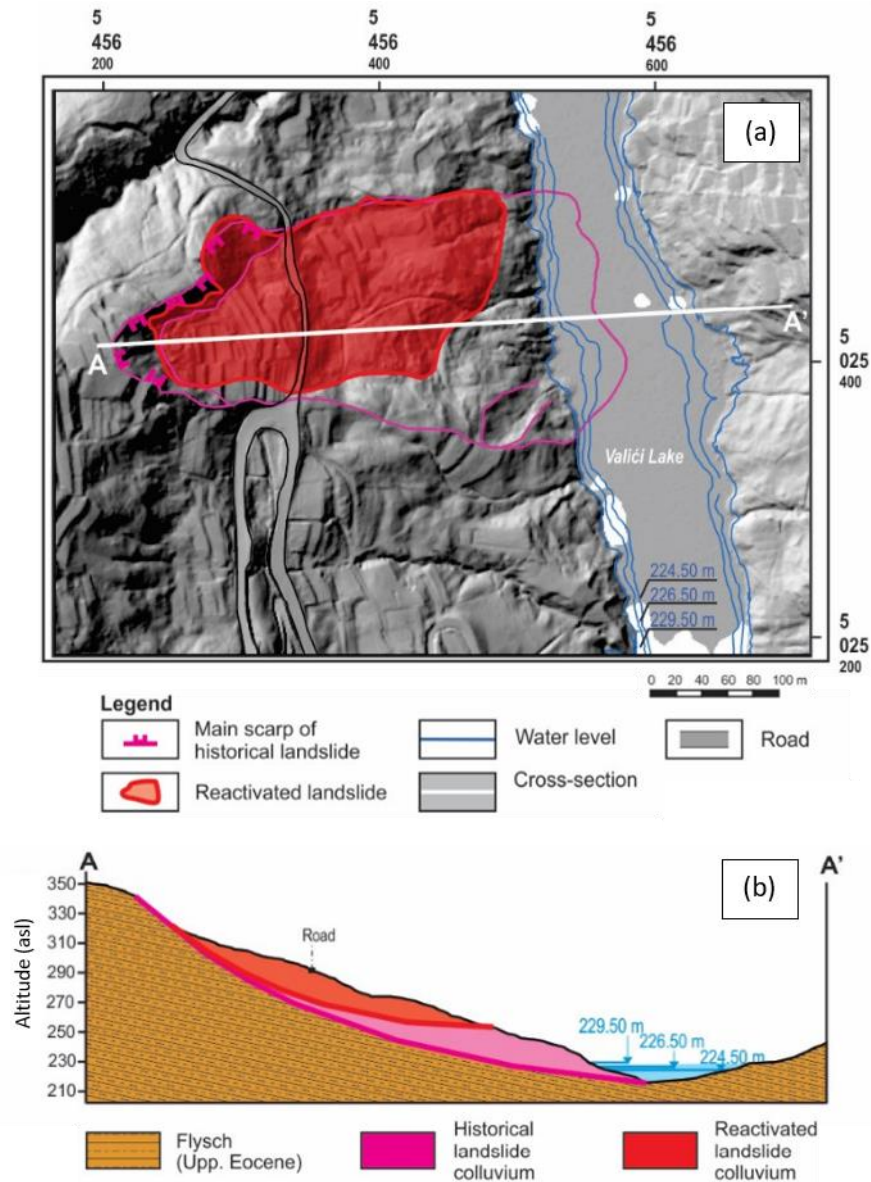


**Figure 2:** Results of preliminary investigations: a) landslide map; and b) engineering geological cross-section of the historic and reactivated Valići Landslide (modified from Mihalić Arbanas et al. 2017).

## 2.2. Physical properties of the soil

Undisturbed soil samples were collected from the sample pit in the central part of the Valići Landslide (location 2 in Figure 4), and a series of tests were conducted to determine the basic index properties of the soil. Sampling was performed from the surface at a small hand-drilled pit by using hard-plastic tubes (Figure 3a). The sampling depths for all the samples varied from 0.5 to 1 m. After pushing the tubes into the soil, they were excavated and sealed to prevent evaporation. The natural water content ranged from 28% at the ground surface to 10% at a depth



of 1 m, while the in situ density varied from 1.91 to 2.13 g/cm<sup>3</sup> (Peranić et al. 2018). Mean values of the basic properties of tested material, including the specific gravity of soil solids (ASTM D854-14), saturated unit weight, particle size distribution (ASTM D1140-17 and ASTM D7928-17), liquid limit ( $w_L$ ), plastic limit ( $w_P$ ), plasticity index ( $PI$ ) (ASTM D4318-17) and classification of material according to the USCS (ASTM D2487-11), are summarized in Table 1.

**Table 1:** Mean values of the basic properties of the residual soil samples used in this study (Peranić et al. 2018).

Specific gravity, $G_s$ [/]	Sat. unit weight, $\gamma_s$ [kN/m <sup>3</sup> ]	Particle size distribution				Atterberg's limits			USCS
		Clay, C	Silt, M	Sand, S	Gravel, G	Liquid limit, $w_L$	Plastic limit, $w_P$	Plasticity index, $PI$	
		[%]	[%]	[%]	[%]	[%]	[%]	[/]	
2.7	20.9	30.3	53	10.4	6.3	44	24	20	CL

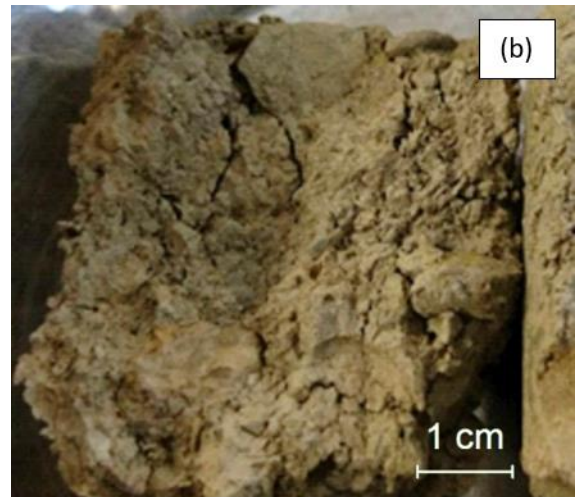


**Figure 3:** a) Sampling pit; b) half of the oven-dried specimen from a depth of 0.75 m.

## 2.3. Grain-size distribution analysis and plasticity limits

The inverse distribution of the solid particles (e.g., the distribution of the voids), for each material type, provides an insight into the possible retention properties and behavior of the unsaturated soil. The distribution of different pore sizes that are present in the material indicate the AEV, desaturation rate and water storage capability of the soil; therefore, the grain-size

distribution (GSD) curves have an important role in unsaturated soil mechanics (Fredlund et al. 2012).

To analyze the GSD characteristics of the material in the landslide body, samples were taken from the landslide surface at ten different locations, which are marked in Figure 4. Wet sieving tests, the hydrometer method and particle sizing by using the SediGraph method were combined to obtain the GSD curves. The obtained results (Figure 5) show that fine-grained particles dominate in the tested samples with the highest average contents of silt and clay. However, larger siltstone grains with different weathering degrees were often present in the undisturbed samples used in these tests. Generally, larger particles of siltstone are surrounded by the fine-grained silty-clayey matrix. Portion, size, and strength of siltstone particles typically increase with depth in the soil profile, as the degree of weathering decreases. Small and soft (easily fractured with fingers) brown siltstone particles become grey, harder, and larger below the first few meters of depth.

GSD curves show a similar grain-size composition of the material along different parts of the landslide surface, indicating similar conditions in material origin due to the weathering process of the bedrock siltstone. The only sample that had a slightly higher content of sand particles (28.2%) was a sample collected from location no. 10, outside the landslide body at the lowest position of the slope. The largest quantity of particles larger than 2 mm was found in samples collected from the central part of the landslide body (locations no. 2, 8 and 9), and sample from location no. 9 had the highest content (9.5%) by weight.

The Atterberg's limits were determined, and most of the samples could be classified as lean clay (CL). Only samples that were taken from locations no. 8 and 10 plot beneath the A-line in the plasticity chart. The obtained results cluster in the plasticity chart, indicating that the near-surface soil has relatively uniform classification properties along the landslide body (Figure 6).



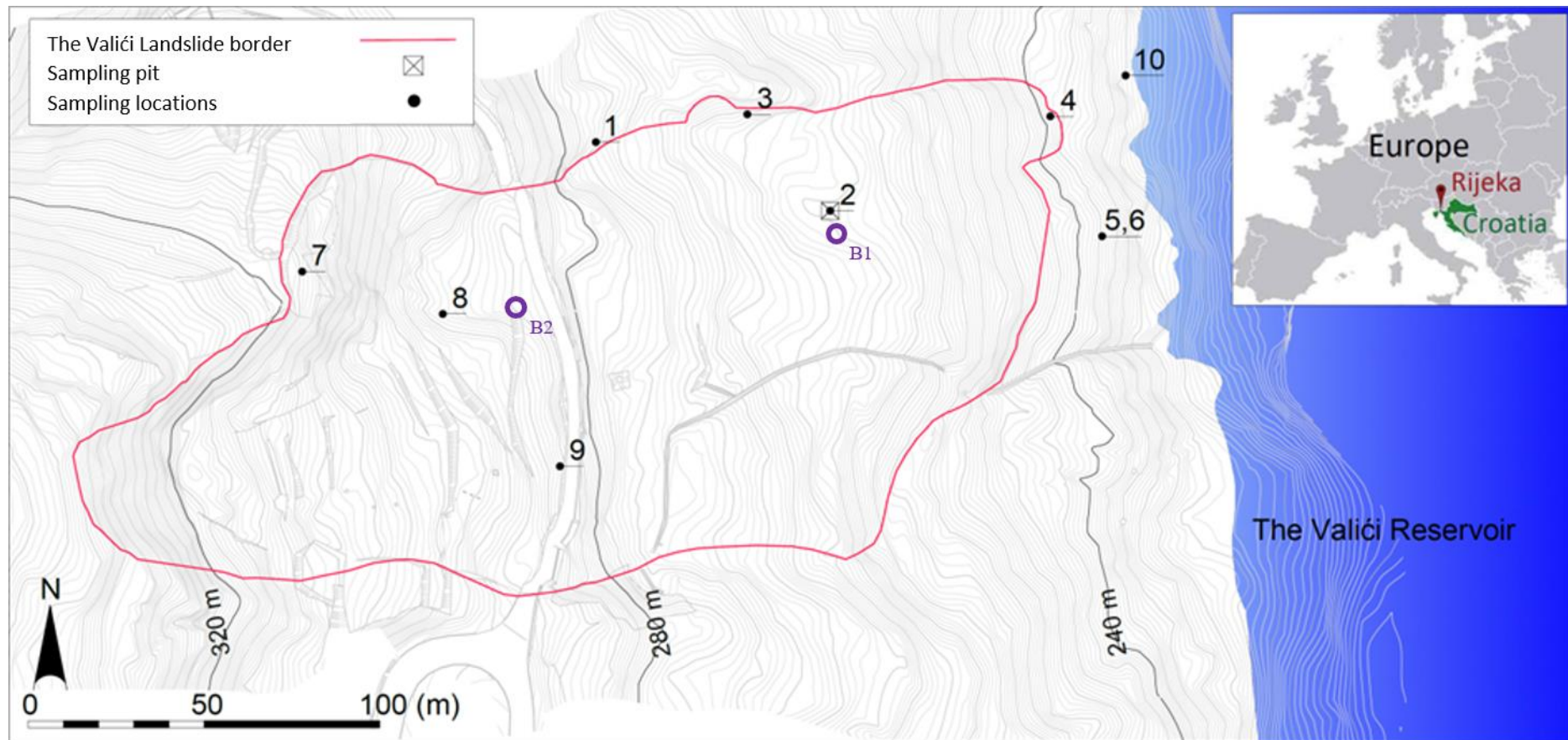


**Figure 4:** Map of the reactivated landslide on a detailed topographic map with sampling locations and borehole B1 and B2 locations (modified from Mihalić Arbanas et al. 2017).

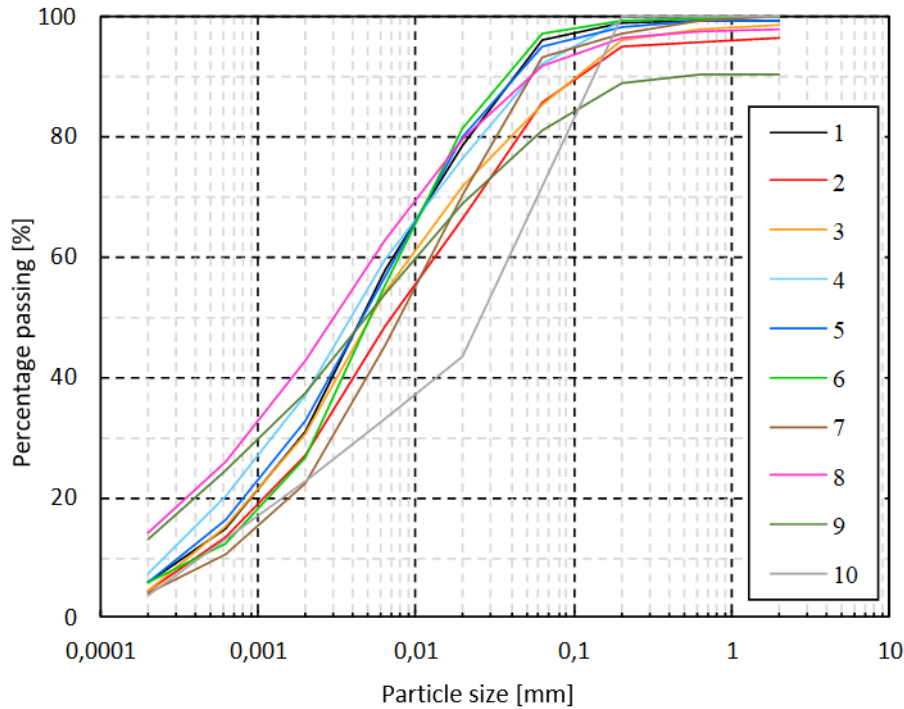


**Figure 5:** GSD results for samples collected at ten locations along the landslide body and slope.

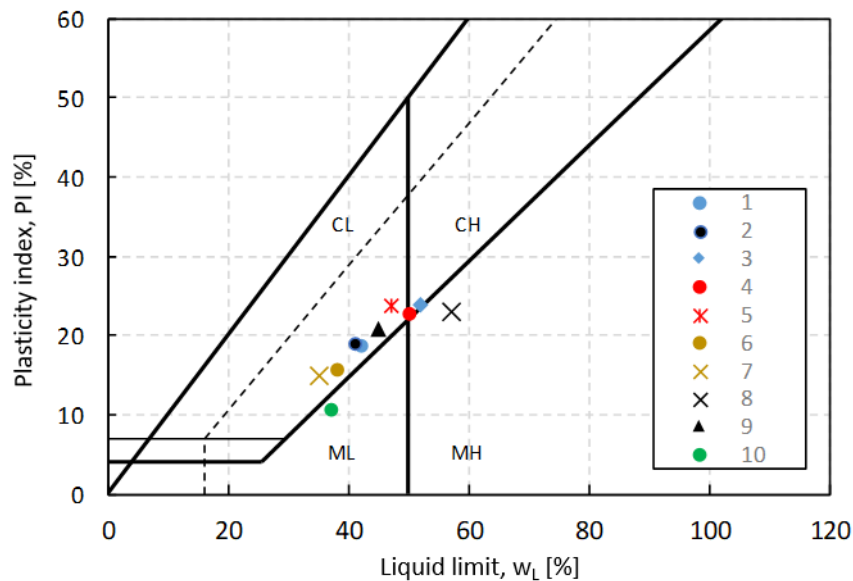


**Figure 6:** Plasticity chart of the samples.

## 2.4. Field investigations

The determination of in-situ water content was performed in several campaigns in the period from October 2017 to June 2018. Superficial undisturbed samples were collected from the sampling pit location using the equipment for undisturbed soil sampling (Eijkelkamp Soil&Water, Inc.) on 14 October 2016, 18 July 2017, 13 September 2017 and 2 October 2017. The equipment employed enabled collection of samples in steel cutters with diameter/height of



50/50 mm, from the surface up to a few meters of depth. Depending on the soil type, sampling depth is very limited in this case, since the drilling is performed by hand. The obtained samples were closed with plastic lids from both sides and sealed in nylon to prevent evaporation. Natural water content and densities at various depths were determined. Depending on the quality of the obtained samples, volumetric water content and the degree of saturation were determined as well. If the SWRCs are known for investigated soil, natural water content can be used to estimate existing in-situ matric suction values. Several details of sample collection in October 2017 are shown in Figure 7, while the obtained results are summarized in Table 2.



**Figure 7:** Collection of near-surface soil samples by using the equipment for undisturbed soil sampling (Eijkelkamp Soil&Water, Inc.) for determination of natural water content and basic physical properties. Sampling depths (0.05; 0.25; 0.45; 0.75; and 1.05 m) are indicated below samples in Figure 7 d).

**Table 2:** Natural water content determination of near-surface soil by hand-drilling using the equipment for undisturbed soil sampling (Eijkelkamp Soil&Water, Inc.).

<b>14 October 2016</b>				
Depth [m]	Natural water content, $w_n$ [%]	Dry density, $\rho_d$ [g/cm <sup>3</sup> ]	Volumetric water content, $\theta_w$ [cm <sup>3</sup> /cm <sup>3</sup> ]	Degree of saturation, $S$ [%]
0.05-0.1	28.1	/	/	/
0.25-0.3	24.5	/	/	/
0.45-0.5	18.8	1.79	0.34	100.0
0.75-0.8	13.0	1.69	0.22	58.6
1.05-1.10	9.9	/	/	/
<b>18 July 2017</b>				
Depth [m]	Natural water content, $w_n$ [%]	Dry density, $\rho_d$ [g/cm <sup>3</sup> ]	Volumetric water content, $\theta_w$ [cm <sup>3</sup> /cm <sup>3</sup> ]	Degree of saturation, $S$ [%]
surface	16.5	/	/	/
0.12-0.17	15.3	1.54	0.23	54.4
0.32-0.37	16.3	1.53	0.25	57.6
0.57-0.62	13.1	1.65	0.22	56.1
0.87-0.92	11.3	1.60	0.18	44.1
<b>13 September 2017</b>				
Depth [m]	Natural water content, $w_n$ [%]	Dry density, $\rho_d$ [g/cm <sup>3</sup> ]	Volumetric water content, $\theta_w$ [cm <sup>3</sup> /cm <sup>3</sup> ]	Degree of saturation, $S$ [%]
0.02-0.05	25.1	/	/	/
0.20-0.25	25.2	1.46	0.37	80.3
0.35-0.40	19.7	1.69	0.33	88.8
0.60-0.65	19.9	1.34	0.27	52.7
0.79-0.84	18.6	1.77	0.33	96.3
0.91-0.96	19.2	1.78	0.34	99.6
1.06	8.5	/	/	/
1.16-1.21	7.3	1.93	0.14	48.9
<b>2 October 2017</b>				
Depth [m]	Natural water content, $w_n$ [%]	Dry density, $\rho_d$ [g/cm <sup>3</sup> ]	Volumetric water content, $\theta_w$ [cm <sup>3</sup> /cm <sup>3</sup> ]	Degree of saturation, $S$ [%]
0-0.05	29.2			
0.21-0.26	21.5	1.46	0.37	80.3
0.32-0.37	19.2	1.69	0.33	88.8
0.63-0.68	21.4	1.34	0.27	52.7
0.80-0.85	13.5	1.77	0.33	96.3
0.87-0.92	12.5	1.78	0.34	99.6
1.10-1.15	15.4	/	/	/
1.28-1.33	10.9	1.93	0.14	48.9

Two investigation boreholes and in total 50 m of material were drilled by conventional machine rotary boring technique in the period from 28 May to 18 June 2018. To measure water content at depths greater than was possible with hand-drilling, drilling fluid was used only after the groundwater table was reached. Table 3 summarizes the natural water content, degree of saturation and volumetric water content measured for samples obtained from different depths during drilling works at the sampling pit location. After being arranged in wooden boxes, samples were trimmed with a knife and sealed in nylon. When possible, wax dipping and the water displacement technique (ASTM D7263-09) were used to determine the total density of irregularly-shaped samples. Natural water contents and volumetric water contents determined for superficial soil at the sampling pit location during various field investigations are summarized in Figure 8.

**Table 3:** Natural water content determination during machine borehole drilling at sampling pit location.

May and June 2018				
Depth [m]	Natural water content, $w_n$ [%]	Total density, $\rho$ [g/cm <sup>3</sup> ]	Volumetric water content, $\theta_w$ [cm <sup>3</sup> /cm <sup>3</sup> ]	Degree of saturation, $S$ [%]
0	32.6	1.71	0.42	80.8
0.20	22.4	1.89	0.35	80.9
0.55	19.1	1.94	0.31	78.6
0.80	12.8	2.05	0.23	71.5
1.10	14.6	2.03	0.26	74.9
1.60	17.8	1.96	0.30	77.5
2.00	14.6	2.10	0.27	83.0
2.50	10.2	2.23	0.21	82.3
3.00	18.2	/	/	/
3.40	10.8	/	/	/
3.90	9.8	/	/	/
4.10	14.0	/	/	/
6.50	11.8	2.31	0.24	103.6
7.60	5.3	2.51	0.13	107.1
9.40	10.9	2.15	0.21	74.9
18.00	12.2	2.29	0.25	101.9
18.00	11.2	2.29	0.23	96.4
18.00	11.7	/	/	/

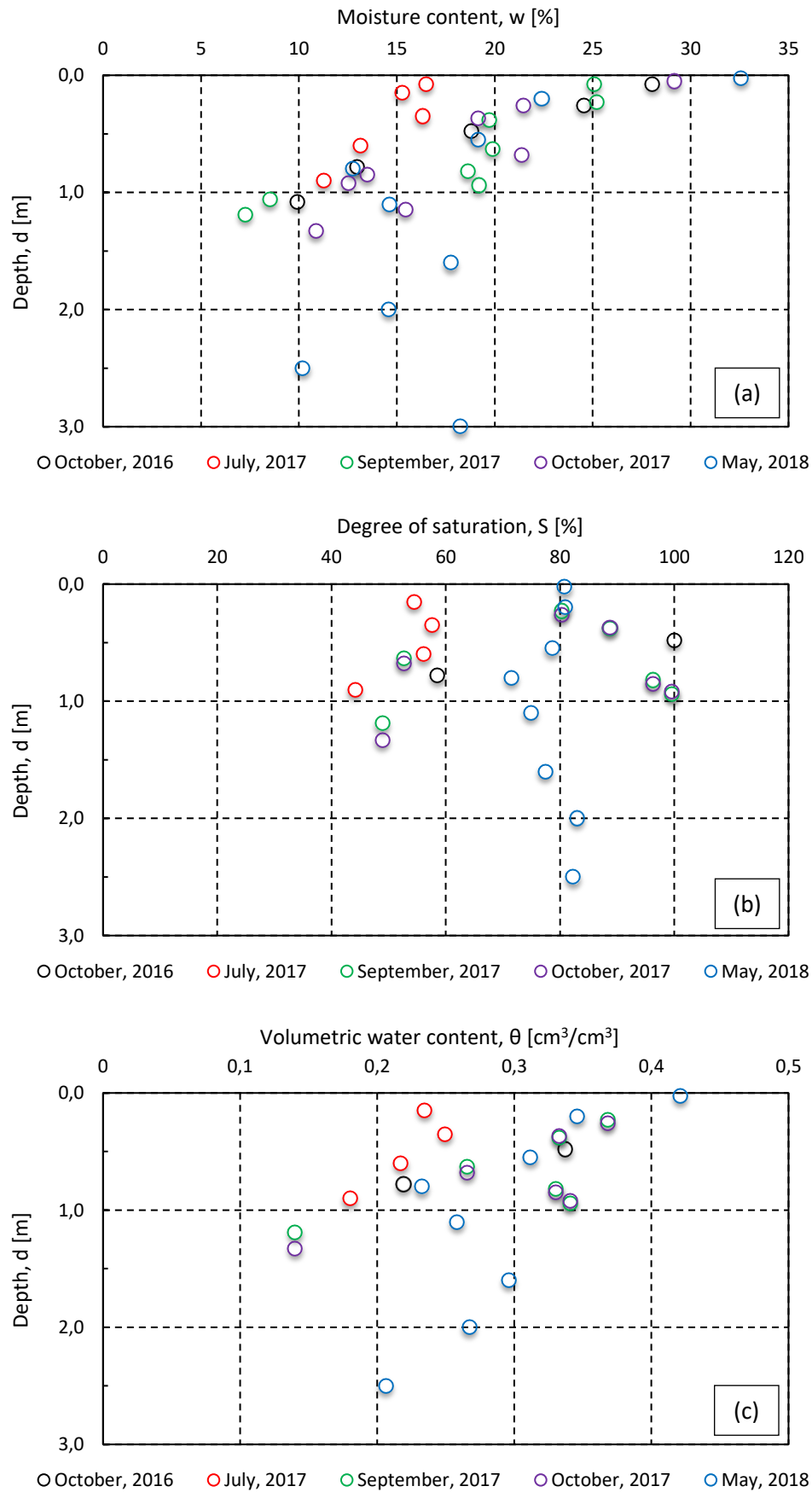


**Figure 8:** Determination of a) natural water content; b) degree of saturation; and c) volumetric water content for superficial soil at sampling pit location (B1) during various field investigations.



Borehole B1 was performed next to the sampling pit location up to 30 m of depth (marked with B1 in Figure 4). Dry boring was performed in the first 4.5 m of depth, without the use of drilling fluid. Groundwater was found at around 2.7 m of depth. A change of material color from brown to grey was observed at a depth of approximately 3 m. Possible indication of the shearing plane was observed at a depth from 18.3 to 18.5 m, where the zone of highly disturbed brownish material with very soft consistency turns into hard siltstone, extracted in the form of intact rock cylinders. The hardness of the rock from 18.5 until 22.5 m of depth required the use of the diamond crown, while sampling of the drilled material by using the knife was not possible. The return of the drilling fluid at the ground surface was observed continuously. Figure 9 shows the core material obtained with machine drilling arranged in wooden boxes with marked depths. Upon reaching the target depth of 30 m, inclinometer casing was installed, and grouting was performed. After a few days of rest, the first (null-reading) survey was performed using the portable inclinometer measuring system Digitilt Classic Inclinometer System (Durham Geo-Enterprises, Inc.) to obtain the initial profile of the casing. Subsequent measurements were performed approximately every two weeks. Measurements were collected using the Digitilt DataMate II (Durham Geo-Enterprises, Inc.), while the interpretation of results was performed with DigiPro2 software (Durham Geo-Enterprises, Inc.). Several details of borehole drilling and installation of inclinometer chasing at location B1 are shown in Figure 10. Inclinometer reading during the first few months indicates that shearing occurs at a depth of approximately 18 m at the B1 location, which corresponds to observed characteristics of core material during in-situ drilling works. The slope stability results obtained in previous and this study indicated that the surface of rupture is located at 17.7 m below the ground surface at the B1 location. Inclinometer readings are reported in Figure 11.



**Figure 9:** Core samples obtained by machine-drilling at the B1 location with marked depths.

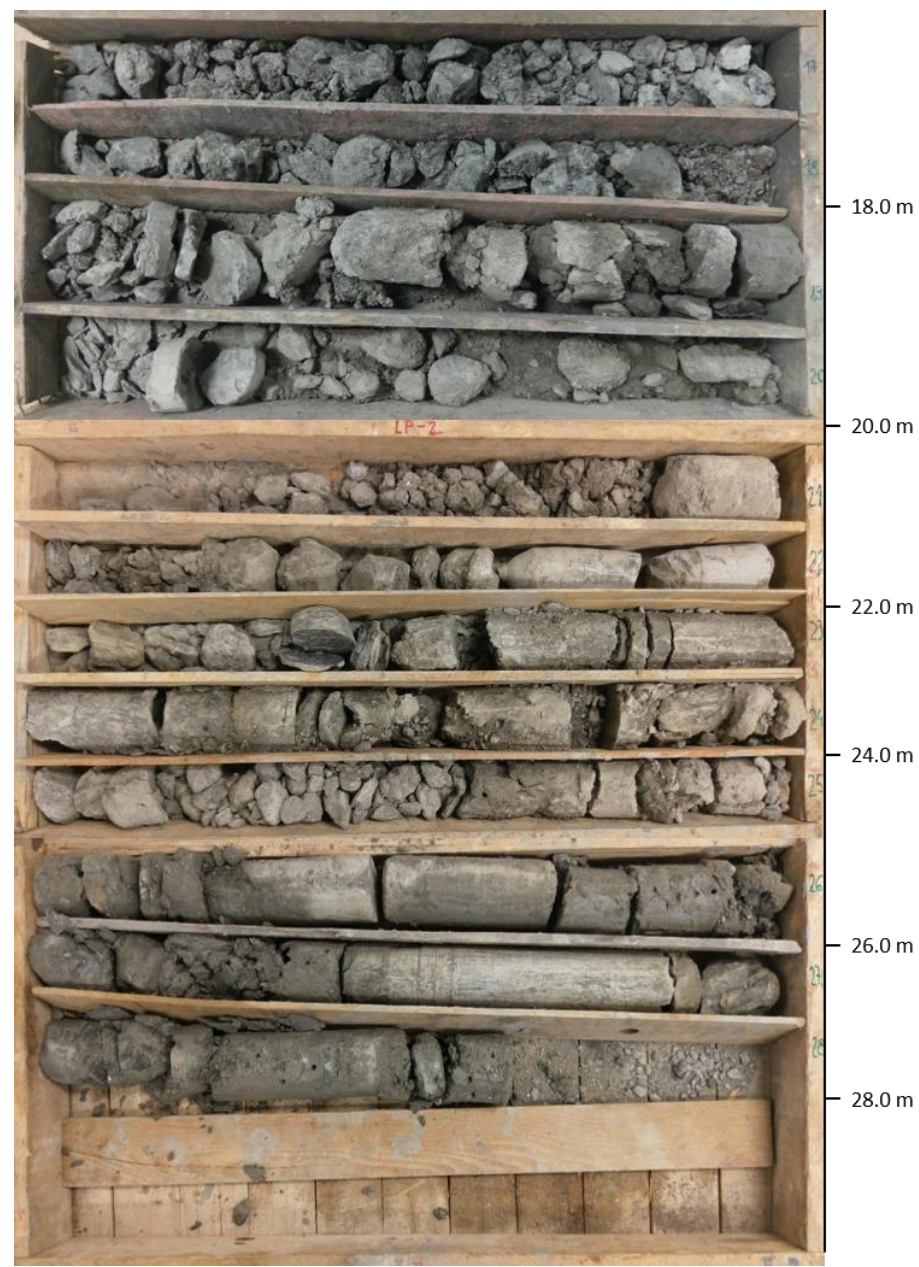
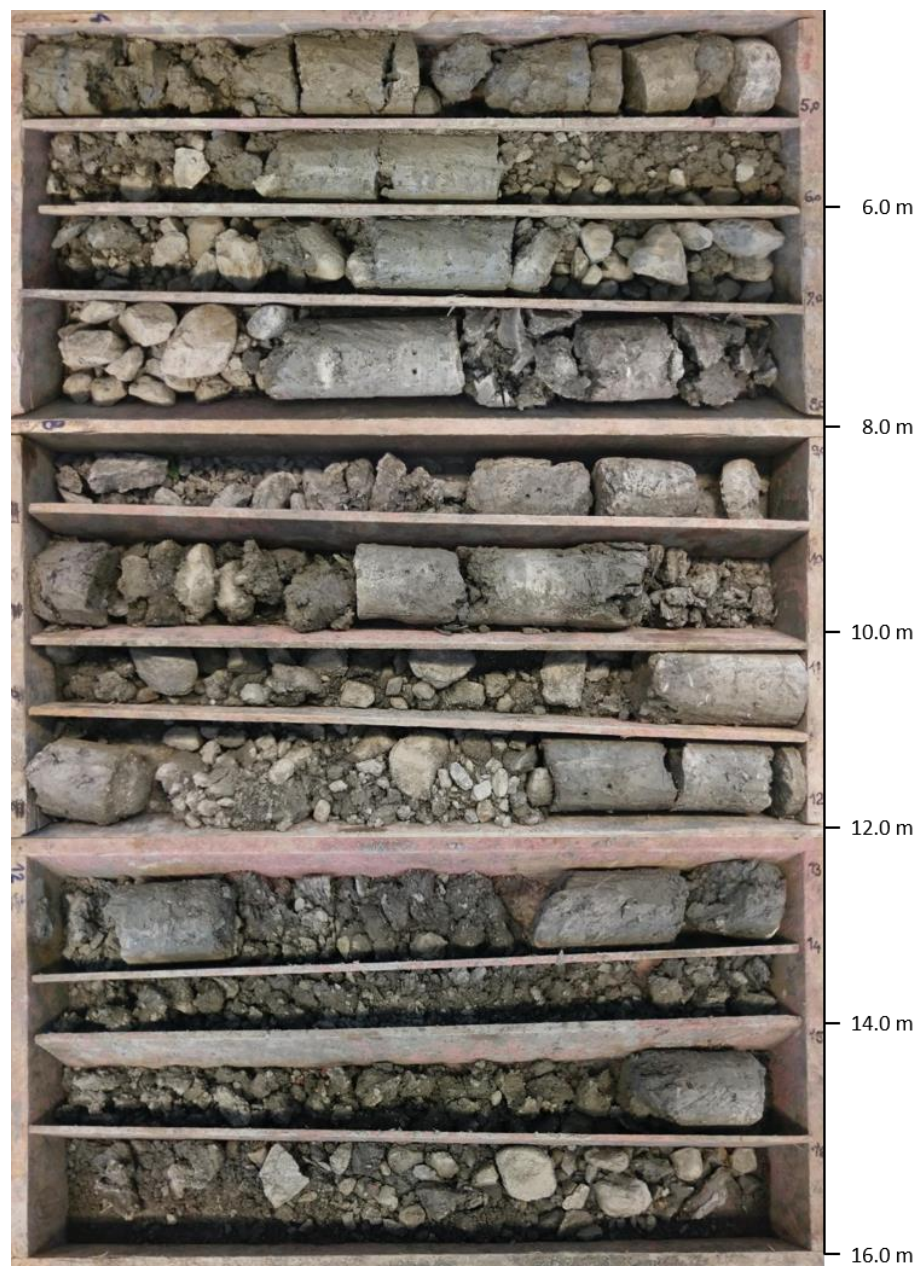


**Figure 9:** Continued.





**Figure 10:** Details of a) inclinometer chasing installation at the B1 location; b) portable inclinometer measuring system Digitilt Classic Inclinometer System (Durham Geo-Enterprises, Inc.); and c) measurements in progress.

Due to the inaccessibility of the terrain, borehole B2 was performed at a higher location next to the existing road damaged during the landslide reactivation (marked with B2 in Figure 4). Groundwater level was found at approximately 8 m of depth. Unlike for the B1 borehole, the occasional presence of isolated sandstone blocks at a depth of 4 m made drilling more difficult and required the use of a diamond crown with drilling fluid. Material at a depth from 7.5 to 8. m was highly disturbed, indicating a possible zone at which shearing has occurred. Slope stability results closely match the those regarding the sliding surface depth at the B2 location as well. Also, the change of color from brown to grey was observed at a depth of 8.5 m. A return of the drilling fluid at the ground surface was not observed, probably due to lateral outflow to the nearby road embankment with high conductivity. When the drilling garniture reached a depth of 20 m, a piezometer standpipe was inserted into the boring hole, the space between the perforated tube and borehole was filled with coarse-grained material and grouted close to the surface. Rugged TROLL 100 Data Logger was installed in piezometer for

continuous measuring and logging water level, non-vented (absolute) pressure and temperature. Readings were started on 21 June 2018 at 30 min recording intervals. Rugged BaroTROLL Data Logger (In-Situ Inc.) was used for compensation of atmospheric pressure, while the Rugged TROLL Docking Station was utilized for periodical download of recorded data on a laptop with installed Win-Situ 5 software (In-Situ Inc.). Some details of data collection during a site visit on 9 July 2018 are shown in Figure 12. Groundwater level was checked occasionally with Water Level Meter 100 (In-Situ Inc.) or fox whistle as well. The data obtained indicate a slow lowering of the groundwater level in piezometer with respect to the soil surface, from 7.5 m at the end of June to 7.8 m at the end of August. The results are summarized in Figure 13.

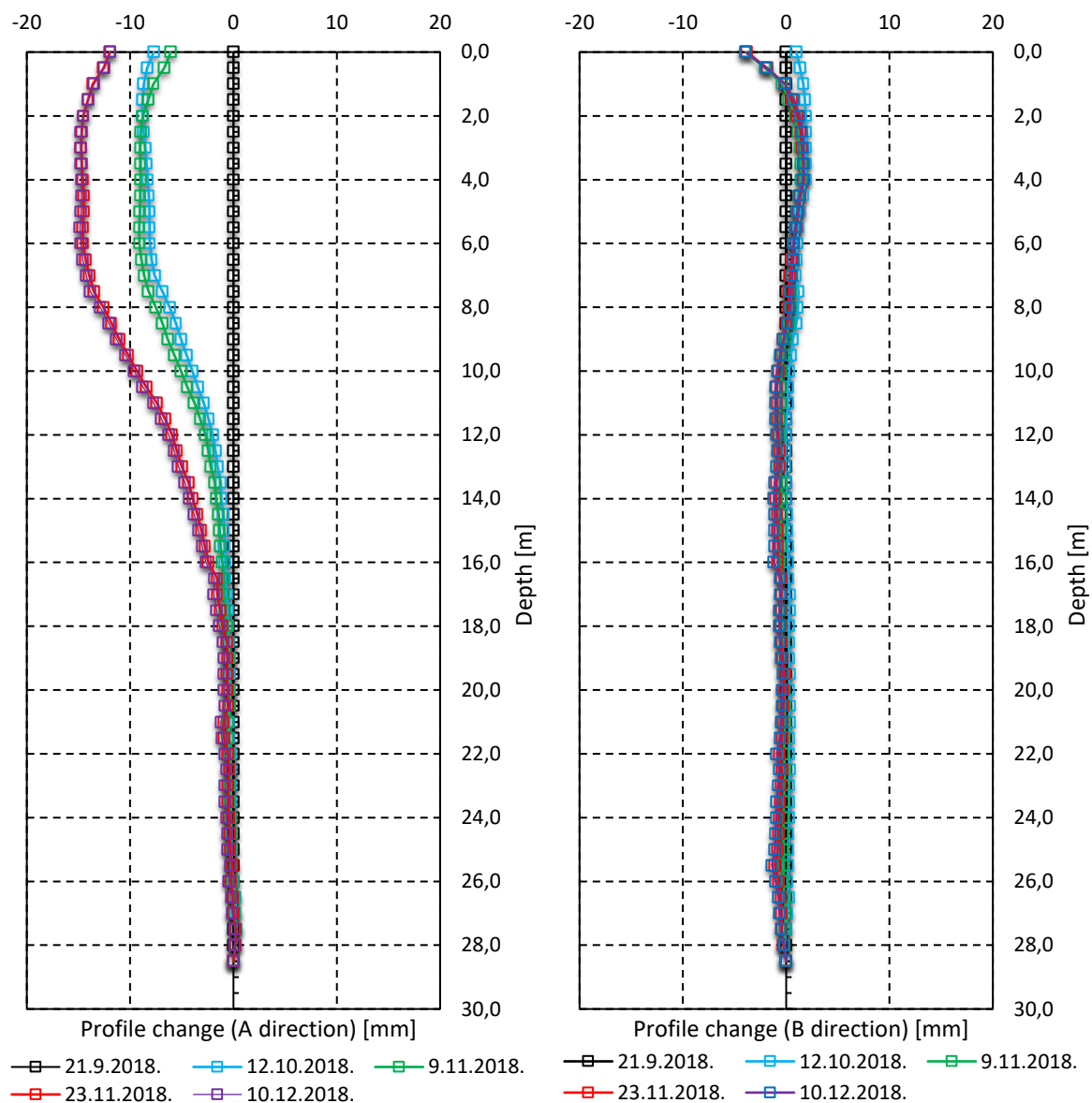


**Figure 11:** Inclinometer surveys at the B1 location.





**Figure 12:** Collection of continuous groundwater pressure measurements at the B2 location: a) Rugged TROLL 100 Data Logger and BaroTROLL Data Logger (In-Situ Inc.), and b) TROLL Docking Station for periodical download of the recorded data with the Win-Situ 5 software (In-Situ Inc.).

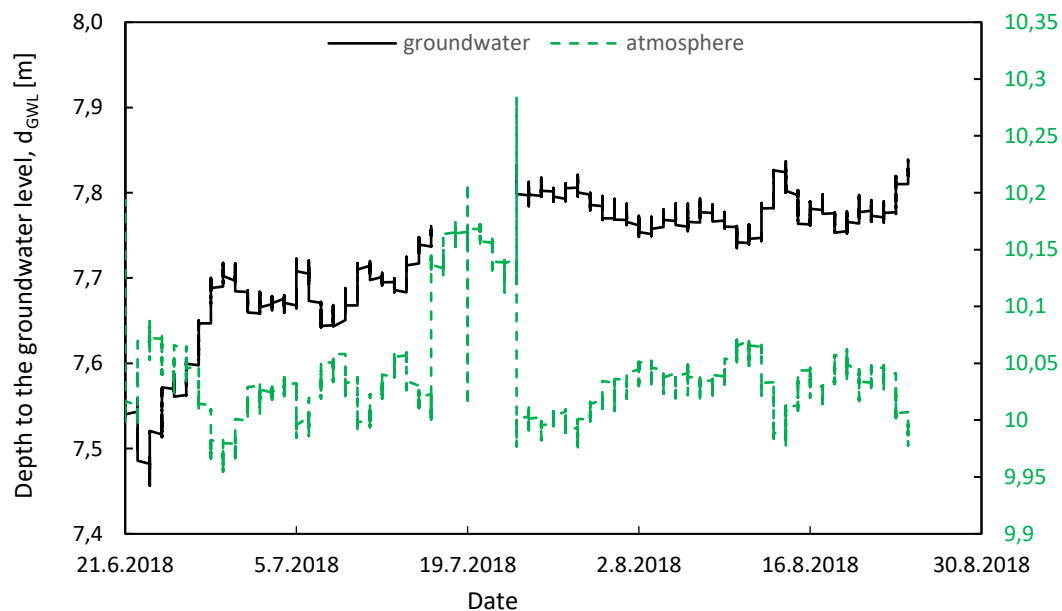


**Figure 13:** Groundwater level and atmospheric pressure measurements expressed as the pressure height.

## 2.5. Climate conditions and rainfall measurements

Due to the complex interaction occurring between the soil surface and the atmosphere, where unsaturated soil existing beneath the topsoil is periodically exposed to the precipitation (rainfall and/or snow) and evapotranspiration events, quantification and defining of the boundary conditions becomes crucial when dealing with near-ground surface problems involving unsaturated soils, such as rainfall-induced landslides (Fredlund et al. 2012). “Net moisture flux”

or actual infiltration, potential evaporation (PE), actual evaporation (AE), evapotranspiration, ponding water, soil cover, runoff, rainfall intensity and pattern, etc., are some of the quantities that, depending on the nature of the problem, have to be defined and calculated when performing advanced numerical analysis of a “flux-driven” problems. Long-term and short-term climate conditions and atmospheric events, along with the hydro-mechanical properties of the unsaturated soils included in the analysis, determine the conditions existing in the slope cross-section. The above determine the flow rates through the unsaturated zone when the slope is exposed to a rainfall event. The latter is typically applied across the ground surface in the form of Neumann-type boundary conditions. Although the assessment of the water balance and calculation of the actual evapotranspiration, which should account for reduced evaporation comparing to the fully saturated soil due to matric suction, go beyond the calculus and needs of this study, some basic climate conditions existing in the investigation area are presented in the following part. Historical rainfall characteristics and obtained in-situ rainfall measurements that were used in the numerical simulations are presented and discussed in greater detail.

Great time and spatial variations of air temperature in Croatia are mostly affected by the sea and land distribution. For example, the mean annual temperature in Croatia ranges from 3°C in the highest mountain areas, to 17°C in coastal areas (Zaninović et al. 2008). In the northern Adriatic area, where the investigation site is located, the mean annual air temperature ranges around 14°C and 15°C (Zaninović et al. 2008). The lowest average daily air temperature in the period from 1948 to 2017 increased from around 5°C in January and February to around 25°C in the mid of July and August ([http://meteo.hr/klima.php?section=klima\\_pracenje&param=srednja\\_temperatura&Grad=ri\\_sred&Godina=2018](http://meteo.hr/klima.php?section=klima_pracenje&param=srednja_temperatura&Grad=ri_sred&Godina=2018)), with the greatest differences typically occurring in March (Zaninović et al. 2008). Although during the winter period negative temperatures are not unusual, according to the probabilities of occurrence, from November to February, the most frequent mean daily air temperatures on the northern Adriatic range from 5°C to 10°C (Zaninović et al. 2008). The mean annual temperature for Croatia is shown in Figure 14, while a comparison of the average air temperature for Rijeka in the period from 1948 to 2017 is shown in Figure 15.

The mean annual amount of precipitation in Croatia ranges from 300 mm on some of the most distant islands, up to slightly over 3500 mm in mountainous areas (Zaninović et al. 2008). According to the Thorntwaite climate classification system, a humid climate prevails in the wider investigation area of the Northern Adriatic (Zaninović et al. 2008). The City of Rijeka with its surrounding is well known to have extremely high precipitation amounts during the wet part of the season. Beside the cyclogenetic effect, the mountainous hinterland and its orographic

effect greatly intensify precipitation in this area (Zaninović et al. 2008). According to the Zaninović et al. (2008), the investigation area falls into the maritime type of annual course of monthly precipitation amounts, where the month with the lowest precipitation amount occurs during the warm period of the year (April to September). For this type of annual course, the main maximum rainfall amounts occur in November, while the main minimum rainfall amounts typically occur in July. Although there are some changes on the seasonal scale, the mean annual precipitation amount hardly changed in the period from 1971-2000 (Zaninović et al. 2008). The rainiest period along the Adriatic coast is from November to May, whereby the Kvarner Littoral gets a slightly higher amount of rainfall during summer than the rest of the shore (Zaninović et al. 2008).

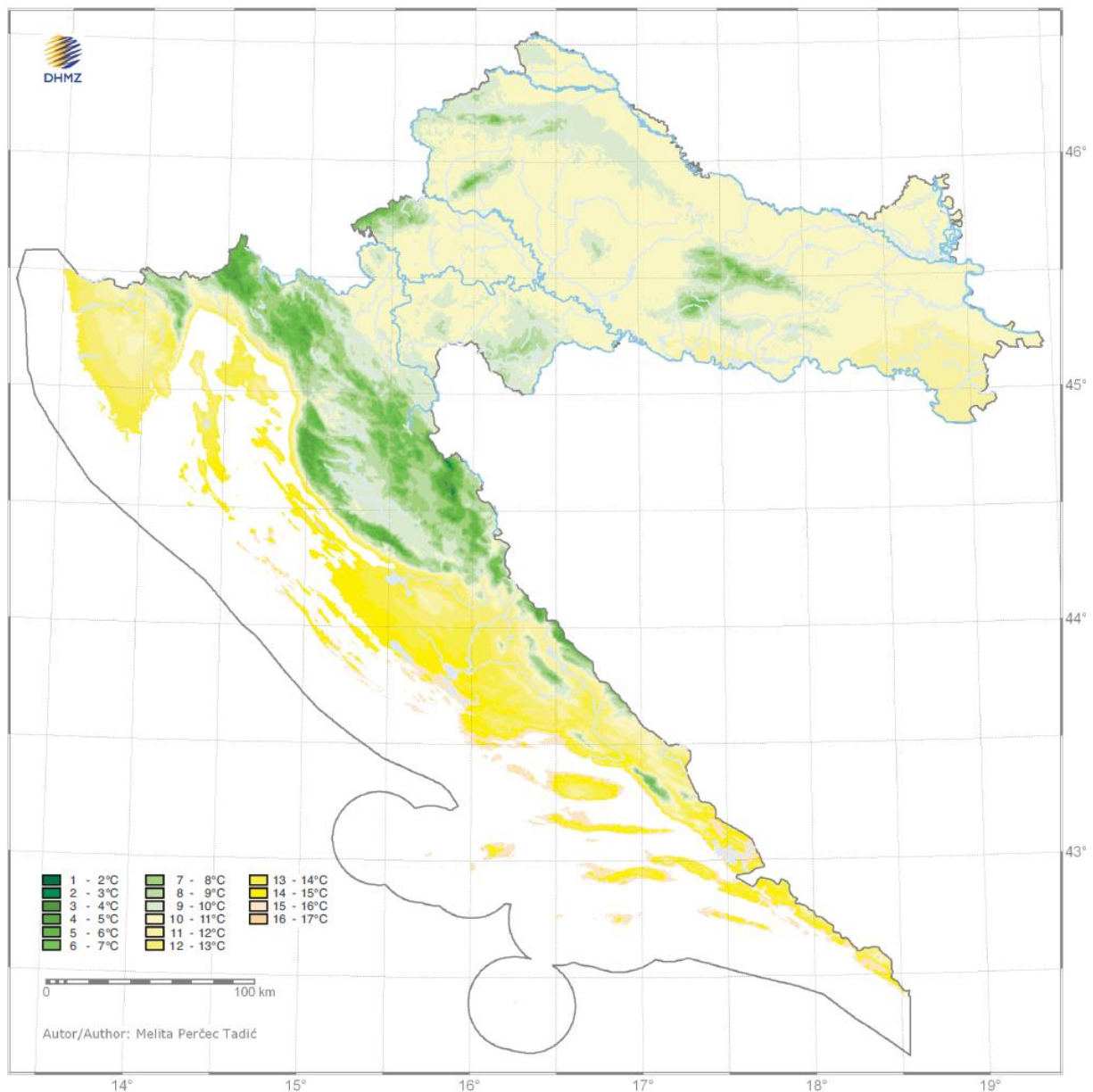


**Figure 14:** The mean annual air temperature for Croatia (Zaninović et al. 2008).

Unlike for the inland, where the days with the highest amounts of precipitation occur more often during summer and are the result of short-term heavy precipitation, for the mountainous areas, and on the Adriatic coast they occur more frequently during the cold part of the year as a result of long-term precipitation (Zaninović et al. 2008). Zaninović et al. (2008) state that from 1971-2000 a change in seasonal precipitation occurred in a way that the number of days with precipitation decreased for the winter, spring and summer, while it increased in autumn. They highlight that these changes are smaller and more pronounced for rainy days with smaller intensities, which have contributed to the changes in seasonal and annual precipitation amounts. Rainfall is the most common form of precipitation in Croatia, while snowfall is very rare in the investigation area, comprising only from 3% to 5% of days with precipitation along the Adriatic coast (Zaninović et al. 2008). Figure 16 shows the mean annual precipitation amounts for Croatia.

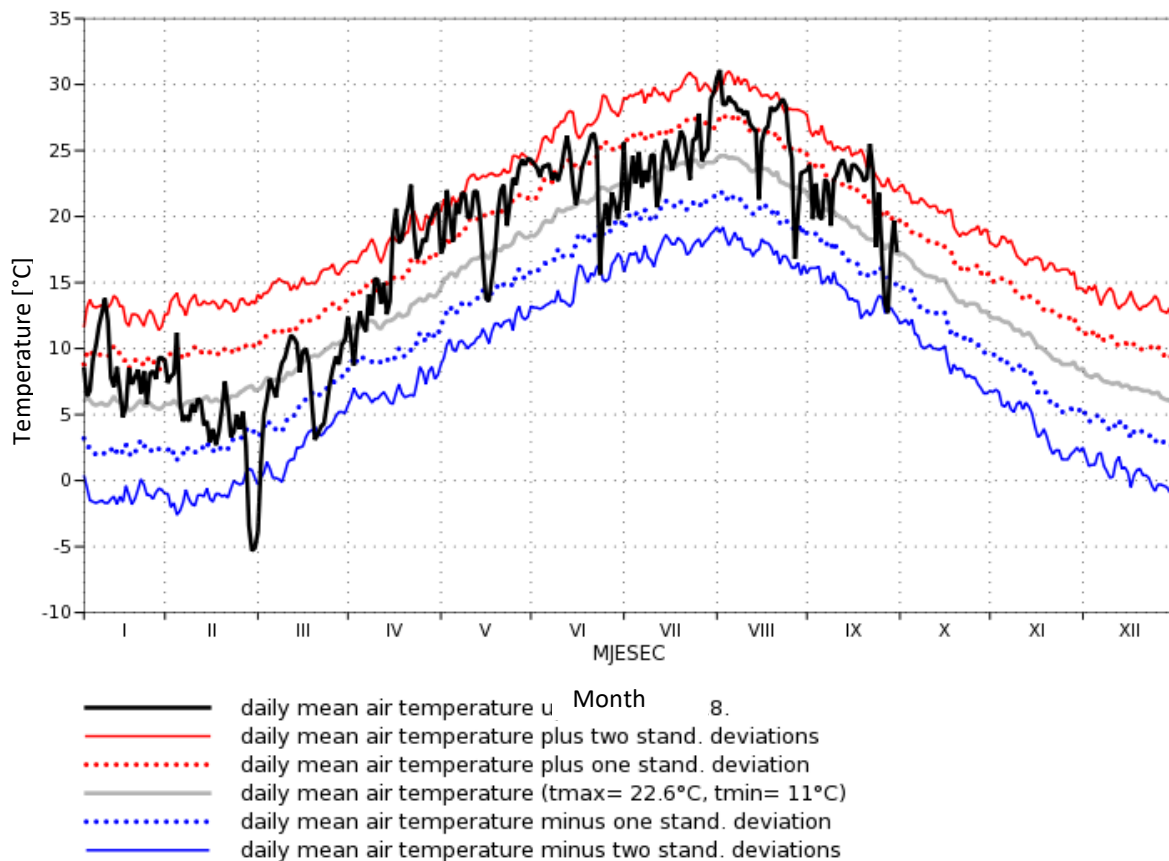
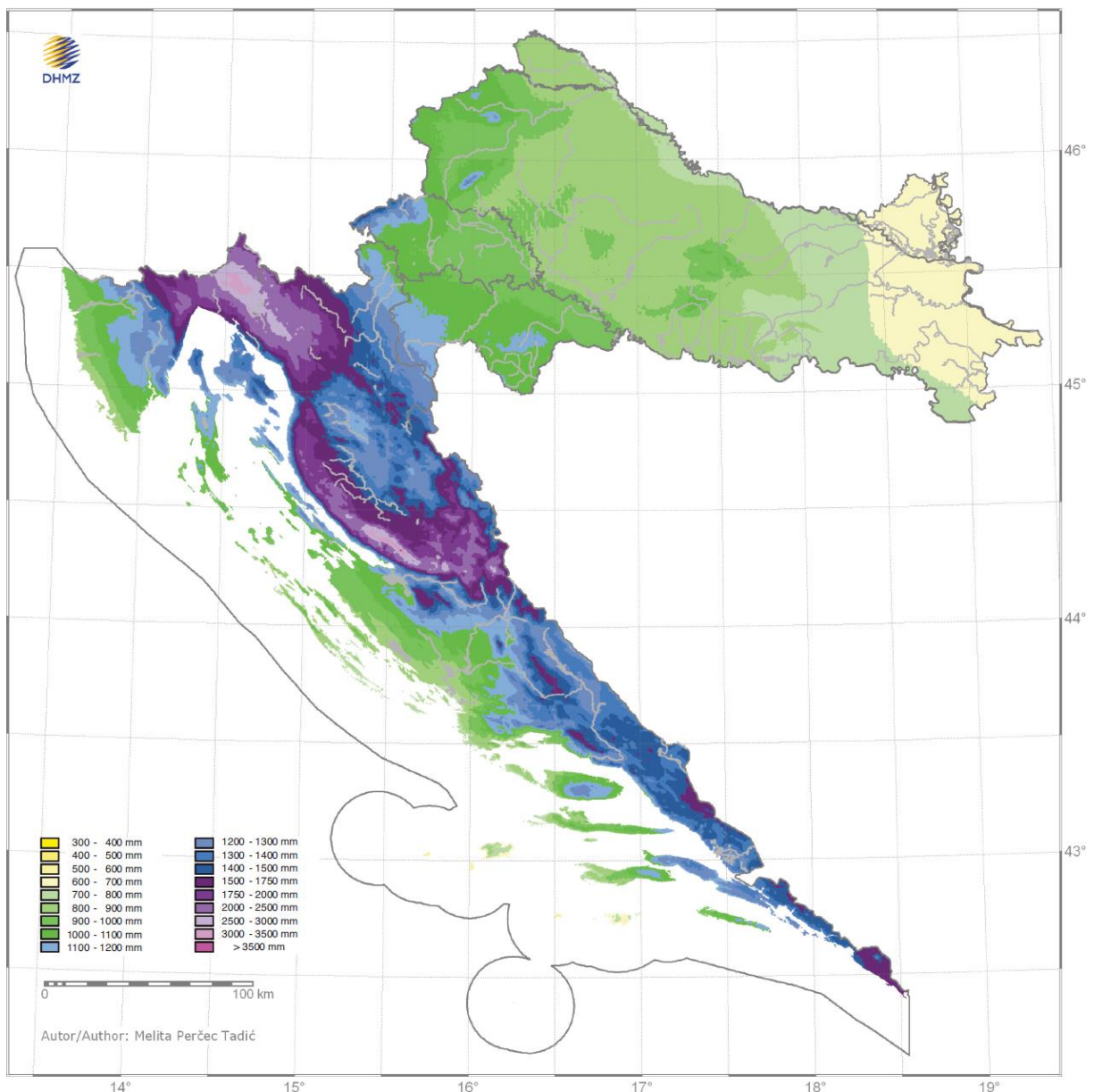


**Figure 15:** Comparison of the average air temperature in Rijeka for the period from 1948 to 2017 ([http://meteo.hr/klima\\_e.php?section=klima\\_pracenje&param=srednja\\_temperatura&Grad=ri\\_en\\_sred&Godina=2018](http://meteo.hr/klima_e.php?section=klima_pracenje&param=srednja_temperatura&Grad=ri_en_sred&Godina=2018)).

Daily rainfall amounts for the period from 1958 to 2015 were obtained on request from the Meteorological and Hydrological Service of Croatia (DHMZ) and statistically analyzed. The measurements were collected at the meteorological station Kozala in Rijeka, located



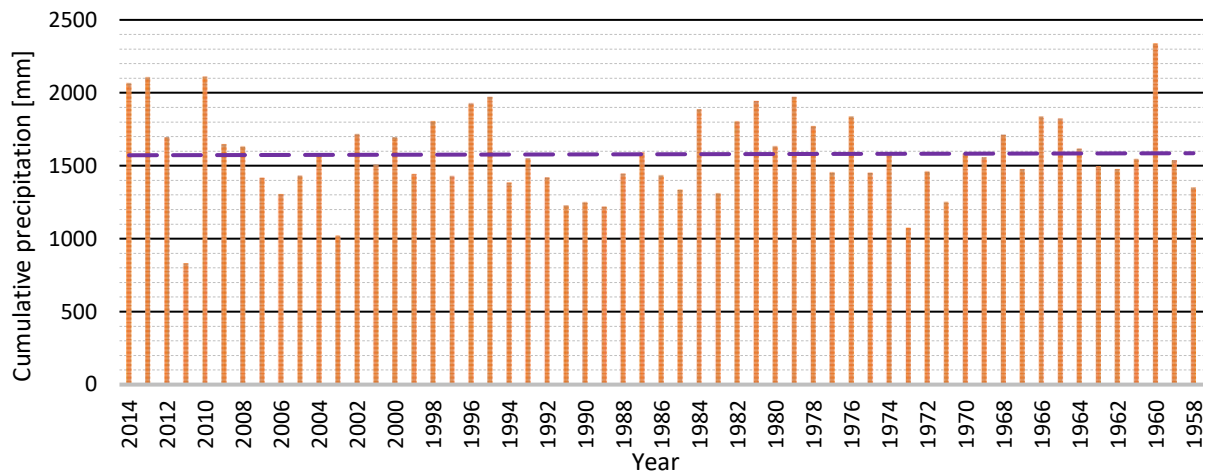
around 4 km south from the Valići Landslide. According to the data obtained, the average annual precipitation amount in the analyzed period was 1,567 mm with the maximum of 2,339 mm in 1960 and the minimum amount of 832 mm recorded in 2011. Average, maximum and minimum monthly and annual precipitation values for the analyzed period are summarized in Table 4. For the same period, Figure 17 shows cumulative annual precipitation amounts with linear trend-line indicating no changes over the analyzed period. Interestingly, the year 2010 had the same or even higher cumulative amount of precipitation than the year 2013, or 2014, in which the Valići Landslide was triggered. In the period from 1994 to 2015, there were several years with the cumulative precipitation much higher than the average value for the analyzed period as well.



**Figure 16:** The mean annual precipitation for Croatia (Zaninović et al. 2008).

**Table 4:** Average, maximum and minimum monthly and annual precipitation amounts analyzed for the period 1958-2015, according to DHMZ data for the meteorological station Kozala (Rijeka).

Month	I	II	III	IV	V	VI	VII	VIII	IX	X	XI	XII	Annual
Avg	134	119	118	112	105	106	75	103	178	180	187	162	1579
Max	448	347	388	248	276	230	201	351	481	527	483	456	2339
Min	1	3	0	1	2	19	2	1	11	0	13	28	832

**Figure 17:** Cumulative annual precipitation analyzed for the period from 1957 to 2015 for the meteorological station of Kozala, Rijeka (data obtained on request from DHMZ).

A change of precipitation trend on an annual basis is visible if the cumulative precipitation is summarized for two distinct parts of each year: the part of year with a small amount of precipitation (i.e., start of March till the end of August) and the part of the year with higher amounts of precipitation (start of September till the end of February). Despite the regular fluctuation of derived data, results summarized in Figure 18 a) and b) reveal that the cumulative rainfall amount continuously decreases in the period from March to September, while the amount of precipitation steadily increases from September to March. Amounts seem to be inversely proportional, which means that if the trend continues, the wet period of the year will receive increasingly higher amounts of rainfall, while the amount of the rainfall will be reduced for the same quantity in the dry period of the year. Again, cumulative annual precipitation amounts should remain unaltered.

Another interesting observation is that in the year before the landslide occurrence, cumulative precipitation during the autumn and winter 2012/13, even in the autumn and winter 2000/2001, was higher than in the year 2013/2014. Figure 19 summarizes cumulative precipitation measured in the period from September till March for the more recent years with extreme quantities, marked with red color in Figure 18 a). Although the cumulative precipitation for the year 2012/13 was the highest (1645 mm), and the year 2000/01 had the same amount of precipitation (1469 mm) as the year 2013/14 (1469 mm), the rainfall intensities



of the year 2013/14 were much lower, which, as the results of numerical analysis will show, affects the slope stability in an unfavorable manner. The total precipitation of the year 2013/14 was distributed over a larger number of days (89), respective to the year 2012/13 (79), and especially of the year 2000/01 (65), which was characterized by shorter precipitations of higher intensity. According to this analogy and given the low permeability of material covering slopes of the Rječina River Valley, precipitation from the years 1996/97 and 1993/94 could have a more critical pattern for the stability of slopes in the investigated area (Figure 19 b), although the cumulative precipitation was not as extreme as for the years 2012/13 and 2000/01 (Figure 19 a). Indeed, the precipitation from 1996/97 is responsible for the triggering of the Grohovo Landslide at the end of December 1996. Finally, the daily precipitation was normalized relative to the saturated coefficient of permeability of the investigated soil, which was found to be around  $k_s = 3.6\text{e-}08$  m/s (Table 11). The latter indicates the approximate rate at which rainfall can infiltrate into the soil. The precipitation from the year 2013/14 had the most days with the daily quantity of precipitation above the  $k_s$  value (58). The second one is, again, the rainfall from the 1996/97 period with 55 days of rainfall with the average intensity above the  $k_s$  value. Results obtained from numerical simulations performed for different values of constant flux boundary conditions (details in Chapter 7), showed that the rainfall intensities of  $2k_s$  reduce the slope stability at the highest rate. Rainfall intensities higher than  $2k_s$  were found to have a negligible effect on the time required to reach slope failure (Figure 120). The rate at which FoS is reduced remains unaffected for flux boundary conditions higher than  $4k_s$ . The above-mentioned quantity of  $2k_s$  corresponds to 0.33 mm of rainfall per hour, or 7.95 mm/day, and could be considered a critical rainfall intensity in this study. Again, rainfall characteristics for the year 2013/14 summarized in Figure 19 c) and d) support the simulation results. To conclude, it seems that the rainfall pattern of the year 2013/14 was the most unfavorable with respect to the triggering of the Valići Landslide due to several reasons:

- i) among the considered years with extreme precipitation quantities, the precipitation from 2013/14 was distributed along the highest number of days (58 days with rainfall,  $q > 0$ ), ensuring the required duration to trigger the landslide;
- ii) intensities were high enough to cause the reduction of slope stability state through time at the highest rate (of 58 days, 52 days with rainfall  $q > 2k_s$ );
- iii) intensities were not too high to cause excessive runoff. The year 2013/14 had the least days with the daily amount of precipitation above  $4k_s$  (only 25 days with rainfall  $q > 4k_s$ ), as summarized in Figure 19 d).

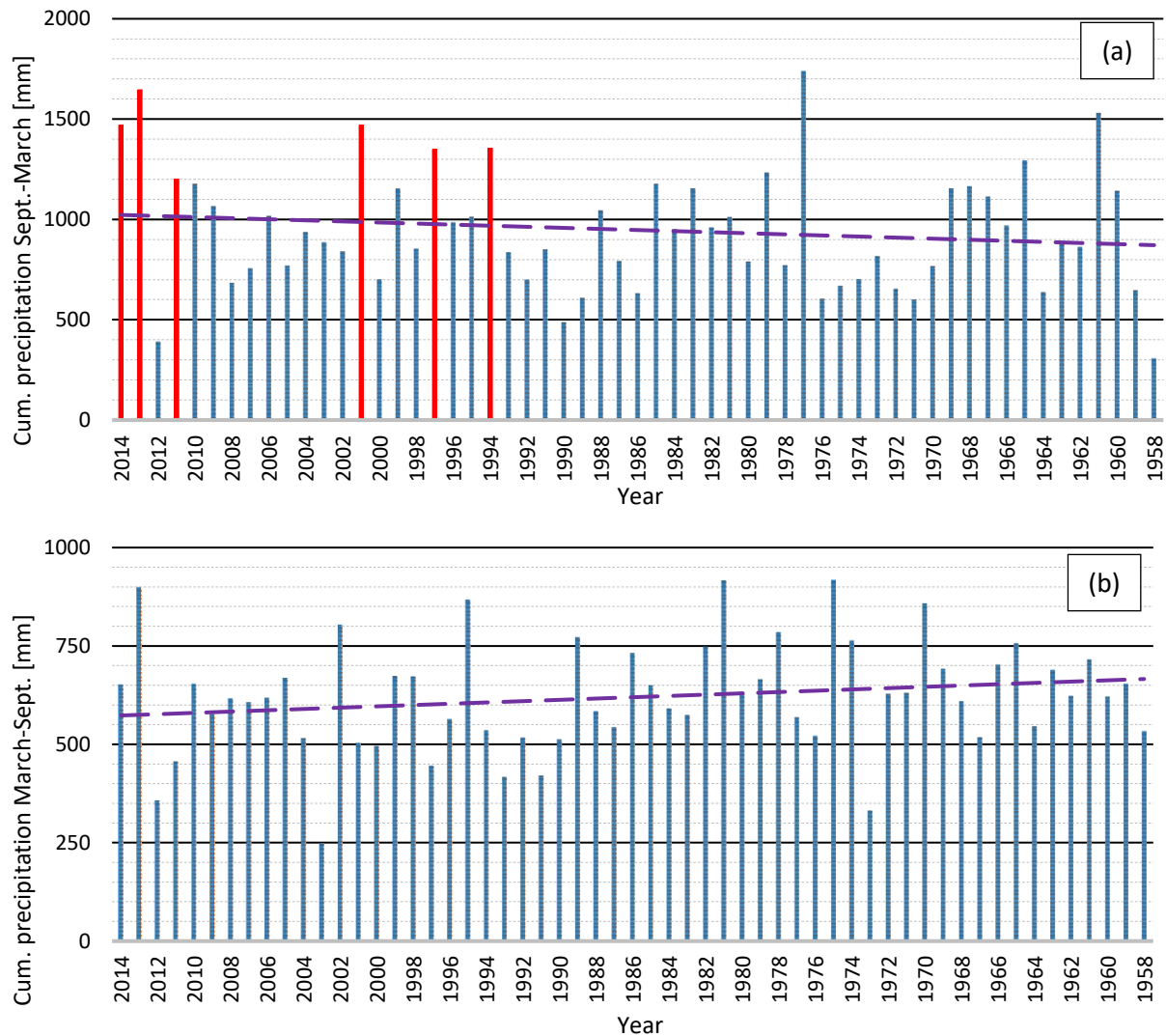


**Figure 18:** Cumulative precipitation summarized from a) the start of September till the end of February (wet part of the season); and b) from the start of March till the end of August for the period analyzed (1957 to 2015).

Precipitation measurements used to define the flux boundary condition for analysis performed in this study were obtained with the Tipping Bucket Rain Gauge and Transmitter RS-2 with Precipitation Data Logger NetLG-201E (Osasi Technos Inc.) and Vantage Pro2<sup>TM</sup> Weather Station (Davis Instruments). The instruments were installed on the nearby Grohovo Landslide in the frame of the Croatian-Japanese joint research project “Risk Identification and Land-Use Planning for Disaster Mitigation of Landslides and Floods in Croatia”. The aerial distance from the Valići Landslide is around 900 m for both devices. Precipitation measurements were performed every 10’ with measuring resolution (minimum quantity of rainfall generating tip of the bucket) of 0.5 and 0.2 mm, respectively. Precipitation measurements obtained with the above-mentioned devices matched closely and are summarized in Figure 20 for the period considered to be relevant for the triggering of the Valići Landslide.

These measurements were used to define a boundary condition in the performed analysis of transient rainfall infiltration in different forms (10', hourly and daily records).

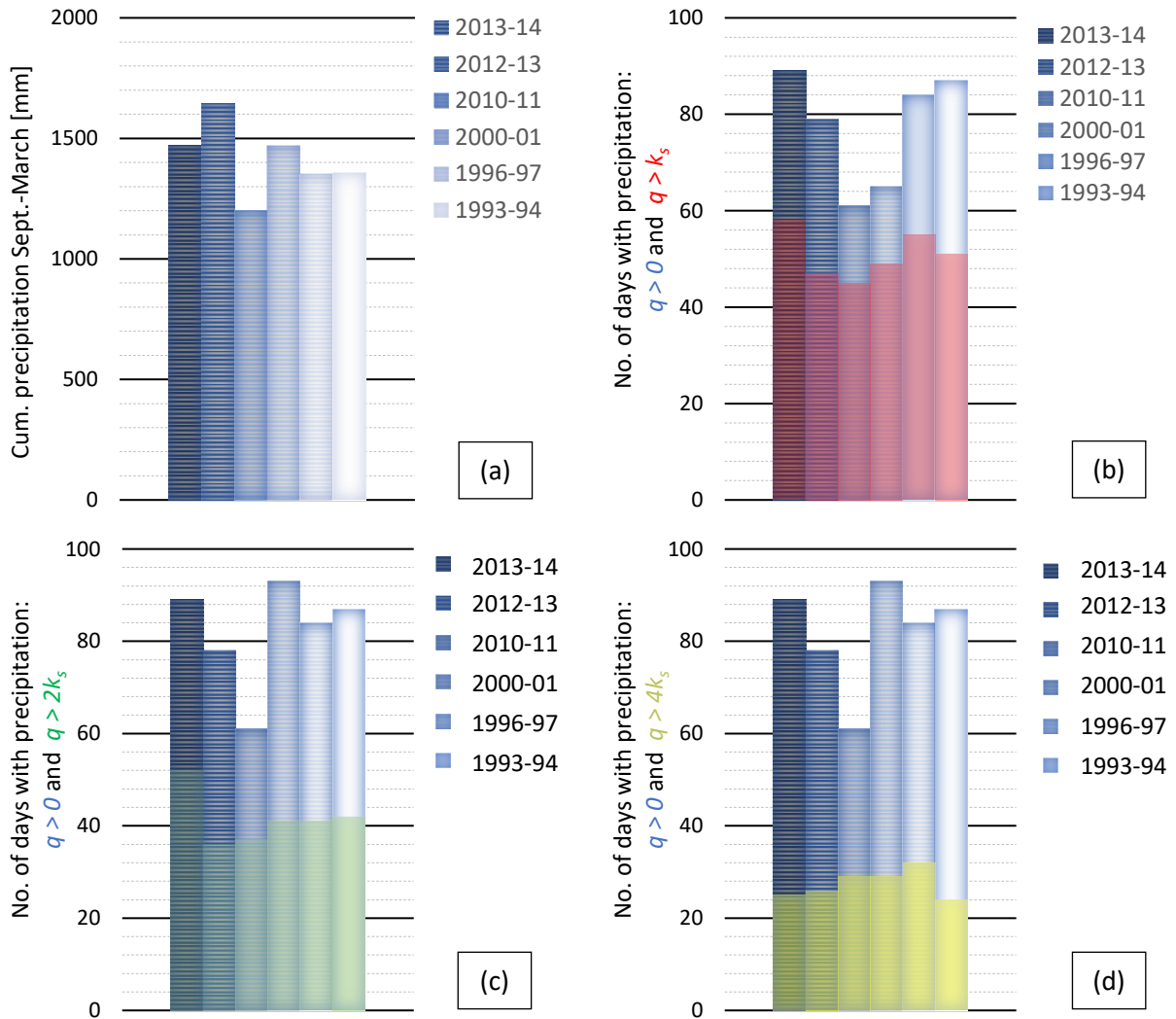


**Figure 19:** Precipitation characteristic of the latest years with extreme quantities during the wet period of the season (September to March): a) cumulative precipitation; b) a number of days with precipitation and number of days with precipitation intensity higher than  $k_s$ ; c)  $2k_s$ ; and d)  $4k_s$  of the soil.

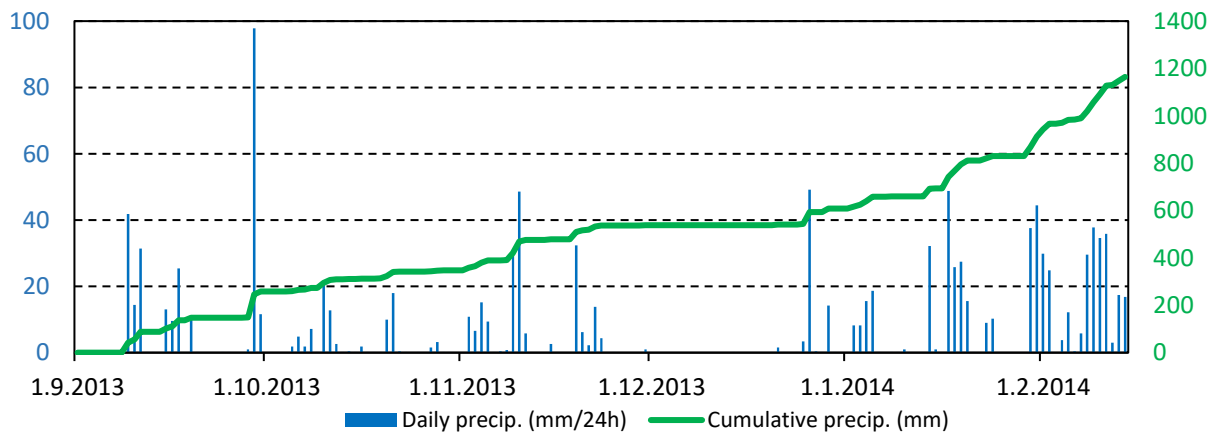


**Figure 20:** Precipitation measurements in period preceding the landslide event: daily rainfall for the period 1 September 2013 to 14 February 2014.

Figure 21 and Figure 22 show the average air temperature and precipitation amounts for summer, autumn and winter of 2013/2014, compared with the multi-annual average in a period from 1961 to 1990. According to the data available at the DHMZ website, thermal conditions at the investigation site were extremely warm during summer 2013, warm during the autumn (September to November) 2013, and extremely warm during the winter 2013/2014 (December to February). According to the precipitation amounts, the same periods could be classified as dry for the summer, and very wet for both the autumn and winter.

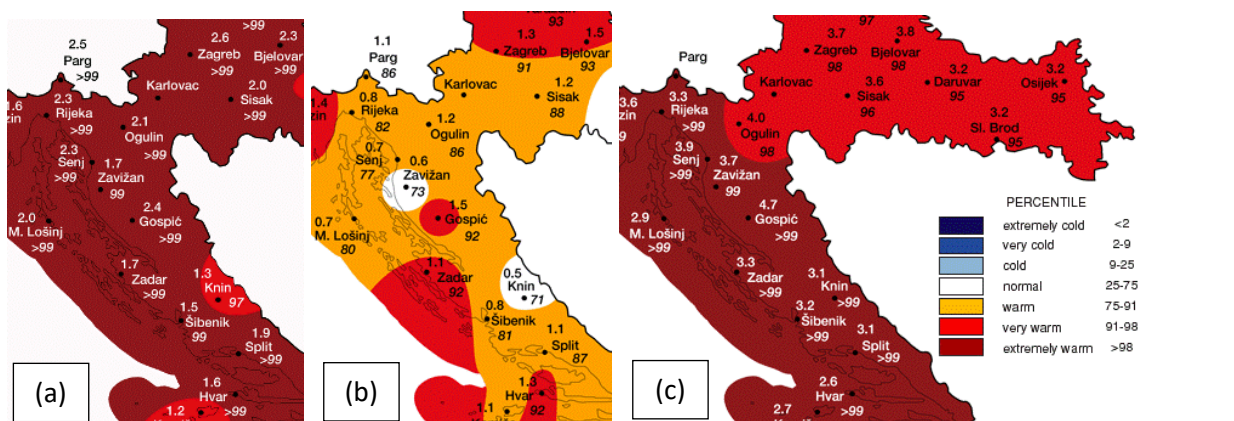


**Figure 21:** Average air temperatures in Croatia for a) summer 2013; b) autumn 2013; and c) winter 2013/2014 compared with the corresponding multi-annual average in the period from 1961 to 1990, according to the DHMZ ([http://meteo.hr/klima\\_e.php?section=klima\\_pracenje&param=ocjena](http://meteo.hr/klima_e.php?section=klima_pracenje&param=ocjena)).

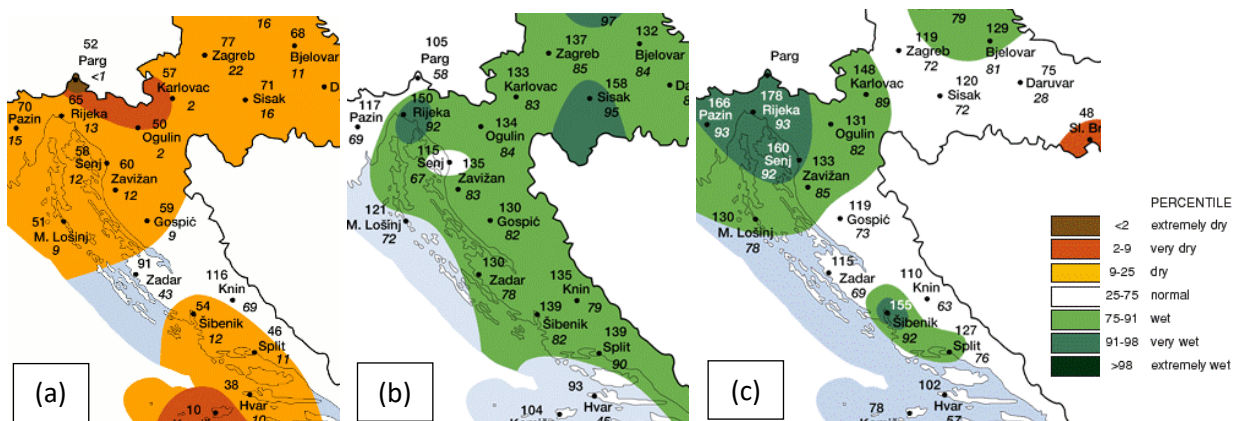


**Figure 22:** Average precipitation amounts in Croatia for a) summer 2013; b) autumn 2013; and c) winter 2013/2014 compared with the corresponding multi-annual average in the period from 1961 to 1990, according to the DHMZ ([http://meteo.hr/klima\\_e.php?section=klima\\_pracenje&param=ocjena](http://meteo.hr/klima_e.php?section=klima_pracenje&param=ocjena)).



### **3. THE BASIC CONCEPTS OF THE UNSATURATED SOIL MECHANICS**

The basic concepts of unsaturated soil mechanics, such as surface tension, capillary phenomena and Kelvin's capillary model, four phase soil model, different variables of unsaturated soil and basic relations for their quantification are presented in this chapter. Soil suction components are defined, and their importance for the rainfall-induced landslides is discussed.

### 3.1. Phase properties of unsaturated soil

Saturated soil below the groundwater table consists of two phases: solid particles and the water phase filling all voids between them. In unsaturated soil, the air and water phases can occupy voids in different portions. Hydro-mechanical properties of unsaturated soil greatly depend on water content (e.g., the degree of saturation). The interface between air and water, called the contractile skin, has some unique physical features and is distinguished as a fourth phase when considering the stress–strain relationship in unsaturated soil. An element of unsaturated soil consisting of solid particles, water, air, and contractile skin is sketched in Figure 23, along with the phase diagram defining volume and mass relationship of the multiphase soil system.

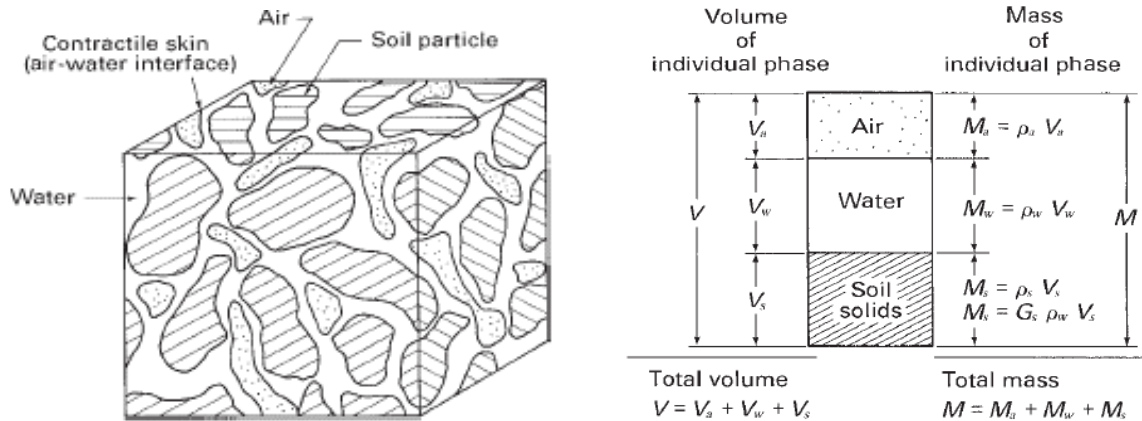


**Figure 23:** An element of unsaturated soil consisting of solid particles, water, air, and contractile skin (left), and phase diagram (right) describing volume and mass relations for unsaturated soil (Fredlund et al. 2012).

With the thickness of only a few molecular layers, the contractile skin can be considered as part of the water phase when establishing volume-mass relations of an unsaturated soil (Fredlund et al. 2012). In this case, the three-phase system can be used without introducing significant error. From the stress-strain point, the contractile skin has to be considered as a separate phase since it affects the soil structure and stress state of unsaturated soil through its essential property called surface tension. It is the contractile skin that provides equilibrium conditions between two fluid phases in unsaturated soil and, thus, an independent flow of air and water (Fredlund et al. 2012).

### 3.1.1. Quantifying each phase

The basic quantities used for the determination of volume and mass properties of the multiphase system shown in Figure 23 b) are defined here. A specific volume or density has to be known for each phase in order to solve the phase diagram.

The density of solid particles,  $\rho_s$ , is defined by the equation

$$\rho_s = \frac{M_s}{V_s} \quad (1)$$

where  $M_s$  is mass of solid particles or dry soil, and  $V_s$  volume of solid particles.

The ratio of the density of solid particles to the density of water presents the specific gravity of the solid soil particles,  $G_s$ , and is defined by the equation

$$G_s = \frac{\rho_s}{\rho_w} \quad (2)$$

where  $\rho_w$  is the density of water, which is exactly  $1,000 \text{ kg/m}^3$  at usual atmospheric pressure conditions (101.3 kPa) and a temperature of  $4^\circ\text{C}$ .

The density of air,  $\rho_a$ , strongly varying with pressure and temperature changes, can be derived from the ideal gas law and Boyle's law as follows:

$$\rho_a = \frac{M_a}{V_a} = \frac{\omega_a}{RT_K} \overline{u_a} \quad (3)$$

where  $\omega_a$  is the molecular mass of air,  $R$  is the universal (molar) gas constant,  $T_K$  is the absolute temperature in (K) and  $\overline{u_a}$  is the absolute air pressure.

For the geotechnical application, it is important to note that the amount of water vapor in the air can vary the most of all air components (Harrison 1965; Fredlund et al. 2012). Air not containing water vapor is called dry air. Relative humidity,  $RH$ , is a term used to quantify the concentration of water vapor in the air

$$RH = \frac{u_v}{u_{v0}} (100) \quad (4)$$

where  $RH$  is relative humidity (%), while  $u_v$  and  $u_{v0}$  are the partial pressures (kPa) of water vapor in the air and the saturation pressure of water vapor at the same temperature, respectively.

A nonlinear relationship between saturated vapor pressure and the temperature is described by several empirical equations (e.g., Lowe 1977). One part of experimental equipment used to measure suction in soil is based on the calculation of  $RH$  of an air-water



mixture by precisely measuring the dew-point temperature  $t_d$  and the actual air temperature  $T$ . For example, the Bosen (1958) equation can be used

$$RH = 100 \left[ \frac{t_d - 0.1T + 112}{112 + 0.9T} \right]^8 \quad (5)$$

if the dry bulb temperature  $T$  (°C) and dew-point temperature  $t_d$  (°C) are known.

Several important relations are used to express different properties of soil in geotechnical engineering application. Porosity  $n$ , void ratio  $e$ , and degree of saturation  $S$  are basic quantities that are defined in the same way as for the saturated soil. However, the volumetric portion of each phase in the unsaturated soil can be defined respective to the total volume. Water porosity,  $n_w$  (%), and air porosity,  $n_a$  (%), are defined by the following relations

$$n_w = \frac{V_w}{V} (100) \quad (6)$$

and

$$n_a = \frac{V_a}{V} (100) \quad (7)$$

where  $V_w$  and  $V_a$  are the volumes of water and air inside the soil pores, while  $V$  represents the total volume of soil.

The quantity used to describe the volume of water relative to the total volume of soil is called the volumetric water content,  $\theta$  (cm<sup>3</sup>/cm<sup>3</sup>), and is defined as

$$\theta = \frac{V_w}{V} = Sn = \frac{SwG_s}{S + wG_s} \quad (8)$$

where  $w$  (%) is the gravimetric water content, which can be commonly measured in the geotechnical laboratory.

Volumetric water content is among the essential quantities used in unsaturated soil mechanics since it is used to derive the equation describing the water flow through unsaturated soil, or the relationship between water content and (matric) suction in SWRC- $\theta$  form. Change in (matric) suction does not cause only changes in the volume of water, but, depending on the soil texture, stress history, etc., can cause smaller or greater total volume changes of soil. In the case of deformable soil, it is essential to measure the instantaneous total volume of soil  $V$  when results are used to describe the relationship between volumetric water content and (matric) suction.

The effective degree of saturation (Corey 1954) accounts only for the free part of the water in soil pores between the residual and saturated water content and is defined as

$$S_e = \frac{S - S_r}{1 - S_r} \quad (9)$$

where  $S_r$  (%) is the residual degree of saturation and can be graphically determined from the SWRC as suggested by Brooks and Corey (1964).

Similar to the effective degree of saturation, van Genuchten (1980) used the normalized volumetric water content  $\theta$ , between saturated and residual water content conditions, expressed by the following relation

$$\theta = \frac{\theta - \theta_r}{\theta_s - \theta_r} \quad (10)$$

where  $\theta_r$  and  $\theta_s$  ( $\text{m}^3/\text{m}^3$ ) are residual and saturated volumetric water contents, respectively.

Both the effective degree of saturation and normalized volumetric water content are often used when defining various USPFs and will be defined in more detail later. They are part of the equations that describe stress state, retention and conductivity properties or shear strength of soil in unsaturated conditions.

### **3.2. Air-water interaction and implications in geotechnical engineering**

The air compressibility and solubility of air in water have a direct impact on many experimental techniques used to control or measure matric suction of soil. The equation (3) states that, under constant temperature conditions, the density of air depends only on the absolute air pressure value. Air can exist in the form of free air or as air dissolved in water. In the case of soil with continuous air phase, the pressure of air in voids is generally equal to the ambient air pressure surrounding the soil. If the pressure of free air is changed, the pressure differential between free and air dissolved in water would cause diffusion of air through the water until equilibrium conditions are reached. Boyle's law can be used to relate air volume and pressure changes in the closed system. Henry's law can be used to relate the quantity of air dissolved in water due to a change in air pressure. Henry's law states that, at the constant temperature, the mass of gas dissolved in a liquid is directly proportional to the absolute pressure of the gas above the

solution (Sisler et al. 1953). Fick's law of diffusion can be used to describe the rate at which air passes through water

$$q_a = \frac{\partial M_a}{A \partial t} = -D \nabla C \quad (11)$$

where  $q_a$  is the air flux ( $\text{mol/s} \cdot \text{m}^2$ ),  $M_a$  is the mass of air (mol),  $A$  is the area of cross-section through which the flow process takes place ( $\text{m}^2$ ),  $C$  is the air concentration ( $\text{mol/m}^3$ ), and  $D$  is the diffusion coefficient ( $\text{m}^2/\text{s}$ ). The diffusion coefficient  $D$  is an intrinsic material property of a specific gas in a particular liquid under specific thermodynamic conditions (Lu and Likos 2004).

Instead of measuring the gradient of the air concentration, an alternative way to assess the air concentration gradient is to estimate the air pressure gradient. For a one-dimensional air diffusion problem (commonly encountered in laboratory application), using the ideal gas equation (3) and Henry's law, the equation (11) can be re-written in the following form (Lu and Likos 2004)

$$q_a = \frac{\bar{u}_a \omega_a}{RT_K} \frac{\partial V_a}{A \partial t} = -D \frac{h_{air} \omega_a}{RT_K} \frac{\partial \bar{u}_a}{A \partial z} = \frac{u_a \omega_a}{RT_K} v_a \quad (12)$$

where  $h_{air}$  is the volumetric coefficient of solubility. The discharge velocity of the dissolved air  $v_a$  (m/s) can be calculated by the following expression

$$v_a = -D \frac{h_{air}}{\bar{u}_a} \frac{\partial \bar{u}_a}{\partial z} = -D \frac{h_{air} \rho_a g}{\bar{u}_a} \frac{\partial h_a}{\partial z} \quad (13)$$

where  $h_a$  is the head of dissolved air (m) (Lu and Likos 2004).

Equations (12) or (13) can be useful for practical application with the axis translation technique. The volume of water expelled from the specimen or imbibed by the specimen during the test has to be corrected for the amount of air dissolved in water inside the measuring system itself. A flux of dissolved air can be calculated if the value of air pressure dissolved in water in the compartment below the high air-entry value porous disc (HAEPD), and air pressure inside the pressure chamber with the soil specimen are known. The manufacturer usually provides the information required to calculate the total volume of air that diffused in water during the time of the test: porosity, thickness and the area of the HAEPD. Another way of accounting for the volume of air diffused in water during the test when using the axis translation technique is using some of the flushing techniques to physically remove the air accumulated below the HAEPD in water compartment. Some of these techniques and devices are described later, where the employed laboratory devices are presented.

### 3.3. Surface tension and capillary phenomena

Surface tension is an important property of the contractile skin, which enables it to exert a tensile pull. Surface tension,  $T_s$  (N/m) is measured as the tensile force per unit length of contractile skin and acts tangentially to the contractile skin surface (Fredlund et al. 2012). It slightly varies with temperature (Table 5) and is equal to 72.75 mN/m at 20°C (Kaye and Laby 1973). Figure 24 shows balanced forces acting on molecules in the interior of water and unbalanced forces acting on molecules in the contractile skin. The latter causes the phenomenon of surface tension – the resultant force which maintains a mechanical equilibrium of the system (Lu and Likos 2004).

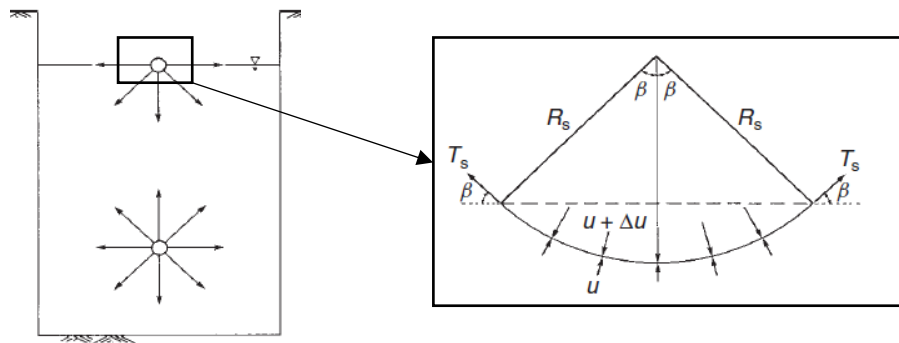


**Figure 24:** Surface tension phenomenon at the air-water interface: intermolecular forces acting in the contractile skin and interior of water, and tension forces associated with a curved two-dimensional surface (modified from Fredlund et al. 2012).

**Table 5:** Surface tension of contractile skin at various temperatures (Kaye and Lany 1973).

Temperature [°C]	Surface tension [mN/m]
0	75.7
10	74.2
20	72.75
30	71.2
40	69.6
60	66.2
80	62.6
100	58.8

The contractile skin acts as a thin elastic membrane with the radius of curvature  $R_s$ , subjected to the pressure differential  $\Delta u$  acting across its curved surface and a surface tension force  $T_s$  (Figure 24). Equilibrium of the vertical forces provides the relationship between the

pressure differential  $\Delta u$ , the radius of curvature of the membrane  $R_{s,s}$ , and the surface tension force  $T_s$

$$\Delta u = \frac{T_s}{R_s}. \quad (14)$$

The equation (14) can be extended for a case of the three-dimensional membrane with the same radii of curvature in two orthogonal principal planes equal to  $R_s$ , using the Laplace's equation as follows (Fredlund et al. 2012):

$$\Delta u = \frac{2T_s}{R_s}. \quad (15)$$

The vertical component of the surface tension holds the water column of height  $h_c$  inside the capillary tube with radius  $r$ , shown in Figure 25. If  $\alpha$  is the contact angle between the contractile skin and wall of a capillary tube, equilibrium of vertical forces provides the height of the water column inside the tube of radius  $r$  (Fredlund et al. 2012):

$$h_c = \frac{2T_s \cos \alpha}{r \rho_w g}. \quad (16)$$

A capillary phenomenon occurs when a contact angle between the liquid and solid surface  $\alpha$ , is less than  $90^\circ$ . In this case, the liquid is said to wet a surface since the drop of the

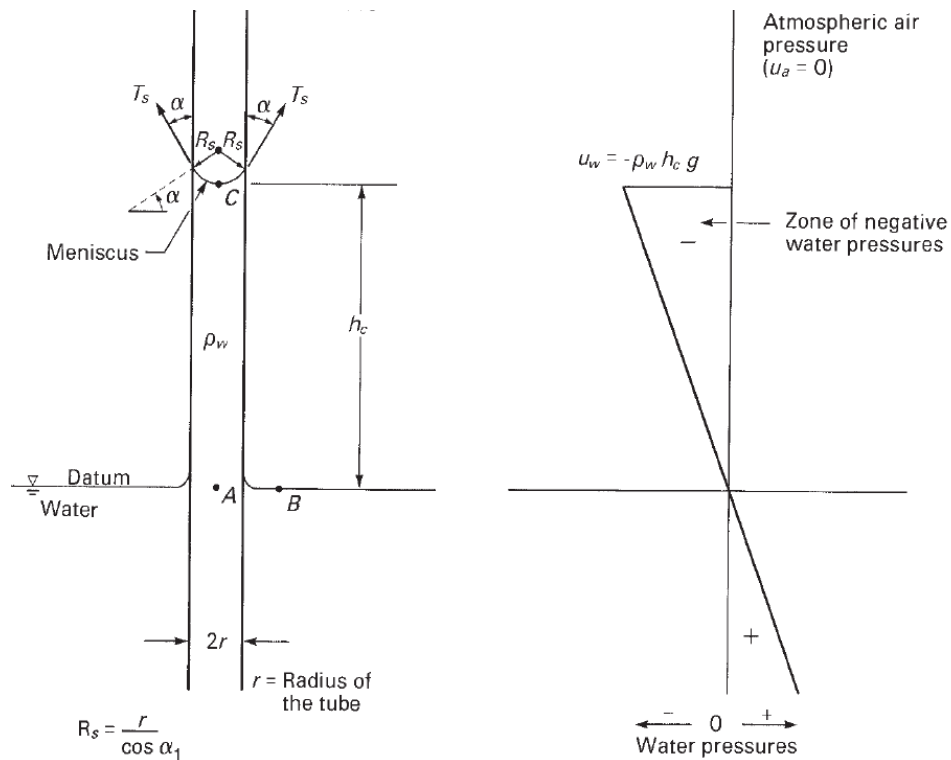


**Figure 25:** Physical model of capillarity (Fredlund et al. 2012).

liquid tends to spread over a solid surface (Marinho et al. 2008). The value of the contact angle depends on cohesive forces in the liquid and the adhesive forces between solid and liquid, and, like many other quantities in unsaturated soil mechanics, exhibits hysteretic behavior (Johnson and Dettre 1969). A critical review and brief explanation on surface tension and capillarity from the multidisciplinary point of view is provided by Sophocleous (2010).

All of the above analogies can be applied conceptually to soil. For example, in unsaturated soil with continuous air and water phases, contractile skin is subjected to the pressure differential  $\Delta u$ , which is equal to the difference between the pore-air pressure  $u_a$ , and pore-water pressure  $u_w$ . For the unsaturated soil, the pore-water pressure is generally lower than the pore-air pressure. In the case of soil in-situ, such as natural slope, pore-air pressure  $u_a$ , is equal to the atmospheric pressure,  $p_{atm}$ . For the sample installed in the laboratory device implementing the axis translation method, the pore-air pressure is equal to the value of the air pressure inside the testing chamber, which is artificially raised to some value  $p_a > p_{atm}$ . In both cases, the pressure differential  $u_a - u_w$  is called a matric suction in unsaturated soil mechanics, and the equation (17) is known as Kelvin's capillary model:

$$u_a - u_w = \Delta u = \frac{2T_s}{R_s}. \quad (17)$$

Matric suction is a component of the total soil suction responsible for holding the weight of a water column with height  $h_c$  in a capillary tube (Figure 25). The radius of a capillary tube is analogous to the pore size in the soil. At some depth below the soil surface, the phreatic line exists where atmospheric and pore-water pressure is equal. The pore-water pressure becomes negative relative to the atmospheric pressure above this level. According to the equation (17), water can be elevated at higher distances above the water table as the radius of capillary tubes (voids in the soil) decreases. In other words, more negative values of pore-water pressure can be expected in case of fine-grained soils with a small size of voids. Figure 26 shows observations of silica microspheres by the Environmental Scanning Electron Microscope with indicated water menisci at the air-water interface and measurable contact angle (Lourenço et al. 2008). However, the conceptually simple capillary model cannot correctly explain the mechanical behavior of unsaturated soil (Fredlund et al. 2012). Limitations arise from many complex properties of natural soil, such as non-uniform distribution of voids, hysteresis between the drying and wetting process in natural soil, varying contact angles between pore fluid and solid particles, adsorptive forces between clay particles, air entrapment and volume changes occurring in deformable soils, and many more.

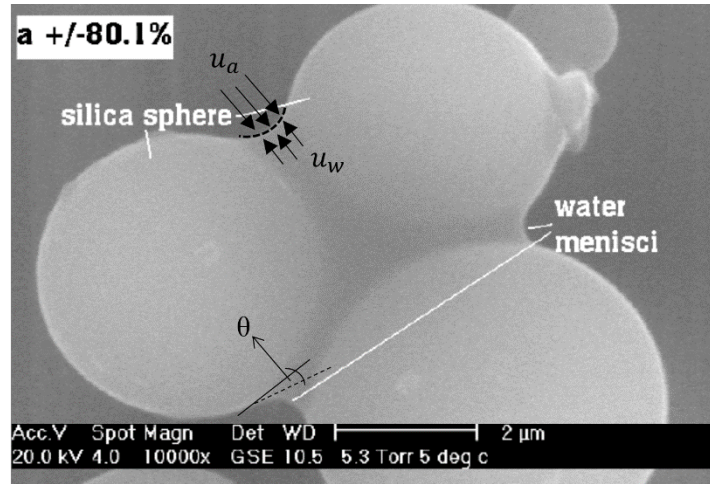


**Figure 26:** The Environmental Scanning Electron Microscope micrographs of silica spheres with indicated pressures along the air-water interface (water menisci) and measurable contact angle (modified from Lourenço et al. 2008).

### 3.4. Soil suction components

The free energy of the soil-water can be measured with respect to the partial vapor pressure adjacent to the soil-water (Richards 1965). The ratio between the partial pressure of pore-water vapor with saturation pressure of water vapor over a flat surface of the pure water at the same temperature is defined in equation (4) as the RH (%) (Fredlund et al. 2012). The thermodynamic relationship between soil suction and the partial pressure of the pore-water vapor, written using Kelvin's equation in terms of the total suction,  $\psi$  (kPa), and RH (%) can be written as follows

$$\psi = -\frac{RT_K}{v_{w0}\omega_v} \ln(RH) \quad (18)$$

where  $\omega_v$  is the molecular mass of water vapor (18.016 kg/kmol),  $v_{w0}$  is the specific volume of water (0.0094 m<sup>3</sup>/kg), and  $RH$ ,  $R$ , and  $T_K$  were defined before in (3) and (4). Various laboratory devices and techniques use the above equation to calculate total suction in a soil sample. The theoretical relationship between RH and total suction  $\psi$ , is shown in Figure 27 by plotting the equation (18) for a complete range of suction and RH at a constant temperature of 20° C (293.16 K). In the case of the rainfall-induced landslides and probably most of the problems encountered in engineering practice, suctions existing in the area with high values of RH are of particular interest.

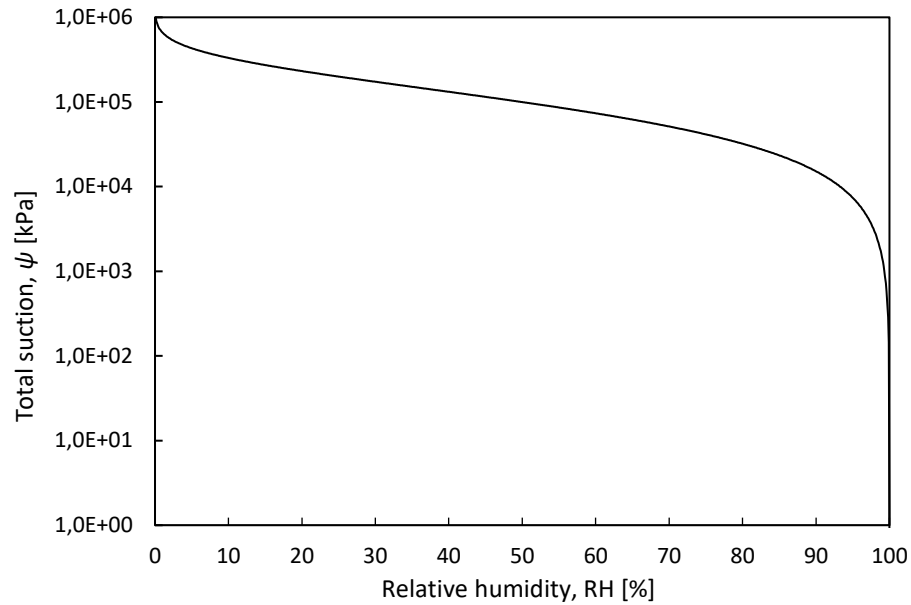


**Figure 27:** Theoretical relationship between relative humidity,  $RH$ , and total suction,  $\psi$ , according to Kelvin's equation for a constant temperature of  $20^\circ\text{C}$  (293.16 K).

Among numerous factors that have been suggested as contributing factors to the total soil suction,  $\psi$  (kPa), matric suction,  $u_a - u_w$ , and osmotic suction,  $\pi$ , appear to be the two primary components:

$$\psi = (u_a - u_w) + \pi. \quad (19)$$

According to Fredlund et al. (2012), the terms *total suction or free energy of soil-water*, *matric or capillary component of free energy*, and *osmotic (or solute) component of free energy* were defined by Aitchison (1964) as follows:

- matric suction is the equivalent suction derived from the measurement of the partial pressure of the water vapor in equilibrium with the soil-water relative to the partial pressure of the water vapor in equilibrium with a solution identical in composition to the soil-water;
- osmotic suction is the equivalent suction derived from the measurement of the partial pressure of the water vapor in equilibrium with a solution identical in composition to the soil-water relative to the partial pressure of water vapor in equilibrium with free pure water;
- total suction is the equivalent suction derived from the measurement of the partial pressure of the water vapor in equilibrium with the soil-water relative to the partial pressure of water vapor in equilibrium with free pure water.

The partial pressure of the water vapor above the curved contractile skin of soil water is less than the partial pressure of water vapor above the flat surface of the same soil (Fredlund et al. 2012). According to equation (4), the  $RH$  will decrease as the radius of curvature of the water surface decreases and the first component of total suction, called matric suction,



contributes to a reduction in the RH and to an increase in soil suction (Figure 27). The water vapor pressure over a flat surface of salt solution is less than the water vapor pressure over a flat surface of the pure water (Fredlund et al. 2012). In other words, an increase of the concentration of dissolved salts in a pore-water of soil causes a decrease of the RH (Figure 27). An increase in soil suction due to a decrease in RH caused by the presence of dissolved salts in a soil pore-water is referred to as the osmotic suction.

Change of any or simultaneous change of both suction components can cause a change in soil (total) suction. Changes in pore salt concentration can affect consolidation and swelling properties of clays (Rao and Shivananda 2005; Rao and Thyagaraj 2007a; Rao et al. 2017), changes in effective stress (Rao and Thyagaraj 2007b), and become relevant when dealing with problems that include problems such as infiltration of chemical solutions through soil, sea-water intrusion in coastal aquifers or lowering of groundwater table caused by excessive pumping (Barbour and Yang 1993; Carretero et al. 2013; Pulido-Leboeuf 2004). A detailed review of the osmotic suction of high plastic clays and its role on soil behavior is provided by Arifin and Schanz (2009) and Rao (2019). Osmotic suction due to the presence of dissolved salts in soil pore-water exists both in the saturated and unsaturated soil. However, in most cases, it is the matric suction component that is of primary interest in geotechnical engineering practice. Experimental evidence shows that the influence of osmotic suction on soil behavior is relatively small compared to the effects of changes in matric suction (Miller and Nelson 2006; Leong and Abuel-Naga 2017).

Most of the engineering problems in unsaturated soil mechanics, including rainfall induced landslides, are commonly the result of weather-imposed conditions (Fredlund et al. 2012). These weather-imposed conditions are primarily manifested by changing the water content of the soil, through the infiltration or evapo(transpi)ration process, which have a dominant effect on the matric suction component. Figure 28 presents changes of the total, matric and osmotic suction due to the change of water content in the soil. While the osmotic suction component is relatively constant over a considered range of water content, matric and total suction curves seem to be almost congruent (Fredlund et al. 2001). In other words, the change of soil suction is practically equal to the change of matric suction when the water content is changed.

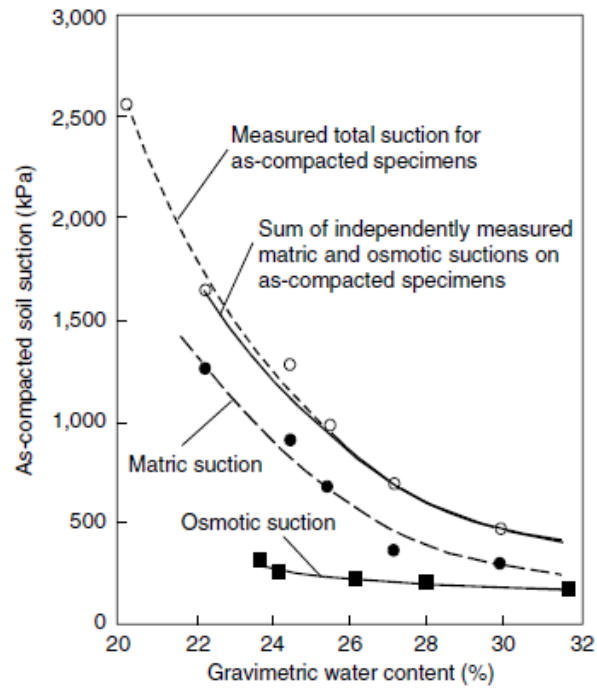


**Figure 28:** Total, matric, and osmotic suction measurements on compacted Regina clay (Krahn and Fredlund 1972).

To emphasize another critical reason why it is unnecessary to account independently for the osmotic suction component, Fredlund et al. (2012) outline that most of the laboratory procedures used to relate soil behavior to changes in matric suction, essentially simulate changes in osmotic suction that occur in the field.

Although common engineering problems include relatively low values of matric suction and high water contents of the soil, sometimes it is useful to define USPFs for the entire range of possible water contents, that is, from saturated to residual conditions. One example is a determination of the residual water content of soil for obtaining SWRC fitting parameters. Since the standard techniques used to measure soil matric suction can be used only up to approximately 1,500 kPa, it is common practice in engineering to use the total suction as a substitute for matric suction. The latter especially pertains to the higher range of total suctions (above 1,000 kPa) where psychrometric techniques have found broad application. Finally, in the case where the salt content of the soil is altered by chemical contamination or deliberate chemical change, the effect of the osmotic suction change on the soil behavior may be significant, and the two main suction components have to be examined separately (Fredlund et al. 2012).



## 4. SOIL-WATER RETENTION CURVE

Defining the relationship between water content and soil suction, the soil-water retention curve (SWRC) is one of the most important features in unsaturated soil mechanics. To date, no single technique has been developed, which can be used to attain the complete water retention curve in all types of soil ranging from sand to clay. This chapter provides a review of the measurement methods and devices used to determine the SWRCs of different soil textures. The material properties that were found to control the water retention properties of soil are discussed. Methodology and laboratory procedures used to determine the SWRC of the investigated soil are described and the obtained results are presented. The influence of matric suction change on volume and the effective stress changes are presented and discussed, as well. The best-fit parameters of the Brooks and Corey, van Genuchten and Fredlund and Xing SWRC equations, obtained by performing a non-linear regression on experimentally measured data are presented and compared with parameters of similar materials that were found in the literature. Finally, the two models that can be used to predict SWRCs of fine-grained soils were tested and compared with the obtained results.

The experimental test results included in this chapter were obtained in three different Laboratories of geotechnics: (i) University of Rijeka (Croatia), (ii) University of Salerno (Italy), and (iii) University of Ljubljana (Slovenia). A major part of the chapter was published as a research article in the journal *Geofludis* (Peranić et al. 2018).

## 4.1. Role of the SWRC in unsaturated soil mechanics

SWRC is one of the most important features in unsaturated soil mechanics and relates to the potential energy of a liquid phase, which is usually characterized by the suction  $\psi$ , to the variations in the water content  $w$  in the soil (Salager et al. 2010). Depending on the material behavior as the suction varies, the soil water content is commonly designated in terms of the gravimetric water content  $w$ , volumetric water content  $\theta$ , or degree of saturation  $S$ . For compressible soils that undergo volume deformations with the variation of suction, both the changes in water content and total volume should be measured (Fredlund and Houston 2013). For the same type of material, the SWRC should be presented in terms that take into consideration both phenomena ( $\theta$ ,  $S$ ). Various approaches were developed for the accurate determination of the SWRCs of different types of soils. Different measuring techniques and devices were designed to measure the water retention characteristics at different suction ranges. Laboratory equipment and testing procedures were often modified to adjust for different factors that affect the measurement results. For highly deformable Regina clay specimens prepared from a slurry under various consolidation pressures during the compaction process, Fredlund and Houston (2013) combined the shrinkage curve and measurements in a standard pressure plate device for the interpretation of the SWRC results.

## 4.2. Literature overview

Many studies were conducted to assess the influence of various factors on the water retention properties of the soil in geotechnical engineering applications. Vanapalli et al. (1999) studied the influence of the initial water content, soil structure and stress history on the soil-water characteristics of statically compacted clayey till specimens. They combined a pressure plate apparatus and osmotic desiccators to develop the SWRC for the entire suction range (0-300,000 kPa). Ng and Pang (2000) developed a new stress-controllable volumetric pressure plate apparatus to investigate the influence of the stress state on the SWRCs of undisturbed, completely decomposed volcanic soil from Hong Kong. Using varying net vertical stress values, they identified a strong relationship between the soil-water characteristics and confining stress. Tarantino (2009) performed an experimental study on the water retention behavior of two reconstituted soils (silty clay and sandy clayey silt) and two compacted soils (silty clay and

silty sandy gravel) using a modified oedometer apparatus. Covering a wide range of soil types and soil fabrics, he showed that the AEV and the residual degree of saturation  $S_r$  of a given soil are inversely proportional to its void ratio  $e$ . Zhang et al. (2017) investigated the influence of lime-treatment of statically compacted London Clay on the drying and wetting water retention properties. By using the contact filter paper method, pressure plate apparatus and a suction-controlled triaxial system incorporating the axis translation technique, they showed that the treatment with lime increased volumetric stability but reduced water retention ability (Zhang et al. 2017).

Numerous investigations noted that the void ratio, water content and stress state of soil have a strong influence on the SWRC. Standard laboratory equipment based on the axis translation technique, such as the pressure plate, volume extractor, suction controlled oedometer, modified triaxial apparatuses, and standard tensiometers are the most common devices used to control or measure matric suction. Although every type of equipment mentioned above has some advantages and limitations, they can be combined to measure or control matric suction up to 1,500 kPa. Generally, capillary forces dominate the wet range, and adsorptive surface forces dominate the dry range of the SWRC. Measurement accuracy in the dry area of the SWRC, such as those above 1 MPa of suction, has greatly benefited from the development of precise chilled hygrometers (Gee et al. 1992). Gee et al. (1992) used a water activity meter (CX-1 model, Decagon Devices Inc.) based on a chilled mirror dew-point technique to obtain water potentials for soils ranging in texture from sand to clay. After measuring water potentials on air-dried surface soils, Gee et al. (1992) noted that the structural changes induced by sampling should have a minimal impact on the measured water potential at low water contents. They concluded that, for low water contents, SWRCs are controlled by a surface area rather than a pore geometry. Vanapalli et al. (1999) came to similar conclusions using the osmotic desiccators to create suctions as high as 300,000 kPa on statically compacted clayey till specimens. They found that, unlike for the low-suction range, the soil-water characteristic behavior appeared to be consistent at higher suction levels (i.e., 20,000-300,000 kPa), unaffected by the stress history or initial water content. They concluded that the inter-aggregate structure appears to be the same for all of the specimens at high suction values, presuming that the films of water are so thin that all of the water is within the range of influence of the osmotic and adsorptive fields. Tuller and Or (2005) used a WP4 dew-point potentiometer (Decagon Devices Inc.) on oven-dried samples mixed with small amounts of water to achieve targeted gravimetric water contents at the dry end of the SWRCs. The obtained results indicate that for a wide range of soil textures, the capillary contributions became negligible for suction values

higher than 10 MPa. Leong et al. (2003) used the same device for measuring the total suction of compacted residual soils from Singapore. By comparing independent measurements of the matric and osmotic suctions using the null-type axis translation apparatus and pore fluid squeezer, they concluded that more research is needed to improve the accuracy of suction measurements.

Cardoso et al. (2007) performed measurements on two compacted clayey soils to study the performance of two different high-range psychrometers. Thakur et al. (2006) took measurements for the drying path by determining the gravimetric water content after each reading step with the WP4 apparatus on air-dried fine-grained soils. The specimens were dried and mixed with the required amount of demineralized water and compacted at a desired dry unit weight. Using the dry and wet weights of the specimen, the gravimetric water content  $w$  was computed for each stage of suction measurements. Agus and Schanz (2005) compared four laboratory methods commonly used for measuring total soil suction by using two bentonite-sand mixtures: the noncontact filter paper method, the psychrometer technique, the relative humidity sensor, and the chilled-mirror hygrometer technique. They concluded that the chilled-mirror hygrometer technique was the most accurate among the four methods used in the study. Campbell et al. (2007) presented a procedure for specimen preparation, suction and water content measurements during a wetting process using the WP4-T apparatus. Their sample preparation procedure consisted of sieving air-dried samples through a 2 mm sieve and then thoroughly mixing the samples with water before leaving them to equilibrate for a minimum of 24 hours. All samples that were prepared with suction lower than 1 MPa were discarded. Using the above technique, they obtained soil water characteristics of four soil samples ranging in texture from sand to bentonite.

In this study, various testing devices were used to cover the wide suction range, which investigated material can exhibit. All tests were performed to measure both the (matric) suction and volumetric water contents during the drying and wetting processes on undisturbed specimens.

### **4.3. Testing program**

All the undisturbed samples used to determine the SWRC were taken from the sample pit in the central part of the Valići Landslide (location 2 in Figure 4). By using different devices and measurement techniques in their optimum measuring ranges and combining the measurements

results, a SWRC was defined in all three characteristic zones of desaturation. For testing the residual soil from the flysch rock mass at a low range of matric suctions, various testing conditions were used to simulate the field conditions that can affect SWRC. The effect of the overburden pressure on the SWRC was analyzed using different values of the net vertical stress in suction-controlled oedometer-type devices. The measurements collected during the drying and wetting processes were performed using multiple devices to identify the hysteresis and retention characteristics that material exhibits in situ during rainfall infiltration or evaporation. The influence of varied initial water contents and saturation conditions was examined by measuring different scanning curves, starting from initially saturated conditions, natural water content or air-dried conditions. To identify the possible effects of the soil structure and sample preparation method on the suction measurements using a WP4-T device, the measurements were taken on undisturbed specimens that were prepared using commonly adopted specimen preparation techniques for testing with the WP4-T device, as proposed by various authors (e.g., Thakur et al. 2006; Campbell et al. 2007), both for the drying and wetting paths. Due to shortcomings of the axis translation technique for measurements of soil suction at high degrees of saturation (Bocking and Fredlund 1980), mini-tensiometer measurements were used to determine the wet part of the SWRC more precisely.

#### 4.3.1. Standard and volumetric pressure plate extractor apparatus

A pressure plate extractor apparatus (Soilmoisture Equipment Corp.) with 1,500 kPa ceramic plates was used on undisturbed samples to obtain results of the drying branch of the SWRC, for up to 700 kPa of matric suction. The tests were performed on undisturbed specimens with the diameter of 51 mm and the height of 10 mm. A short specimen height was used to shorten the equilibration time. At higher water contents, caliper measurements of the total volume have shown to be inapplicable due to the soft consistency of the samples. Wax dipping and water displacement techniques (ASTM D7263-09) were used to determine the total density of a single specimen after every equilibration step. The volume of a specimen could be calculated from the volume of the water displaced by the immersion of the wax-coated specimen and is determined by using the wax density and weight measurement. The total volume measurement, combined with the gravimetric measurement for the determination of the water content according to ASTM D6836-02, enabled use of the conventional pressure plate extractor apparatus to obtain a more advanced characterization of the soil-water retention properties than is possible with a conventional  $\psi$ - $w$  relationship. The results obtained using this device and adopted testing



procedure enabled evaluation of the change in void ratio  $e$  and degree of saturation  $S$  due to the increase in matric suction during the drying process of the undisturbed samples. Gravimetric water content measurements were performed on multiple specimens during the RP03 test (samples se1 to se7), starting from the natural water content  $w_n$ . To minimize evaporation from the samples during the density measurement, volume measurements were performed only on one sample (RP03-se1) after every equilibration stage.

A volumetric pressure plate (Soilmoisture Equipment Corp.) extractor with 200 kPa ceramic plate and hysteresis attachments was used to determine the hysteresis of the soil in the low matric suction range. Test VE-1w was performed on an undisturbed specimen previously equilibrated in a standard pressure plate extractor apparatus at a matric suction of 300 kPa. The total volume change was measured after every equalization step, using the previously described procedure. The water content was calculated after every equilibration step using the gravimetric or volumetric measurements of the water volume change. Devices used in the Geotechnical laboratory at the University of Salerno, Italy (UniSa) are shown in Figure 29.

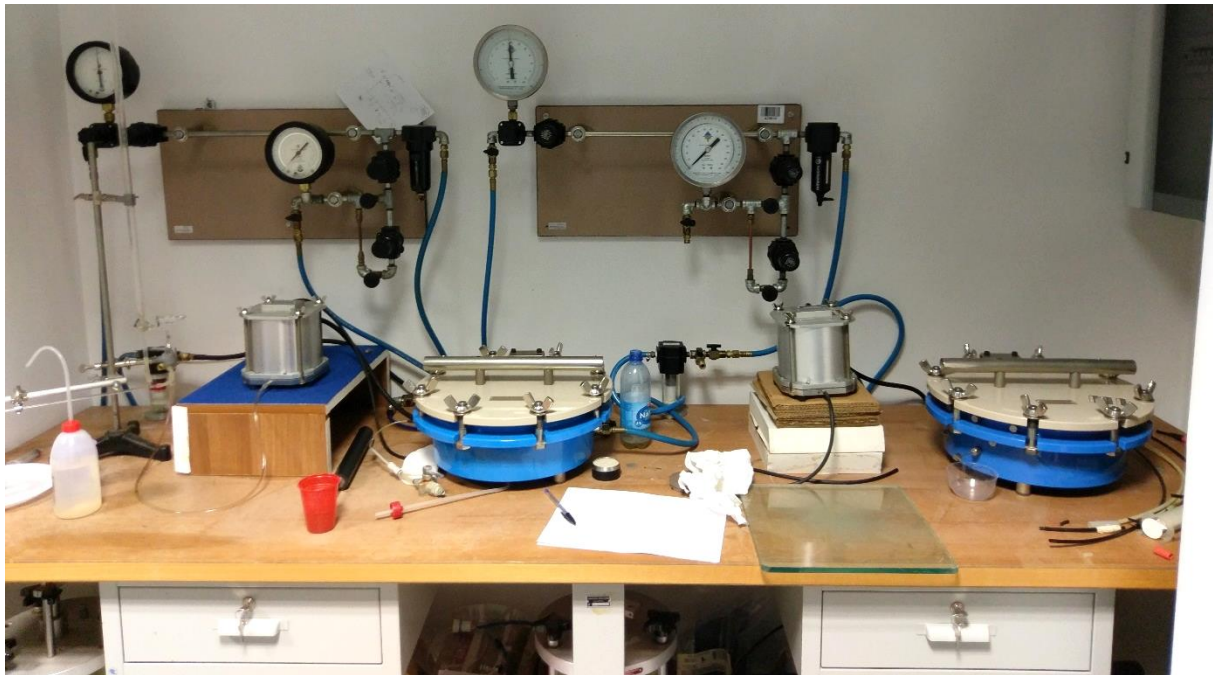


**Figure 29:** Pressure plate extractors and volumetric pressure plate extractors with hysteresis attachments used at the UniSa, Italy.

#### 4.3.2. Suction-controlled oedometer apparatus

Two different suction-controlled oedometer-type devices were used for a more advanced investigation of the soil-water retention properties through control of the stress state variables (net vertical stress and matric suction) and measurements of the axial deformations of the

sample and water volume variations during the test. Automated data acquisition during the test is an important advantage over the previously described null-type axis-translation devices, especially for the long-lasting wetting tests. The main advantage of the suction-controlled oedometer apparatus (SCOED) at UniSa is the advanced air-flushing system, which eliminates the diffused air beneath the HAEPD and consists of two double-wall burettes connected to a differential pressure transducer and a peristaltic pump. HAEPDs with AEV of 200 and 500 kPa were used to perform different types of tests. The Hydrocon hydraulic consolidation cell for unsaturated samples (Controls S.p.A.), used in a Geotechnical laboratory at the University of Rijeka, Croatia (UniRi), enables sample saturation through back pressurization in a confined system. The apparatus was equipped with a 1 MPa HAEPD. The flushing of defused air beneath the HAEPD was performed by rapidly opening a flushing port connected to the water compartment beneath the HAEPD using pressurized water directly from an air/water bladder. These devices, shown in Figure 30, were used to perform multiple (main and scanning) drying and wetting tests on undisturbed specimens under different net vertical stress values. Tests UVH-1, UVH-2 and UVH-3 were performed using the Hydrocon device to obtain the main drying curves under 25, 100 and 200 kPa of net vertical stress, respectively. Test OEUVVCJ01 was performed using the SCOED apparatus and included a scanning drying and wetting test at the net vertical stress of 200 kPa, while test OEUVVCJ03w was performed on an oven-dried sample during the wetting path, using 5 kPa of net vertical stress to measure the vertical deformations during the wetting test. Following this test, the sample was consolidated at 200 kPa, and test OEUVVCJ03 was performed during the drying path.

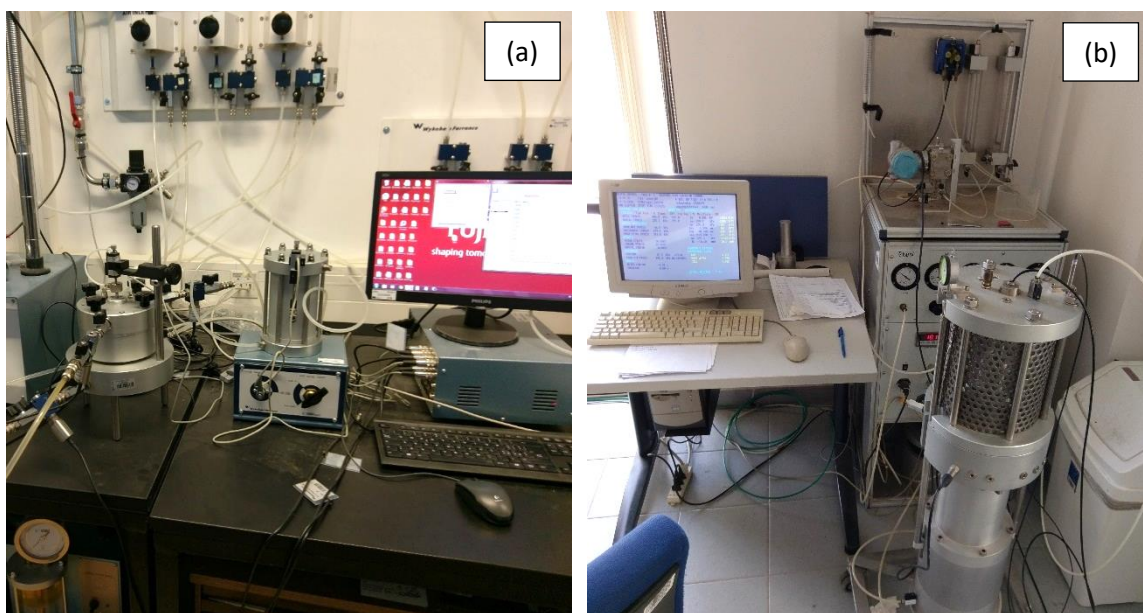


**Figure 30:** Suction-controlled oedometer devices: a) the Hydrocon consolidation cell (Controls S.p.A.) at the UniRi, and b) the suction-controlled oedometer apparatus (SCOED) at the UniSa.

#### 4.3.3. The HYPROP evaporation method device

The HYPROP evaporation method device (Decagon Devices Inc.) shown in Figure 31 a) was used in the Geotechnical laboratory at the University of Ljubljana, Slovenia (UniLj), to determine the wet part of the SWRC more precisely. Tests were performed on three undisturbed specimens with different initial water contents, starting from the saturated or natural water content. Sample saturation prior to testing was performed inside a steel cylinder by either immersion into water or by immersion into water with the application of a small vacuum. The water loss from the sample due to evaporation is automatically recorded by placing the sample on a high-precision scale. The negative water pressures are measured directly using two mini-tensiometers installed in predrilled holes (Figure 31 b) at different heights. Volume changes due to evaporation during the suction increase were not measured; therefore, the obtained results are shown only regarding the gravimetric water  $w$ . Information on the hydraulic gradient between two matric suction-measurement points and the water flux can be used to calculate the unsaturated hydraulic conductivity in the measured range, according to the Darcy-Buckingham law. Due to cavitation problems when using direct tensiometer measurements, the simplified evaporation method (Schindler 1980) is frequently used for simultaneous measuring of the SWRC and the suction permeability curve in sands and silts. By using the tensiometer-preconditioning procedure (Schindler et al. 2010), the results were obtained for matric suction values up to 130 kPa. HYPROP-2 denotes the SWRC results obtained from the sample starting from the natural water content. To decrease the matric suction difference between two tensiometers, the evaporation rate was reduced by putting a screen around the specimen. The heterogeneous cavitation occurred in the upper tensiometer after approximately two weeks.

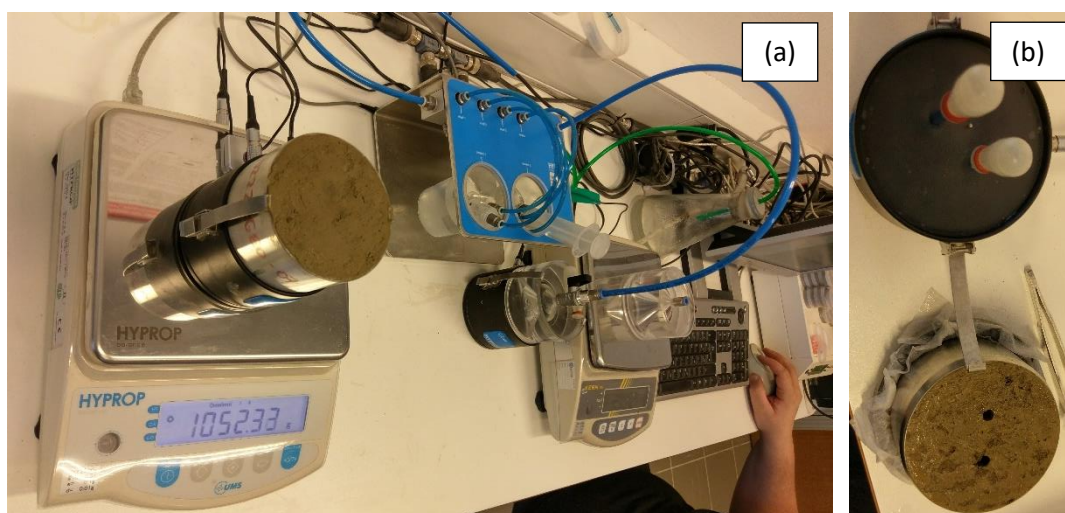


**Figure 31:** The HYPROP evaporation method device (Decagon Devices Inc.): a) test performed at UniLj, and b) pre-conditioned mini-tensiometers and saturated undisturbed specimen.

#### 4.3.4. Dew-point potentiometer WP4-T

The WP4-T (Decagon Devices Inc.) potentiometer device shown in Figure 32 was used in the Geotechnical laboratory at the UniLj to measure soil suction in the dry area of the SWRC, extending into the mid-range. A detailed description of the dew point device that measures the total suction by the vapor pressure method is provided by Leong et al. (2003) and Campbell et al. (2007). The device was used to obtain the water retention characteristics of undisturbed and remolded specimens undergoing drying and wetting processes. Testing procedures were conducted according to ASTM D 6836-02, in combination with density measurements after each suction measurement, by using the wax dipping and water displacement technique (ASTM D7263-09). The measurements were extended into the mid-range of the SWRC for undisturbed and remolded soil specimens to compare the measurement results. In the first test (WP4-T-1), a total of 8 completely remolded specimens were prepared and equilibrated at different water contents, using the specimen preparation procedure similar to that described by Campbell et al. (2007). After a few days of rest in a sealed metal container, the total matric suction was measured using the WP4-T device, and the total density was calculated using the wax and water displacement method. Test WP4-T-2 was performed during the wetting process on 11 completely remolded samples prepared using the specimen preparation procedure proposed by Campbell et al. (2007). In this test, only the water content was measured during the wetting process. Another test (WP4-T-3) was performed on 9 undisturbed samples prepared at a natural water content. The first three specimens (WP4-T-3se1, -2 and -3) were submerged in water and left to saturate for 24 h. The measurements of the next three specimens were taken starting from the natural water content and were slowly air-dried (WP4-T-3se4, -5 and -6). To prevent sample cracking, the evaporation rate was reduced by sealing the sample in a plastic bag. The last three specimens (WP4-T-3se7, -8 and -9) were used to perform measurements during the wetting process, starting from the air-dried condition. Air-dried specimens were wetted with a small amount of water and rested for approximately 24 hours in small sealed plastic bags. After each step of the equilibration, the suction and weight of the specimen were measured. Then, the total density of the specimens was measured, and the procedure was repeated until the suction values became too low during the wetting process or until the air-dried conditions were achieved during the drying process. During both the drying and wetting processes, multiple measurements of the suction and density were performed. Suction values as low as 230 kPa and higher than 90 MPa were measured using the WP4-T device.



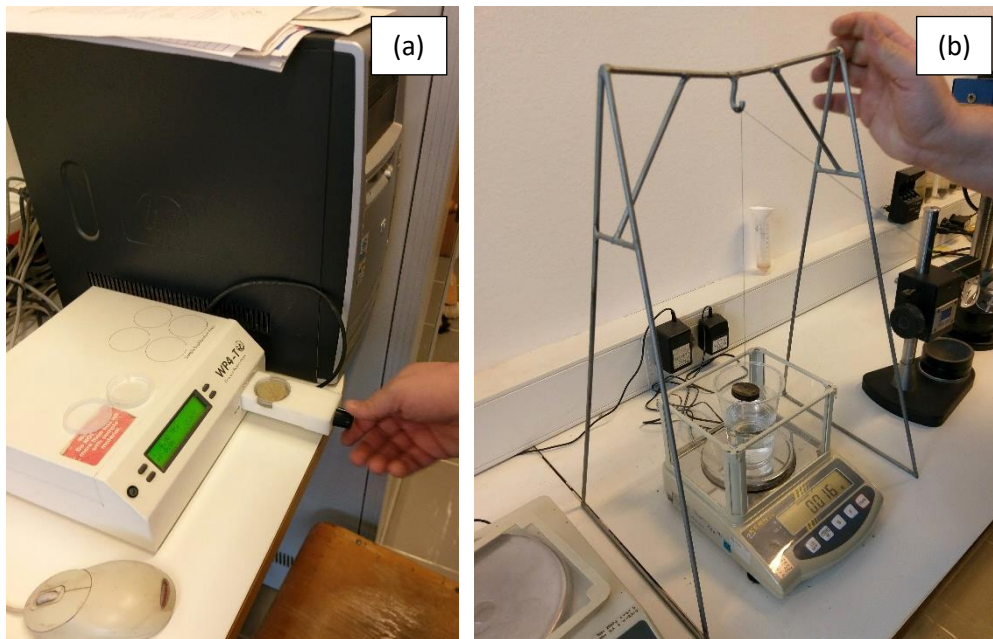


**Figure 32:** The WP4-T (Decagon Devices Inc.) potentiometer device used at UniLj: a) soil suction, and b) density measurements performed on undisturbed sample undergoing the wetting process.

## 4.4. Test results

The results obtained using various measurement techniques and devices are provided in this part. The matric suction and total suction measurements were combined to define the soil-water characteristics from the capillary saturation zone to the zone of residual saturation. All the results were obtained from undisturbed specimens, except for the drying test WP4-T-1 and wetting test WP4-T-2. Different colors are used to highlight different specimen conditions at the start of the test, concerning the saturation and preparation technique. Markers with solid fill indicate that disturbed specimens were used in the test. Red and blue colors indicate drying path starting from the saturated or natural water content conditions, respectively, while the green color is used to represent the measurements obtained from specimens undergoing wetting.

The results obtained from air-dried samples undergoing the wetting path were used for hydraulic characterization of the soil in the wetting process, and results obtained from only undisturbed soil samples were used for the development of the SWRC. The influence of the specimen preparation method and soil structure on the retention properties was evaluated by comparing the results obtained from the disturbed and undisturbed samples using the same device or measurement technique.

The measurement results used to obtain the suction  $\psi$  vs. the water content  $w$  relationship (SWRC- $w$ ) are presented in Figure 33 a). Some of the results obtained using the

standard and volumetric pressure plate extractor devices, suction-controlled oedometer devices, HYPROP, and WP4-T devices are included. The suction  $\psi$  vs. the volumetric water content  $\theta$  (SWRC- $\theta$ ) measurement results are presented in Figure 33 b). The latter representation accounts for changes in both the water volume and total volume (or density) due to the suction change during the test. For the suction-controlled oedometer devices, the total volume was calculated using the measured axial deformations, assuming no sidewall detachment of specimen from the sample ring occur.

A slope of the drying branch in the SWRC before reaching the AEV of the material is visible for both the SWRC- $w$  and SWRC- $\theta$ , indicating that, due to the increase in the stress state of the soil, the material undergoes a volume change when the suction is changed. Many studies (e.g., Pham and Fredlund 2005; Pasha et al. 2016) have concluded that the rate of the volume change in the saturated part of the SWRC depends on the stress history of a soil. For over-consolidated soil, the slope of the SWRC- $w$  before the AEV is generally small and depends on the swelling index  $C_s$  in the  $\log(\psi)$ - $w$  plane. For normally consolidated soil, a steeper slope depends on the compression index  $C_c$  in the  $\log(\psi)$ - $w$  plane (Pham and Fredlund 2005). The slope of the saturated part of the SWRC corresponds to the slope of the unloading-reloading curve in the  $\ln p'$ - $v$  plane for over-consolidated soils or to the slope of the normal compression line for normally consolidated soils (Pasha et al. 2016). However, the total volume change should not affect the degree of saturation  $S$  of deformable soil before the AEV of the soil is reached. The degree of saturation remains equal to unity, and the SWRC- $S$  plot should remain horizontal until the AEV of the material is reached. After this point, desaturation starts at a rate which depends on the features of the material being tested. By plotting a large number of experimental data on a log-log plot of the suction  $\psi$  vs. the effective degree of saturation  $S_e$ , Brooks and Corey (1964) found that the rate of desaturation exhibits a linear shape for the unsaturated part of the SWRC. This approach was used to avoid common difficulties in determination of the true AEV due to the volume changes in the saturated part of SWRC (Wijaya et al. 2015; Pasha et al. 2016).

The SWRC results are shown in the SWRC- $S$  form in Figure 34 a) in a semi-log plot, for tests in which the degree of saturation could be calculated. For the remolded specimens, the density measurements were combined with the standard WP4-T suction and water content measurements for only the drying test WP4-T-1, while the WP4-T-2 test results are not included. In Figure 34 b), the SWRC- $S$  results are presented in a log-log plot. Using the plot and results from the unsaturated linear part of the SWRC, the AEV of 210 kPa and air expulsion

value (AExV) of 56 kPa were determined for the drying and wetting paths, respectively. The regression lines for the drying and wetting processes are parallel, and the pore-size distribution index value  $\lambda = 0.26$  (Brooks and Corey 1964) seems to be unaffected by the ongoing process type. On the other hand, the results obtained from the remolded specimens along the drying path (WP4-T-1) show a deviation from the values mentioned above, with a higher AEV (450 kPa) and higher desaturation rate ( $\lambda = 0.33$ ) (Peranić et al. 2018).

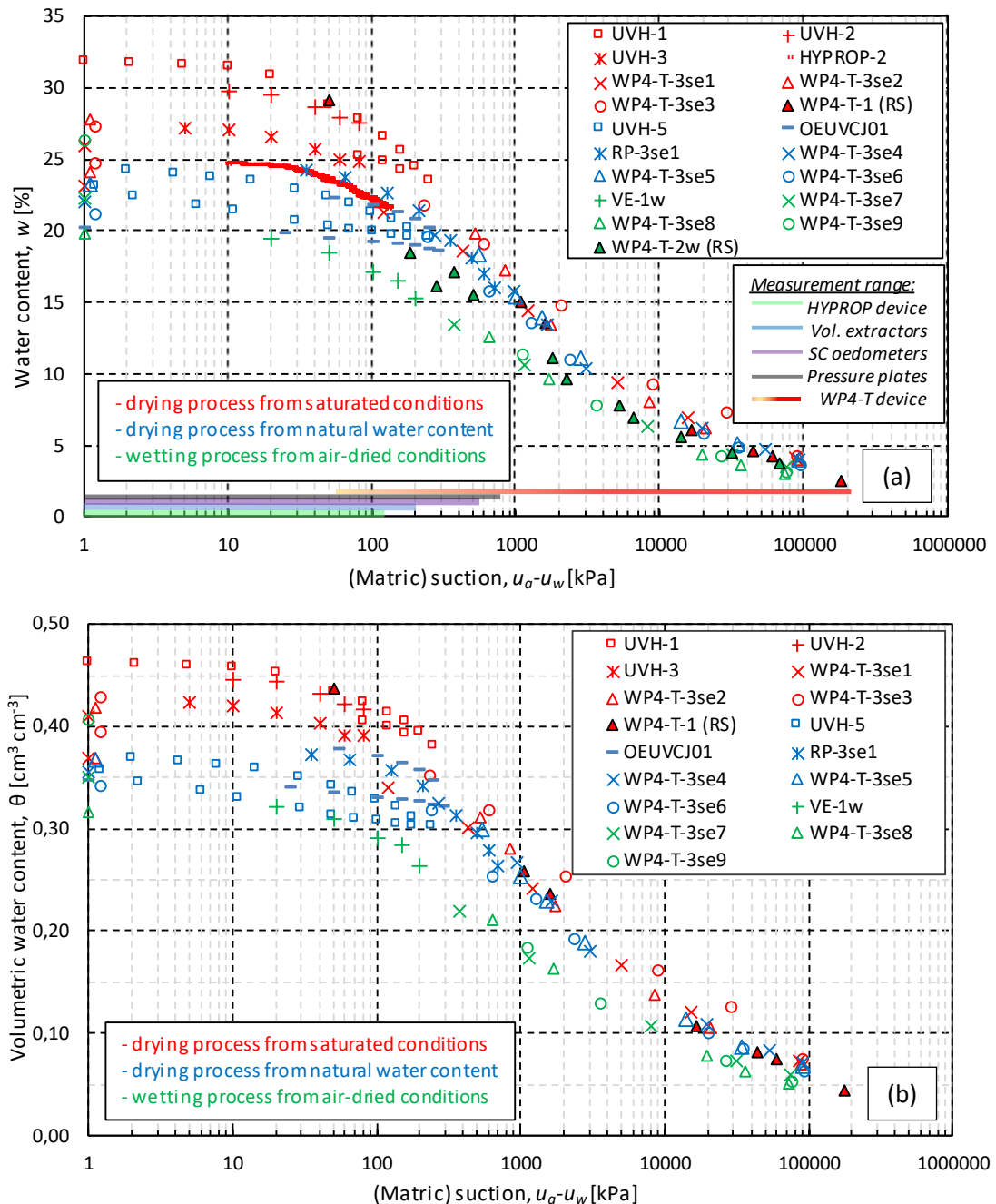


**Figure 33:** SWRC in terms of a) gravimetric water content; b) volumetric water content for the drying and wetting process. Symbol (RS) indicates remolded samples; all other samples are undisturbed (Peranić et al. 2018).

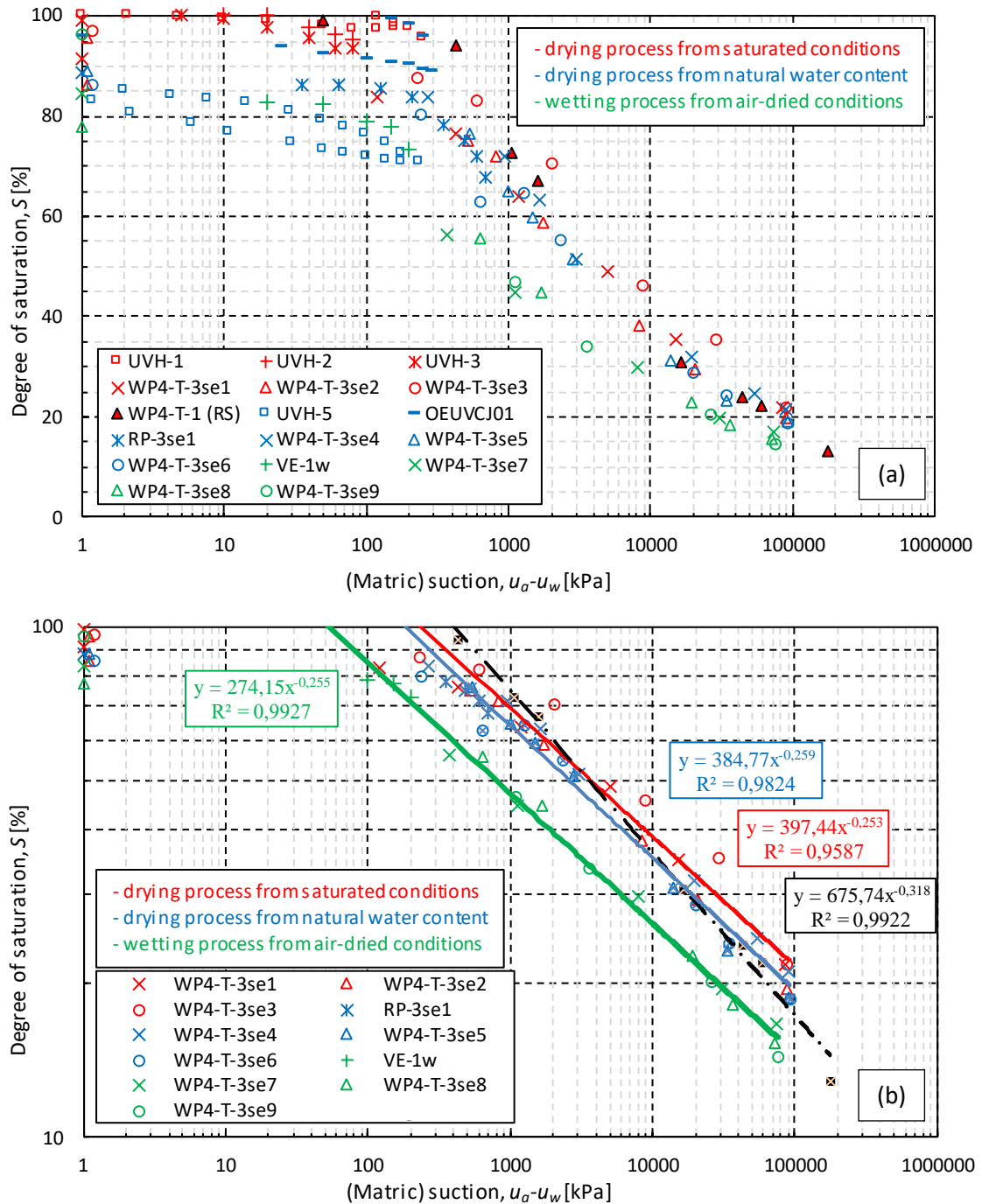


**Figure 34:** Drying and wetting paths of the SWRC- $S$  in the a) semi-log and b) log-log form (Peranić et al. 2018).

Hysteresis between the drying and wetting process is observed for all the SWRC plots. The shape of the SWRC, saturated water contents, and other soil properties associated with the drying and wetting SWRC paths (Fredlund et al. 2012) suggest that the tested material is more similar to silty soil than clayey soil (Fredlund et al. 2011). Another important observation from the wetting tests is that the specimens did not reach full saturation. Similar results are obtained for drying tests performed on samples that were saturated prior to testing by immersion into water. The obtained volumetric water contents typically corresponded to 80-95% of the



saturated water content values. Other researchers reported similar observations. Chiu and Shackelford (1998) obtained maximum volumetric water contents  $\theta_m$  from 0.84 to 0.90 of the saturated value  $\theta_s$  during the wetting process of compacted sand-kaolin mixtures. After several days of soaking, Perera et al. (2005) determined that the degree of saturation was 87% - 100% for the clayey samples.

The influence of the sample preparation technique on the measurement results obtained using the WP4-T device is highlighted in Figure 33 a), both for the drying and wetting paths. For the drying path, the measured results from the remolded specimens plot higher than the results obtained from the undisturbed specimens, especially for suction values below 1,000 kPa. The effects of the sample preparation method and soil structure on the measurements start to wane above a suction of 1,000 kPa for the drying branch. The influence of the specimen preparation method is even more emphasized in the case of the results obtained during the wetting process (WP4-T-2). The results start to deviate from those obtained from the undisturbed samples when the suction values become lower than 6,000 kPa. In contrast, the measurements obtained from the undisturbed specimens using the WP4-T device seem to be in align with the measurements obtained using the axis translation technique, even for the suction values well below 1,000 kPa. This could indicate that the soil structure does have an important effect on the results obtained using the WP4-T device in the part of the SWRC with lower suction values and that the measurements from the undisturbed specimens should be preferred when using the WP4-T device and when the suction values of interest are lower than 1 MPa (Peranić et al. 2018).

The results obtained on undisturbed specimens underline the smooth and gradual transition between the saturated and unsaturated parts of the SWRC, consistent with the wide range of solid-particle sizes present in the studied material and low value of  $\lambda$ . This feature of the soil is closely related to the water retention and permeability characteristics of the soil, and should thus have a direct influence on the rainfall infiltration process occurring in slopes in-situ. For sands and silts, the transition zone of the SWRC is generally steep, indicating higher rates at which the material can be saturated during the infiltration process or desaturated during evapotranspiration. Consequently, short-duration precipitation with higher intensities are the common triggering factors for landslides occurring in these types of material (Clarizia et al. 1996; Crosta and Fratini 2001; Guzzetti et al. 2008). In contrast, the SWRCs with gentle slopes in the transition zone implies low rates of change in the water content of the soil. Long evaporation periods are required to dry these types of soil significantly, and long infiltration periods are necessary for the water to saturate these types of soil. (Peranić et al. 2018).

The density measurements combined with the standard  $\psi$ - $w$  measurements from the pressure plate and WP4-T devices, and the measurements by the suction-controlled oedometer devices can provide insight into the volume changes affected by the change in suction. Figure 35 presents the  $e$ - $S$ - $\psi$  relationship for the specimens that underwent zero total stress and total density measurements after every measurement of the (total) suction or equilibration step. The results obtained using the standard pressure plate apparatus and WP4-T device were included.

The results obtained using the standard and suction-controlled oedometer apparatuses are shown in terms of the effective stress  $\sigma'$  vs. the void ratio  $e$  in Figure 36 a). The effective stress is defined using the Bishop's effective stress formulation (Bishop 1959) defined by (42) and the Khalili and Khabbaz (1998) expression for the effective stress parameter (49). Some of the more recent findings on the effective stress of unsaturated soils and advanced formulations (e.g., Oh et al. 2012; Chen et al. 2013; Nikooee et al. 2012; Likos 2014; Greco and Gargano 2015, etc.) are presented in the chapter devoted to determination of the unsaturated shear strength of the investigated soil. The results show that the effective stress approach works well for the results obtained on the undisturbed specimens in the range of the effective stress considered in these tests, both during the drying and wetting processes. The undisturbed specimen in the UVH-1 test was saturated using the incremental back-pressurization procedure

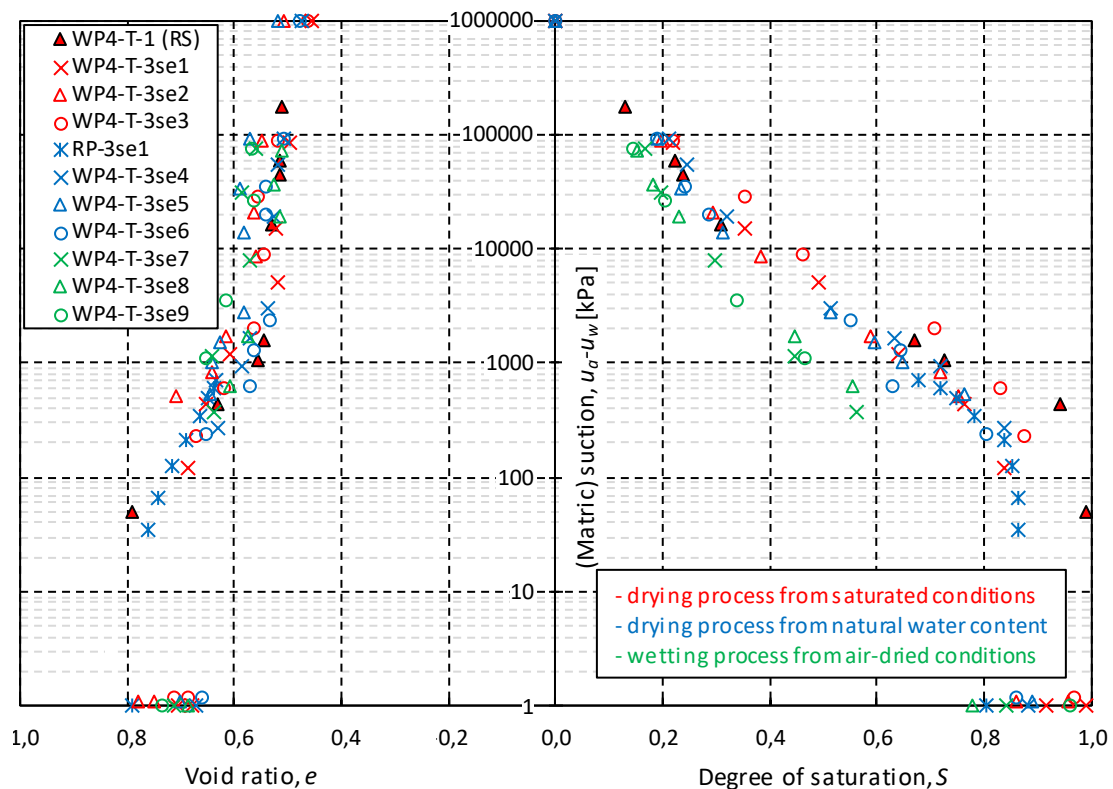


**Figure 35:**  $S$ - $\psi$ - $e$  measurements obtained using the WP4-T and pressure plate extractor apparatus (Peranić et al. 2018).

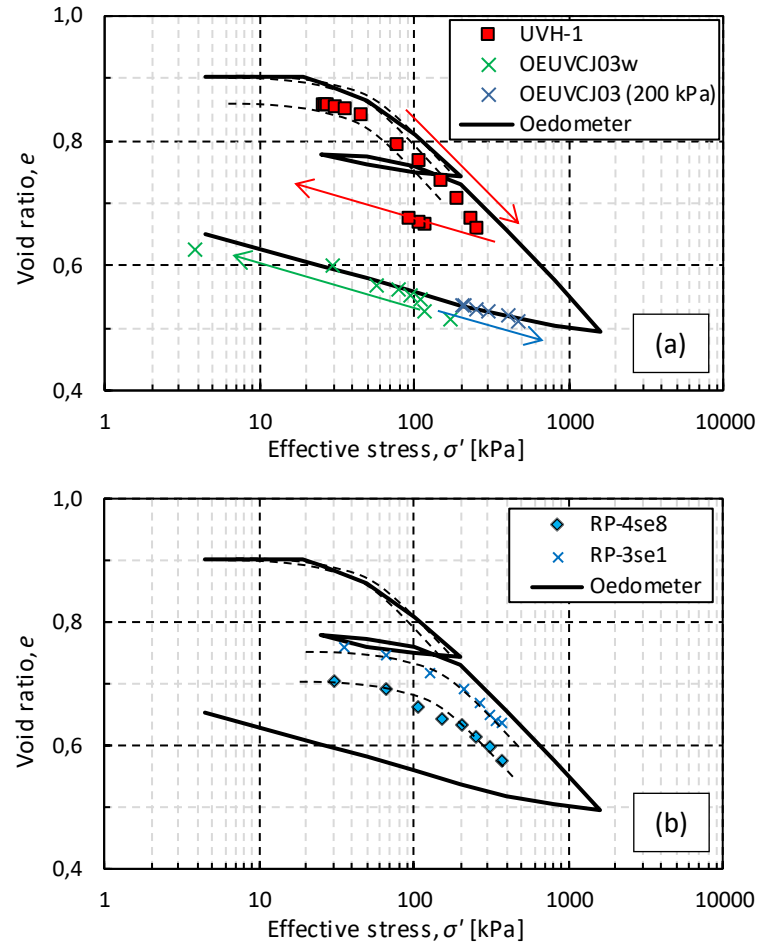


**Figure 36:** Results in terms of  $\sigma' - e$  compared with the conventional oedometer test results for the a) UVH-1, OEUVVCJ03w and OEUVVCJ03; b) RP-3se1 and RP4-se8 tests (Peranić et al. 2018).

and consolidated at 25 kPa of net vertical stress. Next, the specimen was dried by increasing the matric suction up to 250 kPa, and then wetted up to 80 kPa of matric suction. The specimen in the UVH-1 test behaves as an over-consolidated material until the increase in suction causes the effective stress to increase beyond the pre-consolidation pressure of 50 kPa (determined in the standard oedometer test). From this point on, the results follow the slope of the virgin compression line ( $C_c = 0.262$ ). Due to a decrease in the matric suction, the results along the wetting path follow the slope of the swelling curve ( $C_s = 0.065$ ), suggesting a suction over-consolidated material. Similar behavior is observed for the suction-over-consolidated specimen OEUVVCJ03. The oven-dried sample for this test was equilibrated at 490 kPa of matric suction and incrementally wetted to 0 kPa of matric suction. During the wetting process, the specimen follows the swelling line obtained from the standard oedometer test. After absorbing water and reaching equilibration at atmospheric pressure, the specimen was consolidated at the effective stress of 200 kPa. Finally, the matric suction was incrementally increased up to 350 kPa, under a constant net vertical stress. Again, the specimen behaves as a pre-consolidated material,

following the slope of the swelling curve in the  $\log(\sigma') - e$  plane. The results obtained using the standard pressure plate extractor on the samples that start the drying process from the natural water content, the RP-3se1 and RP-4se8 tests, are shown together with the results obtained using the conventional oedometer apparatus in Figure 36 b). Using the same formulation to determine  $\sigma'$ , the pre-consolidation pressure due to the suction seems to be slightly higher for this sample (Peranić et al. 2018).

Using the same formulation for the effective stress, the results obtained using the WP4-T device in the WP4-T-1 and WP4-T-3 tests are shown in Figure 37. Depending on the achieved suction during the drying process, the undisturbed samples from the WP4-T-3 test follow the same behavior pattern as seen in the results from the suction-controlled oedometer tests. A completely different behavior pattern is observed in the case of the remolded specimens in the WP4-T-1 test, where samples behave as a normally consolidated material, undergoing a significant reduction in the void ratio from the beginning of the drying process.

The Khalili and Khabbaz (1998) effective stress parameter seems to predict the effective stress for suctions up to 8,000 kPa correctly. However, according to the standard oedometer results, using a fixed value for the fitting parameter (-0.55) for soil suctions higher than 8,000 kPa, the formulation (49) seems to overestimate the increase in effective stress due to the increase in suction (Peranić et al. 2018).

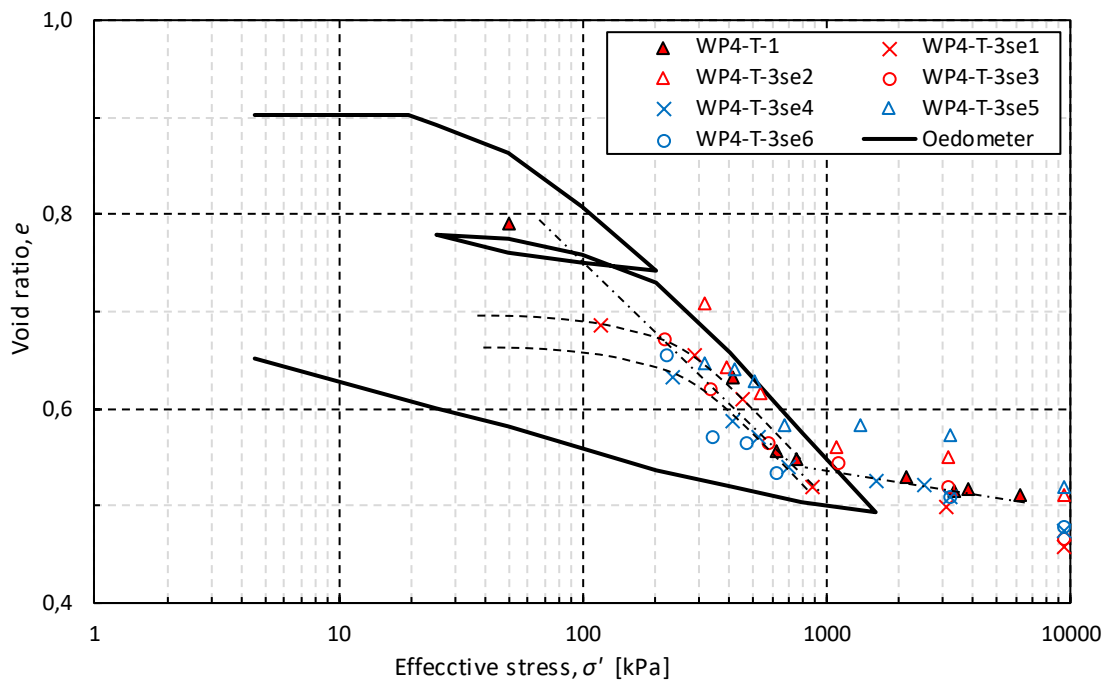


**Figure 37:** Results in terms of  $\sigma' - e$  compared with the conventional oedometer test results for the WP4-T-1 and WP4-T-2 tests (Peranić et al. 2018).

## 4.5. Interpretation of the SWRC results

For modeling, comparison and characterization purposes, it is useful to present the fragmented SWRC laboratory measurements in the form of a mathematical equation. Consequently, a continuous function is obtained for a wide range of suctions. A non-linear regression analysis was performed using the “solver” add-in in Microsoft Excel on the results obtained during the drying and wetting process. The best-fit equation parameters were obtained by minimizing the objective function with respect to the sum of the squared residuals (SSR). Smaller values of the SSR implies a better fit between the measured and calculated values using different SWRC equations. Three of the most frequently used equations were used to fit the obtained measurement data: Brooks and Corey (1964) (BC), van Genuchten (1980) (VG), and Fredlund and Xing (1994) (FX).

The Brooks and Corey (1964) SWRC equation is defined as

$$\begin{aligned} \theta &= \theta_s; & \psi &\leq \psi_b \\ \theta &= \theta_s \left( \frac{\psi_b}{\psi} \right)^\lambda; & \psi &> \psi_b \end{aligned} \quad (20)$$

where  $\theta$  is the volumetric water content,  $\theta_s$  is the saturated volumetric water content,  $\psi$  is the matric suction,  $\psi_b$  is the AEV of the soil and  $\lambda$  is a constant.

The van Genuchten (1980) SWRC equation is given by

$$\theta = \theta_s \left[ \frac{1}{1 + (\alpha\psi)^n} \right]^m \quad (21)$$

where  $\alpha$ ,  $n$ , and  $m$  are constants.

The Fredlund and Xing (1994) SWRC equation is given by

$$\theta = C(\psi) \frac{\theta_s}{\left\{ \ln \left[ e + \left( \frac{\psi}{a} \right)^n \right] \right\}^m} \quad (22)$$

where  $a$ ,  $n$ , and  $m$  are constants, and  $C(\psi)$  is a correction function defined as

$$C(\psi) = 1 - \frac{\ln(1 + \psi/\psi_r)}{\ln(1 + 1,000,000/\psi_r)} \quad (23)$$

where  $\psi_r$  is a constant related to the suction at residual water content,  $\theta_r$ .

Although a sharp discontinuity near saturation in the BC equation very often limits its practical application for modeling purposes, it is one of the oldest equations and is valuable for

comparing the soil-water characteristics of various soils using the existing databases. As it is expected from the obtained SWRC shape, the sigmoidal equations (VG and FX) performed better than the non-sigmoidal (BC) equation, while the FX equation performed slightly better than the VG equation. A higher number of fitting parameters provided a stronger correlation in all the considered cases.

#### 4.5.1. Interpretation for the drying branch of the SWRC

The UVH-1 test results were used for the fitting in the initial part of the desorption branch of the SWRC and determination of the saturated water content  $\theta_s$ . Starting from the saturated conditions and using the results from only those tests with the net vertical stress of 25 kPa, the UVH-1 test results represent the upper bounding curve. The WP4-T-3 test measurements on initially saturated specimens were used to extend the SWRC in the region of higher suction values. The results obtained from the WP4-T-3se3 test plot higher than the rest of the results obtained starting from the saturated conditions. Although this is probably due to the specimen inhomogeneity, the exclusion of the WP4-T-3se3 resulted in a significant decrease in the SSR value, from 0.00270 to 0.00039 in the case of the FX equation and from 0.00283 to 0.00054 in the case of the VG equation. In the case of the BC equation, only a slight decrease in the SSR value, from 0.00702 to 0.00428, was obtained by omitting the WP4-T-3se3 results.

Using the three-parameter form of the FX equation (“correction“ factor  $C(\psi)=1$ ) causes an increase in the SSR value, from 0.00039 to 0.00058. Leaving the  $m$  and  $n$  parameters with no fixed relationship provides a slightly lower value of the SSR (0.00049) than that obtained when fixing these parameters using the relation  $m = 1 - 1/n$  (0.00054), as used in van Genuchten (1980) when trying to obtain a closed-form expression for hydraulic conductivity.

Considering that suctions as low as 2.1 and 1 kPa were used in the fitting procedure for the drying branch, the saturated volumetric water content  $\theta_s$  did not affect the result significantly if kept as a constant value ( $\theta_s=0.4625$ ) or used as another fitting parameter for the VG and FX equations. However, due to the limitation of the BC equation to predict the water contents of soils that exhibit volume changes below the AEV, the best fit was obtained for a slightly lower value,  $\theta_s=0.450$  (Peranić et al. 2018).

The curves and best-fit parameters obtained by using the non-linear regression procedure on measurements performed on undisturbed specimens in the (main) drying and wetting processes are presented in Table 6 and 7, and Figure 38.

#### 4.5.2. Interpretation for the wetting branch of the SWRC

The results obtained from the VE-1w and WP4-T-3se7, -8 and -9 tests were used to fit the parameters of all three equations in the case of the adsorption branch of the SWRC. Only the last measurement from the WP4-T-3se7 test, at a total suction of 370 kPa, was excluded from the non-linear regression procedure, since it plots slightly lower in the  $\psi$ - $\theta$  plane, causing a slight increase in the SSR value from 0.00025 to 0.00047 for the FX equation. The results obtained from air-dried samples represent the lower bounding curve of the SWRC.

The highest volumetric water content of 0.335 did not change significantly when used as a fitting parameter for the FX and VG equations. Again, for the BC equation, the best fit was obtained for a slightly lower value (0.307) (Peranić et al. 2018).

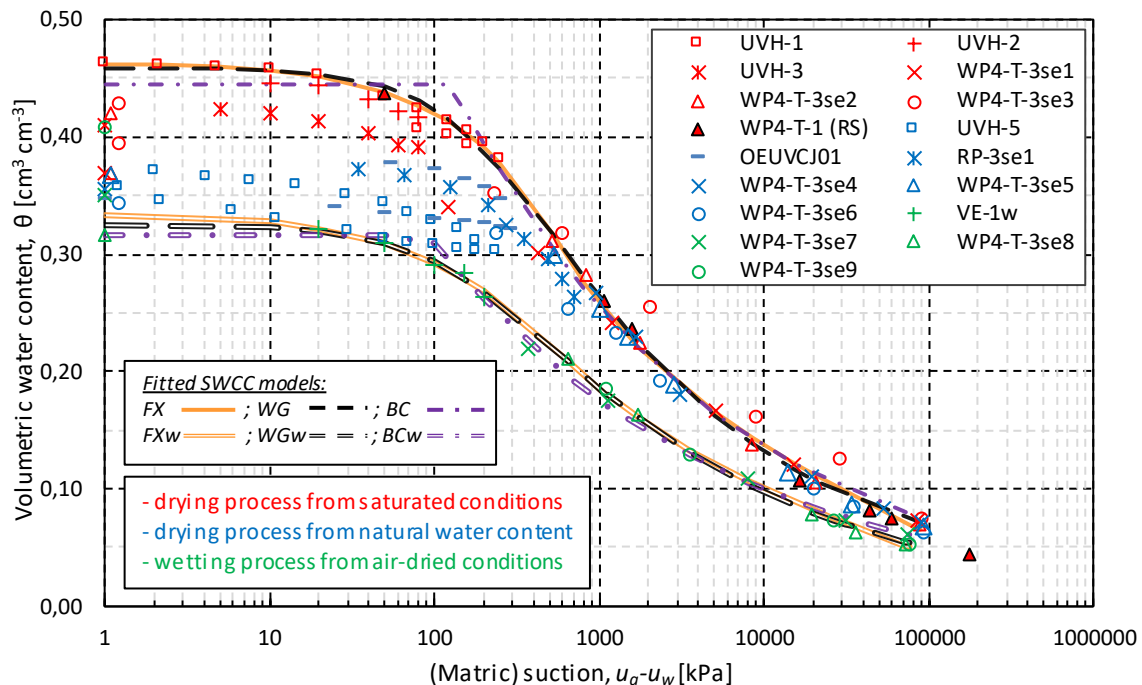


**Figure 38:** Best-fit Brooks and Corey (1964), van Genuchten (1980) and Fredlund and Xing (1994) equations plotted with the measurements in  $\psi$ - $\theta$  plane (Peranić et al. 2018).

**Table 6:** Best-fit parameters and SSR values for the Brooks and Corey (1964) and van Genuchten (1980) three-parameter equations (Peranić et al. 2018).

Brooks&Corey eq. (1964)					van Genuchten (1980); $m^* = 1 - 1/n$				
$\theta_{sd} = 0.4625$ ; $\theta_{sw} = 0.335$	SSR ( $r^2$ )	$\theta_r$	$\psi_b$	$\lambda$	SSR ( $r^2$ )	$\theta_r$	$\alpha$	$n$	$m^*$
Bounding drying curve	0.00428	0	99.491	0.260	0.00054	0.013	0.005	1.332	0.249
Bounding wetting curve	0.00203	0	72.567	0.246	0.00033	0.000	0.008	1.280	0.219

**Table 7:** Best-fit parameters and SSR values for the four-parameter equations: the van Genuchten (1980) and Fredlund and Xing (1994) equations (Peranić et al. 2018).

van Genuchten (1980); $m$ free						Fredlund and Xing (1994)				
$\theta_{sd}=0.4625$ ; $\theta_{sw}=0.335$	SSR ( $r^2$ )	$\theta_r$	$\alpha$	$n$	$m$	SSR ( $r^2$ )	$\psi_r$	$a$	$n$	$m$
Bounding drying curve	0.00049	0.028	0.004	1.186	0.323	0.00039	177720.9	299.753	1.073	0.907
Bounding wetting curve	0.00021	0.011	0.005	0.973	0.348	0.00022	254164.3	284.117	0.859	1.053

## 4.6. SWRC prediction models

Two correlation models that predict the SWRC for plastic materials were tested on the obtained results along the drying and wetting paths. The FX equation parameters were obtained using the correlation models proposed by Zapata (1999) and Perera (2005). Both models use only two basic material properties: the percent passing through a No. 200 sieve ( $P_{200}$ ) and plasticity index (PI). The SSR values indicate the level of convergence between the measured and model-predicted values. The obtained curves are shown in Figure 39, together with the previously derived best-fit FX curve. Table 8 presents the calculated parameter values. During both the drying and wetting process, the Zapata (1999) model seems to perform reasonably well. On the other hand, the model proposed by Perera et al. (2005) was unable to accurately predict the SWRC, especially for the drying process (SSR=0.103). However, it was noted that, if the clay percentage (30.3%) was used instead of  $P_{200}$ , the model performed much better (Figure 39).

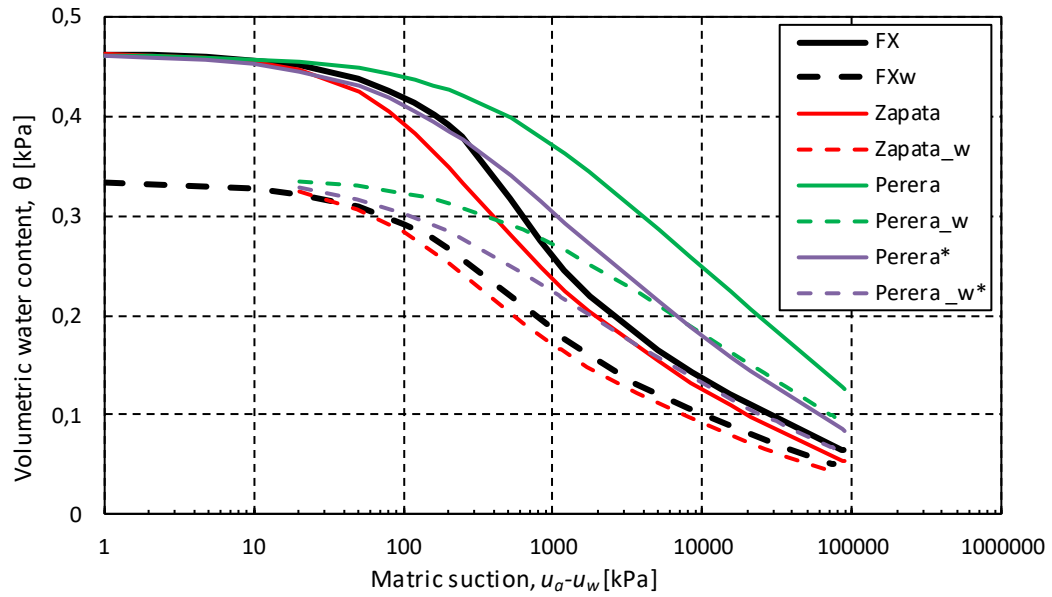
The hydro-mechanical features of the tested soil were compared with Guadalix Red silty clay (Escario and Juca 1989), which is 48% silt, with  $w_L = 33\%$  and  $PI=13.6\%$ . According to the SWRC parameters  $\psi_r = 19.6$  MPa,  $a = 242.1$ ,  $n = 0.81$ , and  $m = 0.79$  (Vanapalli et al. 1998), the two materials closely match. If the obtained retention model parameters are compared with the average values for different soil textural groups (Carsel and Parrish 1988), it is clear that the complex origin process generates interesting hydro-mechanical features in this soil. The saturated and residual volumetric water contents correspond to the silts, while  $\alpha = 0.005$  and  $n = 1.332$  are characteristic values for the silty clay and clay loam textures. On the other hand, the saturated shear strength parameters determined in this and previous studies (e.g., Vivoda Prodan et al. 2017) are commonly obtained in materials with a significant portion of sandy particles.



**Table 8:** Fredlund and Xing (1994) equation parameters and SSR values obtained using the Zapata (1999) and Perera (2005) SWRC correlation models (Peranić et al. 2018).

Fredlund and Xing (1994) equation						
$\theta_{sd} = 0.4625; \theta_{sw} = 0.335$	$SSR_d (r^2)$	$SSR_w (r^2)$	$\psi_r$	$a_f$	$n_f$	$m_f$
Zapata (1999) correlation	0.01109	0.00227	5385.4	121.911	1.085	0.690
Perera (2005) correlation	0.10287	0.07522	500.0	123.599	0.587	0.116
Perera (2005)* correlation	0.01526	0.01237	500.0	91.597	0.801	0.326

\*clay percentage, C (%) instead of P<sub>200</sub>

**Figure 39:** Performance of the two prediction models compared with the Fredlund and Xing (1994) equation obtained by using the non-linear regression procedure on the measured data (Peranić et al. 2018).

## **5. PERMEABILITY FUNCTION**

This chapter presents a methodology for the determination of the unsaturated hydraulic conductivity function of the investigated soil. Along with the soil-water retention function, it is the key-in material property governing the transient rainfall infiltration process. Theoretical basics of the water flow through unsaturated soil are described, and a detailed overview of the available methods for direct measurements or indirect estimation of hydraulic permeability under negative pore-water pressure conditions are presented. Permeability measurement results obtained in saturated and unsaturated conditions and the determined conductivity functions are presented.

## 5.1. Determination of UHCF – literature overview

Hydraulic conductivity or coefficient of permeability  $k$  is a quantity, generally assumed to be a constant in case of saturated soil, which regulates the rate at which water flows through the soil. Although it depends on the size and interconnectivity of voids, it can be considered a constant value for a certain type of soil. Thus, the coefficient of permeability of saturated soil  $k_s$  is often measured at different values of the effective stress, or in another words, for different void ratio values  $e$ . However, this is not the case for unsaturated soil: as the matric suction is increased beyond the AEV, soil starts to desaturate, and the volume of water and volume of voids become unequal. Space available for the water to flow is reduced, along with the reduction of the degree of saturation. The air-water interface (meniscus) separates the air and water phases inside the voids of unsaturated soil, providing the equilibrium for flow through the unsaturated soil (Fredlund et al. 2012). Thus, when describing the flow of water through unsaturated soil with two phases that can flow through voids, air and water, the term coefficient of permeability with respect to the water phase  $k_w$  is often used. Depending on the matric suction value and ongoing process, different values of the degree of saturation can exist in the soil. Depending on the soil type and stress history, change of matric suction can cause negligible or significant total volume change of soil. Consequently, the coefficient of permeability in an unsaturated soil becomes a function of the soil water content, defined by the degree of saturation, volumetric water content, or, in case of non-deformable soil, gravimetric water content, which in turn depend on the matric suction existing in the soil.

The coefficient of permeability is the primary (and the only) soil property required when analyzing the steady-state water flow through the soil (Fredlund et al. 2012). In the case of transient water flow through soil, the water storage properties have to be defined. Since both quantities depend on the water content of a soil, which again depends on matric suction, the latter two are unsaturated soil property functions, known as the unsaturated hydraulic conductivity function and the water storage function. The first one describes the variation of permeability respective to water phase as a function of water content  $k_w(S, \theta)$ , or matric suction  $k_w(u_a - u_w)$ , while the other one describes the ability of the soil to store or release water under some change of matric suction. The water storage function of soil is calculated by differentiation of the SWRC respective to matric suction, where SWRC is always expressed in terms of the volumetric water content  $\theta$  (i.e.,  $d\theta/d(u_a - u_w)$ ) (Fredlund et al. 2012). The slope

of the SWRC on the arithmetic soil suction scale gives the water storage modulus  $m_2^w$  at designated soil suctions (Fredlund et al. 2012).

Among the first measurements of the hydraulic permeability of porous medium under negative pore water pressure values was that performed on glass beads by Mualem (1976). Starting from saturated conditions, the coefficient of permeability was measured at increasing matric suction values at first (drying path) and then for the wetting path. For the non-deformable glass beads, he noticed several important findings that were confirmed in numerous studies conducted on soils with different textures. First, after the matric suction value exceeded the AEV of soil beds, the coefficient of permeability started to decrease significantly. Figure 40 indicates that the coefficient of permeability is equal to some constant value at first and then reduces for several orders of magnitude as the matric suction is increased above 4 kPa, value which seems to be the AEV for used glass beads (Figure 40 b). Another important feature that can be clearly distinguished from Figure 40 is hysteretic behavior. Both the SWRC and permeability function are not unique but strongly depend on whether the soil undergoes drying or wetting process. Any procedure used to measure or predict the hydraulic conductivity function (HCF) should consider the type of flow process occurring in the field (i.e., drying or wetting process). Observed similarities between the SWRC and permeability functions have subsequently become the basis for a wide range of procedure that are used to estimate, rather than directly measure the water permeability function (Fredlund et al. 2012).

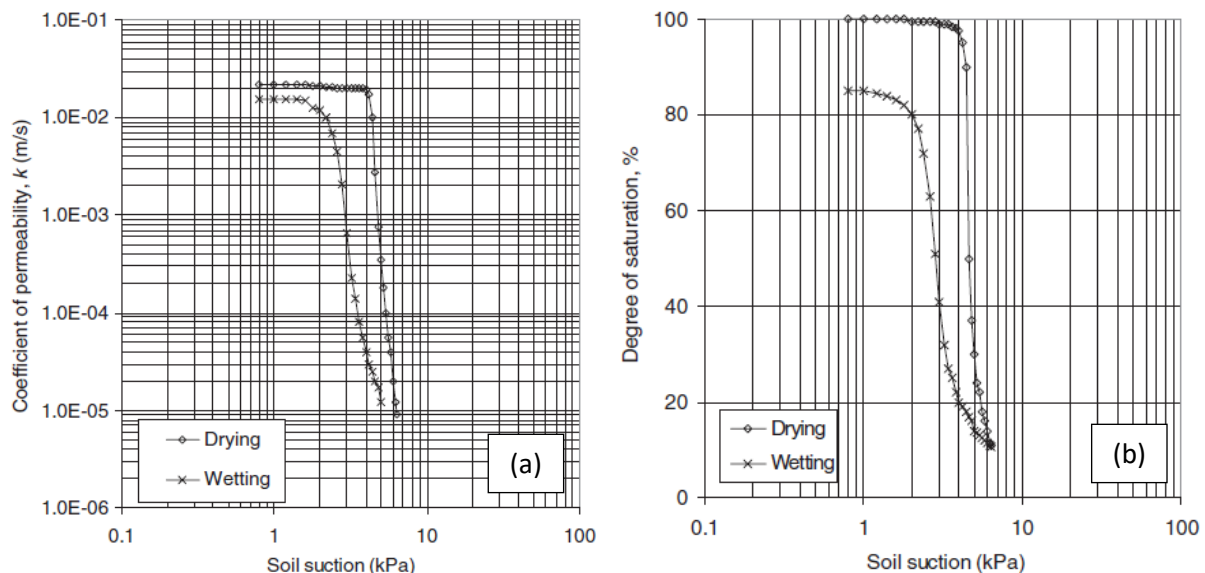


**Figure 40:** Measurements on glass beads undergoing drying and wetting process: a) permeability functions, and b) SWRC (Mualem 1976).

The coefficient of permeability respective to the water phase  $k_w$  in the unsaturated soil can be obtained by using various approaches. Different testing methods and devices can be used to directly measure points on the UHCF for different types of soil. These methods are usually based on Darcy's law for calculation of the hydraulic conductivity from the observed water flow rate due to the imposed hydraulic gradient. However, varying soil textures result in a wide range of matric suction for which the UHCF should be defined. Different stress conditions and hysteresis during the drying and wetting process can cause the need for determination of UHCF under specific conditions. Those usually reflect conditions that soil undergoes in-situ. In many studies problems that are specific for the soils undergoing volumetric deformation due to change of matric suction were reported. Long testing times, issues of control or measurement of matric suction, as well as maintaining the intimate hydraulic contact between tested soil and sensor during the test, result in expensive procedures for the determination of UHCF and very often some degree of uncertainty in measurement results. All of the above results with the fact that, to-date, no single test procedure or device could be used for determination of the UHCF for all types of soils, considering the wide matric suction range and varying testing conditions that might affect hydraulic properties of unsaturated soil. Another approach for obtaining the UHCF is to employ the inverse-analysis on measured water flow response data obtained under certain initial and boundary conditions. In this case, the water flow event is modeled by using some of the available UHCF models, and unknown model parameters are obtained by minimizing the objective function, which is usually defined as a difference between calculated and observed flow quantity. Various types of flow process can be modeled analytically or numerically, using different UHCF models. This technique requires specific engineering analyses but enables quick determination of UHCF by using the data obtained for a wide range of testing set-ups, from both transient and steady-state flow process. The most commonly used procedures to estimate the UHCF combine the coefficient of permeability in saturated conditions, which is much more easily measured in the laboratory, and the SWRC. In this case, similarities in shape of the SWRC and UHCF that were observed from numerous experimental studies are used to predict the shape of the UHCF, given that both the SWRC and  $k_s$  are quantities that are much easier to obtain experimentally than the UHCF itself. Direct and indirect methods for obtaining the UHCF are described in the following chapter.

### 5.1.1. Direct measurement of water flow properties

ASTM D7664-10 describes a family of test methods that can be used to define points on the UHCF for different types of soils, separating them in three main categories.

Category A includes different set-ups of column tests used to obtain UHCF from water content or suction measurements along the column of soil compacted into a rigid wall permeameter, during imposed transient and steady-state water flow process (ASTM D7664-10). UHCF can be obtained on initially unsaturated soil during either the downward infiltration or upward imbibition of water. In case of using initially saturated soil samples, the UHCF can be determined either for downward drainage or evaporation of water. While the first two methods are used for obtaining  $k_w$  values of fine-grained soils for matric suctions ranging from 0 to 80 kPa, the third method is used for coarser soil and matric suction values up to 200 kPa. An evaporation column test can be adopted to perform measurements from 0 to more than 1000 kPa of matric suction on all types of soil, except for high plasticity clays (ASTM D7664-10). For example, McCartney et al. (2007) performed an infiltration test on a clay specimen to obtain the hydraulic conductivity function. The schematic of soil column with a peristaltic pump for applying steady moisture flux at the specimens top, tipping bucket rain gauge for the collection of water draining out of the soil column, and different sensors for measurement of matric suction and water content along the specimen height during the infiltration process are shown in Figure 41 a). They obtained UHCF for both steady-state vertical infiltration of water (i.e., suction is constant with height of column and water flow is gravity-driven, since a unit hydraulic gradient exists in profile), when the hydraulic conductivity was equal to the applied flow rate (McCartney et al. 2007), and, transient flow of water by means of the instantaneous profile method (Watson 1966; Meerdink et al. 1996; Fujimaki and Inoue 2003). As a conclusion, McCartney et al. (2007) outlined several issues when using the transient and steady-state infiltration data for calculation of UHCF, including the outflow boundary effects on the moisture profile, the use of the SWRC to calculate suction values from measured volumetric moisture content values, calculation of the gradient terms, and fitting of the time series with smooth curves. Also, they found that the UHCF predicted by the van Genuchten – Mualem model (1980) generally under-estimated the measured values. Depending on the soil type, the instantaneous profile method can be time-consuming. For example, Cui et al. (2008) used the instantaneous profile method to determine the unsaturated hydraulic conductivity of compacted sand/bentonite mixture specimens by performing infiltration tests under constant volume and free-swell conditions. It took around 2200 h to complete the test. Finally, the accuracy of the

test is proportional to the distance between water content and suction measuring points. A greater number of sensors increases the experimental costs and can involve possible installation difficulties (Li et al. 2009). Li et al. (2009) proposed a wetting front advancing column test for measuring unsaturated hydraulic conductivity, as a modification of instantaneous profile method enabling measurements for a wider range of soils and suction values. This procedure combines theta-probes for monitoring of volumetric water content and tensiometers for matric suction measurements up to 80 kPa. Known SWRC and theta probes are used to predict matric suction values in a higher suction range. The wetting front advancing velocities for initially oven-dried specimen (Figure 41 b) are required for the calculation of the UHCF according to proposed data interpretation procedure. For five different types of soil, calculated UHCF agreed reasonably well with results obtained from the instantaneous profile method. Although observing wetting front advancement reduces the number of monitoring points along the soil column, measuring time is generally shortened and hydraulic conductivity data can be obtained from residual up to saturated conditions, the proposed method depends on an observed wetting front. Therefore, this method is applicable only to wetting tests performed on initially dry specimens, usually starting from high initial suction values, and that change color upon wetting (Li et al. 2009). For example, it can be challenging to observe wetting front in fine-grained soils, such as high-plasticity clays.

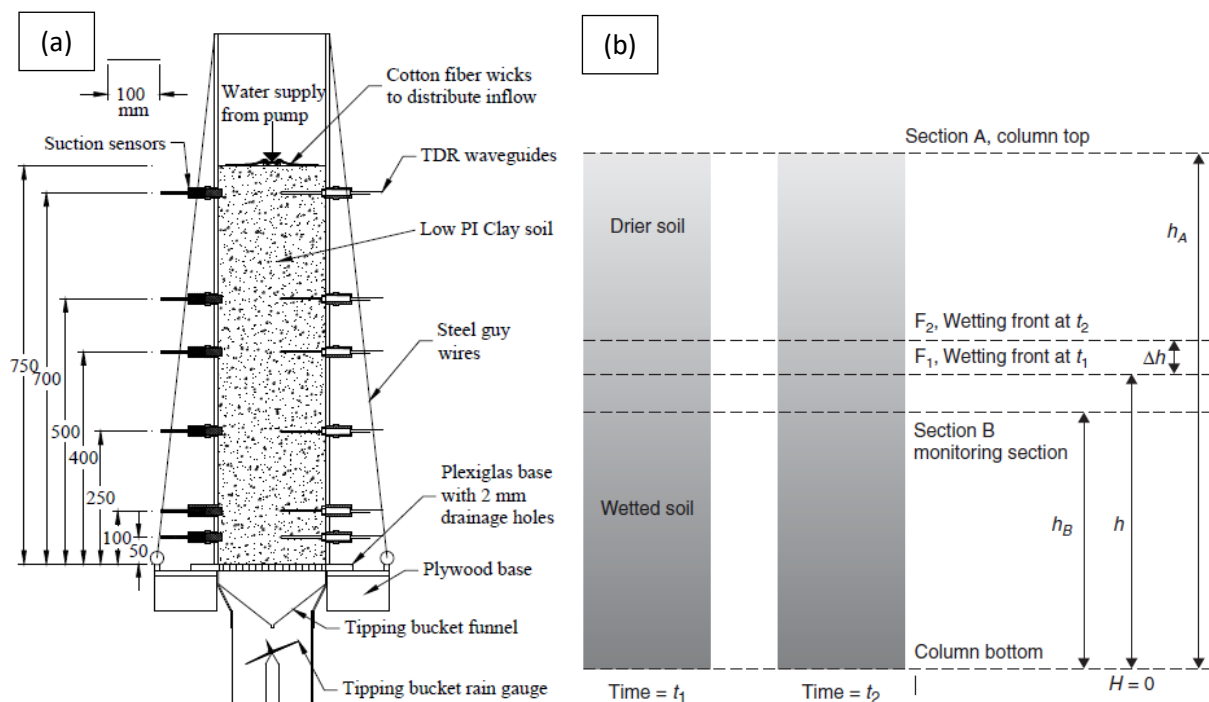


**Figure 41:** a) The schematic of soil column (McCartney et al. 2007), and b) wetting front advancement process in an initially air-dried soil column during the capillary-rise process (Li et al. 2009).

Category B includes two axis-translation methods commonly used for determination of SWRCs (ASTM D7664-10). Both the rigid-wall oedometer and flexible-wall permeameter methods are best suited for direct measurements of  $k_w$  for fine-grained soils, such as clays, from saturated conditions up to several hundred kPa of matric suction. The highest matric suction under which the measurement of permeability can be performed is usually defined by the AEV of the used ceramic disk and the highest air pressure that can be applied inside the testing system. The upper limit for the axis translation technique is usually considered to be 1,500 kPa. The HCF is defined from the outflow measurement when a hydraulic gradient is applied over the unsaturated soil specimen (ASTM D7664-10). The same limitations encountered when performing SWRC measurements exist in case of measuring the hydraulic permeability respective to the water phase at certain matric suction level, or degree of saturation. Those are, for example, the non-uniformity in soil suction value across the specimen height, the impedance to flow due to the low permeability of HAEPD, evaporation of water from the testing system or air diffusion through the HAEPD affecting the water volume change measurements, and low hydraulic permeability of unsaturated soils, especially at high matric suction values, which result in a prolonged testing time (ASTM D7664-10; Romero 1999; Fredlund et al. 2012). Long equilibration times, not reaching equilibration conditions, the effect of moisture loss through compressed air lines, and problems associated with slow rate of air diffusion to the air cavities at high degrees of saturation are problems that were encountered in many studies where the axis translation technique was adopted for measurement or control of matric suction (Leong et al. 2004; Di Mariano 2000; Romero 2001; Marinho et al. 2008). Figure 42 shows a flexible wall permeameter for unsaturated soil testing (a), and the practical limitations when using the axis translation technique for measuring the UHCF (b).

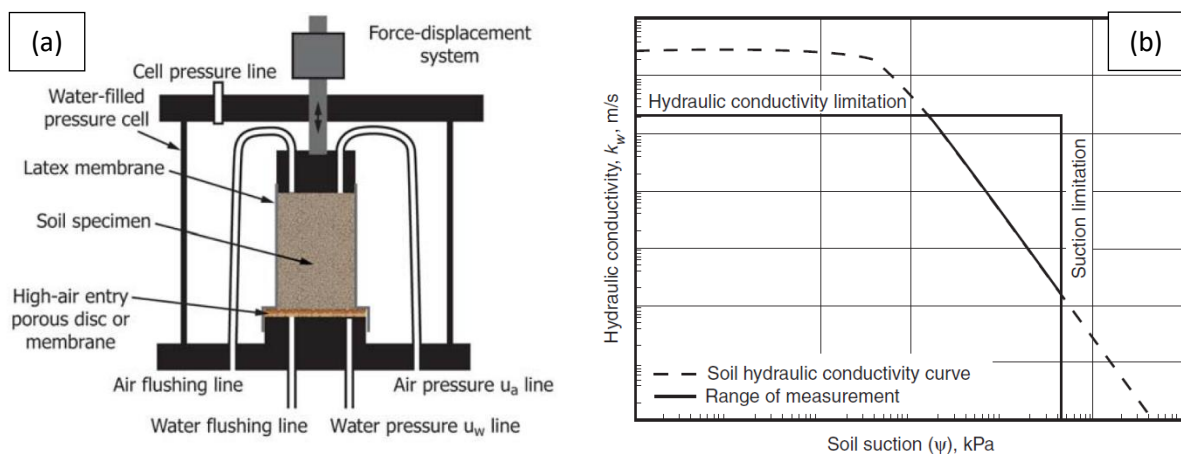


**Figure 42:** a) A schematic of the flexible-wall permeameter for unsaturated soils (ASTM D7664-10); and, b) limitation of the axis translation technique for determination of the UHCF (Fredlund et al. 2012).



However, this method enables measurement of the coefficient of permeability for matric suction up to the capacity of the HAEPD on undisturbed or compacted samples undergoing both, drying and wetting process, considering the effect of overburden pressure by applying different net vertical stress values, with continuous measurement of total volume and water volume changes during the test. Tests are usually performed started from saturated conditions on specimens consolidated under desired confining pressure. The saturated coefficient of permeability can be measured first by applying pressure differential at the top and bottom specimens end. The observed inflow and outflow volume readings and hydraulic gradient values provide data for calculation of  $k_s$  according to Darcy's law. Then the matric suction is usually increased while maintaining constant net stress value, and the flow process leading to desaturation of the soil specimen is induced. Constant hydraulic head gradient across the specimen is held during the equilibration stage. The steady-state condition is obtained when the inflow and outflow of water volume are about the same. For this equilibrium conditions under the constant value of applied matric suction, the water volume flow measurements and the head differential applied on the specimen can be used to calculate the coefficient of permeability  $k_w$ . One point on UHCF is obtained for measurements obtained at imposed matric suction level by using Darcy's law and steady-state flow (Huang et al. 1998). The procedure can be repeated for increased matric suction values in the drying path to obtain more points on the UHCF. If the hysteresis effects are considered, measurements can be obtained for reduced matric suction values in the wetting path, as well. For example, Huang et al. (1998) developed and used a triaxial permeameter to obtain the UHCF of consolidated slurry silty sand. Results showed that the hydraulic permeability is relatively constant for matric suction values between 0 and the AEV. After the AEV, the relationship becomes bilinear on a log-log scale (Figure 43).

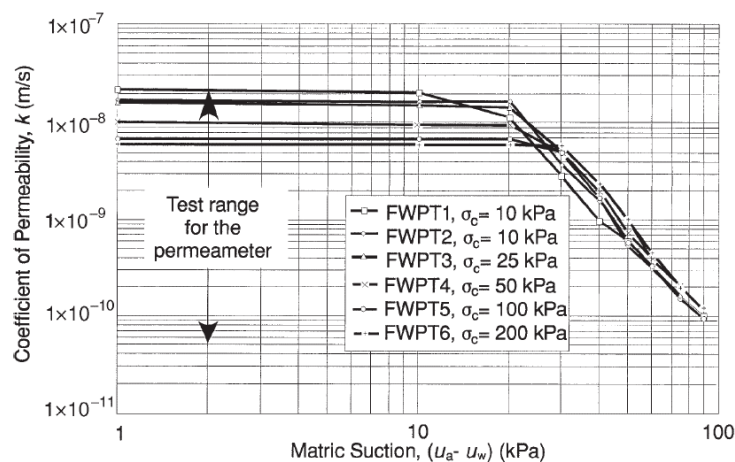


**Figure 43:** Coefficient of permeability respective to the water phase vs. matric suction obtained from flexible-wall permeability tests (Huang et al. 1998).

Agus et al. (2003) developed a flexible wall permeameter system for residual soils that enable measuring of water and air coefficients of permeability under high matric suction values, for specimens undergoing both drying and wetting process with total volume measurements during the test. They described various factors that can have an influence on measured data, such as hydraulic and pneumatic gradients and temperature fluctuations (Samingan et al. 2003). Gallage et al. (2013) developed a new apparatus for obtaining the UHCF of sandy soil over a low suction range (0-10 kPa) using the steady-state method and direct suction measurements by means of two tensiometers. They found that the hydraulic conductivity remained constant up to the AEV. After the matric suction exceeded the AEV of soil, a non-linear decrease of the hydraulic conductivity was observed. As the measurements were performed for drying and wetting process, a significant hysteresis of hydraulic conductivity plotted against the matric suction value became negligible when hydraulic conductivity was plotted against the water content (Gallage et al. 2013).

Category C includes a test method in which permeameter with soil sample is installed inside the spinning centrifuge to impose hydraulic gradients by increasing the effect of the elevation head (ASTM D7664-10). In comparison with standard column infiltration tests, this method allows performing infiltration of water through soil specimen at a much higher rate, with a significant reduction of testing time. UHCF points can be determined for matric suction values between 0 and 200 kPa. The method is applicable to coarse-grained and low-plasticity fine-grained soils (ASTM D7664-10). For example, Singh and Kuriyan (2002) used a geotechnical centrifuge to estimate hydraulic conductivity of silty soil in unsaturated condition from obtained SWRC. The centrifugation method was able to produce matric suction values up to 71 kPa. McCartney (2007) and Zornberg and McCartney (2010) developed a centrifuge permeameter shown in Figure 44. The most essential parts for hydraulic characterization of tested specimens are a water flow control system, instrumentation for measurement of the infiltration rate, volumetric water content (TDR), and matric suction (tensiometers) in flight during steady-state infiltration. McCartney and Zornberg (2010) used newly developed centrifuge permeameter to determine the SWRC and UHCF of a compacted, low plasticity clay under both drying and wetting paths by varying the inflow rate, the  $g$  level or both. Matric suction values ranged from 5 to 70 kPa while the measured hydraulic conductivity values ranged from  $2.0\text{E-}07$  to  $8.0\text{E-}11$  m/s.

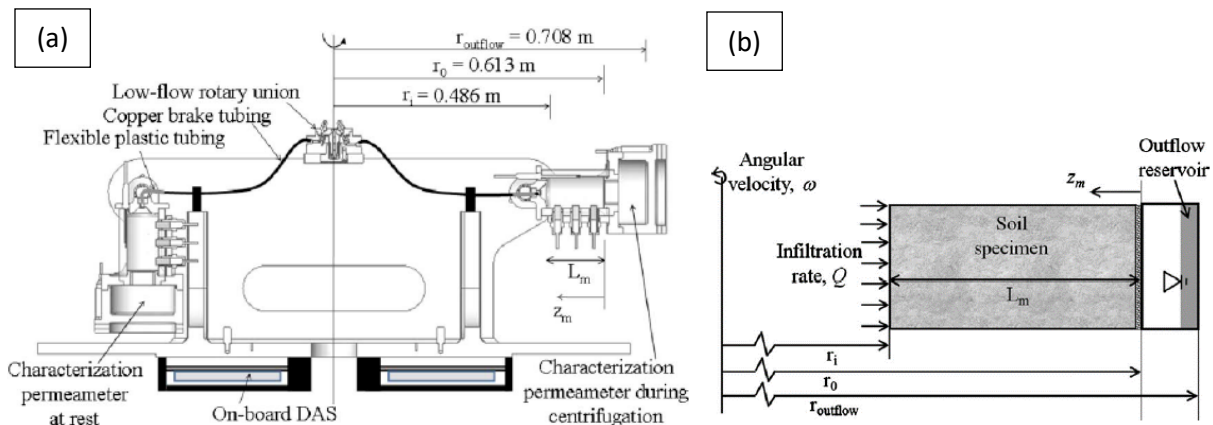


**Figure 44:** Centrifuge permeameter setup: a) testing environment and data acquisition hub; and b) schematic view of a centrifuge permeameter (Zornberg and McCartney 2010).

McCartney and Zornberg (2010) concluded that the obtained SWRCs and UHCFs were consistent with those obtained using pressure chamber and column infiltration tests. Although the obtained UHCFs had the same shape as those derived from predictive relationships, at the lower end of the volumetric water content range the discrepancy between the measured and predicted hydraulic conductivity values were around two orders of magnitude (McCartney and Zornberg 2010).

### 5.1.2. Estimation techniques for determination of UHCF

Experimental procedures used to measure the hydraulic conductivity of unsaturated soil directly are time-consuming and generally expensive. Devices and sensors used for determination of the UHCF are not a part of standard equipment found in geotechnical laboratories. Consequently, determination of the USPFs, especially UHCFs, is usually still too demanding and prohibitive for application in geotechnical engineering practice (Fredlund et al. 2012). As a result, the use of “estimation” techniques for obtaining different USPFs, such as SWRC, UHCF and the unsaturated shear strength from soil properties that are much easier to measure, or measurement results obtained from tests that are performed more routinely in geotechnical laboratories, have received significant attention. Many researchers, for example Zapata et al. (2000), Agus et al. (2003), Aubertin et al. (2003), Fredlund et al. (2012), Zhang and Fredlund (2015), Fredlund (2017), Heyerdahl and Pabst (2018) emphasize that implementation of unsaturated soil mechanics into routine geotechnical engineering practice greatly depends on different estimation techniques used to predict, rather than directly measure USPFs. Different estimation procedures for obtaining the UHCF are described in the following part.

ASTM D7664-10 outlines the possibility of using inverse methods to define the UHCF. Instead of using Darcy's law to calculate the  $k_w$  from measured water flow rate and known hydraulic gradients, this iterative, regression-based approach can be used to estimate the hydraulic properties which tested soil should have in order to obtain observed quantities, such as rate of water outflow from the specimen.

Kool et al. (1985) proposed the parameter estimation approach for determining SWRC and UHCF simultaneously from one-step outflow experiments. In this method, it is assumed that mathematical expression with a small number of parameters accurately describes the relationship between volumetric water content, hydraulic conductivity and, for example, pressure head. If the initially unknown parameters are obtained, the SWRC and UHCF are defined, as well. For the first iteration of numerical simulation, some initial guess values are set for the unknown parameter values. In the following iterations, simulations are repeated with constantly improved values of estimated parameters, until the difference between observed and calculated results is not less than some desired value. For example, Šimunek et al. (1998) used the governing flow equation for radially symmetric isothermal Darcian flow in a variably-saturated isotropic rigid porous medium given by the modified form of the Richard's equation

$$\frac{\partial \theta}{\partial t} = \frac{1}{r} \frac{\partial}{\partial r} \left( rK \frac{\partial h}{\partial r} \right) + \frac{\partial}{\partial z} \left( K \frac{\partial h}{\partial z} \right) + \frac{\partial K}{\partial z} \quad (24)$$

where  $\theta$  is the volumetric water content ( $\text{m}^3/\text{m}^3$ ),  $h$  is the pressure head (m),  $K$  is the hydraulic conductivity (m/s),  $r$  and  $z$  are radial and vertical coordinates (m), and  $t$  is time (s). The unsaturated hydraulic properties, retention and permeability functions, were described by van Genuchten's (1980) expressions

$$\theta_e = \frac{\theta(h) - \theta_r}{\theta_s - \theta_r} = \frac{1}{(1 + |\alpha h|^n)^m}, h < 0; \quad (25)$$

$$\theta_e = 1, h \geq 0.$$

$$K(\theta) = k_s \theta_e^{0.5} \left[ 1 - \left( 1 - \theta_e^{\frac{1}{m}} \right)^m \right]^2, \quad h < 0; \quad (26)$$

$$K(\theta) = k_s, \quad h \geq 0.$$

where  $\theta_e$  is the effective volumetric water content ( $\text{m}^3/\text{m}^3$ ),  $k_s$  is the saturated coefficient of permeability (m/s),  $\theta_r$  and  $\theta_s$  are residual and saturated volumetric water contents, and  $\alpha$ ,  $n$ , and  $m = 1 - 1/n$  are empirical parameters. For a fixed relation between  $n$  and  $m$  parameters, there are 5 unknown hydraulic parameters that define hydraulic properties of soil. Finally, the

objective function,  $\Phi$ , expressing the differences between experimentally measured and numerically predicted flow responses was defined as

$$\begin{aligned} \Phi(b, q, p) = & \sum_{j=1}^{m_q} v_j \sum_{i=1}^{n_{aj}} w_{ij} [q_j^*(x, t_i) - q_j(x, t_i, b)]^2 \\ & + \sum_{j=1}^{m_p} \bar{v}_j \sum_{i=1}^{n_{aj}} \bar{w}_{ij} [p_j^*(\theta_i) - p_j(\theta_i, b)]^2 + \sum_{j=1}^{n_b} \hat{v}_j [b_j^* - b_j]^2 \end{aligned} \quad (27)$$

where the first term on the right side represent deviations between measured and predicted space-time variables, such as cumulative inflow or outflow rate versus time, pressure heads or water contents at different locations and/or time. Here  $m_q$  term is the number of different sets of measurements, while  $n_{qj}$  is the number of measurements in a particular measurement set.  $q_j^*(x, t_i)$  represents specific measurements at time  $t_i$  for the  $j$ -th measurement set at location  $x(r, z)$ ,  $q_j(x, t_i, b)$  are the corresponding model predictions for the vector of optimized parameters  $b$ , in this case  $(\theta_r, \theta_s, k_s, \alpha, \text{ and } n)$ , and  $v_j$  and  $w_{i,j}$  are weights associated with a particular measurement point or set, respectively (Šimuněk et al. 1998). Differences between independently measured and predicted soil hydraulic properties, such as  $\theta(h)$ ,  $K(\theta)$ ,  $K(h)$ , etc. are represented by the second term on the right side of the equation (27), while the rest of the terms here have similar meaning as in the first term on the right side of the equation, but now for the soil hydraulic properties. The last term of the equation (27) represents a penalty function for deviations between prior knowledge of the soil hydraulic parameters  $b_j^*$ , and their final estimates,  $b_j$ , where  $n_b$  represent the number of parameters with prior knowledge and  $\bar{v}_j$  pre-assigned weights (Šimuněk et al. 1998). Levenberg-Marquardt nonlinear minimization method was used for the minimization of the objective function.

The uniqueness of the solution depends on a sufficiency of the input data (Kool et al. 1985). By considering the downward infiltration in vertical column test, Hornung (1983) found that the solution uniqueness is satisfied only if, besides the observed outflow rates from the column, additional information is included. In this case, additional input information was final steady-state pressure head at a certain point inside the soil column (Hornung 1983). Zachman et al. (1981) reported no problem regarding the uniqueness of the solution for a similar problem, involving gravity drainage from an initially saturated column. For a four-parameter model with two unknowns, observation of cumulative drainage in time yielded the best results (Zachman et al. 1981). Kool et al. (1985) obtained good results from one-step pressure outflow

experiments on sandy loam and clay loam, by using the cumulative outflow measurements in time. However, they emphasize that pressure increment should be selected to yield a relatively low final water content, while the input data should include a large portion (at least 50% of cumulative outflow) of the transient flow process. Finally, they concluded that accurate experimental measurements have to be used as input data, since the obtained solutions are sensitive to errors in measured data, while the guess values of initially unknown parameters should be reasonably close to their actual value to reduce chances of obtaining an erroneous solution and to speed-up the convergence process. By using the micro-tensiometer and pressure transducers on different soils, Eching and Hopmans (1993) found that computer optimization of the SWRC by the inverse solution technique using transient one-step and multistep outflow experiments was greatly improved when cumulative transient outflow data were combined with simultaneously measured pore-water pressure head data. Excellent results were obtained for one-step and multistep desorption experiments conducted on Yolo silt loam, Panoche loam, Hanford sandy loam, and Oso-Flaco fine sand. Another advantage of combining cumulative transient outflow data with water pressure head data is that testing time is significantly reduced since the water content data for equilibrium conditions are not required. By using the inverse method for determining the UHCF from one step outflow experiments on four soils with various textures, van Dam et al. (1992) found that reliable estimations of UHCF are obtained when cumulative outflow data are supplemented with the SWRC data. Van Dam et al. (1994) applied Marquardt's optimization algorithm on data collected from multistep outflow experiments performed on a set of 20 soil samples. The method resulted in unique estimates of the SWRC and UHCF, which was not the case for same experimental conditions of the one-step outflow method.

The parameter estimation method was applied for in-situ unsaturated hydraulic conductivity measurements. For example, Šimunek and van Genuchten (1996) used a parameter estimation procedure on data obtained from tension disc infiltrometers. In this procedure, the Levenberg-Marquardt nonlinear parameter optimization method was combined with a quasi-three-dimensional numerical model for solving the equation of water flow through unsaturated soil. Van Genuchten's model parameters were estimated from observed cumulative infiltration during the transient infiltration of water, as well as additional information, such as measured pressure head and water content at different points. They came to several important conclusions on optimal sampling design when using parameter estimation method on tension disc infiltrometer data to estimate hydraulic properties of unsaturated soil, such as number and selection of best measurement points in space and time. First, they concluded that

measurements of the instantaneous or cumulative infiltration rates alone, or with the addition of measured water contents from only one or two locations, do not provide uniqueness of solution for three-dimensional parameter space. Using only pressure head measurements in the profile already guaranteed convergence to the correct solution, while adding the cumulative infiltration rate did not improve the final solution. The best fit was obtained when simultaneously measured pressure head and water content data were included, with several points on the SWRC directly defined. However, the study was performed on numerically generated synthetic data, excluding the errors due to calibration or measurement procedure, which are always present in experimental studies. Gribb et al. (1996) used the parameter estimation method for determining hydraulic properties of fine sand from pore-water pressure and flow rate data obtained by a cone penetrometer method. Inoue et al. (1998) showed that the multistep soil-water extraction procedure could provide accurate soil hydraulic data for in-situ estimation of hydraulic properties of soil undergoing the drying process. Cumulative extraction volume and matric suction data were included in the analysis, which combines a numerical code for unsaturated water flow HYDRUS 2D (Šimunek et al. 1996) with the Levenberg-Marquardt's optimization algorithm. Due to the high sensitivity of the measured soil matric potential head close to the extraction device, Inoue et al. (1998) suggested that tensiometers should be located close the ceramic ring where the extraction vacuum is applied. Parameter sensitivity analysis showed that the method is least sensitive to the residual water content,  $\theta_r$ , and the saturated hydraulic conductivity,  $k_s$ , while strong sensitivity respective to the shape parameters  $\alpha$  and  $n$  of the van Genuchten's model was observed (Inoue et al. 1998). Šimunek et al. (1998) briefly reviewed all of three field methods that can be used for estimating the soil hydraulic properties by way of the parameter estimation method. Again, the HYDRUS-2D code coupled with the Levenberg-Marquardt parameter estimation algorithm was used. Ramos et al. (2006) obtained great estimates of the SWRC using the numerical inversion of tension infiltration data of four coarse- to medium-textured soil in Alentejo (Portugal). The UHCF estimates were reasonable, but less accurate when compared to retention properties. Some of the more recent progress in numerical procedures, sensitivity analysis, identification and estimation of parameters from various models that describe hydraulic properties of unsaturated soils (SWRC and UHCF) by inverse analysis, both for the laboratory or in-situ application, can be found in, for example, Nakhaei (2014), Fatehnia and Tawfiq (2014), Chidichimo et al. (2015), Sprenger et al. (2015), Wassar et al. (2016), Bouchemella et al. (2016), Hayek (2016), Chen et al. (2016), Sedaghatdoost et al. (2017), Naik et al. (2018), etc.

The procedures mentioned above can be used to estimate UHCF without the need for direct measurement of permeability in unsaturated conditions. For example, only SWRC measurements can be used, which are much simpler and cheaper. Despite that, complex calculation procedures and specialized engineering analyses required when estimating the UHCF by inverse methods result in very limited application in engineering practice. Fredlund et al. (2012) distinguish four categories of models used for the estimation of the unsaturated coefficient of permeability functions, namely: (i) empirical models, (ii) statistical models, (iii) correlation models, and (iv) regression models. Among those four, empirical and statistical models appear to be most extensively used in geotechnical engineering (Zhang and Fredlund 2015).

Empirical models make use of the similar character of the SWRC and UHCF, and use this similarity in an empirical manner to estimate the permeability function. An example of the equation for predicting the hydraulic permeability derived in empirical manner is that proposed by Brooks and Corey (1964). In their work, they distinguish the wetting phase, i.e., water, and non-wetting phase, i.e., air, that can exist in soil pores. First, by plotting the water retention curve results in log-log form, with water content expressed in terms of the effective degree of saturation  $S_e$ , defined previously by equation (9), they discovered that, for a wide range of soil textures, soil commences desaturation at linear rate after the AEV of soil is exceeded. The rate of desaturation was defined through the pore-size distribution index,  $\lambda$ , according to the previously defined equation (20). Unknown parameters  $S_r$ ,  $\lambda$ , and  $\psi_b$  can be obtained by fitting the experimentally obtained SWRC data. Further, the effective degree of saturation was substituted into Burdine's equation (1953) for the relative wetting phase permeability to obtain the following expression

$$K_{rw} = \left( \frac{S - S_r}{1 - S_r} \right)^2 \frac{\int_0^S \frac{1}{\psi_b^2} dS}{\int_0^1 \frac{1}{\psi_b^2} dS} = (S_e)^2 \frac{\int_0^{S_e} \frac{1}{\psi_b^2} dS_e}{\int_0^1 \frac{1}{\psi_b^2} dS_e} \quad (28)$$

where  $K_{rw} = K_e/K_w$  is the relative wetting phase permeability,  $K_e$  is the effective permeability respective to part of void filled with water, and  $S$  being the degree of saturation. Finally, by substituting derived SWRC equation (20) into (28) and after performing the indicated integration, Brooks and Corey (1964) obtained the following expression for the relative wetting phase permeability



$$K_{rw} = (S_e)^{\frac{2+3\lambda}{\lambda}} = \left(\frac{\psi_b}{\psi}\right)^\eta; \quad \psi \geq \psi_b \quad (29)$$

where  $\eta = 2 + 3\lambda$ . Today, Brooks and Corey permeability equation is usually expressed as the coefficient of permeability respective to the water phase regarding the matric suction by the following equation

$$k_w = k_s \left(\frac{\psi_b}{\psi}\right)^{2+3\lambda}; \quad \psi \geq \psi_b \quad (30)$$

Statistical models make use of the fact that the pore-size distribution mainly controls both the permeability and retention characteristics of the soil. Consequently, the UHCF was developed based on the interpretation and application of the SWRC (Zhang and Fredlund 2015). To calculate the UHCF by using some of the statistical models, the saturated coefficient of permeability,  $k_s$ , and the SWRC have to be known for considered soil. Three commonly used integral formulas from this group of models are Childs and Collis-George's (1950), Burdine's (1953) and Mualem's (1976) models.

The Brooks and Corey (1964), van Genuchten (1980) and Fredlund and Xing (1994) are the SWRC equations that are most widely used to solve a wide range of problems in geotechnical engineering practice.

By assuming that change of matric suction does not change total volume of soil, Childs and Collis-George (1950) suggested a model for estimating the coefficient of permeability based on randomly interconnected pores with a certain statistical distribution. After some modifications by Kunze et al. (1968), it can be written in the following form

$$k_r(\theta_w) = \frac{\int_0^{\theta_w} \frac{(\theta_w - \xi)}{\psi^2} d\xi}{\int_0^{\theta_s} \frac{(\theta_w - \xi)}{\psi^2} d\xi} \quad (31)$$

where  $k_r = k_w/k_s$  is the relative water coefficient of permeability;  $k_w$  and  $k_s$  are the (unsaturated) coefficient of permeability respective to water phase and saturated coefficient of permeability, respectively,  $\theta_w$  and  $\theta_s$  are the volumetric and saturated volumetric water content, while  $\psi$  and  $\xi$  represent matric suction and a dummy integration variable (Agus et al. 2003). Fredlund et al. (1994) introduced Fredlund and Xing (1994) SWRC equation (22) into the Childs and Collis-George (1950) model to compute a water permeability function. By integrating along the entire SWRC, they proposed the following expression for calculating the coefficient of permeability as a function of matric suction

$$k_w(\psi) = k_s \frac{\int_{\ln(\psi)}^b \frac{\theta(e^y) - \theta(\psi)}{e^y} \theta'(e^y) dy}{\int_{\ln(\psi_{AEV})}^b \frac{\theta(e^y) - \theta_s}{e^y} \theta'(e^y) dy} \quad (32)$$

where  $\psi_{AEV}$  is the AEV of the soil for which hydraulic conductivity is being estimated,  $e^y$  is a natural number raised to the dummy variable power, and  $\theta'$  represent the derivative of the SWRC equation (22) (Fredlund et al. 2012).

The following equation can express the Burdine (1953) model for calculation of the relative coefficient of permeability respective to the water phase

$$k_r(\theta_w) = \Theta^2 \frac{\int_0^{\theta_w} \frac{d\theta_w}{\psi^2}}{\int_0^{\theta_s} \frac{d\theta_w}{\psi^2}} \quad (33)$$

where  $k_r = k_w/k_s$  is the relative water coefficient of permeability;  $k_w$  and  $k_s$  are the (unsaturated) coefficient of permeability respective to water phase and saturated coefficient of permeability, respectively,  $\Theta$  is the normalized volumetric water content previously defined by equation (10),  $\theta_w$  and  $\theta_s$  are the volumetric and saturated volumetric water content, while  $\psi$  denotes the matric suction. The term  $\Theta^2$  is used to account for the effect of tortuosity of water flow path and was found to improve the prediction of permeability significantly, compared with the same equation where the correction factor is omitted (Agus et al. 2003; Fredlund et al. 2012).

By analyzing a conceptual model similar to that of the Childs and Collis-George (1950), Mualem (1976) proposed the following equation for the relative coefficient of permeability

$$k_r(\theta_w) = \Theta^{0.5} \left( \frac{\int_0^{\theta_w} \frac{d\theta_w}{\psi^2}}{\int_0^{\theta_s} \frac{d\theta_w}{\psi^2}} \right)^2 \quad (34)$$

where  $k_r = k_w/k_s$  is the relative water coefficient of permeability. Van Genuchten introduced his three-parameter equation (21) into Burdine's model (1953) to obtain an equation for the UHCF. By fixing the relationship between two fitting parameters according to the following expression

$$m = 1 - 2/n \quad (35)$$

van Genuchten (1980) reduced the number of fitting parameters in his SWRC equation to only two. In this way, the following closed-form permeability equation for calculating the coefficient

of permeability as a function of matric suction was obtained from Burdine's integration procedure

$$k_w(\psi) = k_s \frac{1 - (\alpha\psi)^{n-2}[1 + (\alpha\psi)^n]^{-m}}{[1 + (\alpha\psi)^n]^{2n}} \quad (36)$$

where  $\alpha$ ,  $n$ , and  $m = 1 - 2/n$  are constants from the Van Genuchten (1980) SWRC equation (21) (van Genuchten 1980; Fredlund et al. 2012).

Similarly, van Genuchten (1980) obtained a closed-form equation by using the Mualem's (1976) model. By proposing the following fixed relationship between two fitting parameters,  $n$  and  $m$

$$m = 1 - 1/n; \quad 0 < m < 1, \quad (37)$$

the following expression was obtained for calculating the coefficient of permeability

$$k_w(\psi) = k_s \frac{\{1 - (\alpha\psi)^{n-1}[1 + (\alpha\psi)^n]^{-m}\}^2}{[1 + (\alpha\psi)^n]^{0.5}} \quad (38)$$

Equations (36) and (38) are commonly referred to as the van Genuchten-Burdine permeability equation, and the van Genuchten-Mualem permeability equation, respectively (van Genuchten 1980). Both the van Genuchten (1980) and Fredlund and Xing (1994b) expressions for estimating the UHCF of soil are commonly integrated with software products for modeling groundwater flow problems. Many studies (e.g., Chiu and Shackelford 1998; Leong and Rahardjo 1997; Agus et al. 2003; Cai et al. 2014; Rahimi et al. 2015) evaluated the performance of predictive methods that estimate the UHCF of soil from known SWRC and  $k_s$  against directly measured unsaturated hydraulic conductivity functions for different types of soil, testing conditions, and specimen preparation techniques. By using twenty sets of data found in literature, which included measurements of both SWRC and  $k_w(\psi)$  on different soil types, ranging from sand to clay, Rahimi et al. (2015) concluded that the best-fit SWRC equation has a more significant effect on the estimation of the UHCF than the relative permeability equation used in calculation procedure. Agus et al. (2003) assessed the performance of all three previously described statistical models in combination with different SWRC equations. For the investigated soils (24 sets of data for different soil textures) they have found that all the statistical models provide reasonable estimates of the UHCFs, with a coefficient of determination ( $R^2$ ) ranging from 0.60 to 0.92. For different types of soil, the best fit for the experimental data was generally obtained for Mualem's (1976) model combined with the Fredlund and Xing (1994) SWRC equation (Leong and Rahardjo 1997; Agus et al. 2003).

## 5.2. Testing program for determination of the UHCF

In this section measurement results for the determination of the saturated and unsaturated coefficient of permeability obtained on undisturbed (and disturbed) samples of residual soil from a flysch rock mass are presented. A constant head method was used in the standard triaxial apparatus and falling head method in the conventional oedometer device. SWRC measurement results obtained with the HYPROP device were used to calculate the coefficient of permeability with respect to the water phase for matric suction values up to 130 kPa. Darcy-Buckingham law and the extended evaporation method (Schindler et al. 2015) were used on data obtained from undisturbed specimens undergoing a drying process to calculate the UHCF. Finally, obtained  $k_s$  SWRC equation parameter values were used for estimation of the UHCFs of residual soil from a flysch rock mass undergoing the drying and wetting process.

### 5.2.1. Measurements of the saturated coefficient of permeability

Saturated hydraulic conductivity was measured on both undisturbed and remolded and consolidated samples in the Geotechnical laboratory at UniRi. Falling head method (ASTM D5084-03) was performed with a standard test for determination of one-dimensional consolidation properties (ASTM D 2435-96) in conventional, front-loading oedometer apparatus 26-WF0302 (Controls S.p.A.). Tests were performed on undisturbed specimens under constant total stress increments of 12, 25, 50, 100, 200, 400, and 800 kPa. Change of the water level in burette through time was used to calculate the saturated coefficient of permeability  $k_s$  according to the equation

$$k_s = \frac{a L}{A \Delta t} \ln \left( \frac{h_1}{h_2} \right) \quad (39)$$

where  $a$  refers to the cross-sectional area of the burette tube ( $\text{m}^2$ ),  $L$  is the length of the specimen (m),  $A$  is the cross-sectional area of the specimen ( $\text{m}^2$ ),  $\Delta t$  is time interval (s) over which head loss  $h_1$  to  $h_2$  occurs (ASTM D5084 -03). Readings were taken only 24 hours after the application of load. To account for possible evaporation effects, readings were performed simultaneously on two burettes, where one was exposed only to the evaporation effects.

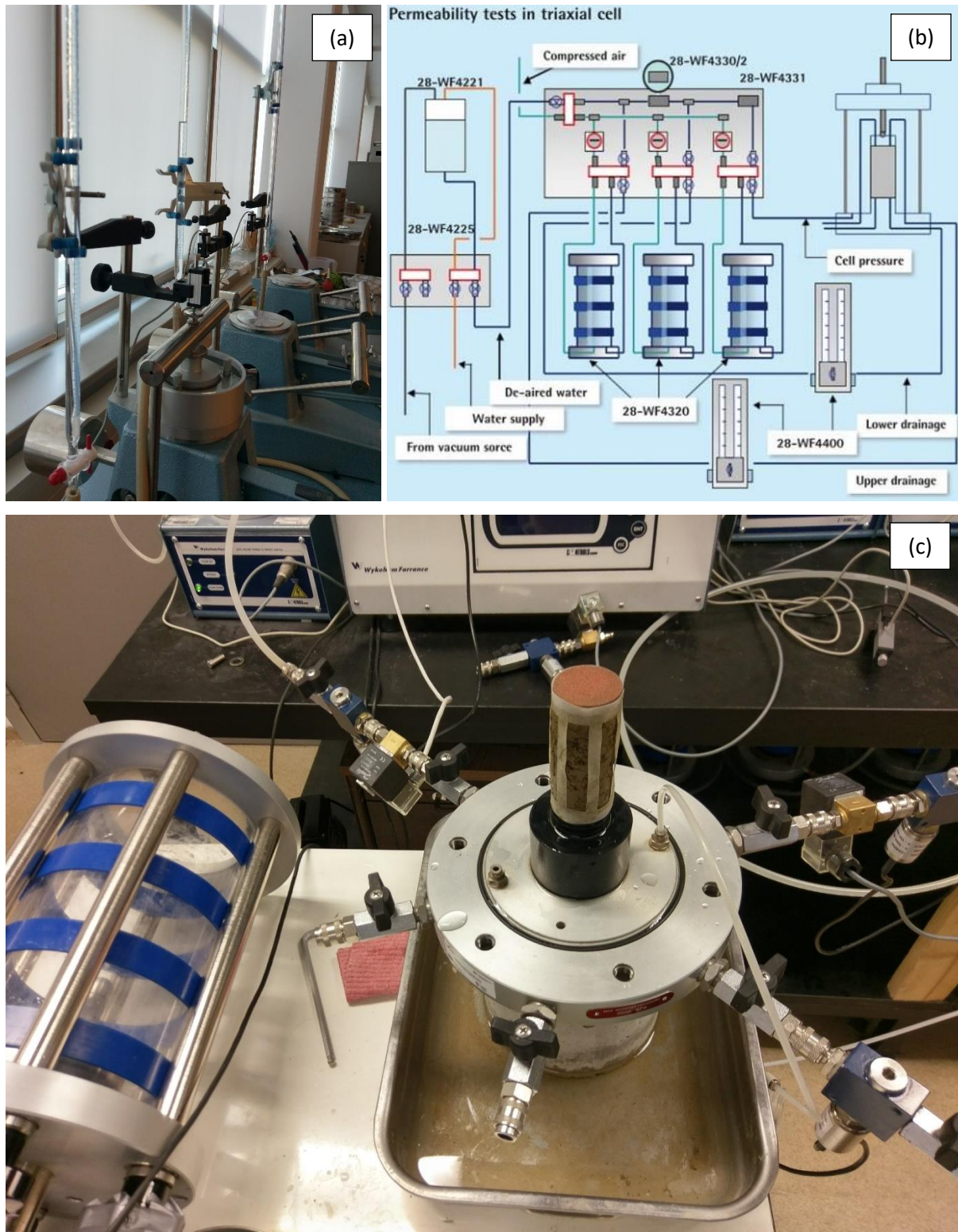
Constant head method tests (ASTM D5084-03) were performed using the triaxial apparatus 28-WF4050 (Controls S.p.A.) with the ability to perform permeability measurements on saturated soil specimens. The test is performed using a triaxial cell fit with 5 no-volume

change valves: 2 for the upper drainage, 2 for the lower drainage and 1 for the water pressure (Wykeham Farrance 2010). Three independent pressure systems are connected to the cell: for the drainage line at the top of the specimen, the drainage line to the base of the specimen, and for the application of cell pressure. Tests were performed on undisturbed and remolded specimens, isotropically consolidated under different effective stress values. Remolded specimens were trimmed from the cake prepared from a thoroughly mixed material having a water content above the liquid limit and consolidated under 50 kPa of vertical stress. Saturation of the test specimens was performed by using the incremental saturation with back-pressure until  $B$  value  $\geq 0.95$  was measured. As confirmed from obtained  $B$  values, specimens trimmed from the cake were practically installed in the cell at the fully saturated condition. In the case of undisturbed samples installed with a different initial degree of saturation values, a back pressure value as high as 350 kPa was applied during the saturation procedure to reach the criteria mentioned above. In the following steps, specimens were isotropically consolidated at the effective stress values of 25, 50, 100, 200, and 400, by increasing the cell pressure and keeping the back pressure at a constant value. After every step of consolidation, at a given effective stress and void ratio, hydraulic conductivity was measured by applying small pressures difference at the top and bottom of the specimen. Specimens with a diameter of 38 mm and diameter to length ratio of 1/2 were used in all tests, with mean values of applied hydraulic gradient  $i$  equal to 6.8. The saturated coefficient of permeability was calculated at given effective stress and void ratio from obtained flow measurement data and applied hydraulic gradient according to Darcy's law and the following equation

$$k_s = \frac{\Delta Q L}{A h \Delta t} \quad (40)$$

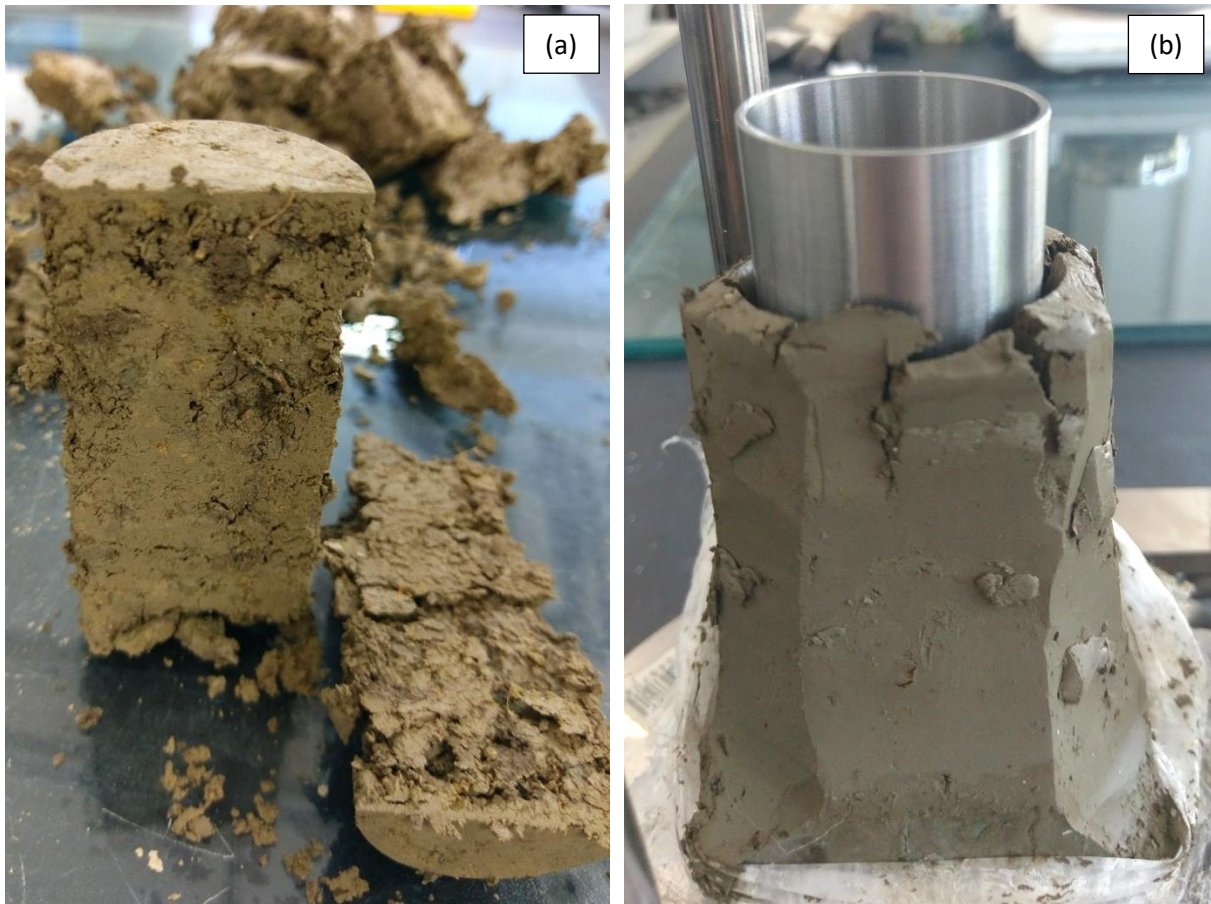
where  $\Delta Q$  (m<sup>3</sup>) represents the quantity of flow for given time interval  $\Delta t$  (s) over which flow occurs, while,  $h$  denotes the average head loss across the specimen (m of water) (ASTM D5084-03).

Figure 45 represent devices used for determination of the saturated coefficient of permeability. Some details on texture difference between undisturbed and remolded specimens are shown in Figure 46. Obtained results are summarized in the following part.



**Figure 45:** Devices used for measurements of the saturated coefficient of permeability  $k_s$  in the Geotechnical laboratory at UniRi: a) front-loading oedometer apparatus 26-WF0302 (Controls S.p.A.) (<http://www.controls-group.com/eng/soil-mechanics-testing-equipment/permeability-system-using-triaxial-cell.php>); b) sketch of the permeability system using the triaxial apparatus 28-WF4050 (Controls S.p.A.), and c) undisturbed specimen with side drains after the permeability test.





**Figure 46:** Samples used for determination of the saturated coefficient of permeability: a) undisturbed, and b) completely remolded and consolidated.

### 5.2.2. Measurements of the unsaturated coefficient of permeability

The HYPROP device (HYdraulic PROPerTy analyzer) can be used to provide measurements of the water retention curve and the hydraulic conductivity function using the extended evaporation method (Schindler et al. 1980). Tests were performed on undisturbed samples taken in a stainless steel cylinder 8 cm in diameter and 5 cm height, starting from the natural water content ( $HYP_{w_n}$ ), or saturated inside a steel cylinder by immersion into water with ( $HYP_1$ ) and without application of a small vacuum ( $HYP_2$ ). Water content, the degree of saturation and the void ratio calculated for each specimen before and after the saturation are summarized in Table 9. Some weight was placed on the top porous stone during the saturation stage to prevent possible swelling during the water imbibition. A void ratio was assumed to be constant during the 24 hours of saturation.

**Table 9:** Water content, the degree of saturation and void ratio for specimens tested in HYPROP device.

Specimen designation	Void ratio, $e$ [ $l$ ]	Before saturation, at $w_n$		After saturation, before test	
		Water content, $w$ [%]	Degree of saturation, $S$ [%]	Water content, $w_i$ [%]	Degree of saturation, $S_i$ [%]
HYP $w_n$	0.86	25.0	78.0	24.7	77.0
HYP $_1$	0.73	20.8	76.0	25.3	93.0
HYP $_2$	0.75	23.2	83.0	27.8	100.0

The coefficient of permeability respective to the water phase can be calculated as a function of matric suction from the HYPROP test results according to the Darcy-Buckingham law according to the following expression

$$k_w(\Psi_{mean}) = \frac{\Delta m}{\alpha A \rho_{H_2O} \Delta t i_m} \quad (41)$$

where  $\Psi_{mean}$  is the mean tension over the upper and the lower tensiometers, geometrically averaged over a time interval of  $\Delta t_i = t_{i+1} - t_i$ , with  $i = 1 \dots n$ ,  $j = 1 \dots n - 1$ ,  $\Delta m$  representing the sample mass difference in time interval recorded by the precise scale (g), which is assumed to be equal to volume of water loss  $\Delta V_w$  due to evaporation from specimen;  $\rho_{H_2O}$  is density of water, assumed to be 1 (g cm<sup>-3</sup>),  $\alpha$  is the flux factor depending on the soil type being tested,  $A$  denotes the cross-section area of specimen (cm<sup>2</sup>), and  $\Delta i_m$  denotes the hydraulic gradient averaged over the time interval (Schindler et al. 2015).

A schematic illustration of the device is shown in Figure 47, with geometric conditions relevant to the calculation of the permeability coefficient. The water loss from the sample due to evaporation is automatically recorded by placing the sample on a high-precision scale, and the negative water pressures are measured directly using two mini-tensiometers installed in predrilled holes at different heights. No volume changes were measured due to evaporation during the suction increase, and results are shown regarding the gravimetric water  $w$ . Cavitation problems associated with suction measurements performed by tensiometers usually limit the use of the simplified evaporation method on coarse-grained soils, and a HYPROP device is thus preferred for measurements on sands and silts. However, by using the tensiometer-preconditioning procedure (Schindler et al. 2010), measurements for the SWRC and UHCF were obtained for the drying process up to 130 kPa of matric suction. To decrease the suction difference between two tensiometers, the evaporation rate was decreased by putting a screen around the specimen.



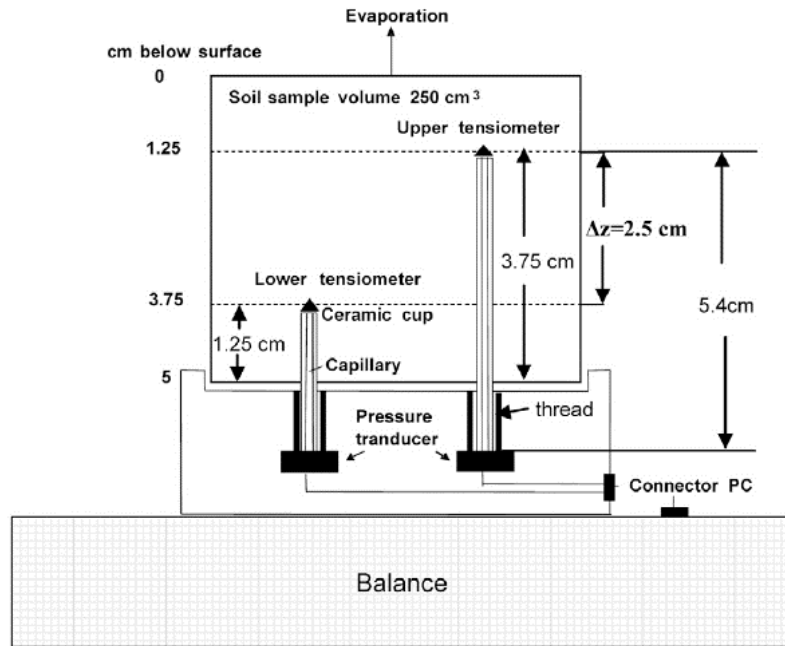


**Figure 47:** Schematic illustration of the HYPROP (Hydraulic PROPerTy analyzer) device (Schindler et al. 2015).

### 5.3. Test results and estimation of the UHCF

Direct measurement results of the coefficient of permeability and the estimated UHCF are presented here. Results obtained from the falling head method performed in standard oedometer apparatus on undisturbed samples under varying values of the effective vertical stress are summarized in Table 10. Results obtained on undisturbed and disturbed samples consolidated at different mean effective stress values, by using the constant head method in standard triaxial apparatus with attachments for permeability tests are presented in Table 11.

**Table 10:** The saturated coefficient of permeability from falling head tests performed in standard oedometer apparatus.

Effective vertical stress, $\sigma_v'$ [kPa]	Void ratio, $e$ [/]	Coefficient of permeability, $k_s$	
		[cm/s]	[cm/day]
25	0.87	/	/
50	0.84	1.30E-08	1.12E-01
100	0.78	2.30E-09	1.99E-02
200	0.72	4.60E-10	3.97E-03
400	0.63	1.20E-10	1.04E-03
800	0.56	6.70E-11	5.79E-04

**Table 11:** The saturated coefficient of permeability from constant head tests performed in conventional triaxial apparatus with attachments for permeability tests.

Mean eff. stress, $p'$ [kPa]	Void ratio, $e$ [ $\text{[]}$ ]	Undisturbed sample		Void ratio, $e$ [ $\text{[]}$ ]	Remolded sample	
		Coeff. of permeability, $k_s$ [cm/s]	Coeff. of permeability, $k_s$ [cm/day]		Coeff. of permeability, $k_s$ [cm/s]	Coeff. of permeability, $k_s$ [cm/day]
25	0.95	4.60E-08	3.97E-01	0.97	3.50E-10	3.02E-03
50	0.90	2.79E-08	2.41E-01	0.93	1.64E-10	1.42E-03
100	0.85	2.71E-09	2.34E-02	0.88	4.98E-11	4.30E-04
200	0.80	3.02E-10	2.61E-03	0.81	2.50E-12	2.16E-05
400	0.75	9.39E-11	8.11E-04	/	/	/

All measurement results of permeability in saturated conditions are summarized respective to the effective vertical stress, in case of the oedometer apparatus, or mean stress, in case of the triaxial apparatus in Figure 48. Variations of the saturated coefficient of permeability with a change in the void ratio are summarized in Figure 49.

Calculated values of the coefficient of permeability respective to the water phase obtained with the HYPROP evaporation method device (Decagon Devices Inc.) are shown in Figure 50, along with the saturated coefficient of permeability values. As expected, the lowest conductivity values under negative pore water pressures were obtained for sample starting from the natural water content, although it had a higher void ratio than two samples which were saturated prior testing. A somewhat greater scatter in measurement results for HYP<sub>1</sub> and HYP<sub>2</sub> tests is due to reduced evaporation rate and temperature effects. Although the heterogeneity of samples could affect measurement results and, due to the duration and costs, the number of performed tests is relatively low, the results obtained on undisturbed samples greatly differ from those obtained on disturbed samples. The latter suggests that use of undisturbed samples should be preferred when measuring hydraulic properties of the residual soil from a flysch rock mass. For example, the coefficient of saturated permeability was found to be around two orders of magnitude lower for remolded samples. Although the degree of saturation was not measured with the HYPROP evaporation method device, results seem to agree reasonably well with the measurements performed on saturated specimens and, in general, the coefficient of permeability decreases as the matric suction is increased during the test. Finally, the saturated coefficient of permeability value of  $k_s = 4.60\text{E-}08 \text{ m/s}$  was adopted along with the SWRC equation parameters obtained for the drying and wetting process to estimate the UHCF of the soil. Van Genuchten-Mualem (1980) and Fredlund and Xing (1994) models were used to predict the UHCF according to equations (38) and (32), respectively. Results are shown in Figure 51.

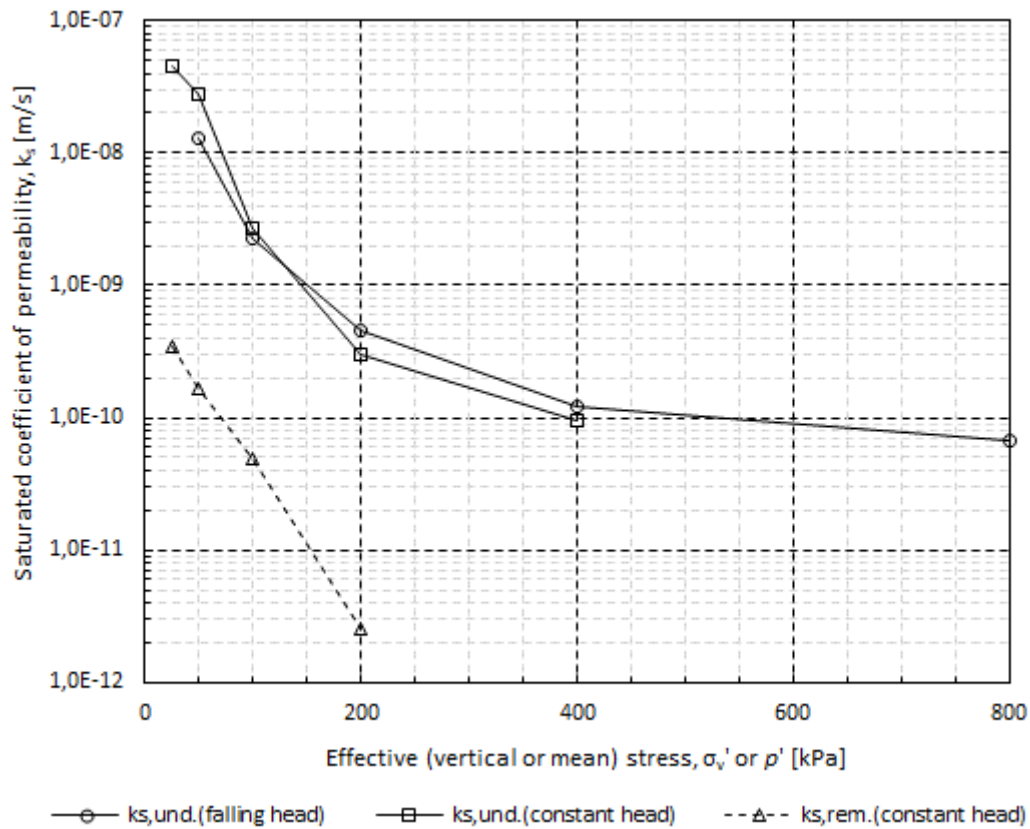


**Figure 48:** The saturated coefficient of permeability vs. effective (vertical or mean) stress for undisturbed and remolded samples of residual soil from a flysch rock mass.

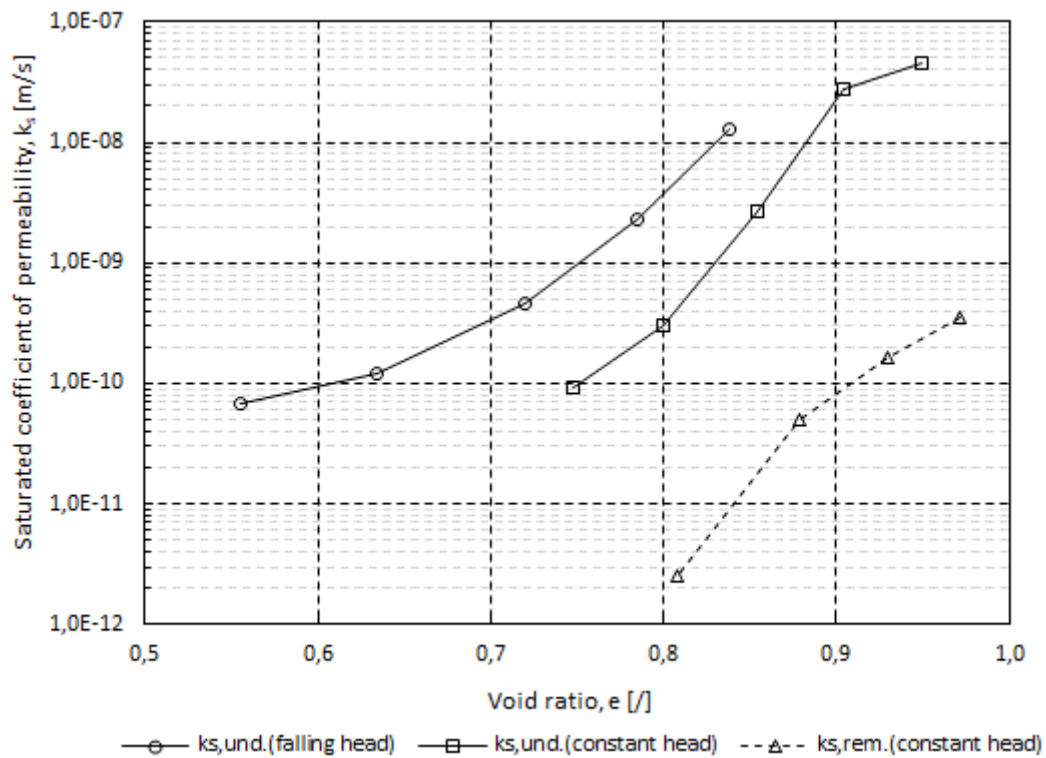


**Figure 49:** The saturated coefficient of permeability vs. void ratio for undisturbed and remolded samples of residual soil from a flysch rock mass.

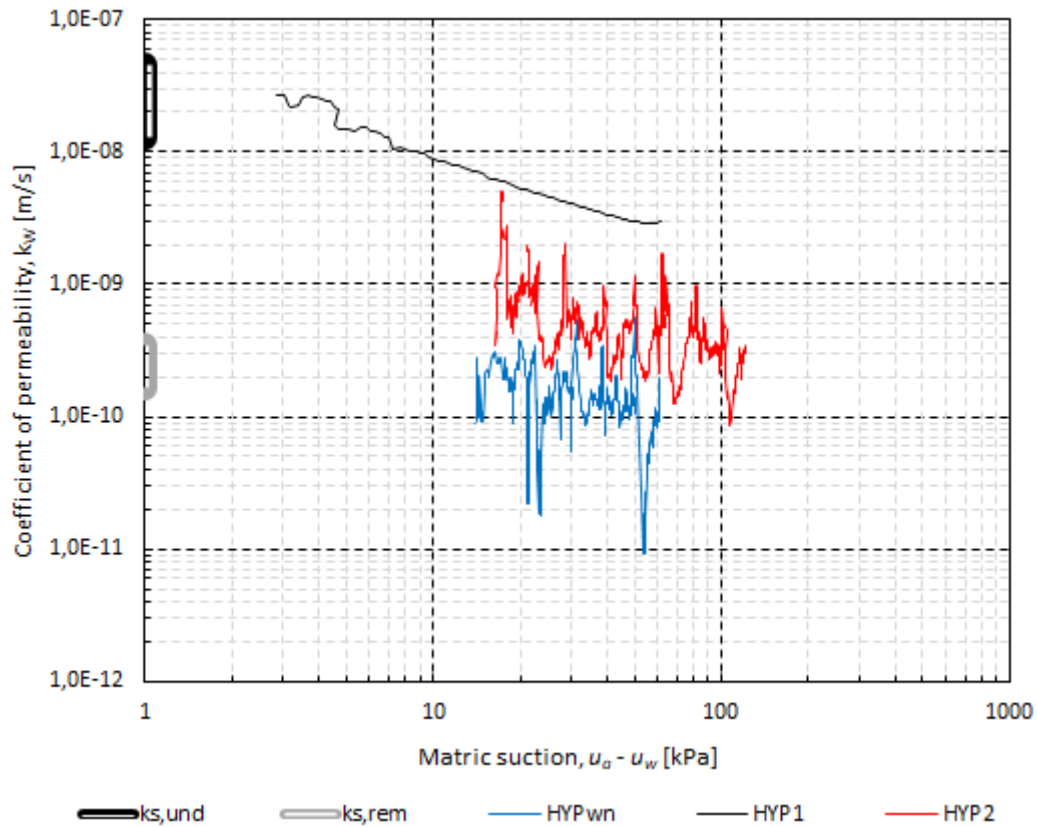


**Figure 50:** Coefficient of permeability respective to the water phase calculated from the HYPROP evaporation method device (Decagon Devices Inc.).

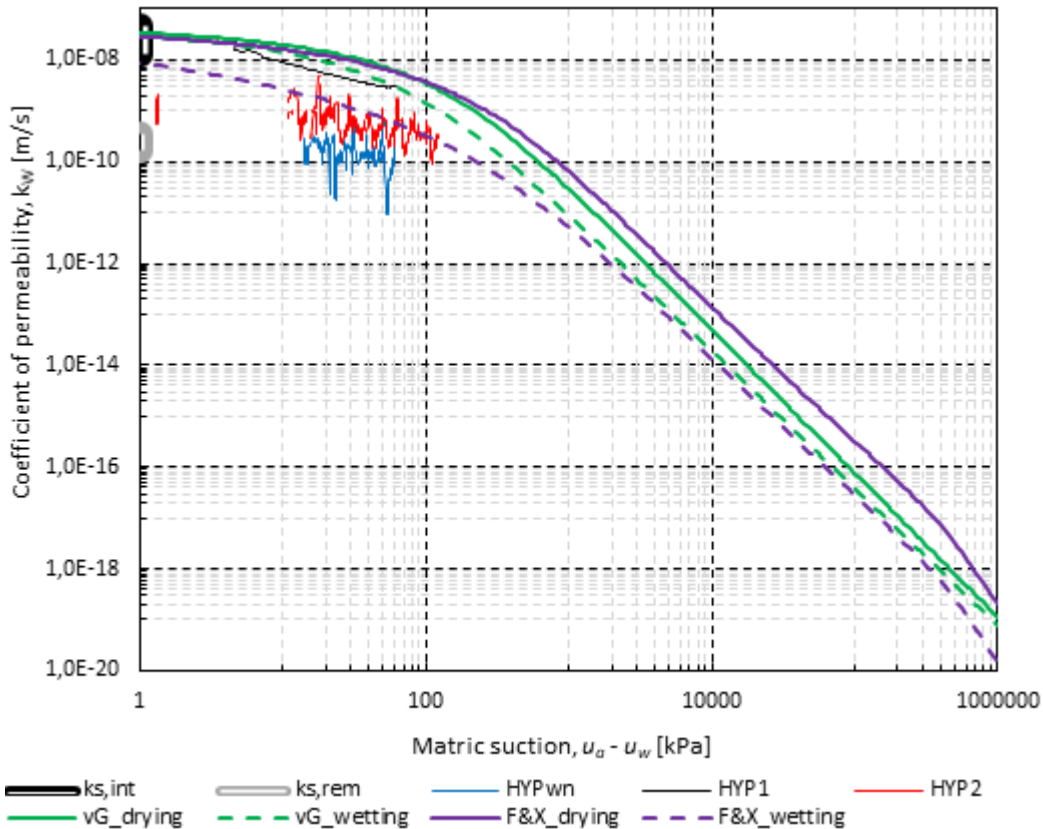


**Figure 51:** The UHCFs of residual soil from a flysch rock mass estimated from the drying and wetting SWRCs and the saturated coefficient of permeability  $k_s$  obtained for undisturbed samples.



## **6. UNSATURATED SHEAR STRENGTH**

This chapter provides a detailed overview of the unsaturated shear strength theory and methodology used to determine the influence of negative pore-water pressure on shear strength characteristics of the investigated soil. The effective stress approach, the independent state variables approach, and some more recently developed concepts are presented. Results obtained in previous studies, where shear strength properties of completely disturbed and consolidated flysch samples from the Rječina River Valley were investigated in conventional direct shear and ring shear apparatuses, are summarized as well. Procedures and laboratory devices used in this study for determination of the shear strength properties in saturated and unsaturated conditions are described. The obtained results are interpreted and some general conclusions on the influence of the matric suction on the behavior of the investigated material during shearing are drawn. The chapter is concluded by presenting and interpreting the results obtained from the long-lasting wetting test.

## 6.1. Literature overview

The shear strength of unsaturated soils is one of the fundamental properties required when dealing with a wide range of geotechnical problems, including the slope stability problems during rainfall infiltration. Since the bearing capacity of the soil, the design of foundations, earth slopes, retaining walls, or pavement constructions often depend on unsaturated soil shear strength, this topic has occupied an important position in the unsaturated soil mechanics for the last few decades. New theories, models, and equations trying to describe the influence of matric suction and different components of pore-water on the shear strength of soil are still being developed. Some of the equations that predict shear strength of partially saturated soils were obtained through regression analyses of experimental data (e.g., Gan et al. 1988; Fredlund et al. 1996) while others were embedded into constitutive models describing the behavior of unsaturated soils (e.g., Alosno et al. 1990; 2010).

Two basic approaches have been used extensively to determine the shear strength of unsaturated soils: the effective stress approach (Bishop 1959) and the independent state variables approach (Fredlund and Morgenstern 1977). Lu and Likos (2006) introduced the suction stress concept, which basically generalizes Bishop's effective stress approach by taking into account all of the possible interparticle mechanisms which affect the effective stress in unsaturated soils. Limitations and advances of these approaches together with numerous modifications that have been proposed in the recent literature are discussed below.

Although basically every conventional device for determination of shear strength properties in saturated conditions was successfully modified for testing in unsaturated conditions (e.g., modified ring shear apparatus Sedano et al. 2007; Hoyos et al., 2014; modified resonant column device Qian et al. 1991; Khosravi and McCartney, 2011), direct shear and triaxial apparatuses modified to implement the axis-translation technique are the laboratory devices most commonly used to investigate the influence of the matric suction on shear strength properties of unsaturated soil. Several general observations on the shear strength of unsaturated soils can be summarised according to numerous shear strength studies that have been undertaken, disregarding of the used approach, equation or device to describe the unsaturated shear strength of soil (e.g., Escario and Saez 1986; Gan et al. 1988; Vanapalli et al. 1996; Wheeler and Sivakumar 2000; Cunningham et al. 2003):

- i) Under the same net vertical stress (or confining pressure), higher matric suction generally results in higher shear strength (Figure 52). An exception could be coarse-grained or silty soils when matric suction value is increased above the residual water content conditions (e.g., Vanapalli et al. 1996).
- ii) Under the same matric suction, higher net vertical stress (or confining pressure) results in higher shear strength (Figure 52).
- iii) The relationship between shear strength and the matric suction is nonlinear: at low matric suction levels below the AEV of soil, when most of the voids are filled with water, the shear strength increases most rapidly (for example,  $\phi^b \approx \phi'$ ). When matric suction is increased above the AEV of soil, the shear strength envelope gradually flattens or even decreases at high suctions (Sheng et al. 2011).

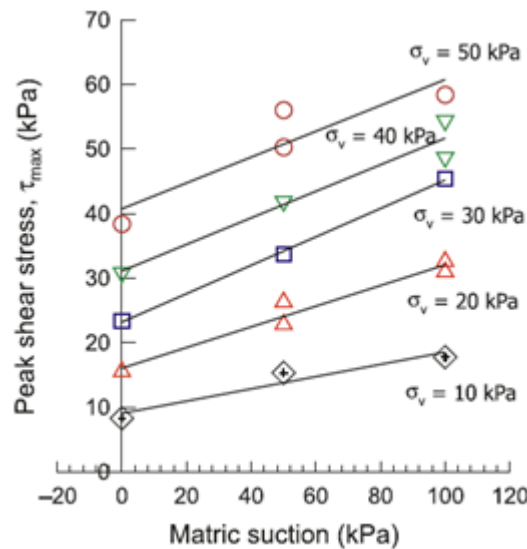


**Figure 52:** Relationship between shear strength and matric suction for different values of net stress (Kim et al. 2010).

Another important topic regarding the shear strength properties for soil in unsaturated conditions is a sample preparation technique. Fredlund et al. (2012) emphasize that to be considered identical, samples should be prepared at the same initial water content and with the same compaction effort. After this, specimens can be consolidated under a range of applied stress conditions and shear to obtain relevant strength parameters. All published test results can be classified into three main categories concerning specimen preparation procedure (Sheng et al. 2011):

- i) Slurry soil can be first consolidated to a desired effective stress value. Following this, specimens are allowed to air-dry to a certain suction level or to reach equilibrium conditions by imposing desired value of matric suction. Finally,



specimens are shared under the constant matric suction value or constant water content.

- ii) Compacted specimens are prepared by using the static or dynamic compaction technique of soil that has been pre-mixed with a certain quantity of water. For a known initial water content, the matric suction can be controlled or measured during the shear stage of the test.
- iii) Using the undisturbed samples taken from the field. Sheng et al. (2011) highlight the need for further research on undisturbed specimens since laboratory research studies performed using the undisturbed specimens are rare.

### 6.1.1. Unsaturated shear strength based on the effective stress approach

Among the earliest attempts of applying Terzaghi's (1943) effective stress principle to unsaturated soils are those of Bishop (1954, 1959) and Bishop and Blight (1963). The expression commonly referred to as Bishop's effective stress equation for unsaturated soils is a modification of Terzaghi's effective stress equation. Bishop (1959) modified the pore water pressure term by introducing the effective stress parameter  $\chi$ , proposing the following form of the equation for effective stress in partially-saturated soil

$$\sigma' = (\sigma - u_a) + \chi(u_a - u_w) \quad (42)$$

where  $\sigma'$  and  $\sigma$  are the effective and total stress (kPa), the difference between total stress  $\sigma$  and air pressure  $u_a$  represents the net stress  $(\sigma - u_a)$ , the difference between the air and water pressure  $u_w$  represents a matric suction  $(u_a - u_w)$ , while  $\chi$  is called the coefficient of effective stress which is a constitutive property of soil related to the water content of soil.

Bishop proposed that the effective stress parameter is simply a degree of saturation ( $\chi = S$ ), ranging between 1 and 0 for saturated or completely dry soil, respectively. In the case of completely saturated soil ( $\chi = S = 1$ ), the term representing air pressure  $u_a$  vanishes and the equation (42) reduces to Terzaghi's effective stress equation

$$\sigma' = \sigma - u_w. \quad (43)$$

In the case of dry soil ( $\chi = S = 0$ ), matric suction term vanishes and the effective stress becomes equal to the difference between total stress and pore air pressure

$$\sigma' = \sigma - u_a. \quad (44)$$

Although the matric suction can be measured or controlled with a certain degree of confidence, to date it is not possible to directly measure a change of the effective stress in soil due to change in matric suction. Consequently, the effective stress parameter  $\chi$  cannot be determined directly from the equation (42) (Lu and Griffiths 2004). However, Bishop (1954) proposed an indirect way to obtain the effective stress parameter from the stress conditions at failure. The following shear strength equation is obtained by substituting the effective stress expression (42) into the conventional Mohr-Coulomb failure criteria

$$\tau_f = c' + [(\sigma - u_a) + \chi(u_a - u_w)]\tan\phi' \quad (45)$$

where  $\tau_f$  is the shear strength of unsaturated soil,  $c'$  is effective cohesion,  $\phi'$  is the effective angle of internal friction, while  $(\sigma - u_a)$  and  $(u_a - u_w)$  are the net normal stress and matric suction at failure, respectively. The latter two can be obtained at the failure by using, for example, the axis translation technique in modified direct shear or triaxial apparatus.

For a known SWRC of the soil, relating the matric suction with the degree of saturation, a one-to-one relationship between the effective stress parameter  $\chi$  and the degree of saturation  $S$  can be established (Lu and Likos 2004). By rearranging the equation (45), the following expression for the effective stress parameter is obtained

$$\chi = \frac{\tau_f - c' - (\sigma - u_a)\tan\phi'}{(u_a - u_w)\tan\phi'}. \quad (46)$$

Following the above-described approach and shear strength results obtained by using the modified direct shear apparatus, Bishop (1959) proposed a slightly nonlinear form of the effective stress parameter shown in Figure 53, along with some more recent solutions offered by various other authors.

Although the effective stress approach is commonly used in case of saturated soils, Bishop's proposal of the effective stress formulation has encountered several difficulties to quantify the contribution of the matric suction to the effective stress of unsaturated soil (Seboong and Lu 2014). For example, by performing a series of consolidation tests on various soils, Jennings and Burland (1962) concluded that the effective stress principle could not explain the collapse phenomenon of unsaturated soil upon wetting. The non-existence of the unique relationship between the effective stress parameter and the saturation degree (Coleman 1962), and the fact that the effective stress equation (42) contains the parameter which is material property (Fredlund and Morgenstern 1977) are limitations which are often noted in the literature. Lu et al. (2010) emphasized that in case of fine-grained soil in a relatively dry state,

the effective stress due to high suction (i.e., suction stress) could be as high as several thousand kPa and it is unphysical that the effective stress parameter is bound to be zero or extremely small (for example, see Figure 61 b).

Several authors proposed modifications in the formulation of Bishop's effective stress parameter. For example, Vanapalli et al. (1996) make use of the SWRC and the saturated shear strength parameters to develop a model for predicting the unsaturated shear strength of soil. The expressions (47) and (48) are referred to as the “first approach ” and the “second approach”

$$\tau_f = [c' + (\sigma - u_a)]\tan\phi' + (u_a - u_w)[(\theta^\kappa)(\tan\phi')], \quad (47)$$

$$\tau_f = c' + (\sigma - u_a) \tan\phi' + (u_a - u_w) \left[ \left( \frac{\theta - \theta_r}{\theta_s - \theta_r} \right) (\tan\phi') \right] \quad (48)$$

where  $\Theta = \theta/\theta_s$  is normalized water content, and  $\kappa$  is a fitting parameter (Vanapalli et al. 1996).

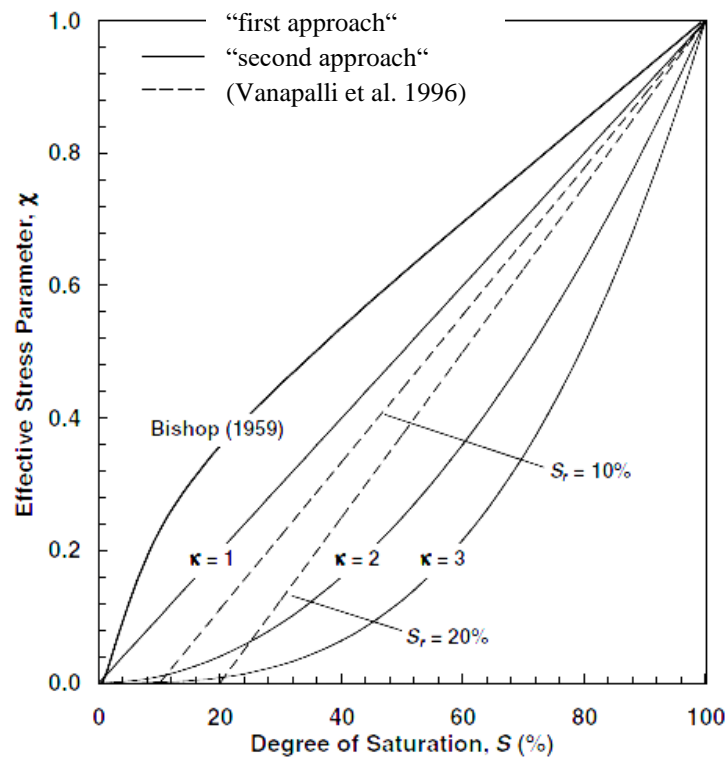


**Figure 53:** Various forms for the effective stress parameter as a function of the degree of saturation (modified from Lu and Likos 2006).

Based on the regression analysis of experimental data from the literature, Khalili and Khabbaz (1998) proposed the following formulation of the effective stress parameter

$$\chi = 1 ; \quad (u_a - u_w) < (u_a - u_w)_{AEV}$$

$$\chi = \frac{(u_a - u_w)_{AEV}^r}{(u_a - u_w)} ; \quad (u_a - u_w) \geq (u_a - u_w)_{AEV} . \quad (49)$$

where  $(u_a - u_w)_{AEV}$  is a matric suction at the AEV of soil and  $r$  is a material parameter which was found to best fit with experimental results if set  $r = -0.55$ .

Tarantino and Tombolato (2005) concluded from experimental data that the effect of water menisci has a negligible impact on the ultimate shear strength and suggest that the ultimate shear strength should be modeled by using the degree of saturation of the macropores,

$$\chi = S_M$$

$$\chi = S_M = \frac{\theta - \theta_m}{\theta_s - \theta_m} . \quad (50)$$

However, all these approaches are fundamentally the same since they make use of the SWRC to relate the matric suction and degree of saturation (Lu and Griffiths 2004). Another group of authors (Lu and coworkers) invoke the effective stress approach: the effective stress parameter  $\chi$  is omitted, and the concept of suction stress is used to define the effective stress.

### 6.1.2. Unsaturated shear strength based on the independent state variables approach

A different approach for the determination of the stress state in unsaturated soil was provided by Fredlund and Morgenstern (1977), following the previous theoretical and experimental findings from, e.g., Coleman (1962), Bishop and Blight (1963) and Matyas and Radhakrishna (1968), who first introduced the concept of “state parameters” in describing the volume change behavior of unsaturated soils. Following the results of null tests, Fredlund and Morgenstern (1977) concluded that any two of three stress variables: (1)  $(\sigma - u_a)$ ; (2)  $(\sigma - u_w)$ , or (3)  $(u_a - u_w)$  are sufficient to fully represent the stress state in unsaturated soil. However, if the in-situ conditions are considered, the pore-air pressure in soil  $u_a$  is generally assumed to be equal to the atmospheric pressure, while the distribution of pore-water pressure in soil profile depends on local conditions, such as groundwater table, vegetation influence or flux conditions occurring at the interface between soil surface and atmosphere. The latter can be estimated or measured by means of direct or indirect methods. In case of the laboratory conditions, it is preferable to keep air pressure at some constant value (usually above the atmospheric pressure in case of the axis translation technique) and control or measure matric

suction value by changing the pore-water pressure  $u_w$ . In this way, the influence of the air compressibility on the test data is reduced as well (Jommi 2000; Fredlund et al. 2012). Considering the above, the following two stress variables are commonly adopted in unsaturated soil mechanics to represent the stress state: net stress ( $\sigma - u_a$ ) and matric suction ( $u_a - u_w$ ). Stress state at the point based on surface tractions extracted from the soil structure force equilibrium equation for unsaturated soil is shown in Figure 54, along with the two independent stress tensor (Fredlund et al. 2012). In the case when matric and osmotic suction influence the unsaturated soil behavior equally, both quantities should be included in the soil suction stress tensor (i.e.,  $(u_a - u_w) + \pi$ ) (Fredlund et al. 2012).

Following the independent stress state variables approach to define stress state in unsaturated soil, Fredlund et al. (1978) extended the Mohr-Coulomb failure criterion to unsaturated soils, obtaining the following equation

$$\tau_f = c' + (\sigma - u_a)\tan\phi' + (u_a - u_w)\tan\phi^b \quad (51)$$

where  $c'$  represent the “effective cohesion” located on the extended M-C failure envelope as the intercept on the shear stress axis where the net normal stress and the matric suction at failure are equal to zero, while  $(\sigma - u_a)$  and  $(u_a - u_w)$  represent the net normal stress state and matric suction on the failure plane at failure,  $\phi'$  is the angle of internal friction associated with the net normal stress state variable, while  $\phi^b$  represents the contribution to the shear strength due to matric suction, and is generally a function of matric suction. The extended Mohr-Coulomb failure envelope for the unsaturated soils and definition of values from the equation (51) are shown in Figure 55.

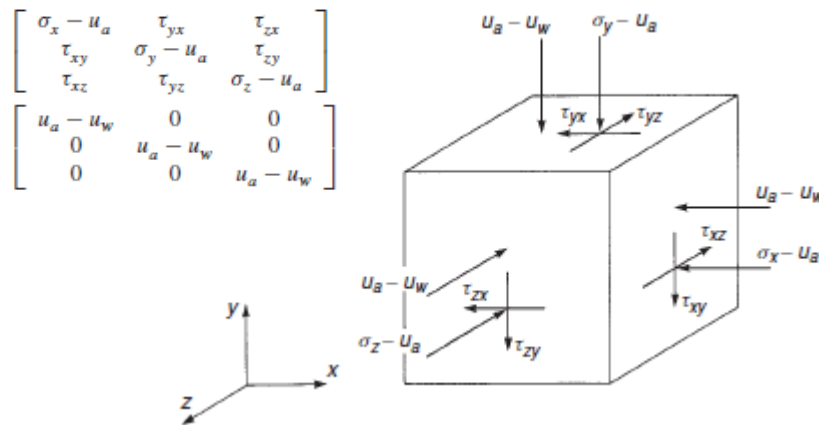


**Figure 54:** Stress state at the point of the unsaturated element of soil and two independent stress tensors: net stress and matric suction (modified from Fredlund et al. 2012).

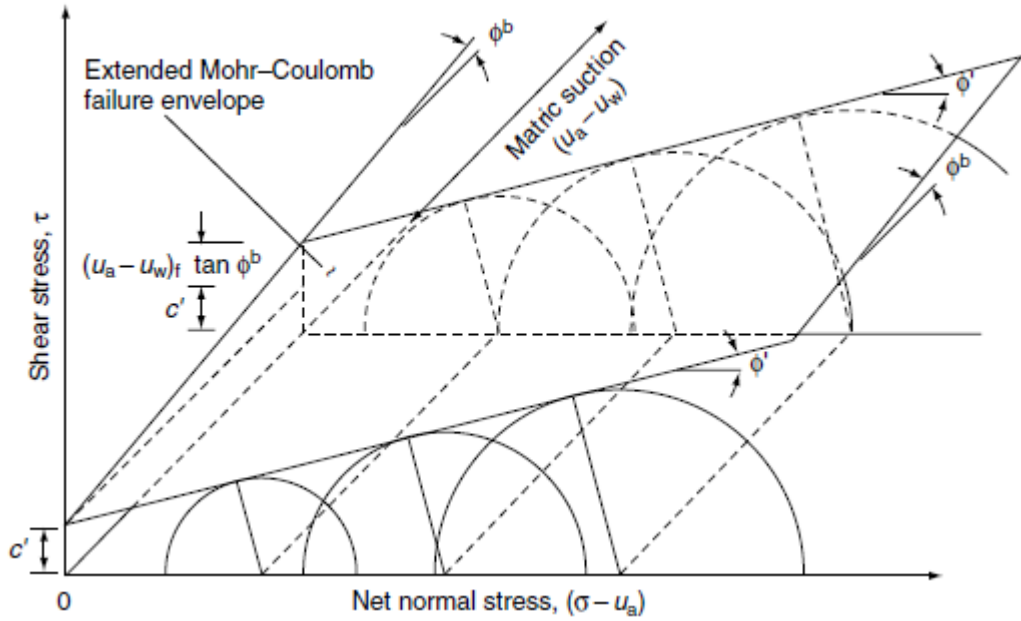


**Figure 55:** Extended Mohr-Coulomb failure envelope for unsaturated soils (from Ng and Menzies 2007 after Fredlund and Rahardjo 1993).

The three-dimensional failure envelope can be observed in two two-dimensional planes: net normal stress vs. shear stress plane parallel to matric suction axis provides contour lines of the failure envelope defining values of the angle of internal friction  $\phi'$  and the effective cohesion  $c'$  for saturated conditions,  $(u_a - u_w) = 0$  or apparent cohesion  $c$  (Taylor 1948) for  $(u_a - u_w) > 0$ , where apparent cohesion is defined, according to Figure 55, by the expression

$$c = c' + (u_a - u_w) \tan \phi^b \quad (52)$$

Another plot can be provided for matric suction vs. shear stress plane. This plot provides a relationship between the angle indicating the rate of increase in shear strength  $\phi^b$  with respect to a change in matric suction, representing the contribution to the shear strength due to matric suction (Fredlund et al. 2012).

Although a linear relationship between  $\phi^b$  and  $(u_a - u_w)$  might exist over a limited range of matric suction values, where linear approximation of shear strength provided by the equation (51) can be adopted, experimental results obtained for wide range of suctions on different types of soil (e.g., Escario and Saez 1986; Gan and Fredlund 1988; Vanapalli et al. 1996; Huat et al. 2005; Kim et al. 2010; or Marinho et al. 2013) showed a non-linear relationship between  $\phi^b$  and an increase in shear strength of unsaturated soil with respect to matric suction  $(u_a - u_w)$ . Results obtained by Gan et al. (1988) are shown in the Figure 56 in terms of the failure envelope obtained from unsaturated glacial till in a) shear stress  $\tau$  vs. matric suction  $(u_a - u_w)$  plane and b) corresponding  $\phi^b$  values.

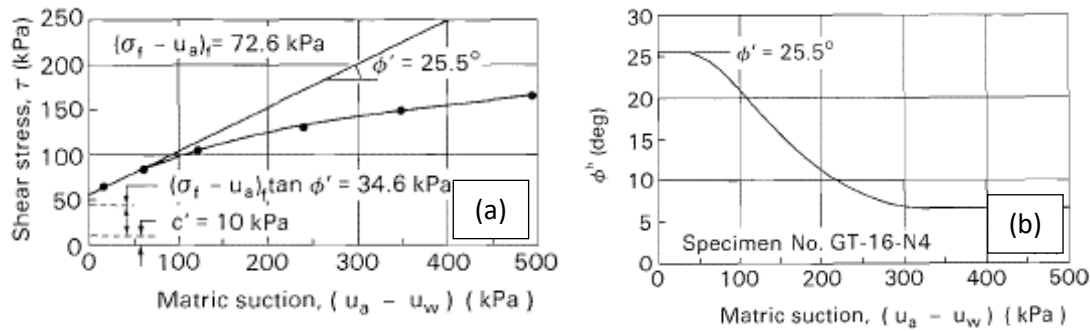


**Figure 56:** Shear strength results obtained from unsaturated glacial till specimens GT-16-N4 using the modified direct shear apparatus: a) failure envelope on  $\tau$  vs.  $(u_a - u_w)$  plane and b) corresponding  $\phi^b$  values (Gan et al. 1988).

Again, the observed dependency between the shear strength of unsaturated soil and the amount of water contained in soil pores was used through the SWRC to develop various models that describe the relationship between shear strength and matric suction (e.g., Vanapalli et al. 1996 or Fredlund et al. 1996). Vanapalli et al. (1996) described the relationship between the SWRC and the shear strength of an unsaturated soil with respect to the matric suction. First, the authors have modified the original concept proposed by White et al. (1970), defining three characteristic zones of desaturation on the SWRC, namely: the boundary effect stage, the transition stage (primary and secondary) and the residual stage (Vanapalli et al. 1996). Following this, the authors explain the variation of water area for defined stages of the SWRC and relate it to the rate of change in shear strength. They propose that a linear increase in shear strength exists up to the AEV of soil when a nonlinear increase in shear strength commences. Finally, they suggest that the shear strength of an unsaturated soil may increase, remain constant or decrease when suction is increased beyond the residual conditions (Vanapalli et al. 1996). The generally anticipated shear strength response expected for a wide range of soil textures is summarized in Figure 57.

Finally, the authors interpret that decrease or absence of significant increase in shear strength of coarser soils (such as sands or silts) might be due to the low water content at higher values of matric suction (i.e., at residual conditions), which disables effective transmission of matric suction on soil particles. At the same time, in case of clayey soil, considerable amounts of water might exist at high values of matric suction and, thus, a contribution of the matric suction might result in a significant increase of shear strength of clayey soil (Vanapalli et al. 1996).

However, it seems that the independent stress state variable approach has found only limited application in engineering practice. The need for defining the nonlinear soil property  $\phi^b$  over a wide range of suctions usually implies a large number of experimental procedures

and possible uncertainties in obtained results (Khalili and Khabbaz 1998; Lu et al. 2010; Nuth and Laloui 2008). Even more, whether the matric suction is a stress variable and the physical basis for the additional shear strength parameter  $\phi^b$  are disputed (Lu 2008). A major theoretical and practical obstacle is that two independent stress state variable approach cannot be simply reconciled within the context of classical mechanics for saturated soil, where the effective stress is a single stress variable which can be used to describe both the shear strength (for example, limit state) and deformation (for example, consolidation) analyses Lu et al. (2010).

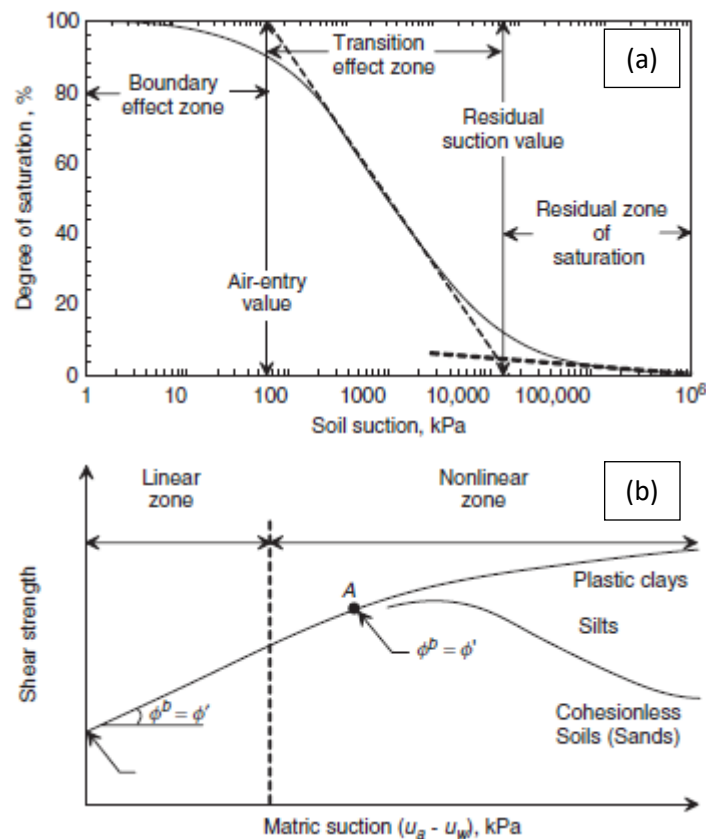


**Figure 57:** Relationship of SWRC to shear strength envelope for different types of soil: a) desaturation zones along the SWRC, and b) variation in shear strength envelopes for different soils in different desaturation zones (Fredlund et al. 2012).

### 6.1.3. The “suction stress” concept

To overcome problems associated with experimental determination and theoretical justification of the effective stress parameter  $\chi$ , non-uniqueness of  $\chi = f(S)$  and the shortcomings mentioned above of the independent stress state variable approach, Lu and Likos (2006) introduce the concept of “suction stress”. They use a series of particle-scale force analyses to distinguish and conceptualize three types of forces that exist and can affect mechanical behavior of saturated and unsaturated soil (e.g., Bolt 1956; Lambe 1960; Skempton, 1960; Bishop 1959;



Mitchel 1976): (1) active “skeletal” forces which are propagated through the soil grains; (2) active “local” forces which are concentrated at or near the interparticle contacts; and (3) passive particle-particle contact forces which counterbalance forces arising from (1) and (2) (Lu and Likos 2006). They propose that the second type of forces, including the van der Waals, electrical double-layer, cementation, surface tension, and forces arising from the negative pore-water pressure, can be conceptually united into macroscopic stress, named “suction stress”. They define the suction stress characteristic curve (SSCC), which describes the relationship between suction stress and the degree of saturation, water content or matric suction.

Local interparticle forces (2) in saturated soil depend jointly on both physical and chemical properties of the soil-water system (e.g., mineralogy, surface area, pore-water chemistry) and include van der Waals attraction, electrical double-layer repulsion, and the net attraction forces arising from chemical cementation at the grain contacts (Lu and Likos 2006). Besides these local interparticle physicochemical forces, additional attractive forces exist in partially saturated soil, arising from surface tension and typically negative pore-water pressure (Lu and Likos, 2006). Each of the above forces (2), which may be considered “active” in nature and independent from the external forces controlling the total stress and pore water pressure, are counterbalanced by “passive” particle-to-particle contact forces (3). As a result, local interparticle forces (2) do not propagate through the granular skeleton. Lu and Likos (2006) conclude that this is probably the reason why they are not explicitly considered in the macroscopic conceptualization according to Terzaghi’s effective stress formulation and equation (43), which accounts only for the active “skeletal” forces (1). Another reason why in saturated soil local interparticle forces do not need to be explicitly considered in the expression for the effective stress is the general assumption that pore fluid chemistry and the strength of cementation bonds remain relatively constant over a wide range of stress variations (Lu and Likos 2006).

Simple one-dimensional microscopic interparticle force and stress equilibrium analysis provided by Lu and Likos (2006) is shown in Figure 58. The forces included in the analyses are:  $F_t$  representing the active “skeletal” forces (1) due to self-weight or external loading;  $F_{pc}$  representing local physicochemical forces (2) and includes for van der Waals attraction ( $F_{vdw}$ ), electrical double-layer repulsion ( $F_{edl}$ ), and chemical cementation effects ( $F_{ce}$ ); and  $F_c$  accounting for passive counterbalancing forces (3) (Lu and Likos 2006). If external force  $F_t$  is set equal to zero, system in Figure 58 b) results with the following equilibrium condition

$$F_{c0} = F_{vdw} + F_{edl} + F_{ce} = F_{pc} \quad (53)$$

and forces (2) and (3) are mutually counterbalanced. Normalization with the cross-sectional area  $A$  of the REV (Figure 58 a), leads to the expression for the  $\sigma_{c0}$  which is physically equal to the intergranular bonding stress that provides cohesion in saturated soil (Lu and Likos 2006)

$$\sigma_{c0} = \sigma_{pc}. \quad (54)$$

If external force  $F_t$  and pore water pressure are considered, the force equilibrium becomes

$$F_t + F_{pc} - F_c - u_w A = 0 \quad (55)$$

from which the equation previously derived by Lambe and Whitman (1969) and Mitchell (1976) follows

$$\sigma_c = \sigma_t - u_w + \sigma_{pc}. \quad (56)$$

The above equation states that the net interparticle stress  $\sigma_c$  is equal to the sum of Terzaghi's effective stress defined by the equation (43) and the interparticle physicochemical stress. As the soil desaturates, physicochemical forces dramatically change and additional local force components arise: a distributed force due to pore-air pressure  $u_a$ , a local capillary force due to surface tension  $F_{cap}$ , and a local hydrostatic force due to negative water pressure (Lu and Likos 2006).

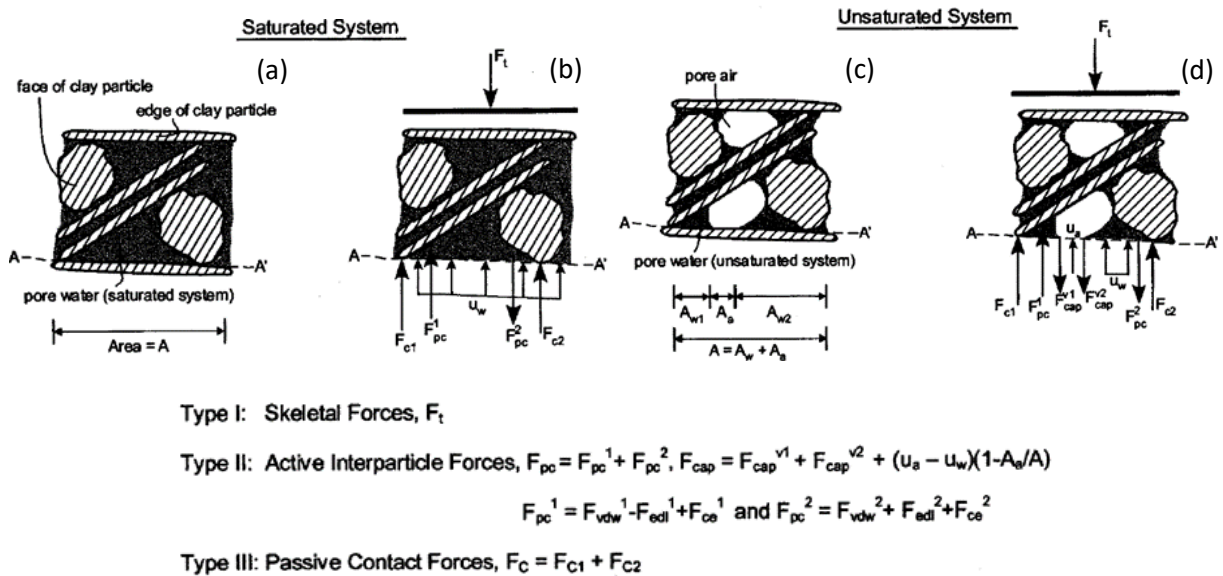


**Figure 58:** Microscopic representation of interparticle force equilibrium: a) and b) REV for saturated; c) and d) REV for an unsaturated fine-grained soil system (Lu and Likos 2006).

Finally, according to the mechanical equilibrium of the forces considered in Figure 58, the following equations are obtained (Lu and Likos 2006)

$$\frac{F_t}{A} + \frac{F_{pc}}{A} + \frac{F_{cap}}{A} - \frac{F_c}{A} - u_w \frac{(A - A_a)}{A} - u_a \frac{A_a}{A} = 0, \quad (57)$$

and

$$\sigma_c = \sigma_t - u_w + \sigma_{pc} + \sigma_{cap} + (u_a - u_w) \left(1 - \frac{A_a}{A}\right), \quad (58)$$

where  $A_a = A - A_w$  represent projected area where the air phase exists. By setting the  $\left(1 - \frac{A_a}{A}\right) = \chi$  in the last equation, the equation proposed by Bishop (42) with two additional terms accounting for interparticle stress due to physicochemical forces or forces arising due to a surface tension was obtained.

By using the analytical equations from various authors (e.g., Verwey and Overbeek 1948; Ingles 1962; Rosen 1989; van Olphen 1991; Israelachvili 1992; Shaw 1992; Santamarina et al. 2001; Cho and Santamarina 2001; Lu and Likos 2004), Lu and Likos (2006) delineate upper boundaries of magnitude of different interparticle stress components as a function of particle size (Figure 59 a) and degree of saturation (Figure 59 b).

Considering the above microscopic analysis, Lu and Likos (2006) finally propose the following expression for the intergranular stress in unsaturated soil

$$\sigma_c = \sigma' = \sigma_t - u_w + \sigma'_s + \sigma_{c0}, \quad (59)$$

where  $\sigma'_s$  is called “suction stress”, a term conceptualized as the resultant of interparticle physicochemical stresses arising from cementation, van der Waals attraction, double-layer repulsion, capillary stress arising from the surface tension and negative pore-water pressure:

$$\sigma'_s = \sigma_{pc} + \sigma_{cap} + \chi(u_a - u_w) - \sigma_{c0}. \quad (60)$$

Again, each of these components forming the suction stress is a function of water content, the degree of saturation, or matric suction, and thus the suction stress is a characteristic function of the soil-water system described by a SSCC (Lu and Likos 2006).

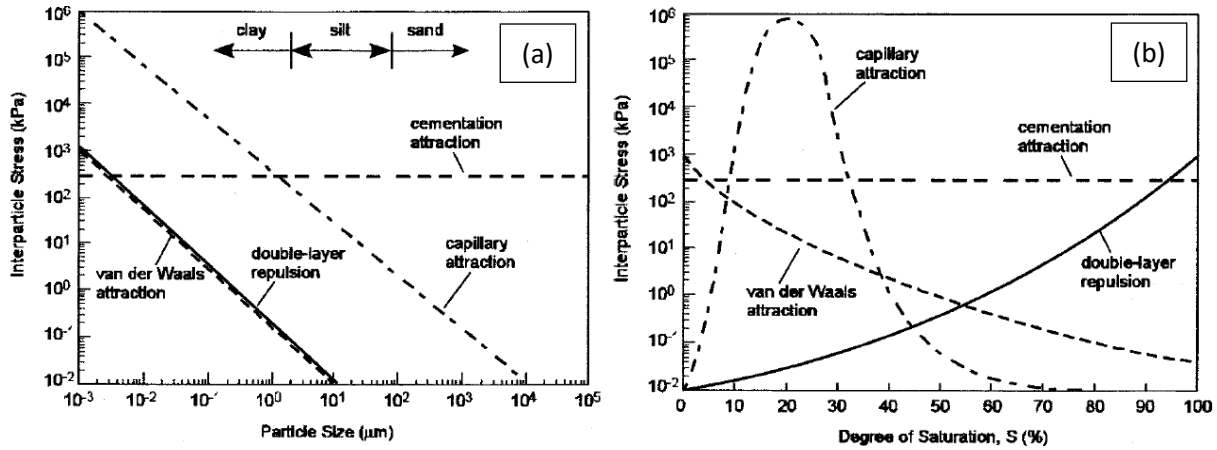


**Figure 59:** Conceptual behavior and magnitude of the interparticle stress components as a function of a) particle size, and b) degree of saturation (Lu and Likos 2006).

To be more consistent with Terzaghi's effective stress equation (43) and previously defined "apparent cohesion" in Mohr-Coulomb failure criterion defined by the equation (52), Lu and Likos (2006) propose the following expression for the suction stress  $\sigma'_s$

$$\sigma'_s = \sigma_s - \sigma_{C0} \quad (61)$$

where  $\sigma_s$  is the "uncorrected" suction stress and  $\sigma_{C0}$  apparent tensile stress at saturated state.

Finally, they provide a conceptual illustration of suction and suction stress variation in the unsaturated state by describing four regimes that have been identified to differentiate the state of saturation and the dominant water adsorption mechanisms active within each (Figure 60). Since the system remains saturated under negative pore-water pressure, suction stress is equal to the matric suction within Regime I (Figure 60 c), while physicochemical interparticle stress remains constant. The start of the Regime II is characterized by the matric suction values exceeding the AEV of soil. Existing pore water is mainly retained by capillary forces and the capillary interparticle stress develops with ongoing desaturation of soil. The rate of desaturation of soil due to the increase in matric suction and related rate of increase of capillary stress and corresponding suction stress, depends on the soil type, while the physicochemical interparticle stress changes only moderately. Rapid changes in physicochemical stress are characteristics of the Regime III, while changes in the capillary stress strongly depend on the soil type. As shown in Figure 60 b, capillary stress and corresponding suction stress remains relatively unchanged for sands while continuously increases for clays. Finally, for the Regime IV, residual water is retained in soil mainly as the absorbed water on particle surfaces as water of hydration, and further increase in matric suction causes only small changes in water content of soil. Again, the suction stress within this zone depends on the soil type: it may diminish to zero for sandy soil or reach several hundred kPa for clayey soil, as shown in the Figure 60 c (Lu and Likos 2006).

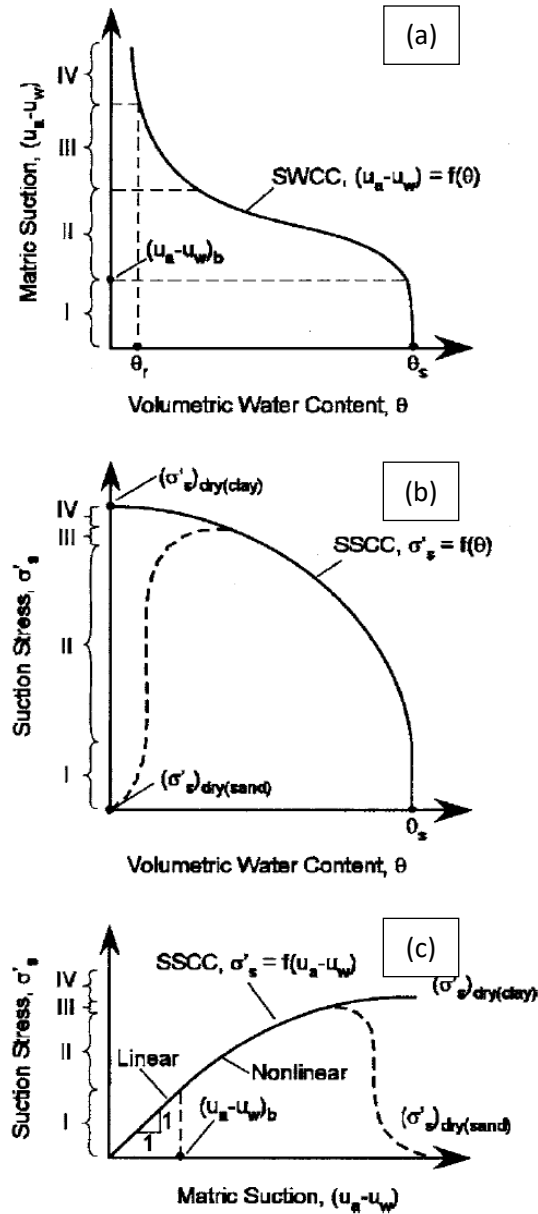


**Figure 60:** Conceptual illustration of behavioral regimes for a) SWRC; b) SSCCs for sand and clay in the form  $\sigma'_s(\theta)$ ; and c) in the form  $\sigma'_s(u_a - u_w)$  (Lu and Likos 2006).

Shear strength test results performed at varying matric suction values can be used to define SSCC, while the intergranular stress (or true effective stress) can be calculated from the equation (59). Lu et al. (2009) used the suction stress concept (Lu and Likos 2006) to develop a theory for the tensile strength of moist granular materials. By using the experimental results from direct tension tests (Kim 2001; Lu et al. 2005; 2007) obtained on Ottawa Sand, Perth Sand and Esperance Sand, they showed that the suction stress concept can accurately predict the tensile strength of moist granular materials if the frictional characteristics ( $\phi$ ) and SWRC of the material are known. Lu et al. (2010) derived a closed-form equation for the SSCC as a function of either soil saturation or matric suction, using a working hypothesis formed on the basis of

experimental observations and thermodynamic justifications. In their work, they focused on a regime where water is held in soil dominately by capillary effects, and changes in residual water content  $V_r$  are ignored. “Free” capillary water  $V_f$  is a part of the total water in soil  $V_w$ :

$$V_f = V_w - V_r. \quad (62)$$

Assuming that for the case when  $V_w > V_r$ , small deformations do not change the volume of solid particles or tightly bound residual water, they obtained that the ratio of the free water volume  $V_f$  to the total available  $(V_v - V_r)$ , where  $V_v$  is the volume of voids, is defined by the effective degree of saturation,  $S_e$  (Lu et al. 2010)

$$S_e \equiv \frac{S - S_r}{1 - S_r} \equiv \frac{V_f}{V_v - V_r}. \quad (63)$$

Assuming that the effective saturation  $S_e$  remains constant and introducing some additional simplifications, Lu et al. (2010) obtained the following approximation for the suction stress for considered case  $V_w > V_r$

$$\sigma^s = -(u_a - u_w)S_e. \quad (64)$$

The obtained equation is very similar to that proposed by Bishop ( $\chi = S$ ), except in part where the residual water content is removed from the tensile stress ( $\chi = S_e$ ). By using the above equation, they finally propose the expression to quantify effective stress as an extension of Bishop’s and Terzaghi’s effective stress for all saturations (Lu et al. 2010)

$$\sigma' = (\sigma - u_a) - [-S_e(u_a - u_w)] = (\sigma - u_a) - \sigma^s \quad (65)$$

Finally, Lu et al. (2010) use van Genuchten’s (1980) SWRC model to obtain a closed-form expression for suction stress  $\sigma'_s(S_e)$  and  $\sigma'_s(u_a - u_w)$  for the full range of saturation or matric suction

$$\sigma'_s = -\frac{S_e'}{\alpha} \left( S_e^{\frac{n}{1-n}} - 1 \right)^{\frac{1}{n}}, 0 \leq S_e \leq 1, \quad (66)$$

and

$$\sigma'_s = -(u_a - u_w), (u_a - u_w) \leq 0 \quad (67)$$

$$\sigma'_s = -\frac{(u_a - u_w)}{(1 + [\alpha(u_a - u_w)]^{\frac{n-1}{n}})^{\frac{n}{n-1}}}, (u_a - u_w) \geq 0. \quad (68)$$

This way, Lu et al. (2010) obtained an equation (68) where the effective stress in unsaturated soil is solely a function of suction and can be determined either from the shear

strength test results or known SWRC parameters. If the latter two equations are substituted into equation (65), the closed-form effective stress equation is obtained which provides a smooth transition from an unsaturated state to a saturated state

$$\sigma' = \sigma - u_a + (u_a - u_w), (u_a - u_w) \leq 0, \quad (69)$$

$$\sigma' = (\sigma - u_a) + \frac{(u_a - u_w)}{(1 + [\alpha (u_a - u_w)]^n)^{\frac{n-1}{n}}}, (u_a - u_w) \geq 0 \quad (701)$$

The above closed-form suction stress equations (68) proposed by Lu et al. (2010) are used in the following part to show general characteristics of SSCCs for different soil textures (i.e., sand, silt, and clay) and the interrelationship with the SWRC. Values of the van Genuchten's SWRC model parameters were obtained by fitting the experimentally obtained results of SWRC measurements performed on varying types of soil and using various testing devices and techniques (e.g., van Genuchten 1980; Rawls et al. 1982; Carsel and Parrish 1988; etc.). Table 12 shows the adopted values of van Genuchten's SWRC model parameters, which are representative of sand, silt, and clay, along with the previously defined parameter values of the investigated material. The designations Flysch RS-d and Flysch RS-w indicate residual soil from a flysch rock mass parameter values derived for the drying and wetting path, respectively. Graphs were plotted using the MathCad 15.0 (Parametric Technology Corporation Inc.). Figure 61 shows that, in case of clayey soil, the suction stress can be very high as matric suction increases and the degree of saturation goes to zero, changing the behavior of soil from plastic to very brittle and difficult to break. Lu and Likos (2010) conclude that, under the proposed framework, effective or suction stress is intrinsically related to the SWRC and values of the  $\alpha$  and  $n$  parameters. They showed that the SSCC monotonically decreases if  $n \leq 2$  and decreases and then increases if  $n > 2$ , while the  $\alpha$  parameter controls the minimum value of suction stress and corresponding matric suction value.

**Table 12:** Common values of van Genuchten's SWRC parameters for different soil textures (sand, silt, and clay) and values of the soil investigated in this study used in Figure 61.

SWRC parameter	Sand	Silt	Material		
			Clay	Flysch RS-d	Flysch RS-w
AEV [kPa]	4	40	400	200	125
$\alpha$ [kPa <sup>-1</sup> ]	0.25	0.025	0.0025	0.005	0.008
$n$	2.5	1.5	1.3	1.332	1.28

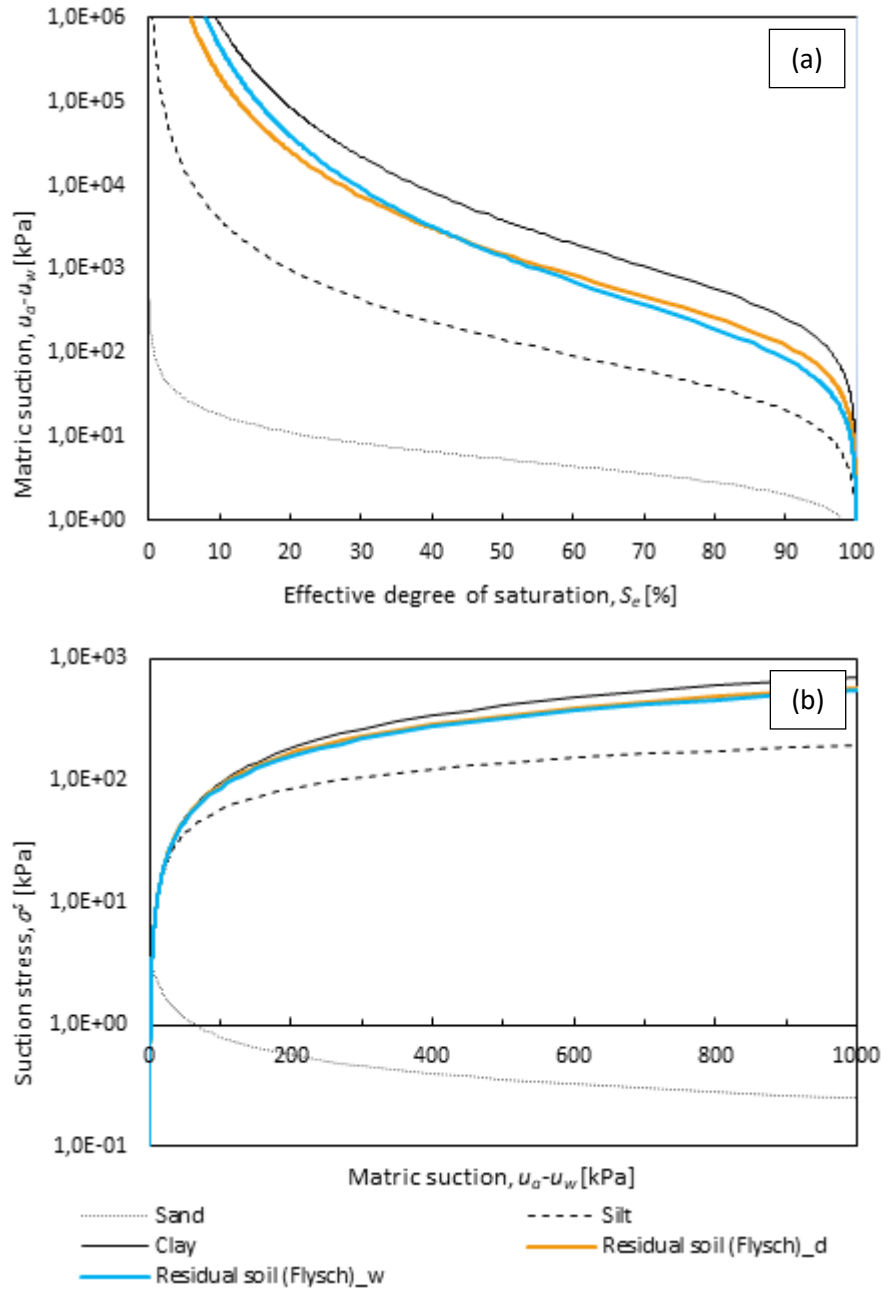


**Figure 61:** Comparison of a) SWRC and b) SSCC ( $u_a - u_w$ ) of residual soil from a flysch rock mass with varying soils textures represented with common SWRC parameter values.

Using the effective degree of saturation and the suction stress formulation as defined by the equation (64), Bishop's form of the shear strength equation (45) is reduced to the following expression

$$\tau_f = c' + [(\sigma - u_a) - \sigma^s] \tan \phi', \quad (71)$$

and direct shear test results can be used to calculate suction stress at a given value of matric suction by using the following equation



$$\sigma^s = \frac{\tau_f - c' - (\sigma - u_a)\tan\phi'}{\tan\phi'}. \quad (72)$$

Lu et al. (2010) used experimental results obtained on various types of soil and demonstrated that the proposed closed-form equation could accurately describe effective stress for different soil textures, ranging from sand to clay. Seboong et al. (2012) performed the quantitative validation of the effective stress based on the SSCC (Lu and Likos 2006) for residual soils. SSCC and SWRC were experimentally measured for various residual soils from Korea prepared under different remolding conditions. The results confirmed the intrinsic relationship between the SWRC and SSCC and, again, proved that a unique set of unsaturated soil parameters (i.e.,  $AEV$ ,  $n$ ,  $\theta_s$ , and  $\theta_r$ ) could be independently defined from either unsaturated shear strength tests or soil-water retention tests, even in the case of residual soils. This could have significant implications in engineering practice since the SWRC results, which are generally easier to perform in the laboratory, could reduce the need for performing shear-strength tests, which are generally more complicated, expensive and time-consuming, especially in the case of low-permeable fine-grained soils. Lu et al. (2013) used the same framework to show the intrinsic relationship between SWRC, UHCF, and SSCC by studying the hysteresis of unsaturated hydro-mechanical properties of sand-silt mixtures. By using varying confining stress values up to 200 kPa, Oh and Lu (2013) investigated uniqueness of the SSCC for a silty sand. They found that for specimens undergoing wetting a process, even though SWRC and SSCC varied for different confining stresses, a unique SWRC or SSCC could be defined if the effective degree of saturation  $S_e$  was used. In the case of the drying process, the uniqueness of the SWRC and SSCC held approximately, which was attributed to the differences in the  $AEVs$ . The uniqueness of the SWRC for drying and wetting processes, considering the wide range of confining pressures still has to be validated for fine-grained soils.

Greco and Gargano (2015) proposed and verified a novel equation for the evaluation of the suction stress in unsaturated soil, which is based on wetted surface area in pores. By assuming that transmission of suction to solid particles occurs only through a wet external surface, they use SWRC to derive the “soil suction characteristic curve”. Verification of the equation against available experimental data obtained for suction stress values below 1 MPa on various types of soils, showed good agreement between predicted and measured values. Consequently, Greco and Gargano (2015) concluded that the proposed equation performs better than other proposed expressions for the evaluation of suction stress.

In their work, the amount of wetted surface is quantified through the normalized wet area index  $\alpha_w$ , as the ratio between the wet surface area of solid particles, contained in a given soil bulk volume  $A_w$ , and the total surface area of solid particles in the same volume  $A_s$

$$\alpha_w = \frac{A_w}{A_s}. \quad (73)$$

First, they show that the normalized wet area index is a function of the matric potential  $\alpha_w(\psi)$  with a shape closely related to the pore size distribution of soil. Further, they change the SSCC equation by replacing the effective degree of saturation from the equation (64), arguing that  $\chi = \alpha_w$ , to obtain the following SSCC equation

$$\sigma^s = -(u_a - u_w)\alpha_w. \quad (74)$$

Theoretical analysis proposed by Greco and Gargano (2015) leans back on Fredlund and Xing's (1994) SWRC definition and concept proposed by Tuller et al. (1999, 2005) where matric potential  $\psi$  and the pore radius  $r$  are strictly related through augmented Young's relationship

$$\psi = \frac{u_a - u_w}{\gamma_w} = \psi_c + \psi_a = -\frac{\alpha T_w \cos(\theta_c)}{\gamma_w r} - \frac{\lambda A}{\gamma_w h^3}, \quad (75)$$

where  $\psi_c$  and  $\psi_a$  account for the effects of capillarity and molecular adsorption of water layer with thickness  $h$  around the solid particles,  $\alpha$  and  $\lambda$  are geometric factors related to the pore shape,  $T_w$  is the water surface tension,  $\theta_c$  is the contact angle between the air-water interface and the surface of solid particles, and  $A$  is Hamaker constant equal to 6E-20 J (Tuller et al. 2005). This model proposes that in the largest pore capillary phenomena dominate, while smaller pores contain mainly adsorbed water. There are pores where curved menisci and adsorbed water layers coexist (Tuller and Or 2007; Philip 1977). Only residual absorbed water is retained in the soil pores for potential below the residual potential,  $\psi_r$ .

On the basis of pure geometrical arguments, Greco and Gargano (2015) assume that there is a threshold water potential value  $\psi_0$  below which ( $\psi < \psi_0$ ) the wet external surface area remains constantly equal to  $A_0$ , ( $A_w = A_0$ ), as shown in the Figure 62.

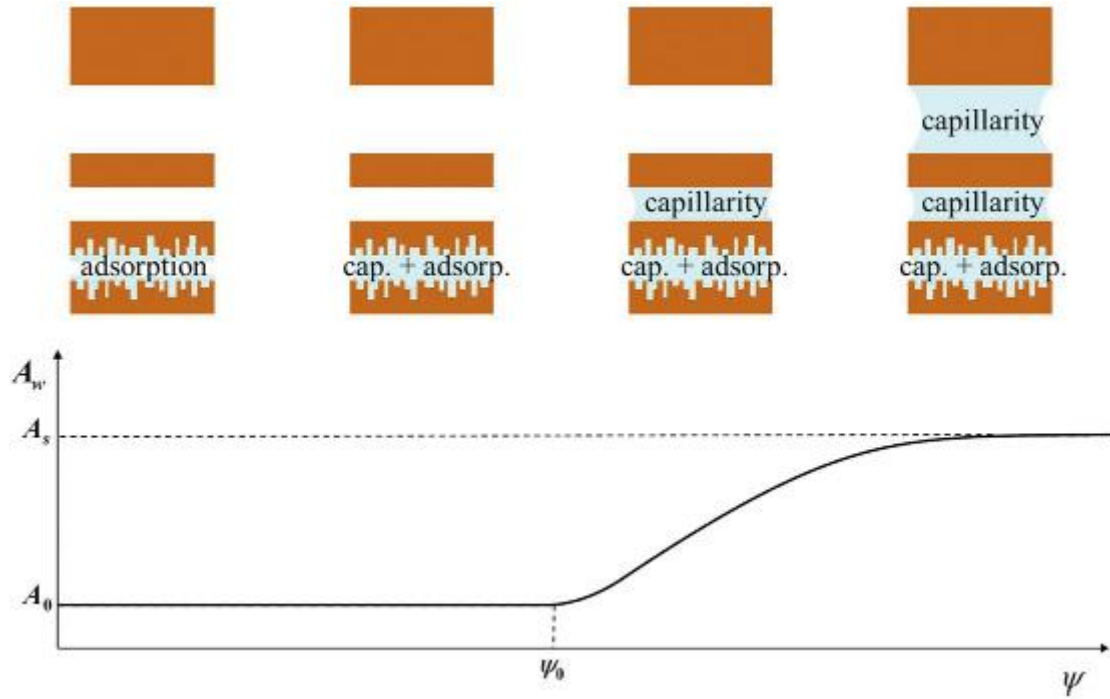


**Figure 62:** Sketch of assumed simplified process of emptying and filling of soil pores and corresponding variation of wetted surface area with water potential (Greco and Gargano 2015).

Revil and Lu (2013) developed a water retention model that extends up to very dry conditions, including the effect of adsorbed and capillary water. In their paper, Greco and Gargano (2015) omit problems related to the determination of  $\psi_0$  value and residual water content conditions by considering only suction values below 1 MPa. These values are typically present in geotechnical engineering practice. For this purpose,  $\psi_0$  is considered only as a fitting parameter of the suction stress model.

Further, they propose the following expression for a simple, yet reasonable estimate of  $A_0$ , based on the assumption of isotropic distribution of the residual water content

$$\alpha_0 = \frac{A_0}{A_s} = \left( \frac{\theta_r}{\theta_s} \right)^{\frac{2}{3}}, \quad (76)$$

arguing that the shape of  $\alpha_w(\psi)$  is only slightly affected by the choice of  $\theta_r$ . By defining the ratio of surface area to volume in pore as  $\kappa/r$ , where  $\kappa$  is a geometric factor related to pore shape being equal to  $\kappa/r = 3/2$  for spheres and regular polyhedrons, and  $\kappa/r = 1$  for cylinders and plane fissures, and for given SWRC, Greco and Gargano (2015) relate the soil water potential  $\psi$ , with the corresponding wet surface area  $A_w$ , by the following expression

$$A_w(\psi \leq \psi_0) = A_0; \quad (77)$$

$$\begin{aligned}
 A_w(\psi > \psi_0) &= A_0 + \int_{S_e(\psi_0)}^1 \frac{\kappa}{r} (\theta_s - \theta_r) dS_e \\
 &= A_0 - \frac{\gamma_w(\theta_s - \theta_r)}{T_w \cos \theta_c} \int_{\psi_0}^{\psi} \frac{\kappa}{\alpha} \omega \frac{dS_e}{d\psi} d\omega.
 \end{aligned} \tag{78}$$

where  $\omega \equiv \psi$  is the dummy variable. Finally, if the above equations are normalized by the total surface area  $A_s$ , of the saturated soil, the wet area index defined by the equation (73) is expressed as a function of the soil water potential, which is referred to as soil wet area curve (SWAC) (Greco and Gargano 2015)

$$\alpha_w(\psi \leq \psi_0) = \frac{A_0}{A_s} = \frac{A_0}{A_0 - \frac{\gamma_w(\theta_s - \theta_r)}{T_w \cos \theta_c} \int_{\psi_0}^0 \frac{\kappa}{\alpha} \psi \frac{dS_e}{d\psi} d\psi} = \alpha_0; \tag{79}$$

$$\begin{aligned}
 \alpha_w(\psi > \psi_0) &= \frac{A_0 - \frac{\gamma_w(\theta_s - \theta_r)}{T_w \cos \theta_c} \int_{\psi_0}^{\psi} \frac{\kappa}{\alpha} \omega \frac{dS_e}{d\psi} d\omega}{A_s} \\
 &= \alpha_0 - \frac{\frac{\gamma_w(\theta_s - \theta_r)}{T_w \cos \theta_c} \int_{\psi_0}^{\psi} \frac{\kappa}{\alpha} \omega \frac{dS_e}{d\psi} d\omega}{A_0 - \frac{\gamma_w(\theta_s - \theta_r)}{T_w \cos \theta_c} \int_{\psi_0}^0 \frac{\kappa}{\alpha} \psi \frac{dS_e}{d\psi} d\psi}.
 \end{aligned} \tag{80}$$

Although based on purely geometrical arguments, the two thermodynamic hypotheses made by Lu et al. (2010) while deriving the suction stress equation are still valid, because the equation (74) was derived without considering the amount of absorbed water, and forces at the contact between the menisci and the solid surface were not considered either. Consequently, the free energy of absorbed residual water remains unaltered due to volumetric deformations of soil and the variation of the energy of air-water interfaces caused by volumetric deformations of soil are negligible (Lu et al. 2010).

By comparing the SWAC and the SWRC of three soils with different textures, Greco and Gargano (2015) argue that commonly adopted assumption  $\alpha_w = S_e$  is acceptable only in the case of poorly graded soils with low residual water contents (like sand), but not in the case of fine-grained soils with wide pore sizes (like clay). Validation of the proposed SSCC was performed by using the experimental data available from the literature, with suction stress corresponding to soil suction well below 1 MPa. By adopting the constant shape factor ratio  $\kappa/r = 1$ , using the equation (76) to estimate the  $\alpha_0$  and by assuming  $\psi_0$  around 1.5 times the water potential corresponding to the inflection point on the  $S_e, \log(-\psi)$  SWRC plot, they obtained excellent agreement with the experimentally obtained results and showed that only

SWRC parameters have to be known to evaluate SWAC, and thus the suction stress (Figure 63).

While comparing the proposed relationship for Bishop's effective stress parameter with those proposed by Khalili and Khabbaz (1998) and Lu et al. (2010), Greco and Gargano (2015) observed that relationships proposed from various authors performed with various levels of success on different types of soil. A wide scatter in the  $(\chi, S_e)$  plane was obtained in some cases. However, as shown in Figure 64, the SSCC equation proposed by Greco and Gargano (2015) fit the experimental data most successfully in all cases.

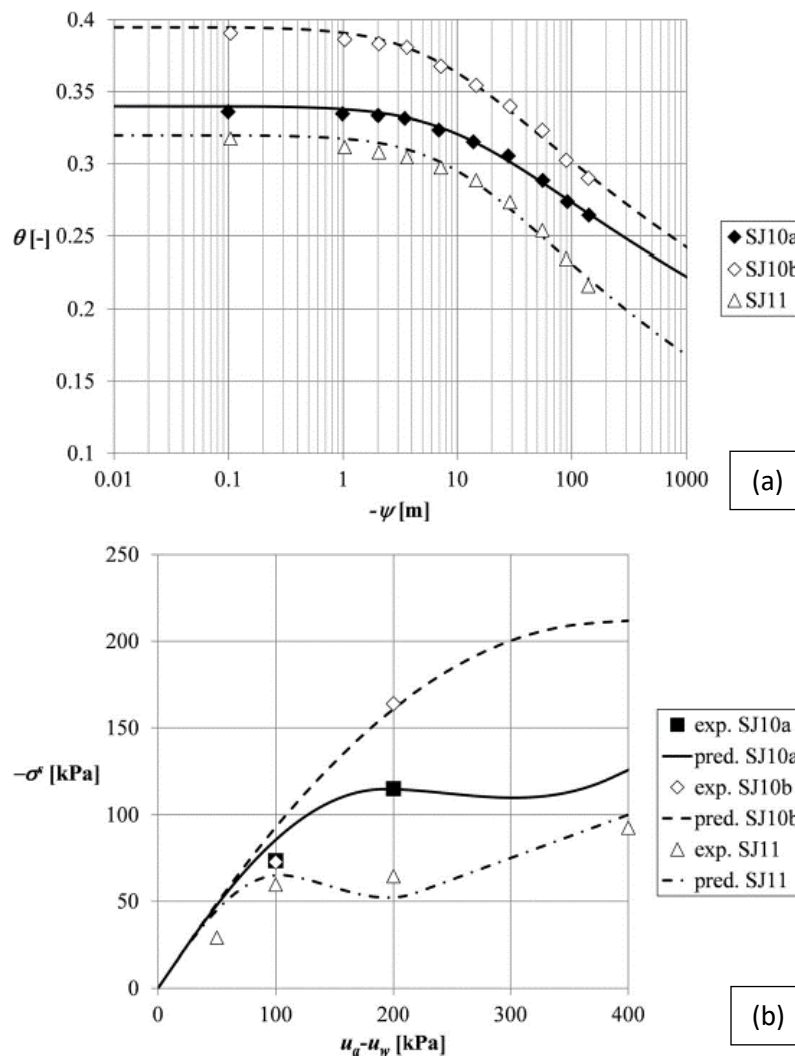


**Figure63:** Hume Dam clay soil a) SWRC data from Khalili et al. (2004), and b) suction stress results: dots indicate experimentally obtained values, while lines represent the theoretical expression for the suction stress based on the approach proposed by Greco and Gargano (2015).

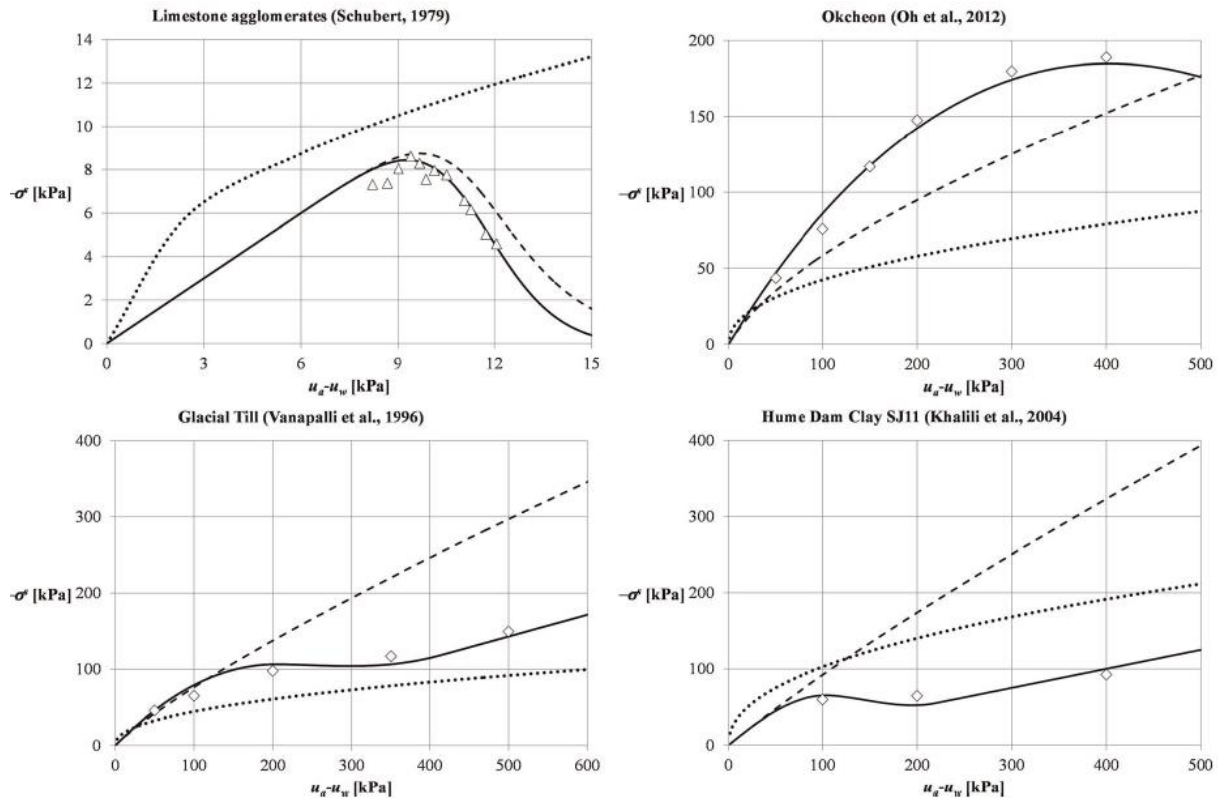


**Figure 64:** Comparison of different expressions for the SSCC curve: dots represent the values calculated from the experimental data; the solid lines represent the wet area index approach; the dotted lines represent the approach proposed by Khalili and Khabbaz (1998); the dashed lines the relationship proposed by Lu et al. (2010) (Greco and Gargano, 2015).

## 6.2. Previous studies of shear strength properties of flysch material from the Rječina River Valley

Shear strength characteristics of the residual soil from a flysch rock mass of the Rječina River Valley were investigated in several studies using various laboratory devices. In all of the previous studies, completely remolded and consolidated specimens were tested in saturated conditions. For example, Oštrić et al. (2012) used the Portable Ring Shear Apparatus, ICL-1 (Sassa et al. 2003, 2004; Okada et al. 2004; Fukuoka et al. 2006) to obtain residual shear strength parameters of the soil samples taken from the flysch outcrop on the Grohovo Landslide. Tests were performed on completely remolded and consolidated specimens under the constant shear rate of 0.002 cm/s in undrained conditions (Oštrić et al. 2012). Steady-state conditions were reached after 1 m of shear displacement, and as a result, the basic parameters values (peak, mobilized and apparent friction angle, so as cohesion), as well as a steady state normal and

shear stress of soil sample were obtained (Arbanas et al. 2014). Peak shear strength conditions were not observed while the friction angle,  $\phi$ , cohesion,  $c$ , and apparent friction angle,  $\phi_a$ , were equal to 25.4°, 15.2 kPa, and 20.4°, respectively (Oštrić et al. 2012).

Vivoda Prodan and Arbanas (2016) studied the influence of weathering process on residual strength of siltstones from flysch rock mass from the Rječina River Valley. Samples with different weathering grades taken from the Valići Landslide were completely remolded to the engineering soil grade and consolidated in the conventional direct shear apparatus (Controls S.p.A.) or ICL-1 Portable Ring Shear Apparatus. After the saturation and consolidation of specimens at normal effective stress values of 100, 200 and 400 kPa, the shearing stage was performed. In case of ring shear apparatus, constant shear speed test was performed (0.01 cm/s) in undrained conditions to obtain basic parameters (peak and residual friction angles and cohesion) and the steady-state normal and shear stress values. A constant shearing speed of 0.15 mm/min was selected for the conventional direct shear tests (Vivoda Proda et al. 2016). Basic geotechnical properties and shear strength parameters obtained in previous studies using the conventional direct shear apparatus and ICL-1 ring shear apparatus are summarized in Table 13. Results were obtained on completely remolded and consolidated samples from the Rječina River Valley in saturated conditions.

**Table 13:** Basic geotechnical properties and residual shear strength parameters of flysch samples with different weathering grades and obtained from various parts of the Rječina River Valley in previous studies by Oštrić et al. (2012) and Vivoda Prodan and Arbanas (2016).

Sampling location	Weathering degree	Particle size distribution		Atterberg's limits			Direct shear test			Ring shear test	
		< 63 $\mu\text{m}$ , C+M [%]	Sand, S [%]	$w_L$ (%)	$w_P$ [%]	PI	Spec. grav., $G_s$ [/]	Friction angle, $\phi_r$ [°]	Cohes- ion, $c_r$ [kPa]	Friction angle, $\phi_r$ [°]	Cohes- ion, $c_r$ [kPa]
Valići* <sup>1</sup>	SW/FR	19	81	Non-plastic			2.51	29	33.5	30	32
Valići* <sup>1</sup>	HW/CW	21	79	Non-plastic			2.62	31	21.5	35	11
Grohovo <sup>2</sup>	HW/CW	/	/	/	/	/	2.66	/	/	25.4	15.2

<sup>1</sup> Material sedimented at the bottom of the Valići Lake originating from the flysch deposits; <sup>2</sup> Sample taken from the flysch outcrop on the Grohovo Landslide; terms FR, SW, HW and CW indicate fresh, slightly, highly and completely weathered material.



### 6.3. Conventional direct shear tests on undisturbed samples

Undisturbed soil samples were collected from the sampling pit location (Figure 4), either by inserting hard plastic tubes into the soil or steel cutters used for testing with different direct shear devices. Prior to sampling, the superficial layer of the soil and organic matter were removed, so that sampling depths were around 0.5 to 1 m for all samples. To preserve a natural water content, undisturbed samples were wrapped in nylon upon collection in the field and sealed with wax after returning to the laboratory. Specimens were installed in testing devices with or without previous saturation, depending on desired initial water content conditions and the need for initial suction measurement. In the case of specimens with natural water content, the latter were considered to be close to the in-situ matric suction values during the time of sampling. Some details on the collection of the undisturbed samples by insertion of hard plastic tubes and using the steel cutters in-situ, sealing and specimen preparation procedure are shown in Figure 65 and Figure 66.



**Figure 65:** Some details on collection of undisturbed soil specimens from the a) sampling pit by insertion of b) hard plastic tubes or c) steel cutter for testing in direct shear apparatus.



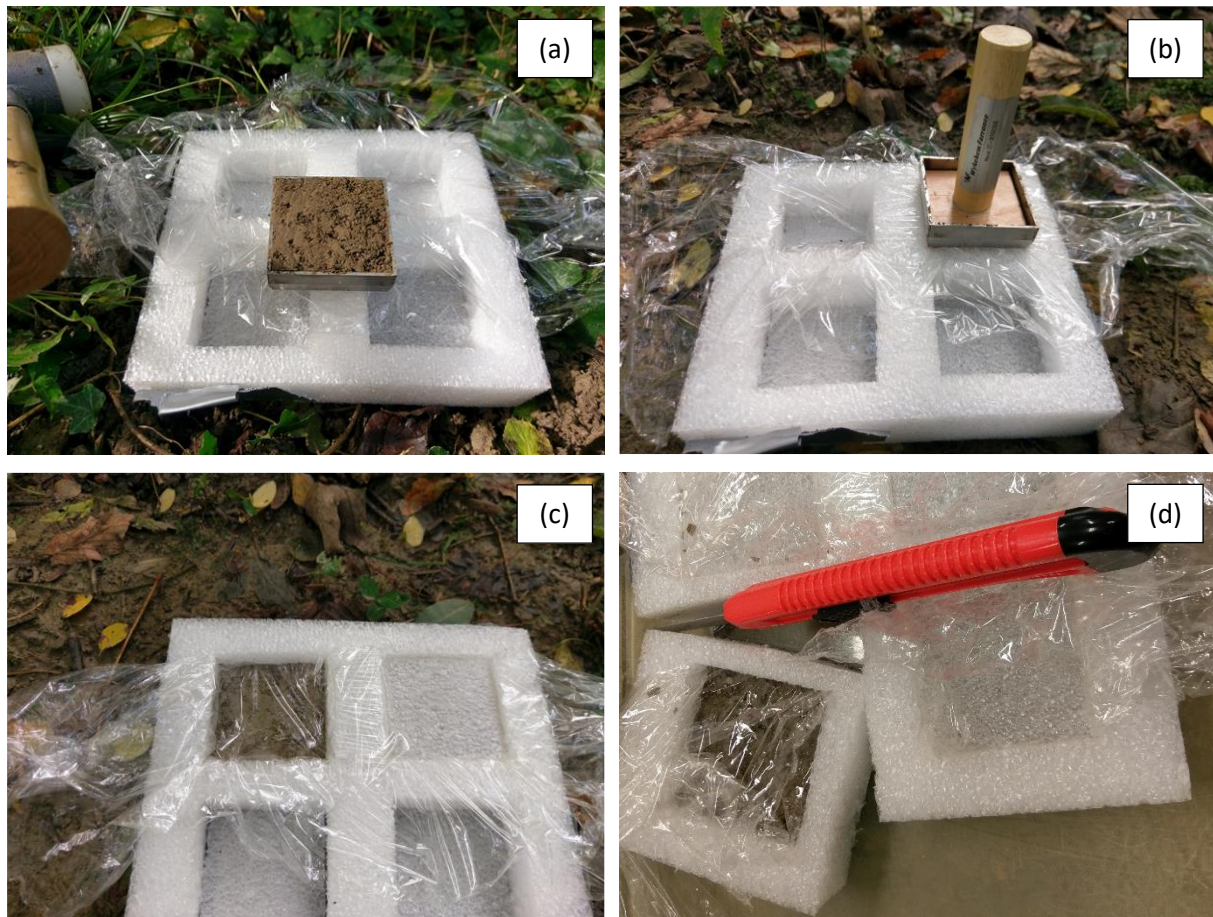


**Figure 66:** The procedure of collecting the undisturbed soil samples for testing in direct shear apparatus by using the steel cutters directly in-situ: a) 60x60 specimen in cutter; b) specimen extrusion into the perforated styrofoam box with removable upper and lower lids; c) sealing of the sample to minimize the water loss due to evaporation; and d) separation of a single specimen for the installation in testing device.

The first tests to determine shear strength characteristics of residual soil from a flysch rock mass were performed by using the conventional direct shear apparatus 27-WF2160 (Controls S.p.A.) in the Geotechnical laboratory at Faculty of Civil Engineering, UniRi. The AutoShear Machine 27-WF2160 is designed to automatically perform direct and residual shear tests (Wykeham Farrance 2010). Input parameters that have to be defined for the shearing stage are the shear rate and value of the horizontal displacement up to which the specimen will be sheared at a constant rate. Additionally, the return shearing rate has to be defined in the case of cyclic shearing in the residual shear tests. Up to 9 cycles can be defined in residual shear test mode while the shear rates can range from  $5.0\text{E-}05$  up to  $11 \text{ mm/min}$  (Wykeham Farrance, 2010). Maximum horizontal and vertical load that can be applied to a specimen is  $5 \text{ kN}$  and  $500/5000 \text{ kN}$  using the 10:1 lever loading device, respectively (Wykeham Farrance, 2010). One of the three devices that were used at UniRi is shown in Figure 67.

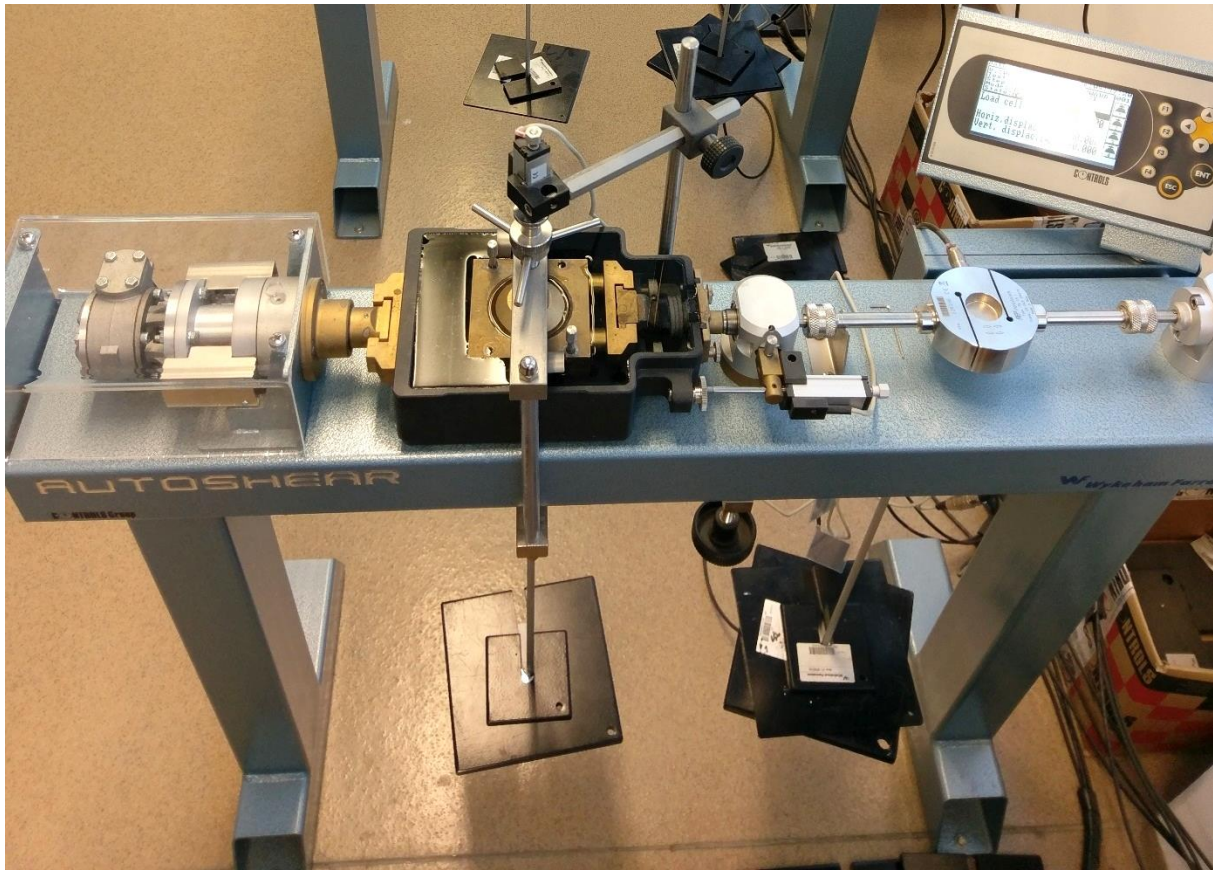


**Figure 67:** The AutoShear Machine 27-WF2160 (Controls S.p.A.) used in the Geotechnical laboratory at the UniRi, during the consolidation stage.

Tests were performed in saturated conditions at a constant shear rate of  $5\text{E-}03 \text{ mm/min}$  to ensure that results were obtained under drained conditions, without generation of significant excessive pore pressure. The adopted shear displacement rate was around half to one order of magnitude lower than the maximum displacement rate calculated from consolidation theory according to equations provided in CEN ISO/TS 1789-10:2004 (E) and ASTM D3080-11 test standards. The time to reach failure conditions was about ten times lower than the default minimum times to failure according to the USCS results suggested by ASTM D3080-11. Normal loads were applied in a single step to produce 50, 100 and 200 kPa of normal stress on square or circle specimens. After 24 h of consolidation, the shearing stage was started until the maximum shear displacement of 15 mm was reached. Then, the test was stopped, devices were dismantled, and the water content was determined. After the tests were performed on undisturbed samples, and final water content was determined, a specimen from each testing device was thoroughly mixed with distilled water by using the spatula or knife, and left to rest overnight to obtain a homogeneous mixture. Following this, the same amount of material was added in the same steel cutter used during the in-situ sampling, and installed in the same testing device. The identical testing procedure regarding the applied vertical stress, consolidation stage



and shearing conditions was repeated on produced specimens. The aim was to identify possible differences in strength or stiffness characteristics of material only due to specimen disturbance effects, avoiding problems of data interpretation and differences due to different shapes and volumes of used samples or differences between three testing devices that were used simultaneously. Several details on testing of the undisturbed specimens in conventional direct shear apparatus, and adopted preparation technique of remolded specimens are shown in Figure 68 and Figure 69. Specimen characteristics and testing conditions are summarized in Table 14.

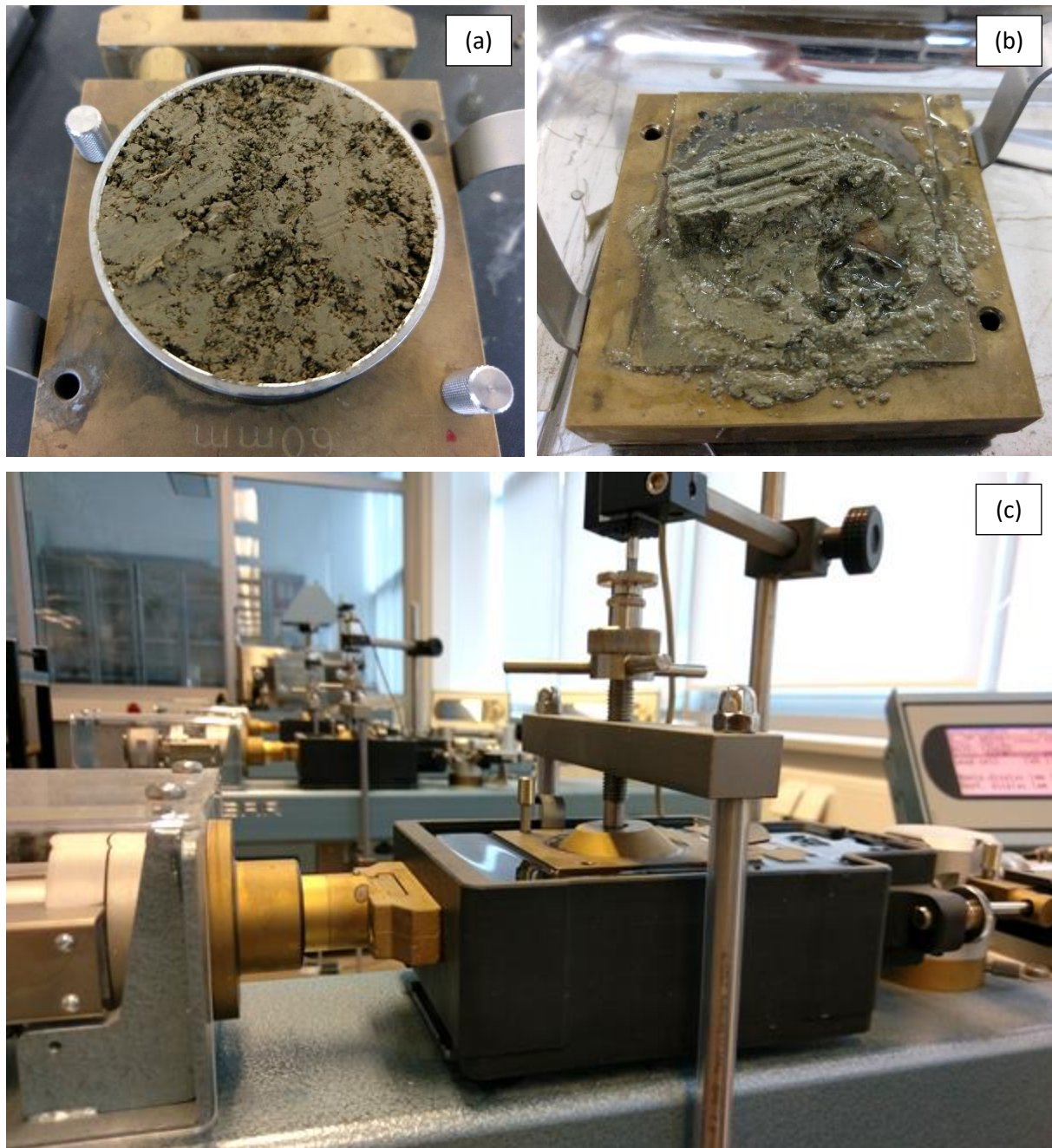


**Figure 68:** Details of conventional direct shear tests on undisturbed specimens of residual soil: a) installation of undisturbed specimen collected by insertion of circle steel cutter directly in-situ; b) undisturbed specimen with visible weathered grain of siltstone at the shearing plane; and c) undisturbed specimen during the shearing stage in conventional direct shear apparatus.

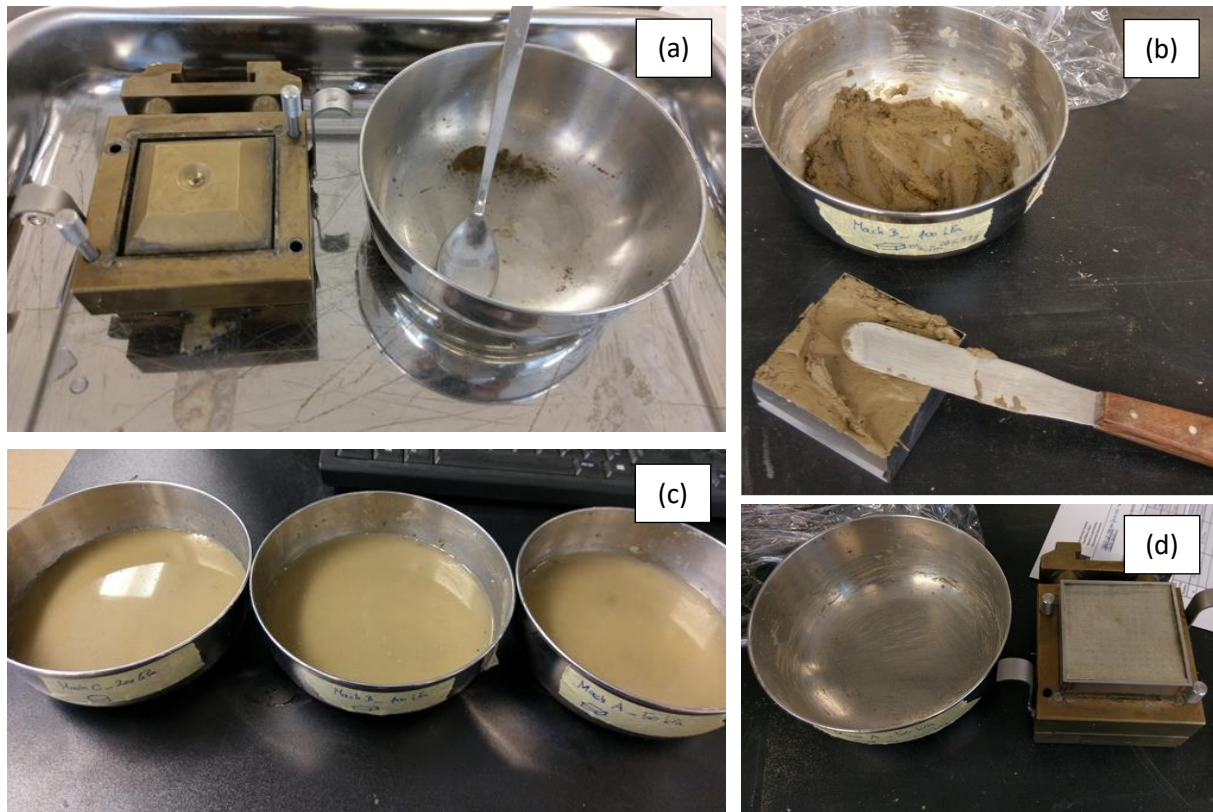


**Figure 69:** Details of the adopted specimen preparation technique: a) collection of the material after testing the undisturbed specimen for water content determination; b) material thoroughly mixed with de-aired water left to rest over-night; c) installation of sample inside the square cutter; and d) remolded specimen ready for the installation in direct shear apparatus.

**Table 14:** Test characteristics of conventional direct shear tests performed on undisturbed and remolded specimens.

Testing machine	Height of the specimen, H [mm]	Shape of the specimen [square/circle]	Shear box area, A [mm <sup>2</sup> ]	Rate of shear displacement [mm/min]	Applied vertical stress [kPa]
A	20.1	square	3600	0.005	50
B	20.1	square	3600	0.005	100
C	20.05	round	2827.43	0.005	200

### 6.3.1. Test results for undisturbed and remolded specimens

Due to test duration and costs, the influence of sample disturbance, specimen preparation technique and stress history on the shear strength characteristics of residual soil from a flysch rock mass was investigated only in saturated conditions, using the conventional direct shear apparatuses. In Figure 70 results of the consolidation stage are shown for applied vertical stress values of 50, 100 and 200 kPa, both for undisturbed and remolded specimens. Results from the shearing stage are shown in Figure 71. A diagram in terms of the horizontal shear displacement

vs. measured shear stress is shown in Figure 71 a), while Figure 71 b) shows vertical displacements during the shearing stage, for all values of applied vertical stress and both for undisturbed and remolded specimens.

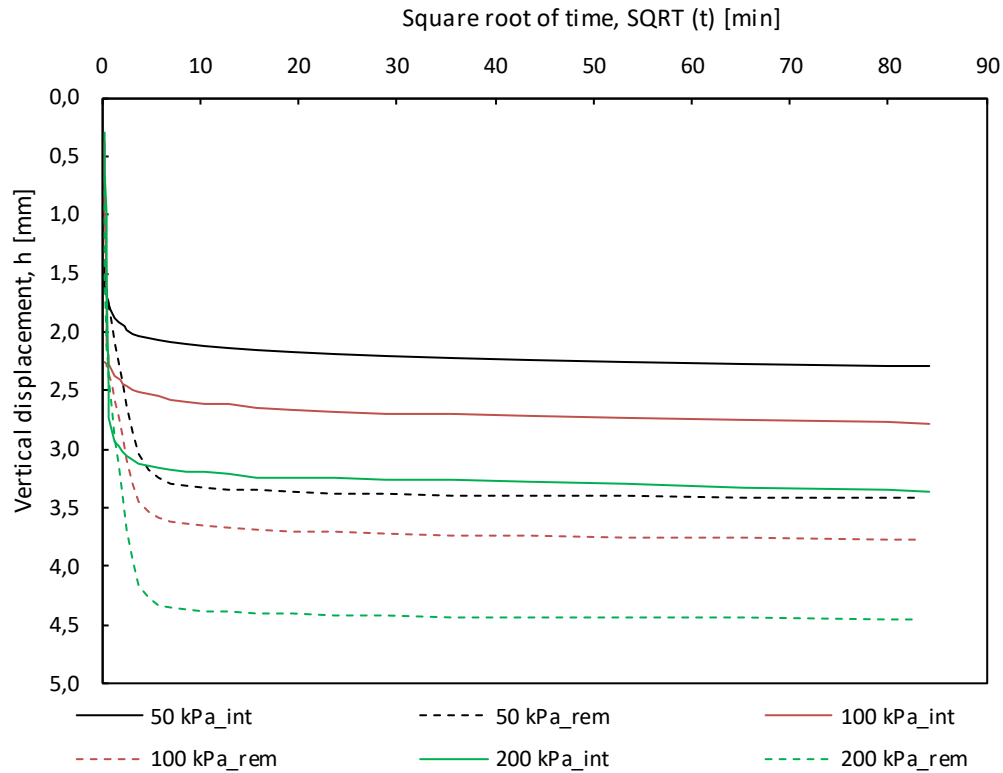


**Figure 70:** Consolidation stage test results for undisturbed (solid line) and remolded (dashed line) specimens. Black, red, and green colors represent 50, 100, and 200 kPa of vertical stress, respectively.

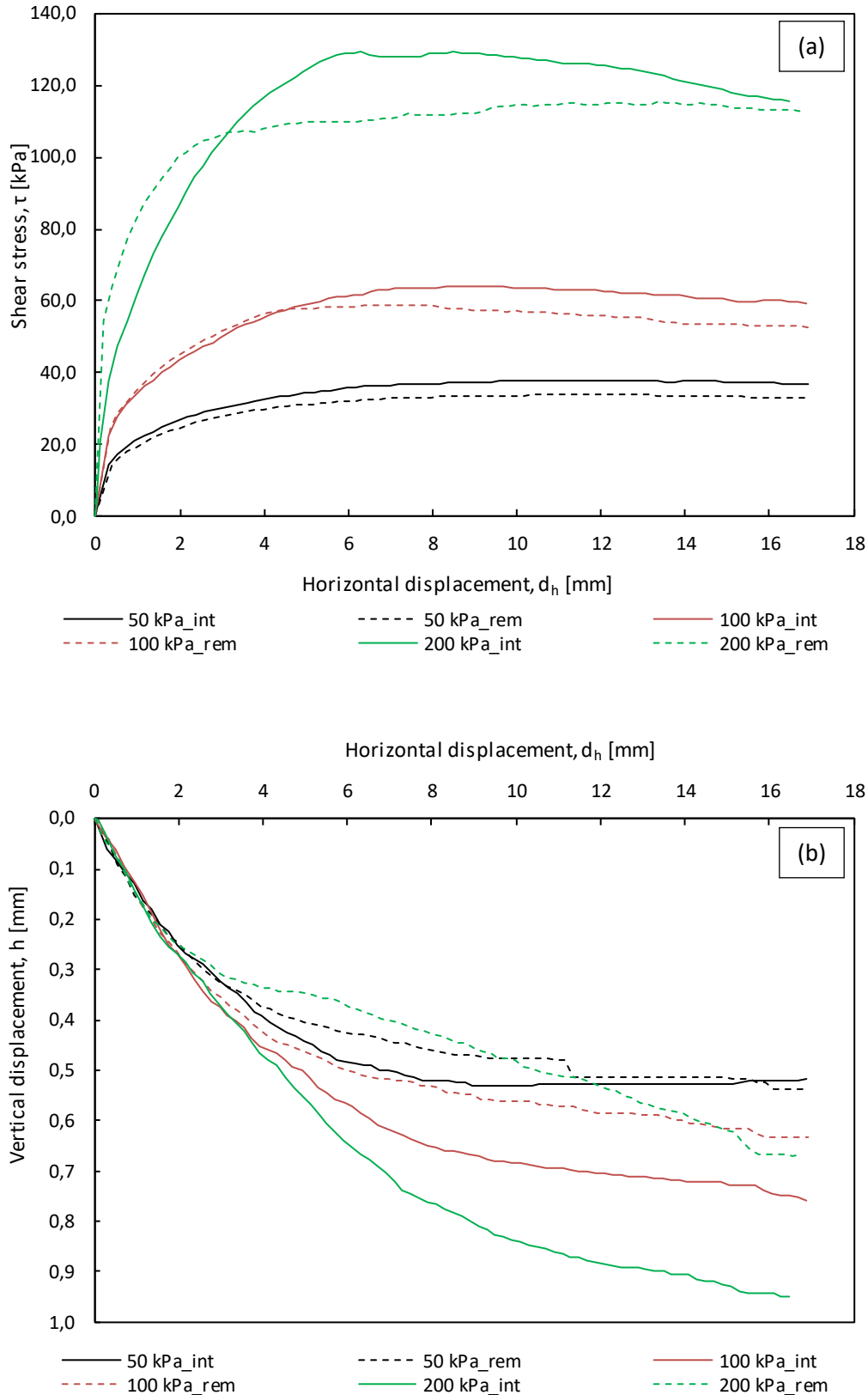


**Figure 71:** Shear stage test results for undisturbed (solid line) and remolded (dashed line) specimens at different vertical stress values in terms of a) horizontal displacement vs. shear stress and b) horizontal displacement vs. vertical displacement. Black, red, and green colors represent 50, 100, and 200 kPa of vertical stress, respectively.

### 6.3.2. Interpretation of conventional direct shear test result

As expected, Figure 70 shows that, under the same value of the applied vertical stress, undisturbed specimens undergo significantly smaller vertical deformation than remolded specimens. However, during the shearing stage, the situation is quite different: undisturbed specimens undergo greater compression than remolded specimens for all values of the applied vertical stress. There is a slight inconsistency in results obtained from remolded specimen consolidated at 200 kPa, since the vertical deformation is smaller than for specimen consolidated at 50 kPa and 100 kPa, up to the horizontal displacement of 10 and 14.8 mm, respectively. Results indicated that the shear strength was fully mobilized at horizontal displacement values of 11.4, 8.5 and 6.3 mm for tests performed on undisturbed specimens at normal stress values of 50, 100 and 200 kPa, respectively. Horizontal displacement values corresponding to fully mobilized shear strength for remolded specimens, under the same values of normal stress were 11.3, 8.6 and 6.6 mm. Figure 71 a) reveals that the results obtained for undisturbed specimens always plot only slightly higher than those obtained for remolded specimens. It seems that the disturbance effects have no significant influence on the stiffness or maximum shearing resistance properties. Shear strength envelopes for undisturbed and remolded specimens are shown in Figure 72.

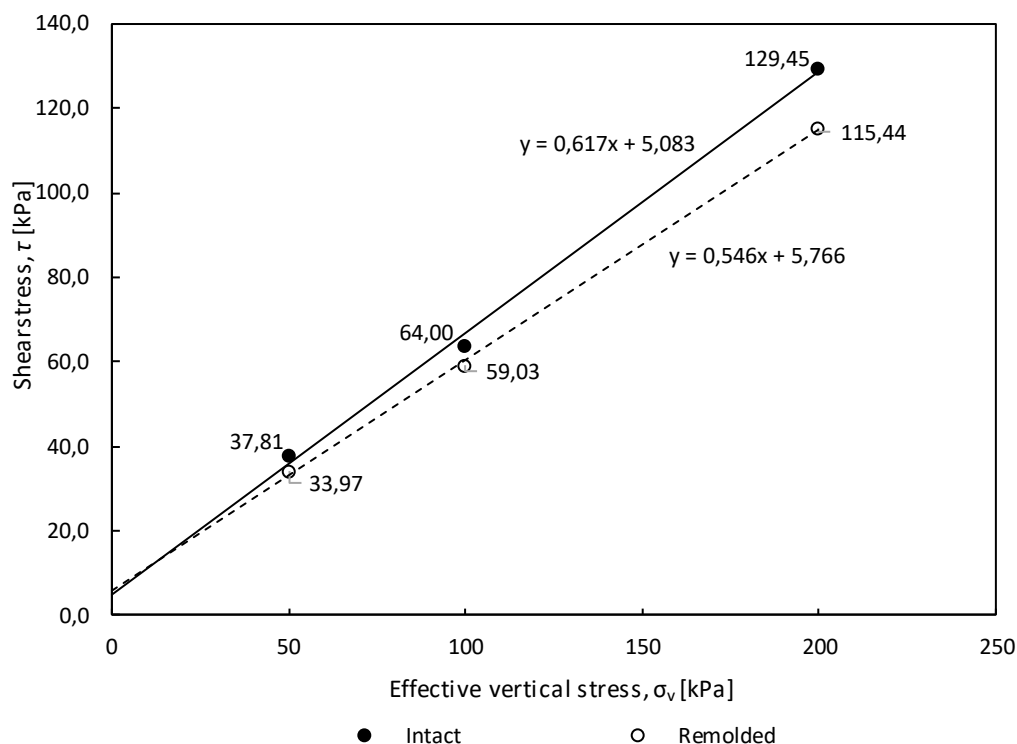


**Figure 72:** Mohr-Coulomb shear strength envelopes for undisturbed (solid line, filled markers) and remolded specimens (dashed line, empty markers), obtained in conventional direct shear apparatus.



Obtained Mohr-Coulomb shear strength parameters, the effective cohesion  $c'$ , and the effective angle of internal friction associated with the effective normal stress  $\phi'$ , were equal to 5.1 kPa and 31.7° for undisturbed specimens, and 5.8 kPa and 28.6° in the case of remolded specimens. While the effective angle of internal friction values closely corresponds to results that were obtained in previous studies on material originating from the same bedrock (Oštrić et al. 2012; Vivoda Prodan and Arbanas 2016), obtained values of the effective cohesion are much smaller. Although there might be some inhomogeneity among the used soil samples, the main reason for different shear strength parameters could be the rate at which samples were sheared. In previous studies, much higher shearing rates were used, which could result in the generation of excess pore water pressure during the shearing stage.

Figure 73 shows the remolded specimen after the shearing stage with a visible part of the shearing surface. Interestingly, even in the case of the remolded specimen, there are visible grains of highly weathered siltstone that were crushed during the shear stage, leaving the trace of lightly brown color which can be clearly distinguished from the grey silty-clay matrix.

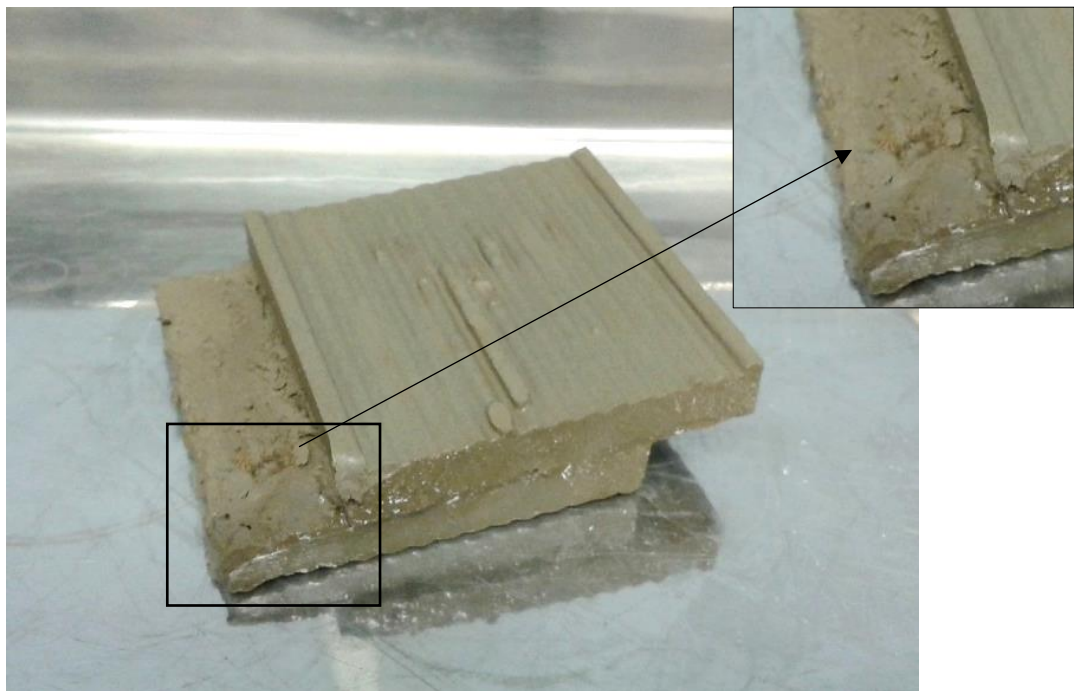


**Figure 73:** Remolded specimen dismantled from direct shear apparatus after the test with visible highly weathered siltstone particle crushed on the shearing plane.



## 6.4. Determination of shear strength characteristics of undisturbed samples in unsaturated conditions

The determination of shear strength properties in unsaturated conditions was performed with two modified, axis-translation based (Hilf 1956) direct shear devices. First measurements of matric suction at natural water content and shear tests were conducted in the Geotechnical laboratory at UniSa, by using the Suction Controlled Direct Shear Apparatus (SCDSA) (Megaris s.a.s.). The shear box apparatus that enables measurement or control of the matric suction through the axis translation technique was developed in cooperation with the Department of Geotechnical Engineering of the University of Naples Federico II ([http://www.megaris.it/en/w\\_geo/tns.asp](http://www.megaris.it/en/w_geo/tns.asp)). This apparatus enables testing of square soil samples with dimensions of 60x60x20 mm under very low values of the net vertical stress (5 kPa), and under a wide range of matric suction values (0-300 kPa) under constant water content or control of the matric suction. A device used at UniSa is shown in Figure 74. It was equipped with 1bar HAEPD, and internal shear and axial load cells with a capacity of 5 kN.



**Figure 74:** Suction Controlled Direct Shear Apparatus (SCDSA) (Megaris s.a.s.) used in the Geotechnical laboratory at the UniSa.

Precise measurements of the water content variations during the test are based on a high accuracy differential pressure transducer, which measures the pressure difference in two double-walled burettes shown in the central part of Figure 74, as proposed by Aversa and Nicotera (2002). One of the burettes is connected to the drainage circuit while the other one is used as a reference. The scheme of the testing system provided in Papa and Nicotera (2011) is shown in Figure 75.

The shear box with a standard porous stone in the upper half and HAEPS installed in the bottom half is located inside a steel cell which is pressurized with air. The bottom (fixed) half of the shear box has the water compartment below the HAEPS where the pore water pressure,  $u_w$ , is measured. The water compartment is connected with the burette for measuring water content variation. The peristaltic pump between the measuring burette and water compartment below the HAEPS can be switched on to flush the system from diffused air. Any air bubbles trapped below the HAEPS or inside tubes are pushed into the water volume measuring burette during the circulation of water, thus providing correct readings of water volume changes during the test, only due to water volume change in the tested soil specimen. The differential pressure transducer reads the water volume changes respective to the reference burette. The pressurized air is connected to the system through the main pressure line with the main pressure regulator. The system can regulate four pressures independently by means of electro-pneumatic regulators with 1kPa accuracy. The pressures that can be used during various test stages are: cell pressure  $p_c$ , pore water pressure  $u_w$ , axial,  $p_a$ , and shear pressure,  $p_s$ .

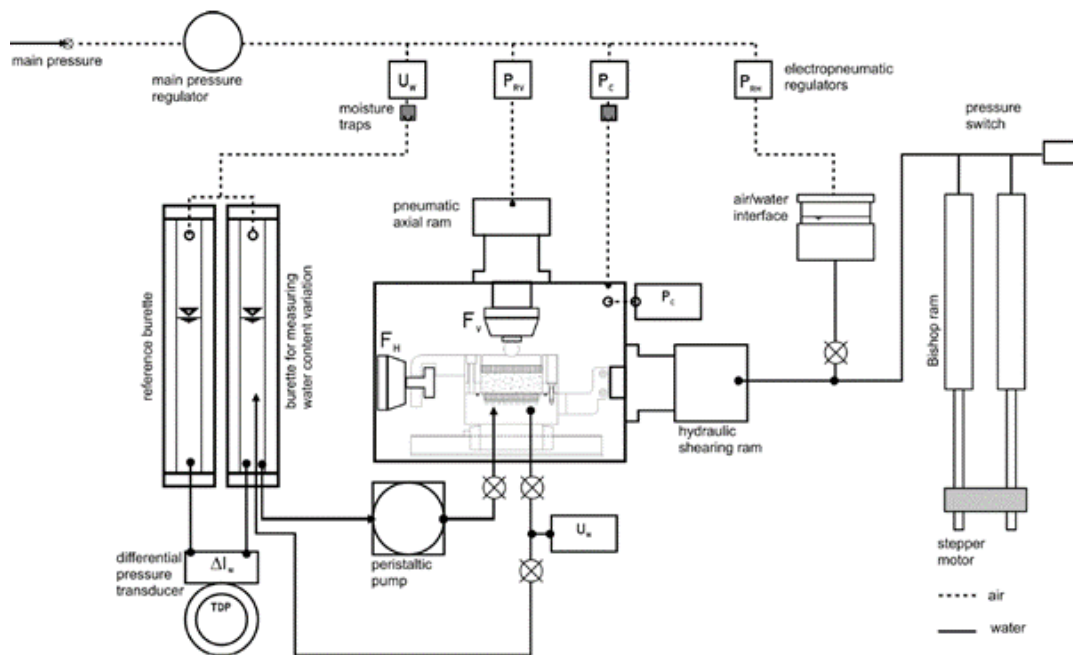
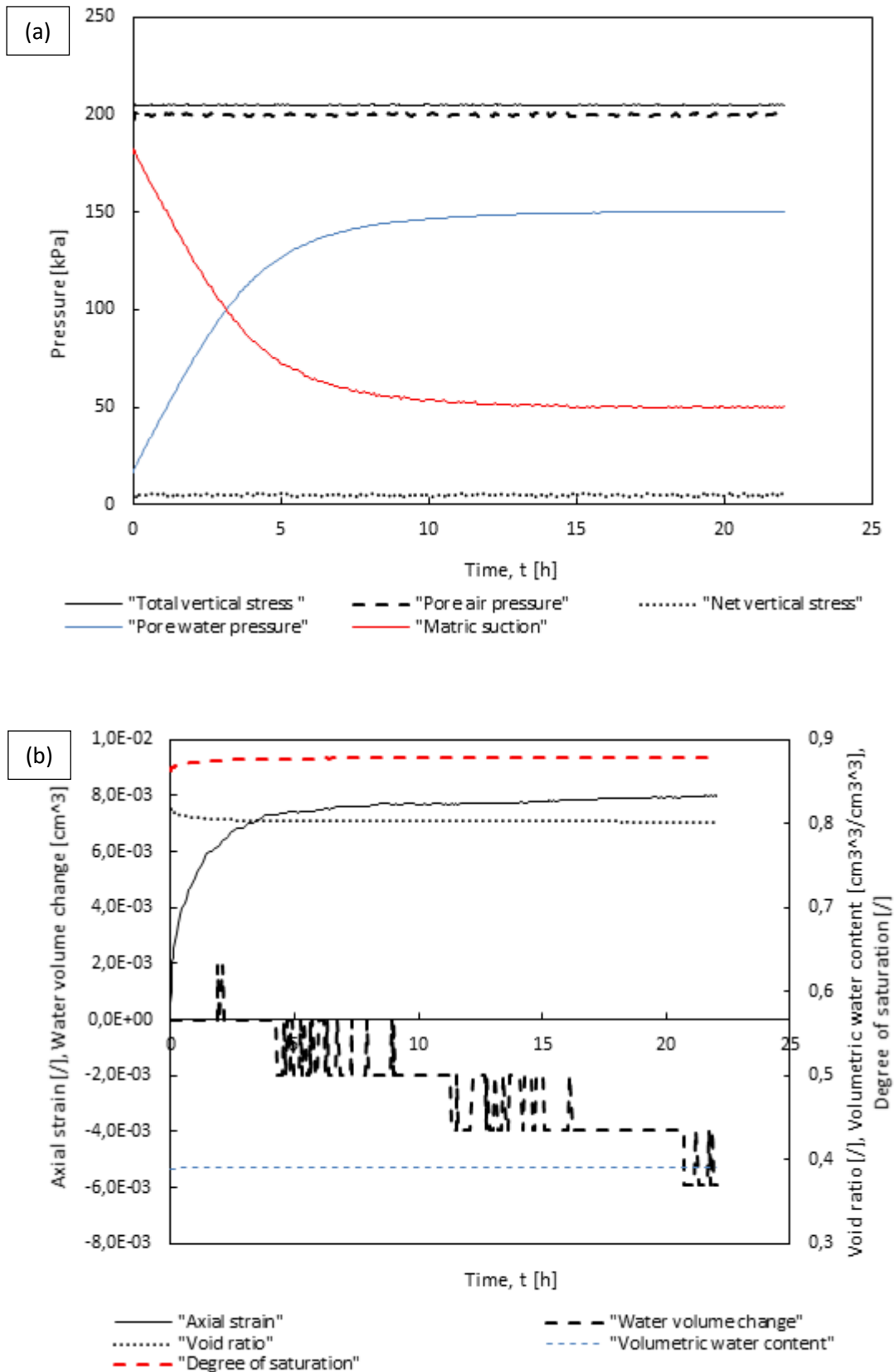


**Figure 75:** Scheme of pressure regulation circuits and transducers used in the suction-controlled direct shear apparatus (Papa and Nicotera 2011).

The cell pressure applied inside the steel chamber is equal to the applied air pressure,  $u_a$ , which is considered to be the same as air pressure inside the pores of the tested specimen. Pore water pressure is equal to the water pressure in the compartment below the HAEPD, while the difference between air and water pressure ( $u_a - u_w$ ) is equal to the matric suction value in tested specimen. Cavitation of water can be eliminated in the described system simply by artificially raising the air pressure inside the testing chamber above the atmospheric pressure, causing the water pressure to increase into a positive domain where cavitation phenomenon does not occur. The limitations of the maximum matric suction that can be measured or controlled inside a such system are defined by the maximum pressure values that can be applied inside the testing system (steel chamber, valves, pipes, pressure transducers, etc.), and the AEV of the high air entry ceramic disk located at the bottom of specimen, in the lower part of the shear box. Two independent hydraulic pistons are used for controlling the axis and shear loads, while inner load cells are used for the measurement. Two LVDTs are used to measure vertical and horizontal displacements during the test. The whole system is connected to the PC unit with an open source software which enables complete control of test and data acquisition.

Three tests (DSUVCJ01, DSUVCJ02, and DSUVCJ03) in total were performed by using the Suction Controlled Direct Shear Apparatus at the UniSa. Tests were performed on undisturbed samples collected with steel cutter directly in-situ, starting from the natural water content. After the specimen installation, drainage valve was closed and air pressure inside the cell was increased. A vertical ram was brought into contact with the top cap by applying a small net vertical stress (contact pressure of few kPa) to keep track on vertical deformations. Initial matric suction value was determined once the pore water pressure value became constant in time. After the measurement of the initial suction for natural water content, the consolidation stage was performed by applying different values of net vertical stress. Net vertical stress values equal to 50, 100 and 200 kPa were used for the DSUVCJ01, DSUVCJ02, and DSUVCJ03 tests, respectively.

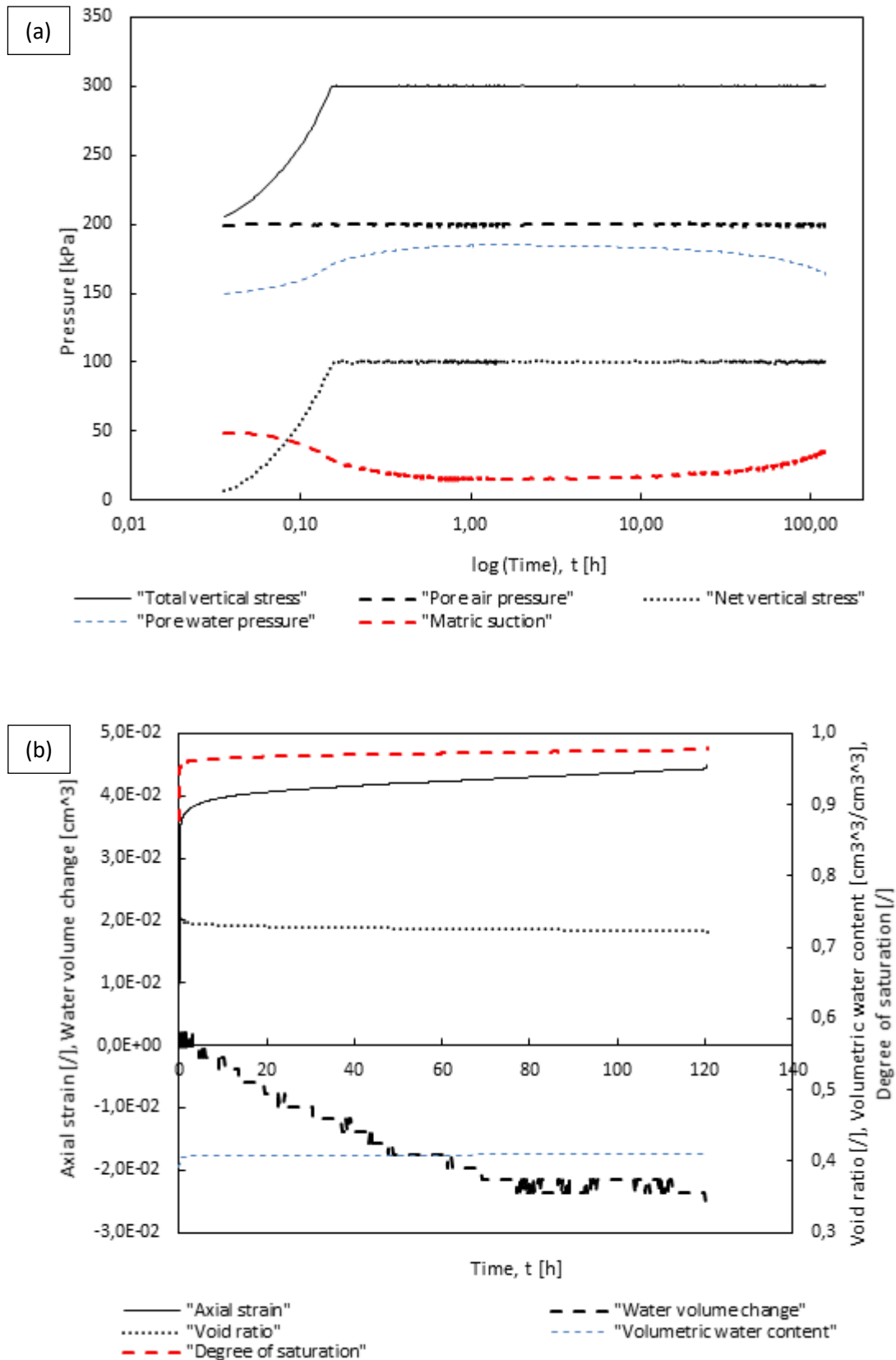
For the first sample in the DSUVCJ01 test, matric suction of 50 kPa was measured for natural water content and 5 kPa of the contact pressure. The detail of the initial suction measurement for the natural water content in the DSUVCJ01 test is shown in Figure 76 a). The pore water pressure value became constant after around 12 – 13 hours. Results regarding the axial strain, void ratio, water volume, volumetric volume content and degree of saturation change for the initial suction measurement stage are shown in Figure 76 b).



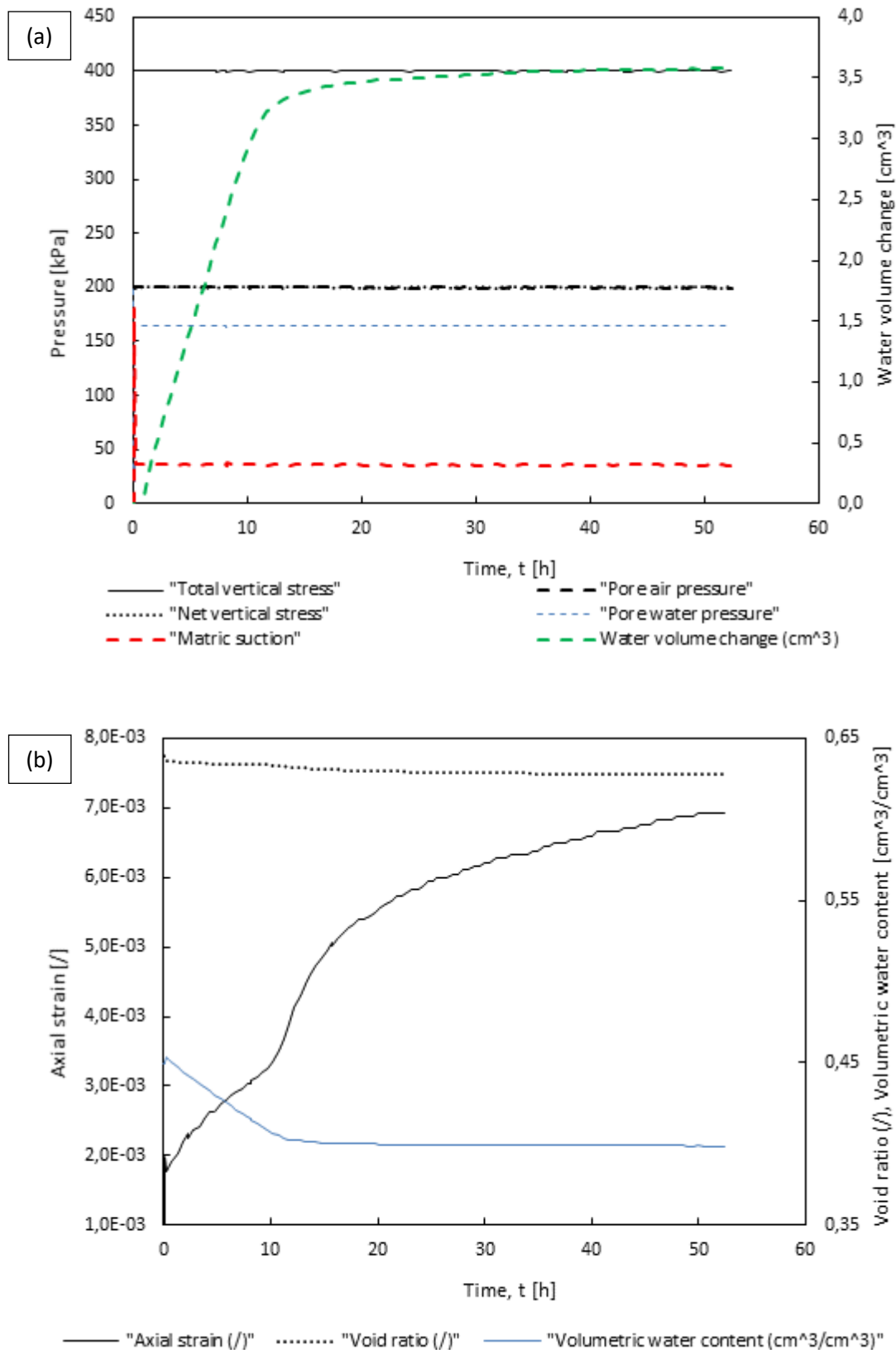
**Figure 76:** Initial suction measurement stage for the natural water content in the DSUV CJ01 test in terms of a) measured stress values with calculated matric suction value; b) measured axial strain and water volume change with calculated variables: void ratio, volumetric water content and degree of saturation.

Following the initial suction measurement stage, the specimen was consolidated for 24 h at 100 kPa of net vertical stress with measurements of axial deformation and matric suction value. As expected, compression of the specimen caused the increase of the volumetric water content and degree of saturation, reducing the matric suction value up to around 16 kPa. After approximately 12h, the matric suction started to increase at a very low rate, probably due to the evaporation process taking place inside the large steel chamber. Matric suction of 36 kPa was measured at the end of the consolidation stage. To save time, matric suction of 36 kPa was chosen to be kept constant during the shearing stage in drained conditions and an additional equilibration stage was omitted. The measurements collected during the consolidation stage in the DSUVCJ01 test are presented in Figure 77. Measured stress values with calculated matric suction value are shown in Figure 77 a), while measurements of the axial strain and water volume change along with computed void ratio, volumetric volume content and degree of saturation change during the consolidation stage are shown in Figure 77 b).

Shearing was performed at a constant shear rate of  $5\text{E-}03$  mm/min under constant matric suction value of 36 kPa up to a maximum shear displacement of around 20 mm. The same testing programme was adopted in DSUVCJ02 and DSUVCJ03 tests, except for the additional equilibration stage before the shearing stage. Varying values of applied net vertical stress during the consolidation stage, along with slightly different initial conditions of undisturbed specimens resulted with varying matric suction values at the end of the consolidation stage. After the 24 h consolidation stage was completed, the drainage valve was opened and pore water pressure beneath the HAEPD was changed to result in 36 kPa of matric suction. Water volume change in the measuring burette was observed during the equilibration process. Finally, when the water flow from or into the specimen ceased, or slow linear change with time was observed, it was considered that the specimen was equilibrated at the imposed matric suction value and tests could proceed to the shearing stage. Figure 78 shows an example of the equilibration stage for the DSUVCJ02 test. The measured stress values, calculated matric suction, and recorded water volume change during the equilibration at imposed matric suction value are shown in Figure 78 a), while the measured axial strain along with calculated void ratio and volumetric water content change during the equilibration stage are shown in Figure 78 b). Specimen characteristics and testing conditions are summarized in Table 15. Some details on specimen preparation, installation, and testing in Suction Controlled Direct Shear Apparatus are shown in Figure 79 and Figure 80. Obtained test results are reported in the following section.



**Figure 77:** Results for the consolidation stage in the DSUVCJ01 test in terms of a) measured stress values with calculated matric suction value; b) measured axial strain and water volume change with calculated variables: void ratio, volumetric water content and degree of saturation.

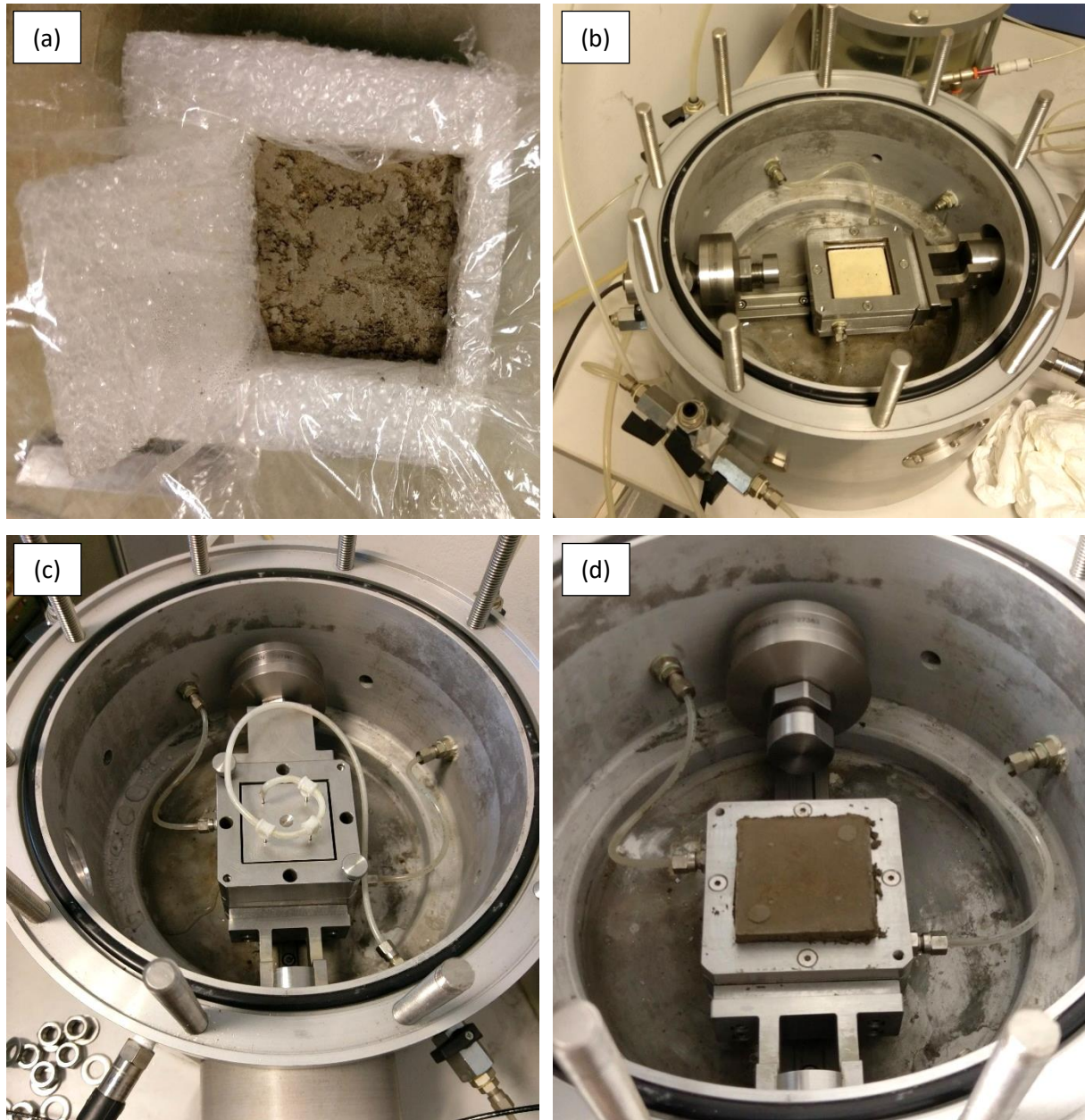


**Figure 78:** Equilibration of the specimen from the DSUVCI02 tests at 36 kPa of matric suction after the consolidation at 200 kPa of net vertical stress, in terms of a) measured stress values, calculated matric suction value, and volume of water drained from the specimen; b) measured axial strain with calculated variables: void ratio and volumetric water content.



**Table 15:** Test characteristics of direct shear tests performed on undisturbed specimens using the Suction Controlled Direct Shear Apparatus in the Geotechnical laboratory at the UniSa.

Testing machine	Test name	Height of the specimen, H [mm]	Shear box area, A [mm <sup>2</sup> ]	Rate of shear displacement [mm/min]	Applied vertical stress [kPa]
SCDS	DSUVCJ01	20	3600	0,005	100
SCDS	DSUVCJ02	20	3600	0,005	200
SCDS	DSUVCJ03	20	3600	0,005	50

**Figure 79:** Some details of Suction Controlled Direct Shear Apparatus used at the UniSa: a) undisturbed sample collected with cutter in-situ; b) disassembled steel chamber with saturated HAEPD; c) installed sample with the attachment for the wetting test connected through the top cap; and d) undisturbed specimen after the shearing stage.



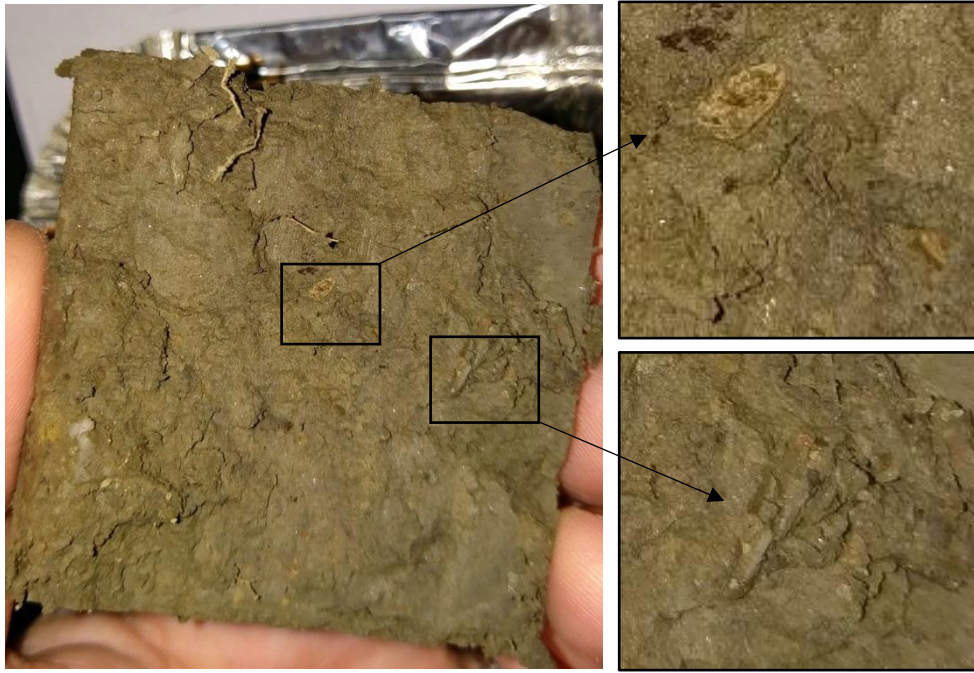


**Figure 80:** Heterogeneity of the undisturbed samples: siltstone grains of different size and weathering degree, along with some roots present at the shear surface of the specimen used in the DSUVCI01 test.

The unsaturated version of the Back Pressured Shear Box (GDS Instruments Ltd.), shown in Figure 81, was used in the Geotechnical laboratory at Faculty of Civil Engineering, UniRi, Croatia to further explore the influence of matric suction on shear strength characteristics of undisturbed samples of residual soil from a flysch rock mass. In the same way as the modified direct shear apparatus used at the UniSa, the device implements the axis translation technique (Hilf, 1956) by means of a high air-entry ceramic disk installed in the lower part of the shear box and precise control of air and water pressure, to control or measure matric suction of soil. Some of the very unique design features from the GDS manufacturer are the ability to manually adjust the shear gap from the outside of the testing chamber in order to minimize the sample disturbance in stages preceding the shearing stage. This is very useful in case of soil testing in unsaturated conditions, where high values of air pressure can be applied inside the testing chamber. A submersible load cell for shear force measurement ensures load measurements with greater accuracy, excluding the need for any ram friction corrections (GDS Instruments Manual 2013). The used device enables testing of square soil samples of dimensions 100x100x20 mm with the application of 10 kN of maximum normal load and 5 kN of the maximum shear load. Maximum shear displacement is  $\pm 12.5$  mm and the maximum working back pressure of 1 MPa can be applied during the test (GDS Instruments Manual 2013). The device is equipped with 5 bar capacity HAEPS installed in the lower part of the shear box, and GDS pressure and volume controlling unit with a nominal volumetric capacity of 200 cm<sup>3</sup>,

connected directly to the water compartment below the HAEPS. A software-controlled GDS pneumatic controller is used to apply air pressure inside the testing chamber. The schematic of the Unsaturated GDS Back Pressured Shear Box (UGDSBPS) fully equipped for testing in unsaturated conditions is shown in Figure 82.



**Figure 81:** Back pressurized direct shear apparatus for soil testing in unsaturated conditions (GDS Instruments Ltd.) in Geotechnical laboratory of Faculty of Civil Engineering, UniRi.

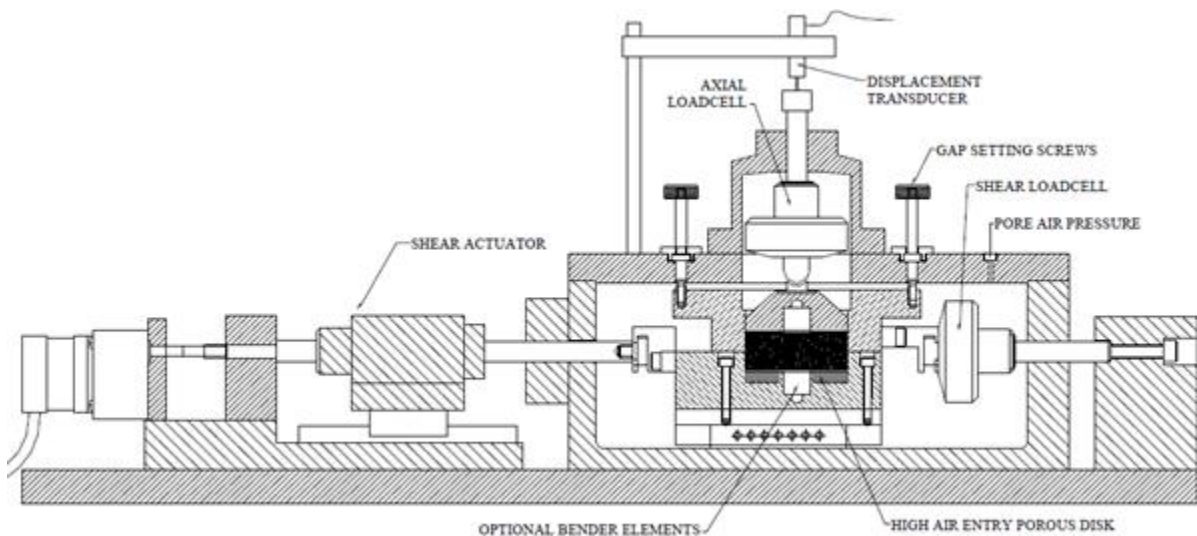


**Figure 82:** Schematic of the UGDSBPS fully equipped for testing in unsaturated conditions options ([www.gdsinstruments.com](http://www.gdsinstruments.com))

The above-described system and GDSLAB software allow the control of the back pressure, back volume, air pressure, shear load, shear stress, shear strain and shear displacement, normal load, normal stress, normal strain and normal displacement in the following manner: constant (the parameter is actively controlled during the test); ramp (the desired parameter value is increased or decreased by a user-defined amount over a user-defined time interval and then kept constant, if not defined otherwise); cycle (the set parameter is cycling according to user requirements) and hold volume (the parameter is not under controlled but usually measured during the test stage). The device can be equipped with GDS bender elements, simply by replacing standard pedestal and top cap with those equipped with bender element inserts, enabling measurement of soil stiffness at very small strains during any test stage. The bender element system master signal conditioning unit and GDSBES software are used to control data acquisition and driving signal generation. Single or repeated sinusoidal, square or user defined waveforms can be generated by using the bender elements.

This advanced testing device enables the performance of various types of standard or advanced shear tests in saturated or unsaturated conditions, such as quasi-static cyclic loading of samples under either load or strain control, multi-stage testing, consolidation, quasi-static (low speed/creep), ramp and cycle pore pressures or volumes, saturation ramp, back pressure cyclic direct shear displacement tests, back pressure cyclic direct shear load tests, geomembrane shear test, constant normal stiffness, stress-dependent soil water characteristic curve determination (SDSWCC), etc. ([www.gdsinstruments.com](http://www.gdsinstruments.com)), with or without using the bender elements.

Various test types were performed using the UGDSBPS device on undisturbed samples starting from the natural water content, with or without initial suction measurement, or saturated conditions. In the case of saturation prior to testing, samples in the steel cutter with filter paper beneath and above were covered with a steel plate to prevent any swell and submerged in de-aired water for a period of a minimum 24 h. Specimen saturation inside the disassembled testing chamber was performed only in the case of the UVSCDS03 test by flooding the specimen inside the shear box with tightened shear-gap screws. De-aired water was added from the top and through the HAEPS at the bottom, by applying a small pressure with the GDS volume and pressure controller (30 kPa). Some details of specimen preparation and described saturation procedures are shown in Figure 83 and Figure 84.

All of the tests that were performed in the UGDSBPS with loading conditions and initial specimen characteristics are summarized in Table 16. Measured water contents and



corresponding matric suction values that were measured for the natural water content indicated two distinct sampling periods.



**Figure 83:** Preparation of undisturbed specimen for testing in the UGDSBPS collected in-situ with dimensions 100x100x20 mm.

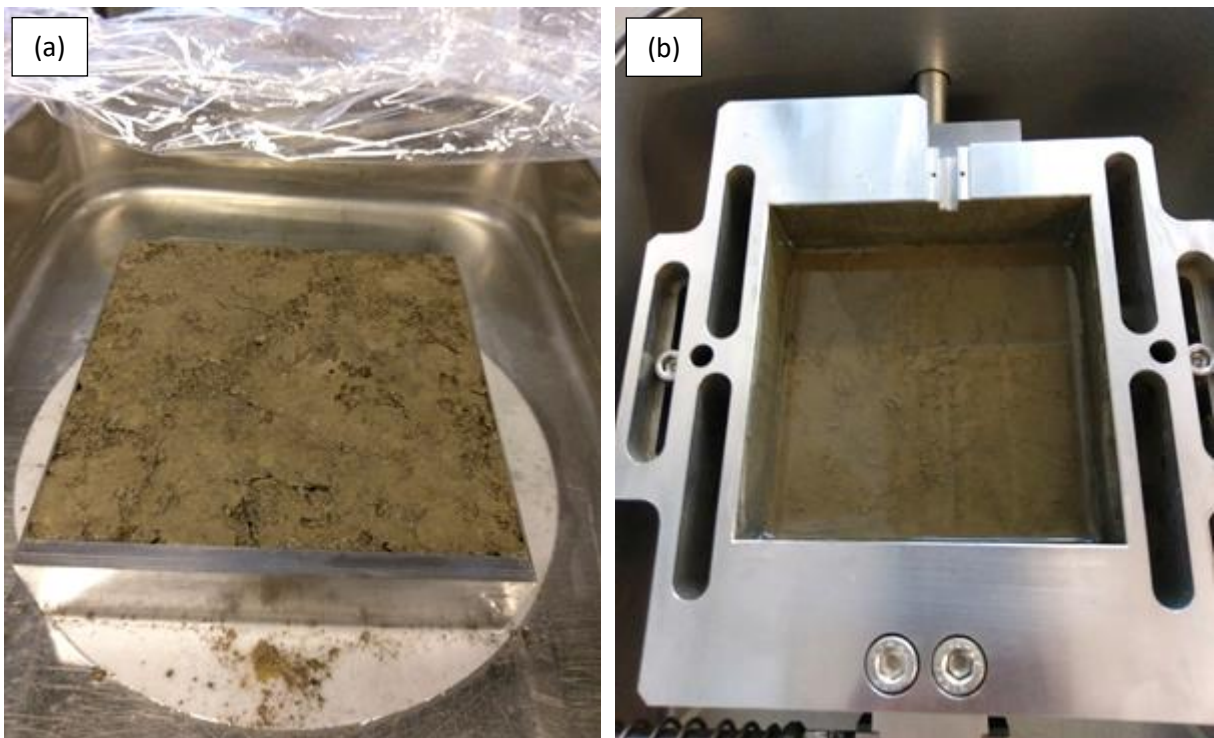


**Figure 84:** Saturation of undisturbed specimens used in the UGDSBPS a) outside the shearbox by submersion in de-aired water along with the cutter, filter papers and steel plate at the top of specimen; b) inside the shear box by adding water from the top and bottom.

Samples with lower natural water content (UVSCDS04, UVSCDS06, UVSCDS11, and UVSCDS12) ranging from 14.1% to 17.4%, were collected at the end of July 2017, during the dry period without any rainfall in one week period preceding the sampling day. Other samples with higher water content values were collected during March 2017 (UVSCDS01, UVSCDS02, UVSCDS03, and UVSCDS07) and September 2017 (UVSCDS08, UVSCDS09, and UVSCDS10) periods with higher amounts of rainfall. In both cases, in-situ conditions for the period preceding the sampling day, such as the actual evapotranspiration and amount of rainfall, resulted in higher values of the degree of saturation for the samples that were collected at relatively small depth ( $<0.5$  m). Consequently, lower matric suction values were measured for the natural water content.

Tests UVSCDS01, UVSCDS02, UVSCDS02b, UVSCDS08, UVSCDS09, and UVSCDS10 were performed as a suction controlled tests under different values of matric suction and net vertical stress, starting from the natural water content and with initial suction measurement. The same shearing rate of  $5.0 \times 10^{-3}$  mm/min was used for all suction-controlled tests. Test UVSCDS02b was performed as a re-shearing test under the increased matric suction value respective to the matric suction value applied in the first test. After the end of the UVSCDS02 test, the specimen was sheared into the opposite direction, until the initial position of the shear box was reached. The specimen was unloaded to a low contact pressure of 5 kPa, and air pressure was decreased to atmospheric pressure. The drainage valve was kept constantly closed after the end of the UVSCDS02 test to prevent a change in the water content of the specimen. Following this, the UVSCDS02b test was started and the specimen was again consolidated and equilibrated at a desired matric suction value, higher than in the previous test. Following the equilibration stage, the specimen was sheared with control of matric suction under the constant shear rate. Stages of initial suction measurement, consolidation at the net vertical stress value of 100 kPa and equilibration 174 kPa of matric suction for the UVSCDS02 test are shown on the same graph in Figure 85. During the stage of initial suction measurement, air pressure inside the cell was ramped at a constant rate from 0 (equal to the atmospheric pressure) to 200 kPa over 16 min. This value was kept constant during the consolidation and equilibration stages. Pressure and volume controlling unit measured a negative pore water pressure (around -20 kPa) at the very beginning of the test since the initial degree of saturation inside the specimen installed at natural water content was below 100 %, and the air pressure inside the testing chamber was still at the atmospheric value. Air pressure increasing is followed by the increase of pore water pressure up to some constant value, defining the initial matric suction value existing in the tested specimen. Again, the difference between pore air and pore

water pressure approaches the value of around 20 kPa. During the application of net vertical stress of 100 kPa in consolidation stage, pore water pressure instantly increases and then, with the dissipation of excess pore water pressure converges to a lower constant value, equal to 8 kPa. At the same time, the void ratio value decreases causing a rapid increase in the degree of saturation. After the consolidation stage, matric suction of 174 kPa was applied by lowering the pore water pressure to generate a difference between air and water pressures. During 24 h of the equilibration stage, around 14 cm<sup>3</sup> of water drained out from the specimen, causing a reduction in the degree of saturation and volumetric water content, and some decrease in void ratio as well. Figure 85 a) shows values of the applied net vertical stress and pore air pressure, measured pore water pressure with calculated matric suction value in semi-logarithmic scale. Figure 85 b) shows changes in the height of the specimen, volume of water inside the specimen, void ratio, volumetric water content and degree of saturation in time for all three stages.

**Table 16:** Summary of tests performed in the UGDSBPS at the UniRi with test labels, measured initial characteristics of tested specimens and definition of applied test conditions.

Test name	Test type: sc/w;w <sub>n</sub> /S*	Testing conditions			Water cont., w <sub>n</sub> [%]	Vol. of solids, V <sub>s</sub> [cm <sup>3</sup> ]	Initial specimen characteristics				Meas. mat. suction, (u <sub>a</sub> - u <sub>w</sub> ) <sub>i</sub> *** [kPa]
		Net vertical stress, σ <sub>v</sub> [kPa]	Mat. suction, (u <sub>a</sub> - u <sub>w</sub> ) [kPa]	Shear displ. rate, d <sub>h</sub> [mm/min]			Dry mass, m <sub>d</sub> [g]	Void ratio, e <sub>i</sub> [/]	Degree of sat., S <sub>i</sub> [/]	Vol. water cont., θ <sub>i</sub> [/]	
UVSCDS01	sc; w <sub>n</sub>	100	28	0.005	23.4	159.4	430.3	0.88	0.88	0.34	21
UVSCDS02	sc; w <sub>n</sub>	100	174	0.005	21.9	171.8	463.8	0.75	0.79	0.34	28
UVSCDS02b	sc; w <sub>n</sub>	100	240	0.005							
UVSCDS03	conv.; S	100	0	0.005	23.2	166.8	450.3	0.80	0.78	0.35	na
UVSCDS03b	sc; S	100	72	0.005							
UVSCDS03c	sc; S	100	140	0.005							
UVSCDS04	sc; w <sub>n</sub>	5; 50; 100		na	15.9	161.8	436.9	0.85	0.50	0.23	328; 328; 303
UVSCDS05	sc; S	200	73	0.005	na			0.79	≈1.00	0.44	na
UVSCDS06	sc; S	50	74	0.005	16.4***	170.0	450.9	0.80	0.56***	0.25***	≈0
UVSCDS07	sc; S	200	138	0.005	22.5***	163.3	440.9	0.84	0.73***	0.33***	≈0
UVSCDS07b	sc; S	200	207	0.005							
UVSCDS07c	sc; S	280	207	0.005							
UVSCDS08	sc; w <sub>n</sub>	245	180	0.005	24.6	163.5	441.4	0.84	0.79	0.36	19
UVSCDS09	sc; w <sub>n</sub>	50	180	0.005	29.7	153.9	415.6	0.95	0.84	0.41	13
UVSCDS10	sc; w <sub>n</sub>	50	144	0.005	24.3	169.3	457.1	0.77	0.85	0.37	17
UVSCDS11	w; w <sub>n</sub>	69		nc**	17.4	166.7	450.0	0.80	0.59	0.26	350
UVSCDS12	w; w <sub>n</sub>	100		nc**	14.1	166.1	448.4	0.81	0.48	0.22	397

\* test type: sc - suction controlled/w-wetting test/conv.-conventional direct shear test without application of matric suction (only in UVSCDS03);

initial saturation condition: w<sub>n</sub>-initial water content/S-saturated prior to testing;

\*\* variable is not controlled in the wetting tests;

\*\*\* specimen taken at natural water content was saturated in steel cutter outside the shear box for several days.

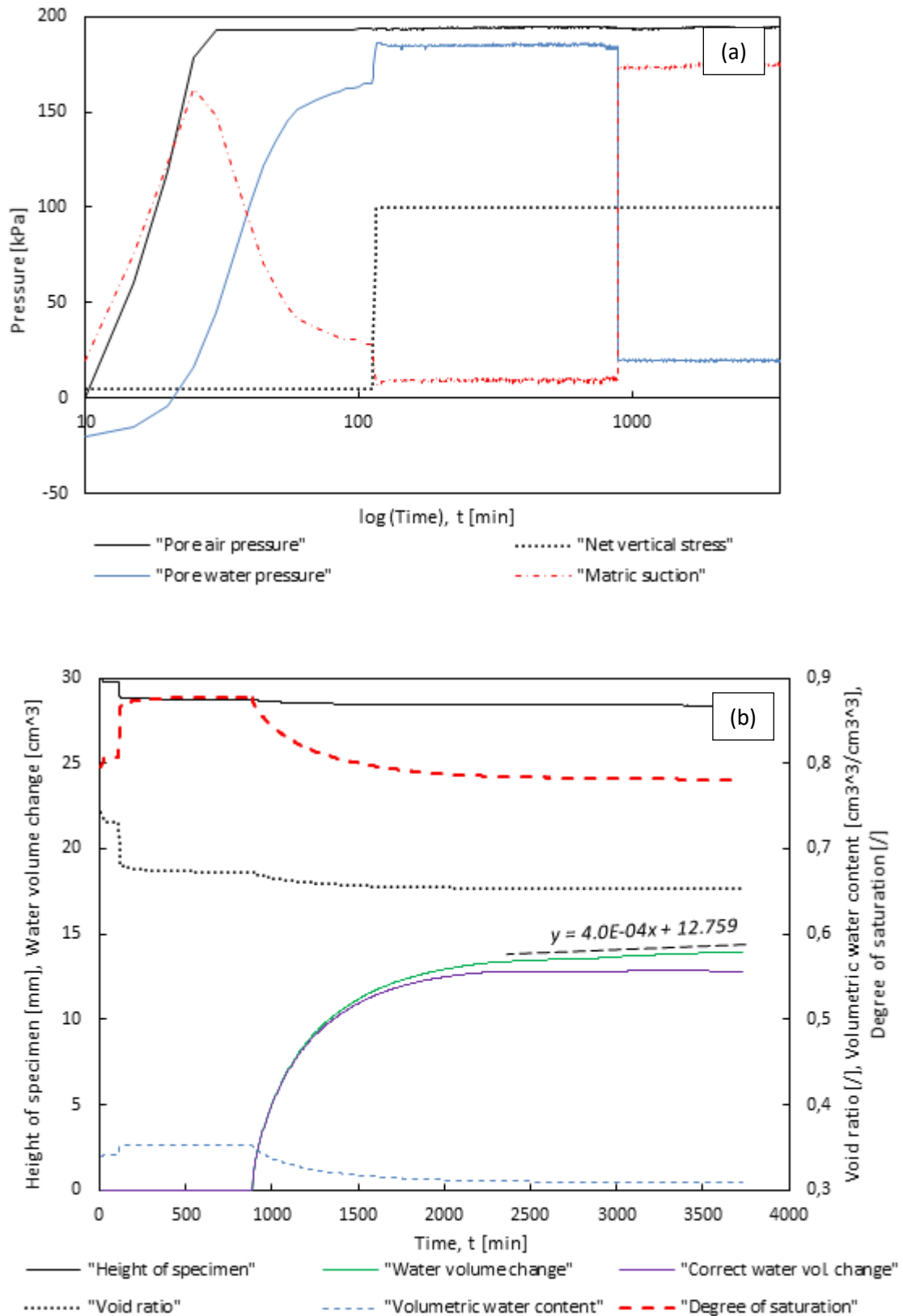


**Figure 85:** Results from the UVSCDS02 test for the initial suction measurement, consolidation, and equilibration at 174 kPa of matric suction in terms of a) applied and measured net vertical stress, pore air, pore water pressure, and matric suction in semi-log graph; and, b) change of the specimen height, volume of water in the specimen, void ratio, degree of saturation and volumetric water content for all stages in terms of absolute duration of test.



The adopted procedure for the correction of the water volume change when using the UGDSBPS is outlined in Figure 85 b) in the case of the UVSCDS02 test. Correction of water volume readings for the volume of diffused air is performed by analyzing the measured outflow reading from the GDS volume and pressure controller. The process of water flow from or into the sample through the HAEPS due to change in pore air pressure caused by modifying the air pressure inside the testing chamber, or/and pore water pressure by changing the water pressure in compartment below the HAEPS, which is in hydraulic contact with the installed specimen, occurs as a nonlinear process in time. When the change of water volume has ceased, and specimen volume changes are negligible, the specimen is considered to be equilibrated at the imposed matric suction value under the applied stress conditions. However, the process of air diffusion through water occurs, in most cases, at a constant rate respective to time. In order to impose positive matric suction value, air pressure inside the testing chamber, which is in equilibrium with the pore air pressure inside the specimen, is usually greater than the water pressure inside and below the HAEPD. The latter is in equilibrium with the pore-water pressure inside the specimen if intimate hydraulic contact between the HAEPS and testing specimen exists. Since the ambient pressure below the HAEPD is generally smaller than above it, once when diffused through the HAEPD, the air expands. If not periodically removed by the flushing technique, diffused air causes erroneous volume readings. However, the amount of diffused air can be calculated from the linear part of the volume change readings after the equilibration of the specimen at imposed suction level is reached. According to the previous assumptions, the rate of volume change and the data collected from the equilibration stage can be used to correct water volume readings.

Test UVSCDS03 was performed as a conventional saturated drained shear test without application or measurement of matric suction. After the specimen's installation, the shear box was flooded with water from the top by adding the de-aired water and from below by applying 30 kPa of water pressure beneath the HAEPD. The specimen was left to saturate for a minimum of 24 hours and then was sheared under a constant shear rate. Following this, the specimen was re-sheared in the two following tests (UVSCDS03b and UVSCDS03c) under the same net vertical stress value but increased matric suction values. Tests UVSCDS03b, UVSCDS03c, UVSCDS05 and UVSCDS07, UVSCDS07b and UVSCDS07c were performed as suction controlled tests on previously saturated specimens, starting from  $S \approx 1$ . Tests UVSCDS07b and UVSCDS07c were performed as re-shearing of the specimen used in the UVSCDS07 test at increased values of matric suction and net vertical stress, relative to the previous test. Test UVSCDS04 was used only to determine matric suction value of the relatively dry specimen

that was collected at the end of July 2017. Measurements were performed under the increasing values of net vertical stress (5, 50, and 100 kPa). Following this, the specimen was unloaded, the testing chamber was opened, and the saturation procedure similar to that described in the UVSCDS03 test was performed. After the saturation was completed, the UVSCDS05 test was started with increased matric suction and consolidation stress of 200 kPa. Figure 86 shows the results for the final stage of matric suction measurement in the UVSCDS04 test. For the 100 kPa of net vertical stress, a corresponding degree of saturation and volumetric water content values of 55.4% and  $0.24 \text{ cm}^3/\text{cm}^3$ , matric suction value of 303 kPa was measured with the axis translation technique.

Except for the suction controlled tests, two wetting tests (UVSCDS11 and UVSCDS12) were performed on relatively dry samples collected at the end of July 2017. Upon the installation of specimens at natural water content, initial matric suction was measured with constant water content and under 5 kPa of contact pressure. Following this, the specimen was consolidated at various net vertical stress values. In the following stage, considering the applied net normal stress, shear stress equal to around 1/2 to 2/3 of the predicted shear strength was applied on the specimen. Imposed stress conditions were kept constant until the axial and shear deformations ceased. Finally, specimens were wetted at different rates, until failure conditions in terms of acceleration of shear displacement under constant stress were reached.

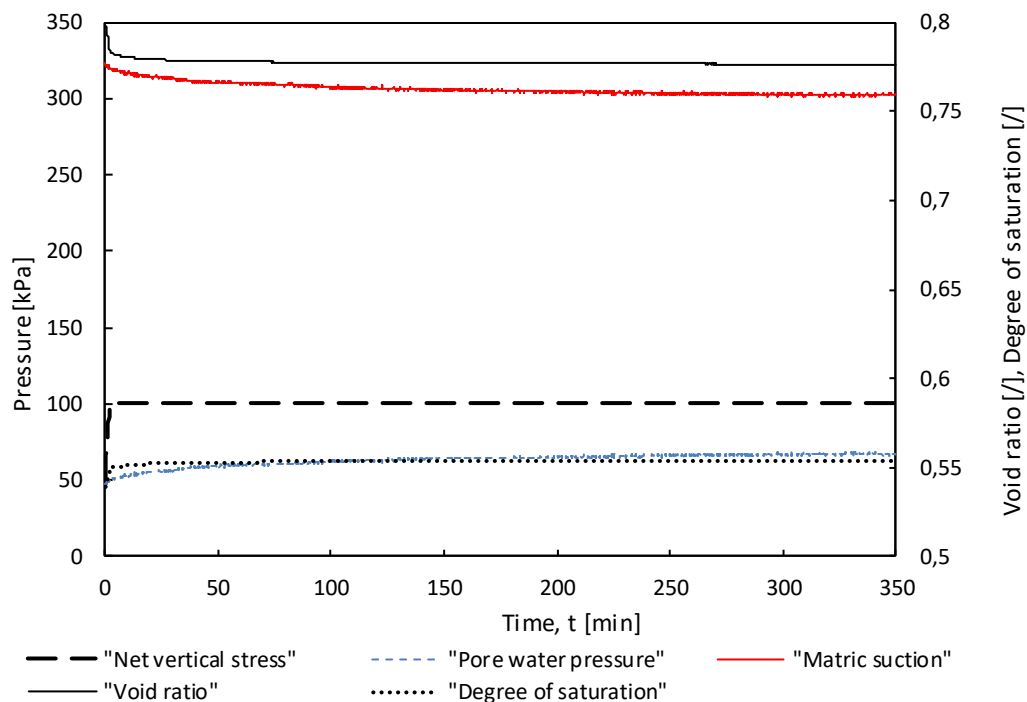


**Figure 86:** Detail of suction measurement from UVSCDS04 test for undisturbed specimen at natural water content collected at the end of July 2017.

The wetting tests intended to study the influence of matric suction decrease due to an increase of water content in tested specimen, and to observe if the reduction of matric suction could cause a decrease of the shear strength, leading to failure of the specimen under imposed loading conditions. Some details on specimen preparation, saturation, and installation in UGDSBPS are shown in Figure 87 and Figure 88.

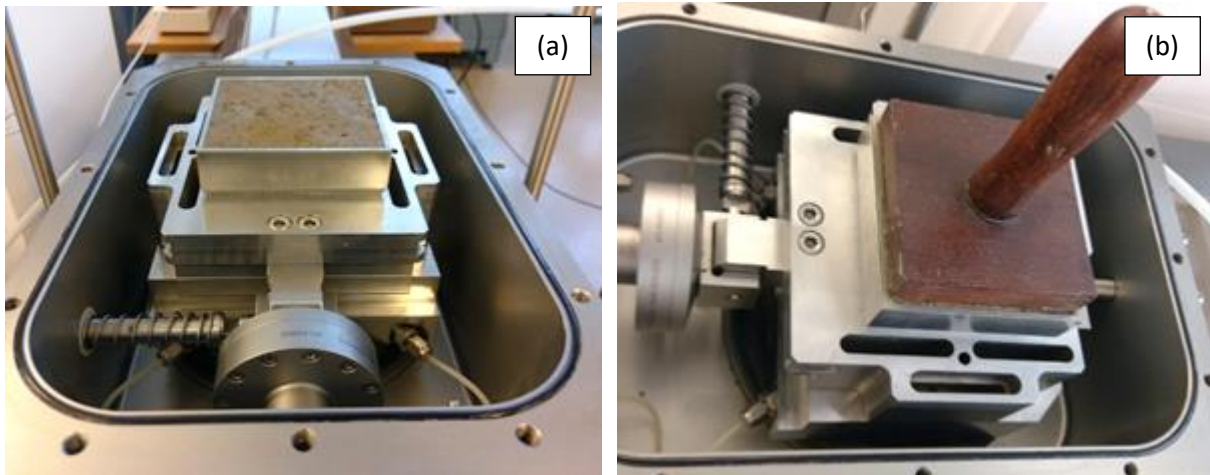


**Figure 87:** Adopted procedure for installation of undisturbed specimens at natural water content a) collected in-situ directly with cutter; and b) extrusion into the UGDSBPS apparatus.



**Figure 88:** Undisturbed specimen used in the wetting tests installed into the UGDSBPS apparatus at a natural water content.

#### 6.4.1. Suction-controlled test results

Some of the shear strength test results obtained by using the SCDSA at the UniSa and UGDSBPS at the UniRi are presented in this part. Results are compared for the shearing stage of tests where shearing was performed under the control of matric suction and under the same value of the applied net vertical stress. Results obtained from conventional direct shear tests are added to outline the influence of the matric suction on the shear strength and stiffness characteristics of the investigated soil, as well. While for the SCDSA and UGDSBPS the volume of water change during the shear stage was actually measured by the volume measuring system, in the case of the conventional tests, the amount of water draining in or out from the specimen was calculated from the measured vertical displacement and known area of cross-section. In case of the conventional tests, it was assumed that the samples were completely saturated and that the matric suction value was equal to 0 kPa, while the total volume change of the specimen was equal to the water volume change.

Results obtained by using all three devices for determination of the soil shear strength under 50 kPa of net vertical stress are summarized in Figure 89. Results are shown in terms of the shear stress, vertical displacement, degree of saturation, and change of water volume vs. horizontal displacement in Figure 89 a), b), c), and d), respectively.

Although the obtained results are not entirely consistent, which might be due to usage of different devices and undisturbed specimens that could vary in terms of homogeneity or the fact that different saturation conditions were used in the different tests, several conclusions could be clearly outlined. In every case, the increasing of matric suction resulted with an increase of the shear strength and stiffness of tested specimens during the shearing. Compressive behavior during shearing in saturated or nearly-saturated conditions changed to dilative as the matric suction was increased during the shearing. On the other hand, as the matric suction value increases, so does the rate at which water drains out from the specimen. Consequently, the degree of saturation rapidly decreases during the shearing at higher matric suction values, due to dilation of specimens and lowering of the water content. Compression and water flow inside the specimen during shearing at low suction values increase the degree of saturation during the shearing stage. The threshold value of matric suction separating the two patterns of behavior during the shearing (between 36 and 72 kPa for the net vertical stress of 50 kPa) was found to increase with the increasing of the net vertical stress.

Results are shown in the same form for the shear tests performed at a net vertical stress value of 100 and 200 kPa in Figure 90 and Figure 91, respectively.

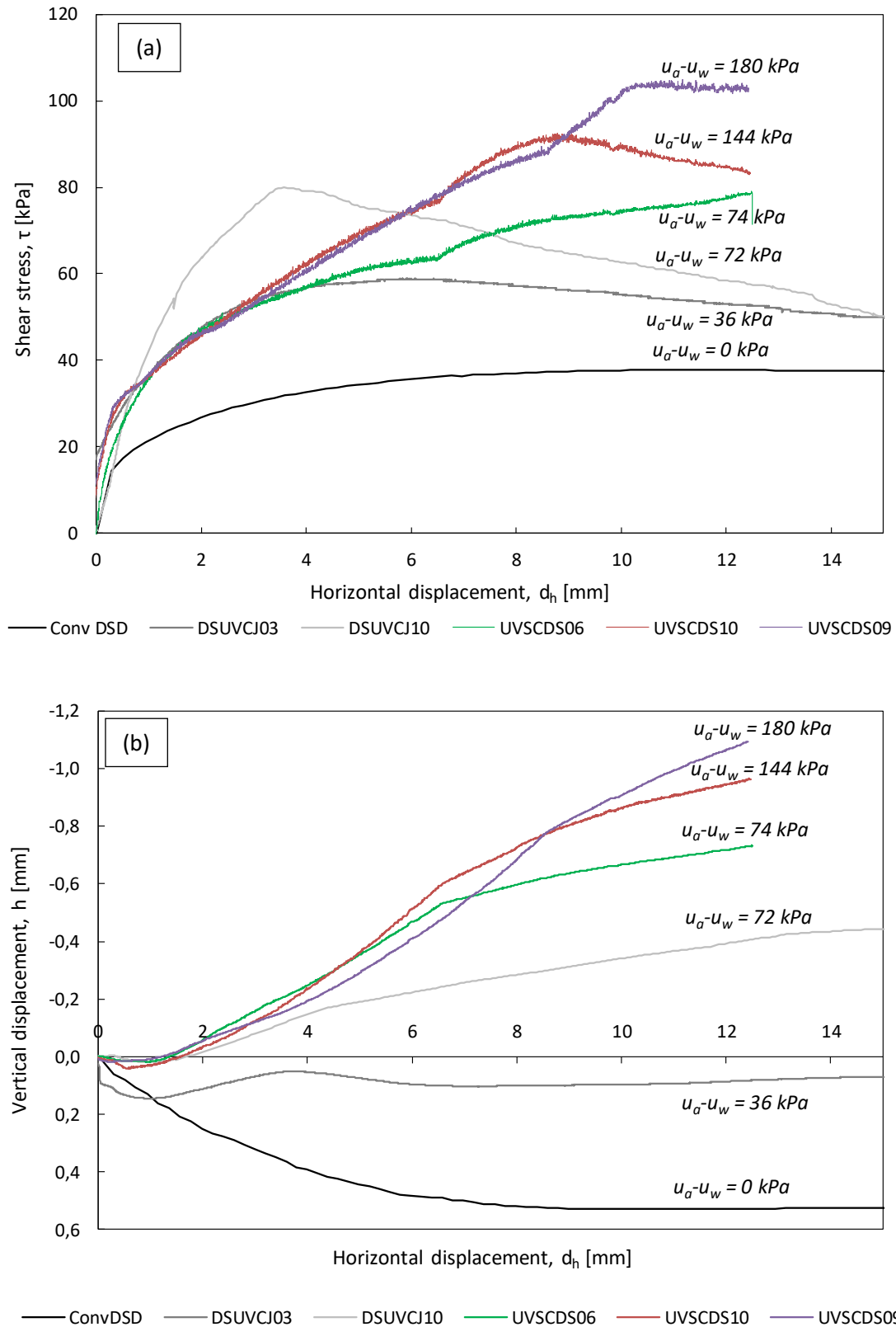


**Figure 89:** Results obtained for shear stage using all three direct shear test devices under 50 kPa of net vertical stress, in terms of a) shear stress; b) vertical displacement; c) degree of saturation; and, d) change of volume of water vs. horizontal displacement.

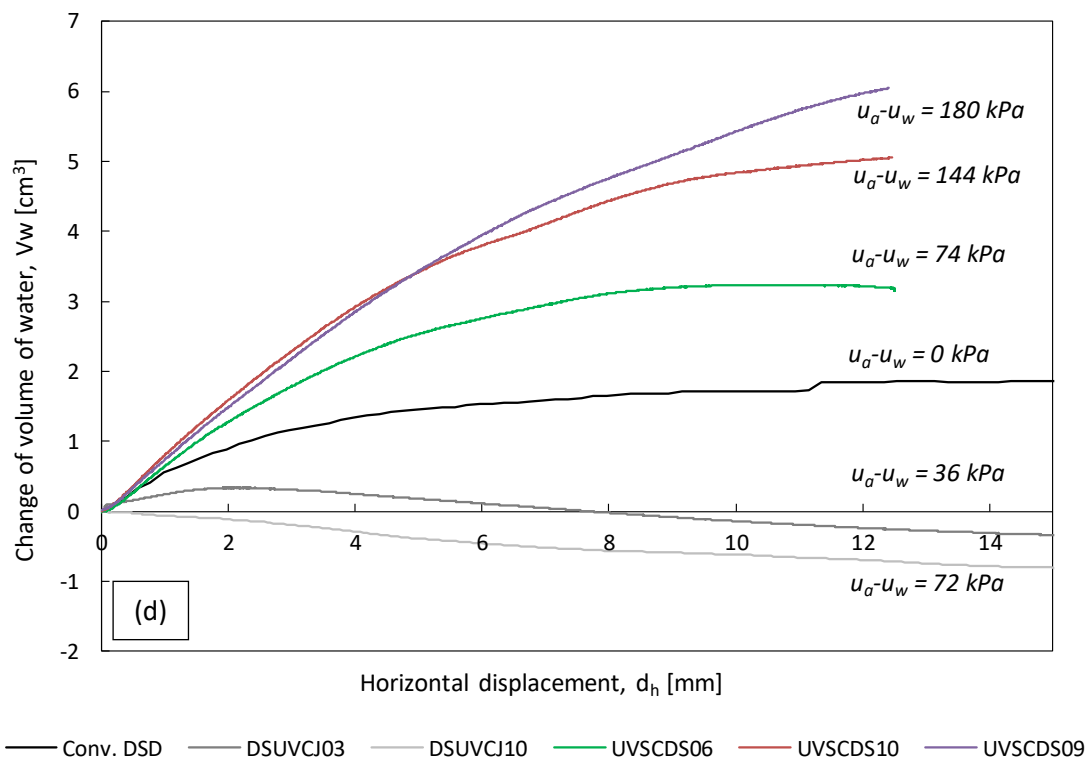
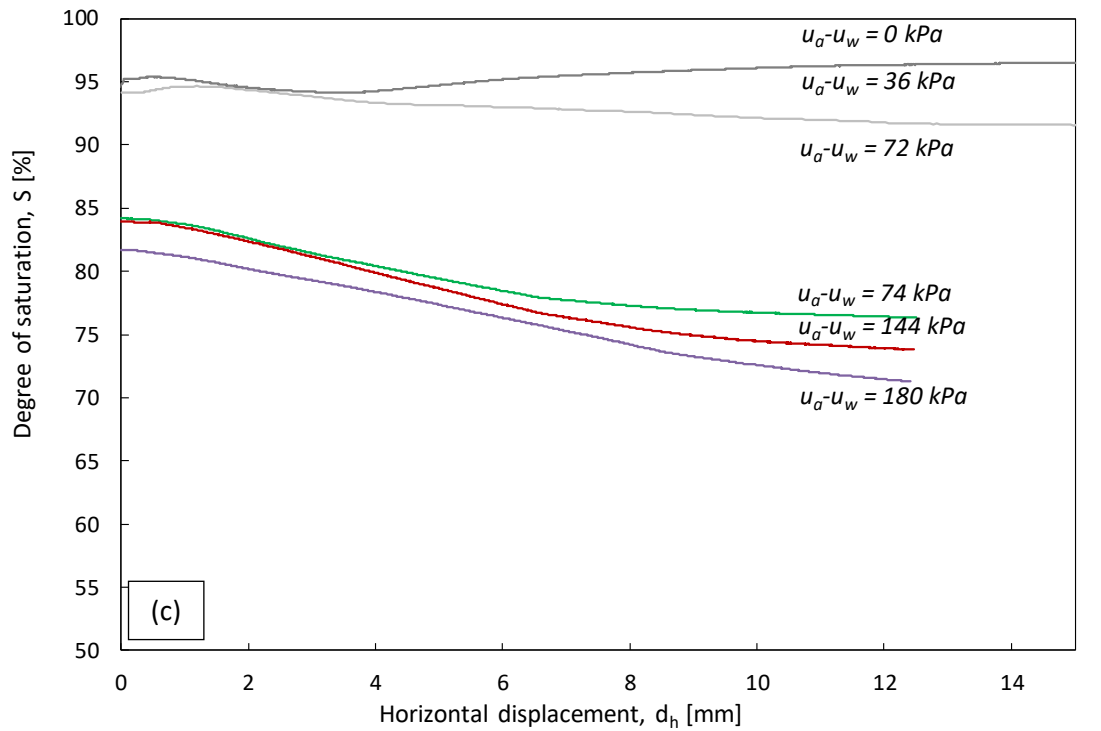
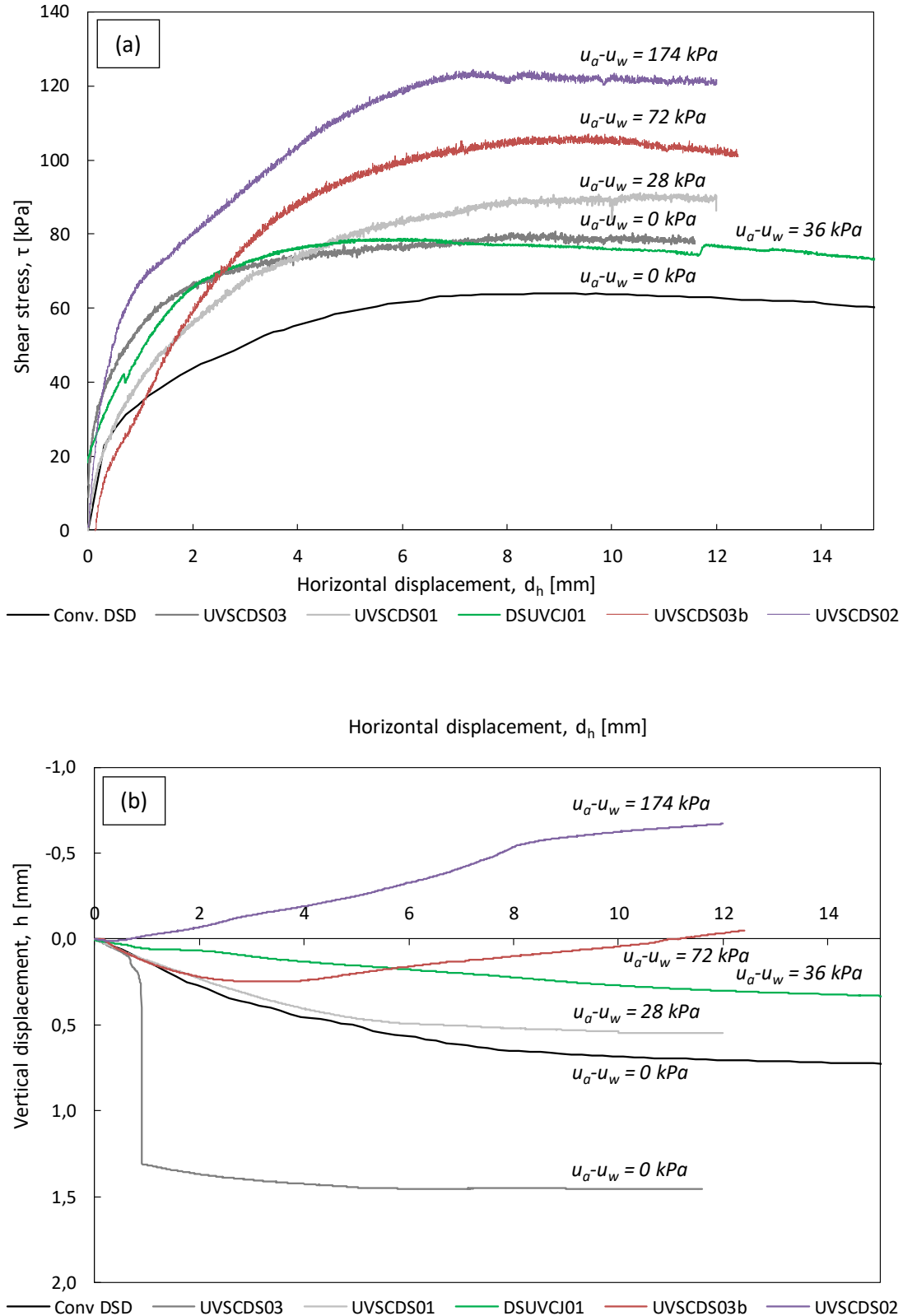


Figure 89: Continued.



**Figure 90:** Shear stage tests results obtained from conventional and modified direct shear devices under 100 kPa of net vertical stress, in terms of a) shear stress; b) vertical displacement; c) degree of saturation; and d) change of volume of water vs. horizontal displacement.

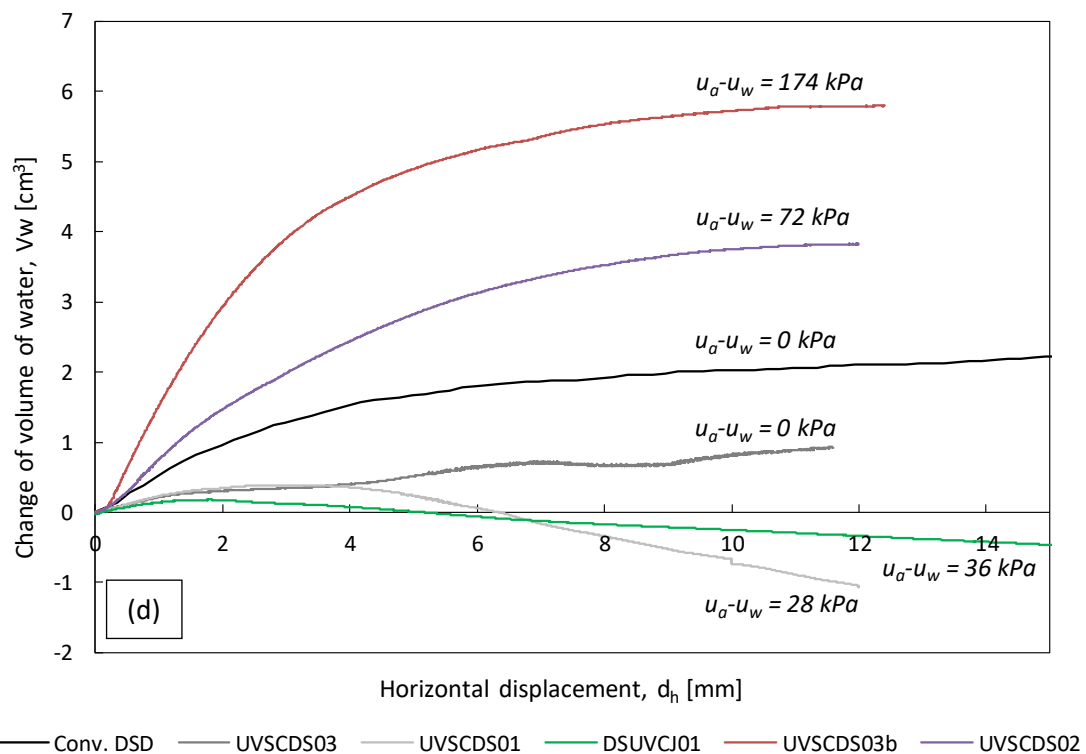
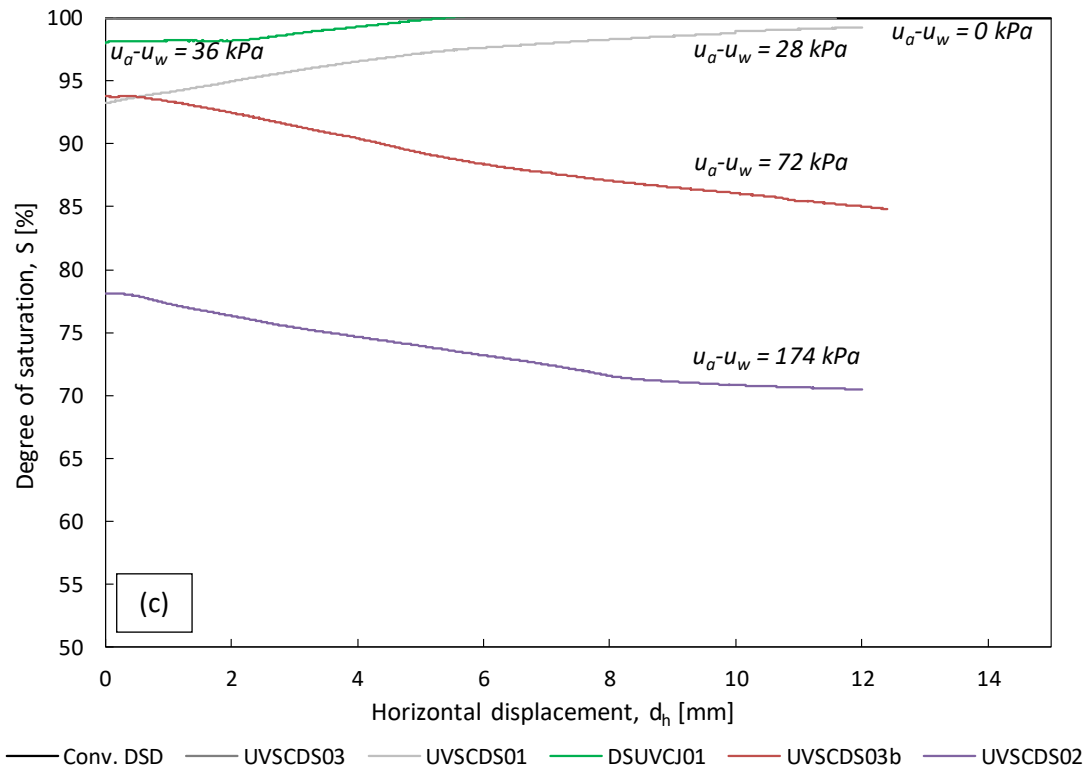
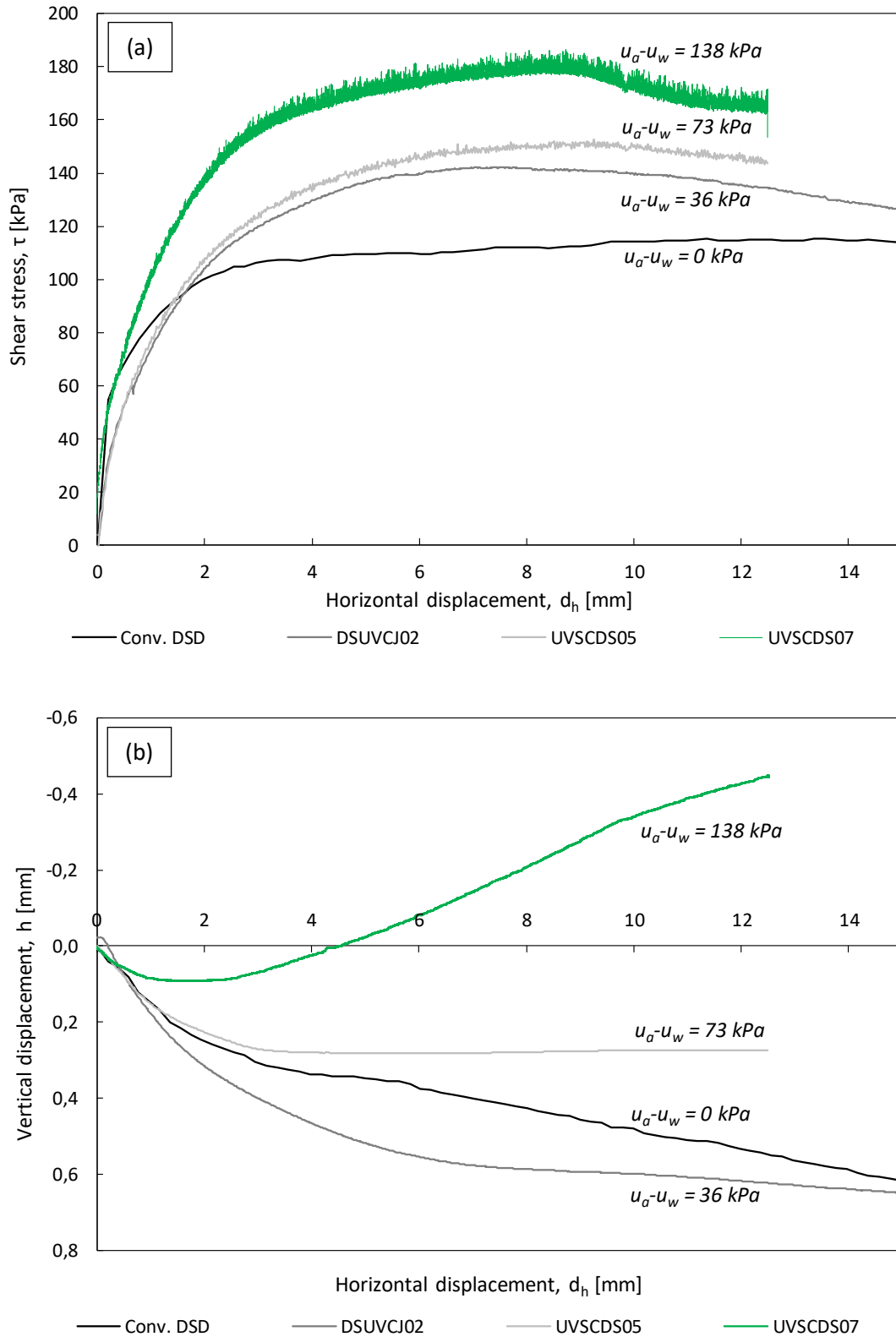


Figure 90: Continued.





**Figure 91:** Shear stage tests results obtained from conventional and modified direct shear devices under 200 kPa of net vertical stress, in terms of a) shear stress; b) vertical displacement; c) degree of saturation; and d) change of volume of water vs. horizontal displacement.

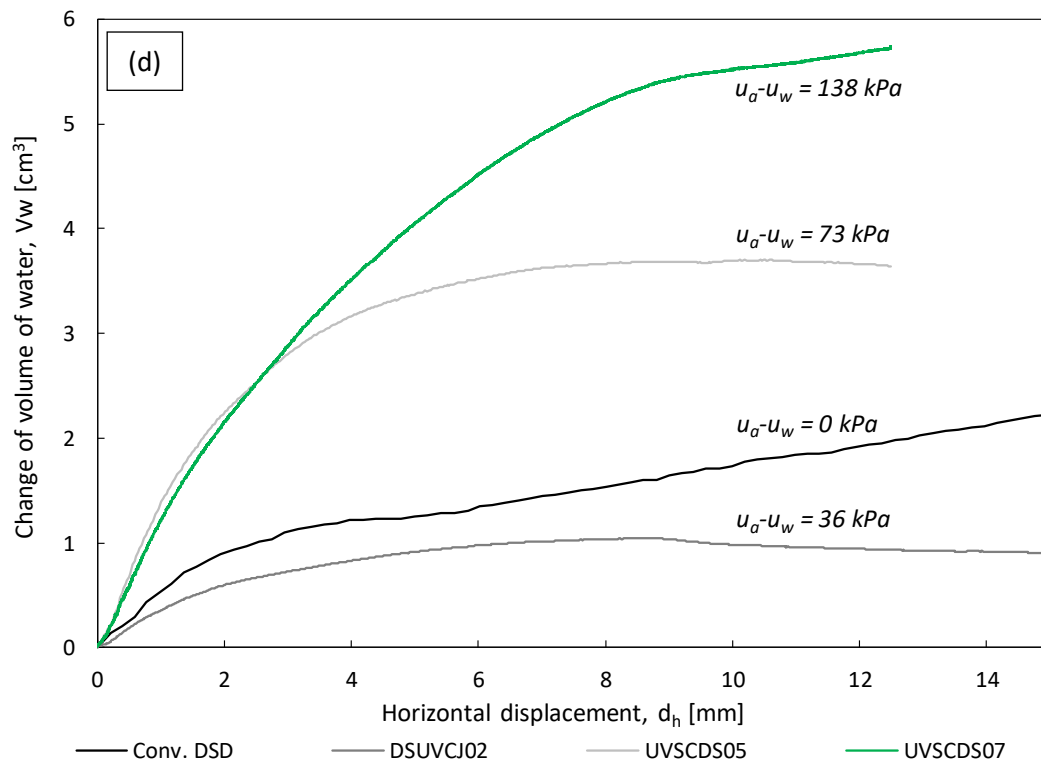
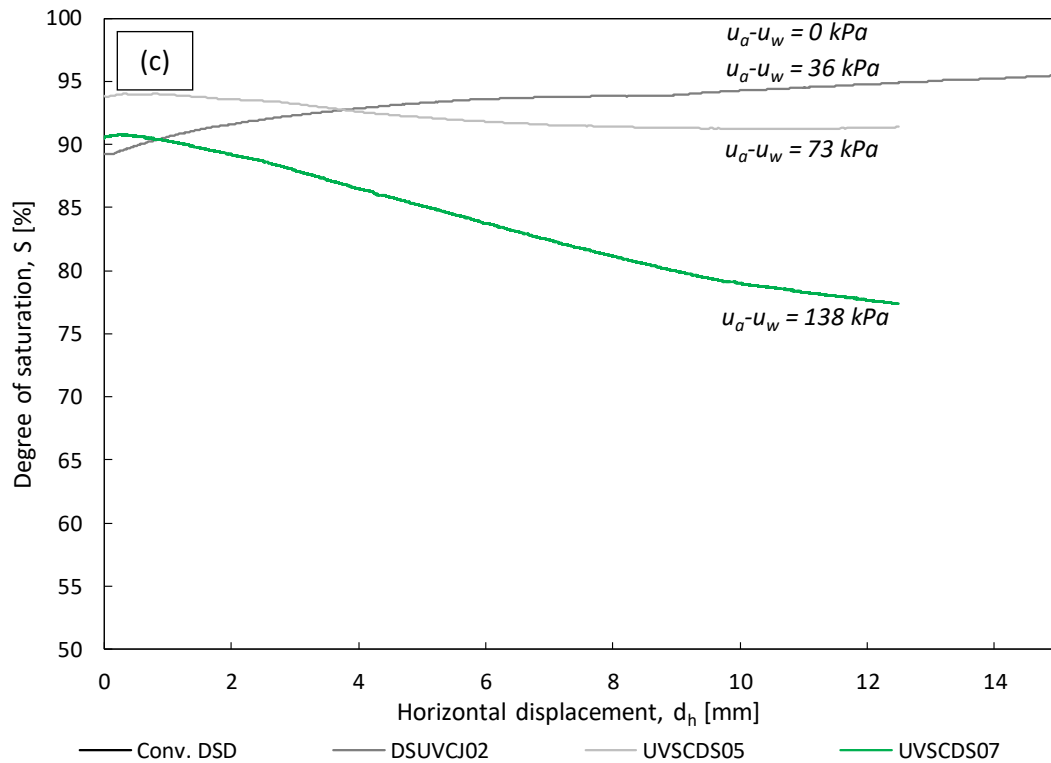


Figure 91: Continued.

As was the case with tests performed at the net vertical stress of 50 kPa, an increase of matric suction resulted with an increase in shear strength of undisturbed samples tested under 100 kPa of the net vertical stress. Results that slightly deviate from this pattern are those obtained for saturated testing conditions by using the UGDSBPS and the UVSCDS03 test, which resulted in 10 kPa higher shear strength compared to the results obtained in the conventional DSD, under the same value of the effective vertical stress. Another deviation is observed when comparing the results obtained from the UVSCDS01 and DSUVCJ01 tests, which were performed at matric suction value of 28 and 36 kPa, but using two different devices. The latter results plot slightly below although shearing was performed at a higher value of matric suction. However, both discrepancies could be considered negligible, considering that the results were obtained on undisturbed samples starting from different saturation conditions and by using different testing devices. Another important reason for discrepancies in results obtained from tests conducted on undisturbed samples of residual soil from flysch rock mass could arise from the heterogeneity of samples, especially for the presence of siltstone particles of varying weathering degrees or roots at the shearing surface. Again, the same patterns were observed when considering the contractive and dilative behavior of specimens during the shearing stage relative to the increase of matric suction: dilative behavior was observed only when the matric suction was increased to 72 kPa, and tested specimens started to desaturate during the shearing. On the other hand, for matric suction values lower than 72 kPa, tested specimens exhibited contractive behavior with the increase of the degree of saturation during the shearing.

The same pattern was obtained for the specimens sheared under the 200 kPa of the applied net vertical stress. However, the threshold limit separating the contractive and dilative behavior is increased: the dilation and significant desaturation of tested samples during the shear were observed only when the matric suction value was increased to 138 kPa. Test results obtained in UGDSBPS clearly outline an increase in stiffness and shear strength with the increase in matric suction, as well. All of the obtained results on undisturbed samples tested in unsaturated conditions are interpreted in the following part.

#### *6.4.1.1. Interpretation of test results*

Conditions at failure from all of the tests performed in this study are summarized in Table 17. According to the results shown in the previous section, the threshold matric suction value separating contractive and dilative behavior increases with the increase of net vertical stress

value applied during the shear stage. Since the AEV of the soil generally increases with the increase of net vertical stress due to the reduction of the void ratio of the tested specimen, the obtained results provide insight into the connection between the SWRC and behavior of fine-grained soil behavior during the shearing in unsaturated conditions. Results obtained from conventional and modified direct shear tests are shown in the following figures, in terms of the different models described in the earlier part of the chapter. For example, Bishop's effective stress formulation is used to present all of the shear strength tests results obtained on undisturbed samples in Figure 92. A continuous line fits the result obtained for saturated conditions by using the conventional direct shear device (Conv. DSD). A dashed line fits all of the results that were obtained in unsaturated conditions by using two modified direct shear test devices (SCDSA and UGDSBPS). Two squared markers without the fill indicate results from the UVSCDS03 and UVSCDS02b tests, which are excluded from the fitting procedure. Test UVSCDS03 was performed as a conventional test by using the UGDSBPS on an undisturbed sample installed at a natural water content inside the shear box. The specimen was saturated by adding the water from the top of the porous disc and from below, through the HAEPS as described earlier. Following this, the specimen was consolidated by applying 100 kPa of the effective vertical stress and sheared at a constant shear rate of  $5.0\text{E-}03$  mm/min. However, the results obtained here suggest that the matric suction of approximately 30 kPa still existed inside the specimen during the shear stage and that the saturation process inside the shear box was not successful.

On the other hand, results could be affected by the specimen heterogeneity, especially if larger siltstone particles (Figure 93 a), or even limestone fragments are present at the shearing plane (Figure 93 b), which could result in increased shear strength related to the case where these particles are absent on the shearing plane. In the case of the UVSCDS02b test, shear stress was still increasing at 12.5 mm of horizontal displacement. After the maximum horizontal displacement was reached, the test was terminated. The maximum recorded shear stress was probably much lower than would be reached if the shear strength was fully mobilized. The reason for this could be the fact that the specimen was re-sheared (a specimen was previously used in the UVSCDS02 test), which might have affected the behavior of the specimen during the following shearing, especially regarding the stiffness, which could be significantly reduced.

**Table 17:** Conditions at failure for all direct shear tests.

Test name	Test type: sc/w;w <sub>n</sub> /S*	Testing conditions		Shear displ. rate, $d_h$	Shear stress, $\tau_f$	Mat. suction, ( $u_a - u_w$ ) <sub>f</sub>	Conditions at failure		Vol. water cont., $\theta_f$	Void ratio., $e_i$	Bishop's ef. stress, $\sigma_v'$
		Net vertical stress, $\sigma_v$	Mat. suction, ( $u_a - u_w$ )				Hor. displ., $d_{hf}$	Degree of sat., $S_f$			
		[kPa]	[kPa]				[mm]	[/]			
Conv. DSD	conv.; S	50	nc**	0.005	37.8	0	11.4	1			50
Conv. DSD	conv.; S	100	nc**	0.005	64	0	8.5	1			100
Conv. DSD	conv.; S	200	nc**	0.005	129.5	0	6.3	1			200
DSUVCJ01	sc; w <sub>n</sub>	100	36	0.005	78.8	36	5.7	1	0.41	0.71	136
DSUVCJ02	sc; w <sub>n</sub>	200	36	0.005	142	36	7.4	0.94			233.8
DSUVCJ03	sc; w <sub>n</sub>	50	36	0.005	52	36	6.4	0.95			84.2
DSUVCJ10	sc; w <sub>n</sub>	50	72	0.005	79.5	72	3.9	0.94	0.37		117.7
UVSCDS01	sc; w <sub>n</sub>	100	28	0.005	87	28	7.5	0.98	0.39	0.65	127.5
UVSCDS02	sc; w <sub>n</sub>	100	174	0.005	124	174	7.1	0.72	0.29	0.68	226
UVSCDS02b	sc; w <sub>n</sub>	100	240	0.005	131	240	12.2	0.72	0.28	0.64	272.1
UVSCDS03	conv.; S	100	0	0.005	80.3	0	8.0	1	0.32	0.48	100
UVSCDS03b	sc; S	100	72	0.005	106.2	72	8.2	0.87	0.25	0.41	162.6
UVSCDS03c	sc; S	100	140	0.005	118,4	140	5.5	0.84	0.22	0.35	217.3
UVSCDS04	sc; w <sub>n</sub>	5; 50; 100		na							
UVSCDS05	sc; S	200	73	0.005	152,6	73	9.3	0.94	0.19	0.27	268.5
UVSCDS06	sc; S	50	74	0.005	67.7	74	7.3	0.78	0.32	0.70	107.7
UVSCDS07	sc; S	200	138	0.005	165	138	8.9	na	na	0.48	
UVSCDS07b	sc; S	200	207	0.005	180	207	13.9	na	na	0.44	
UVSCDS07c	sc; S	280	207	0.005	202	207			na	0.36	
UVSCDS08	sc; w <sub>n</sub>	245	180	0.005	233	180	10.0	0.85	0.30	0.53	398.7
UVSCDS09	sc; w <sub>n</sub>	50	180	0.005	102	180	10.4	0.73	0.34	0.87	180.7
UVSCDS10	sc; w <sub>n</sub>	50	144	0.005	92.4	144	8.7	0.74	0.31	0.74	155.8
UVSCDS11	w; w <sub>n</sub>	69	decrea.	nc**	75	74.4	na	0.68	0.29	0.75	100.7
UVSCDS12	w; w <sub>n</sub>	100	decrea.	nc**	90	16.9	na	0.79	0.33	0.71	113.4

\* test type: sc - suction controlled/w-wetting test/conv.-conventional direct shear test without application of matric suction (only in UVSCDS03 and Conv. DSD);

initial saturation condition: w<sub>n</sub>-initial water content/S-saturated prior to testing;

\*\* variable is not controlled in the wetting tests;

\*\*\* specimen taken at natural water content was saturated in steel cutter outside the shear box for several days.

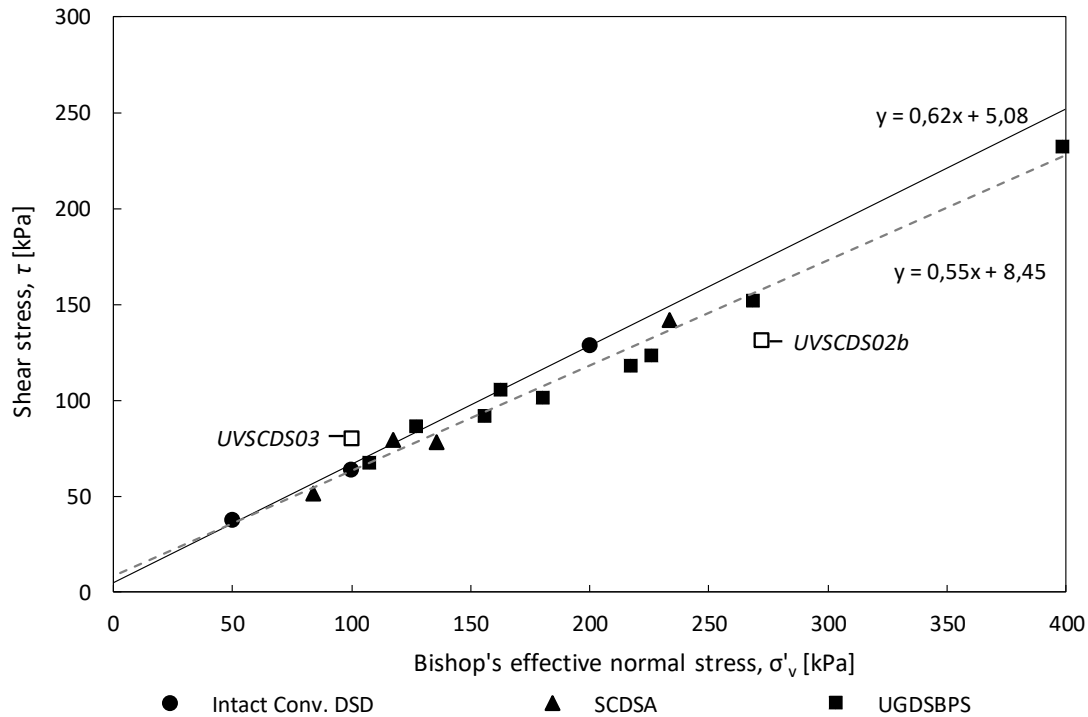


**Figure 92:** Shear strength test results in terms of the Bishop's effective stress formulation (Bishop 1959), obtained on undisturbed samples of residual soil from a flysch rock mass by using conventional (DSD) and modified (SCDSA and UGDSBPS) direct shear test apparatuses.

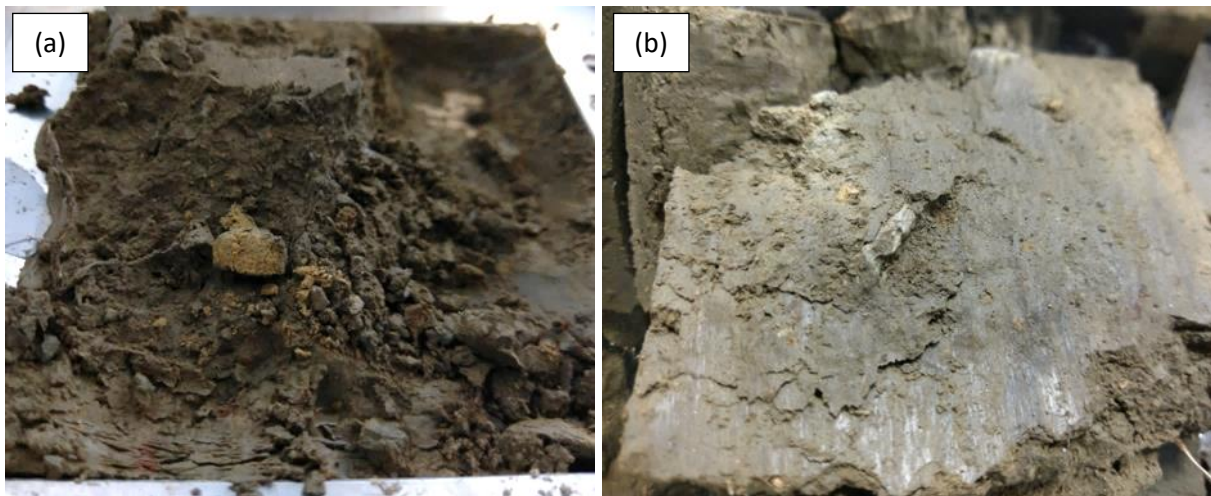


**Figure 93:** Heterogeneity at the shearing plane of undisturbed samples: a) occasional presence of roots and siltstone fragments of different weathering degree and size, and b) lime-stone fragment.

Figure 94 shows obtained shear strength results in two planes of the extended Mohr-Coulomb's failure envelope. Figure 94 a) shows plot for matric suction ( $u_a - u_w$ ), vs. shear stress  $\tau$ , plane, providing a relationship between the angle of internal friction related to the matric suction  $\phi^b$ , and matric suction value. Obtained results indicate that the  $\phi^b$  value is close to or equal to the value of the effective friction angle  $\phi'$  (i.e.,  $30^\circ$ ) for the matric suction values up to approximately 75 kPa. Then there is a small range of matric suction in which  $\phi^b$  vs. ( $u_a - u_w$ ) relationship becomes non-linear, and a sharp reduction of  $\phi^b$  value occurs afterwards. As

the matric suction is increased above 100 kPa,  $\phi^b$  becomes equal to a constant value of around  $9^\circ$ , with very little variation for the considered range of matric suction. Figure 94 b) shows the plot for net normal ( $\sigma - u_a$ ) vs. shear stress  $\tau$ , a plane parallel to matric suction axis, providing values for the  $\phi'$  and the effective  $c'$  or apparent cohesion,  $c$ .

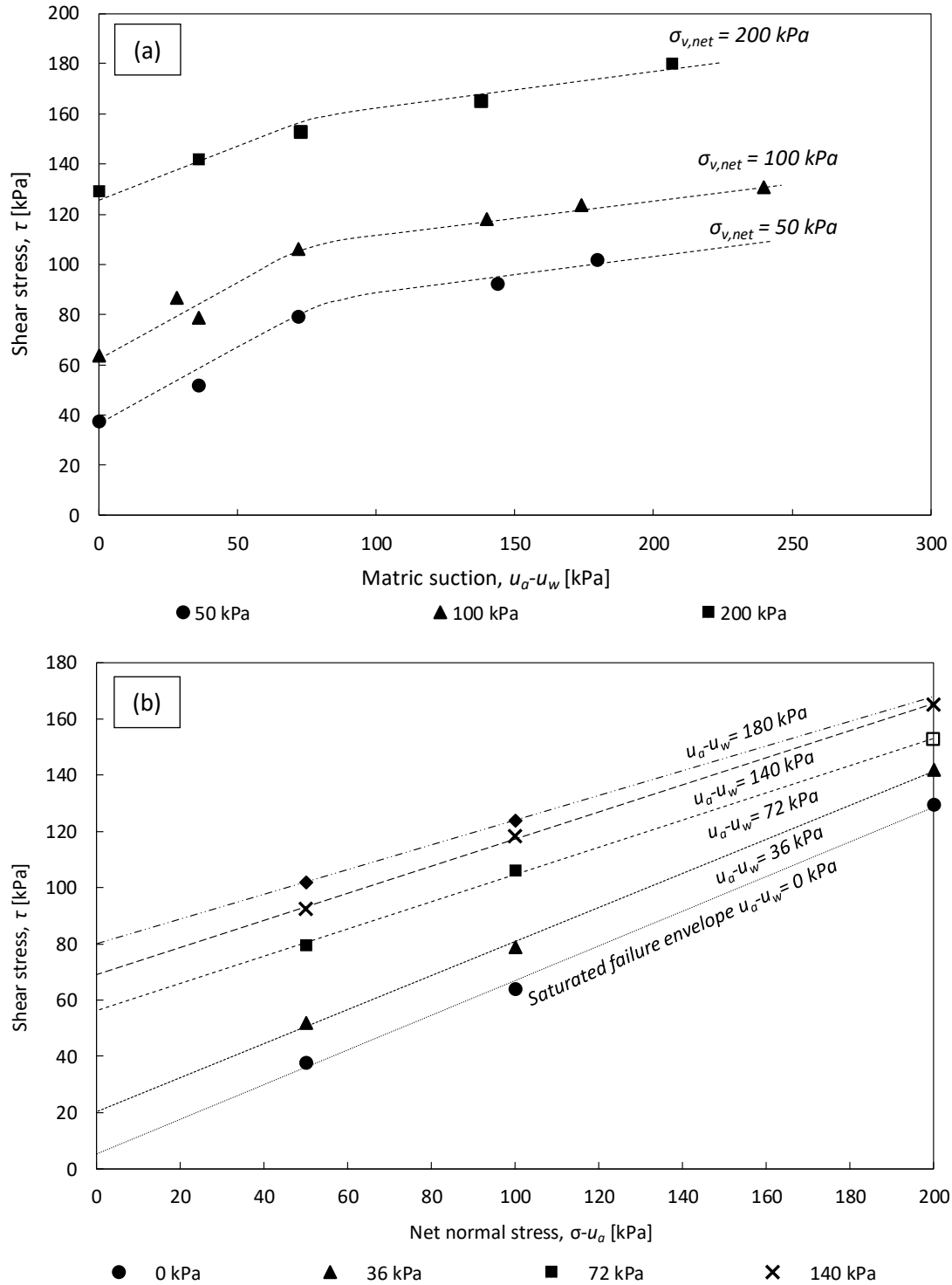


**Figure 94:** Failure envelope obtained from conventional and modified direct shear tests performed on undisturbed samples, projected onto: a)  $\tau$  versus  $(u_a - u_w)$  plane; and b)  $\tau$  versus  $(\sigma - u_a)$  plane.

The above results are used for the determination of the quantities required for the evaluation of the suction stress under the matric suction values for which the envelopes were obtained, as proposed by Lu et al. (2010). The procedure for obtaining values of the effective cohesion  $c'$ , apparent cohesion  $c$ , effective friction angle  $\phi'$ , apparent tensile stress,  $\sigma_{c0}$ , uncorrected suction stress,  $\sigma_{ci}$ , and corrected suction stress  $\sigma_{c0}'$ , is outlined in Figure 95.

Table 18 and Table 19 summarize the calculated values for determination of the suction stress and considered failure envelopes. Figure 96 represents verification of the experimentally obtained results against the SSCC of residual soil from a flysch rock shown (Figure 61 b) obtained by using a closed-form suction stress equation (68) proposed by Lu et al. (2010).

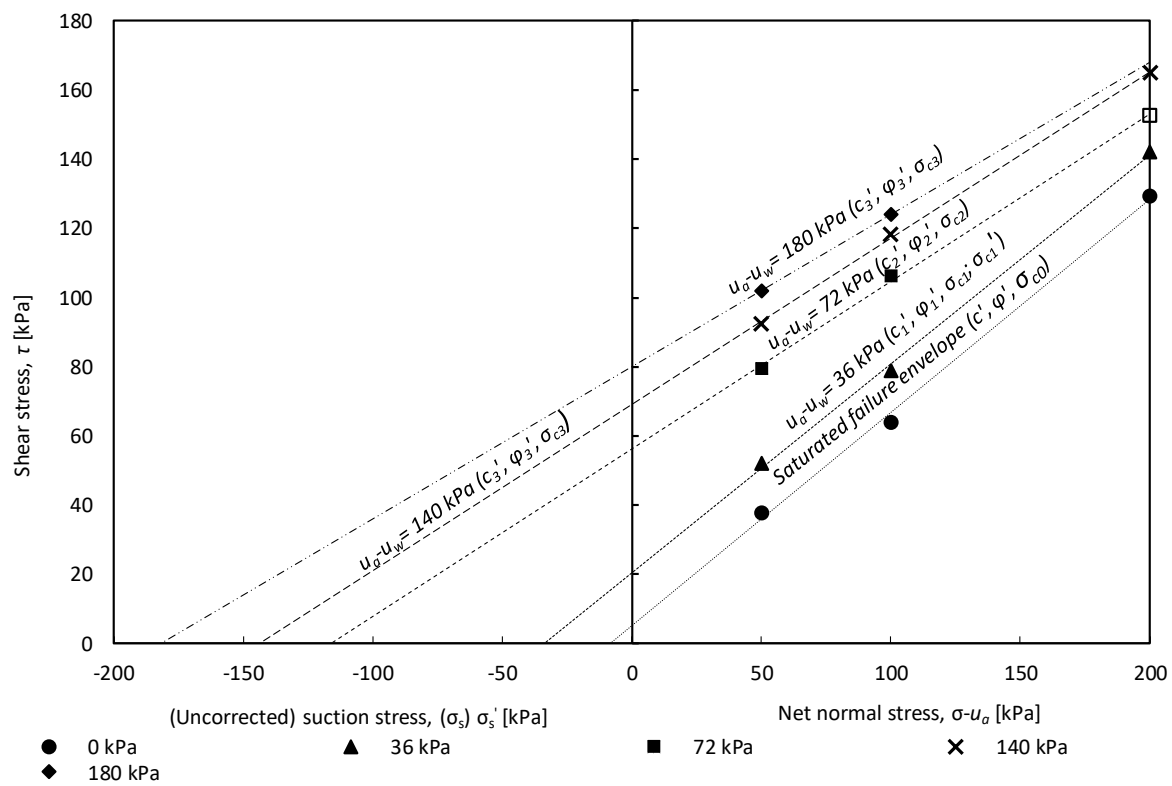


**Figure 95:** Experimentally obtained shear strength test results for quantification of the SSCC (Lu and Likos 2006) of residual soil from a flysch rock mass.

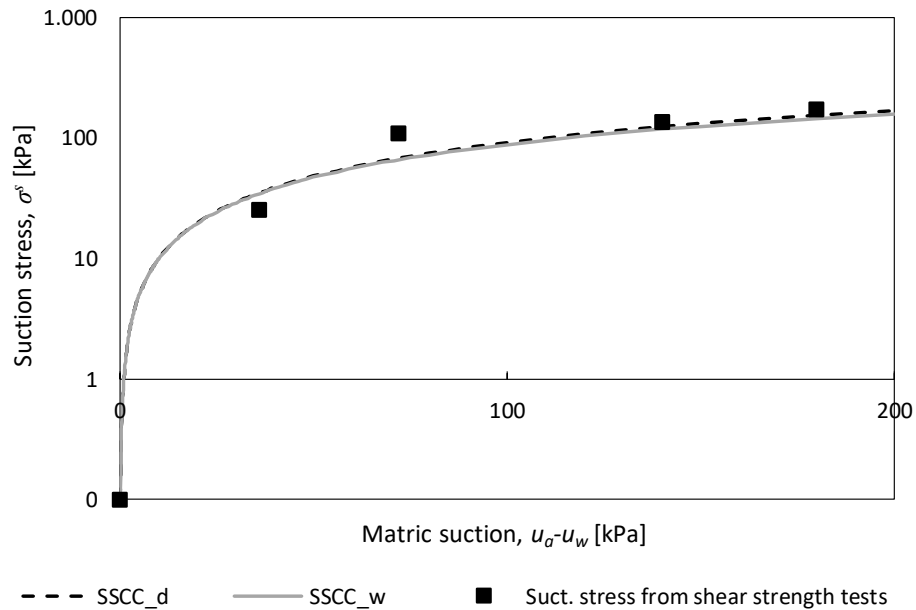
**Table 18:** Determination of the apparent tensile stress and effective cohesion from the conventional direct shear test results performed on undisturbed samples.

Failure envelope	Mat. suction, $(u_a - u_w)$ [kPa]	Failure envelope equation, $\tau_f$ [kPa]	Ef. cohesion, $c'$ [kPa]	Ef. friction angle, $\phi'$ [°]	App. tensile stress, $\sigma_{c0}$ [kPa]
Saturated	0	$\tau_f = 0.617\sigma_n' + 5.1$	5.1	31.7	8.1



**Table 19:** Determination of the suction stress from suction-controlled direct shear test results performed on undisturbed samples.

Failure envelope	Mat. suction, $(u_a - u_w)$ [kPa]	Failure envelope equation, $\tau_f$ [kPa]	Apparent cohesion, $c'$ [kPa]	Ef. frict. angle, $\phi'$ [°]	"Uncor." suc. stress, $\sigma_{ci}$ [kPa]	Suc. str., $\sigma_{ci}'$ [kPa]
Unsaturated	36	$\tau_f = 0.605\sigma_n' + 20.4$	20.4	31.2	33.7	25.6
Unsaturated	72	$\tau_f = 0.484\sigma_n' + 56.3$	56.3	25.8	116.4	108.3
Unsaturated	140	$\tau_f = 0.481\sigma_n' + 69.1$	69.1	25.7	143.5	135.4
Unsaturated	180	$\tau_f = 0.440\sigma_n' + 80.0$	80.0	23.7	181.8	173.7

**Figure 96:** SSCC of residual soil from a flysch rock mass presented by closed-form expression (68) and experimentally obtained values from direct shear tests.

Although the shear strength tests were performed on undisturbed samples and under a limited range of matric suction values, the obtained results show very good correlation with the SSCC predicted by the equation (68). To be considered as identical, samples used for determination of unsaturated shear strength characteristics of soil should be homogeneous, not only with the same dry density and stress history but with the same water content as well. The last term provides a strong motivation for the use of samples prepared under controlled conditions in the laboratory, rather than performing long-term experimental studies on undisturbed specimens, for which inconsistencies in measurements are a common feature, while the interpretation of the tests results is usually much more difficult.

#### 6.4.2. Wetting test results

In this part, the results of two experiments performed as wetting tests are presented. The first wetting test, UVSCDS11 was performed under 50 kPa of net vertical and 75 kPa of shear stress. The second test, UVSCDS12 was performed under 100 kPa of net vertical and 90 kPa of shear stress. In both tests, undisturbed samples collected during the dry period of the year (end of July 2017) with relatively low water content were used. After the installation of specimens, contact pressure was applied, and initial matric suction values were measured by using the similar approach described for the suction controlled direct shear tests. Depending on the applied net vertical stress value, one or multiple suction measurements for the natural water content were performed with a closed drainage valve. After the final step of consolidation was completed, shear stress was applied in one or multiple stages. When equilibrium conditions were reached for the imposed stress state, and when horizontal deformation ceased, matric suction was measured once again, and the wetting part of the test began. Matric suction was decreased in various ways: by increasing the water pressure in the water compartment below the HAEPS, by decreasing the air pressure inside the testing chamber, or by a simultaneous change of both. Depending on the stage of the test and moisture conditions, matric suction was reduced at different rates. In some cases, water pressure was increased instantly by using the GDS volume and pressure controlling unit and water volume changes were observed during the time. Alternatively, the increase of pore water pressure was controlled by software. The desired value of the pore water pressure increasing was applied linearly during the defined time interval. In the case of the reduction of air pressure, the software was used to decrease matric suction value at the aimed rate. For example, rates at which matric suction was decreased in some cases were from 0.5 up to 2 kPa/h. In general, a low hydraulic conductivity of investigated soil and relatively safe  $\tau/\sigma_{net}$  ratio applied at the beginning of tests resulted in a long duration of both tests. For example, UVSCDS11 test lasted for 30.5 days, while it took 28 days to complete the UVSCDS12 test. The fact that these were the first wetting tests performed on this type of material, and that matric suction values imposed during the wetting stages were controlled in the following steps to check if the selected rate was appropriate for the equilibration process to take place, have contributed to the long duration of tests as well. Both tests and obtained results are briefly described below.

After the application of low contact pressure (5 kPa) in the UVSCDS11 test, the initial matric suction of 350 kPa was measured at constant water content. Tested specimen had initial water content of 17.4%, the degree of saturation equal to 58.6 %, volumetric water content of

26.0%  $\text{cm}^3/\text{cm}^3$  and a void ratio of 0.80. Following this, the specimen was consolidated under 50 kPa of net vertical stress, causing a slight increase of the volumetric water content and 20 kPa decrease of the matric suction. Shear stress was applied incrementally through three stages with a ramp of 25 kPa per minute. As shown in Figure 97, equilibrium conditions were reached at approximately 5.5 mm of horizontal displacement. All of the variables were measured during the application of initial loading conditions. After the last stage of shear stress application, and when the horizontal displacement ceased, the wetting part of the test was performed. Measurements of the volumetric water content, void ratio and shear stress vs. horizontal displacement are summarized in Figure 97. The obtained results indicate that void ratio increases and the volumetric water content of the specimen decreases as dilation occurs after 1.5 mm of horizontal displacement. In the following part of the UVSCDS11 test, imposed normal and shear loads were kept constant, while the water content was slowly increased by reducing the matric suction. During the next ten days ( $t_{\text{abs}} = 15500$  min in Figure 98), matric suction was incrementally decreased to 190 kPa, causing the increase of the degree of saturation to approx. 63%. Matric suction change, horizontal displacement, and calculated values of the pore water volume and degree of saturation during the following 20 days are summarized in Figure 98 a). Figure 98 b) shows the final part of the experiment in which yielding of the specimen starts to occur at an increased rate, as the matric suction is decreased below 65 kPa.

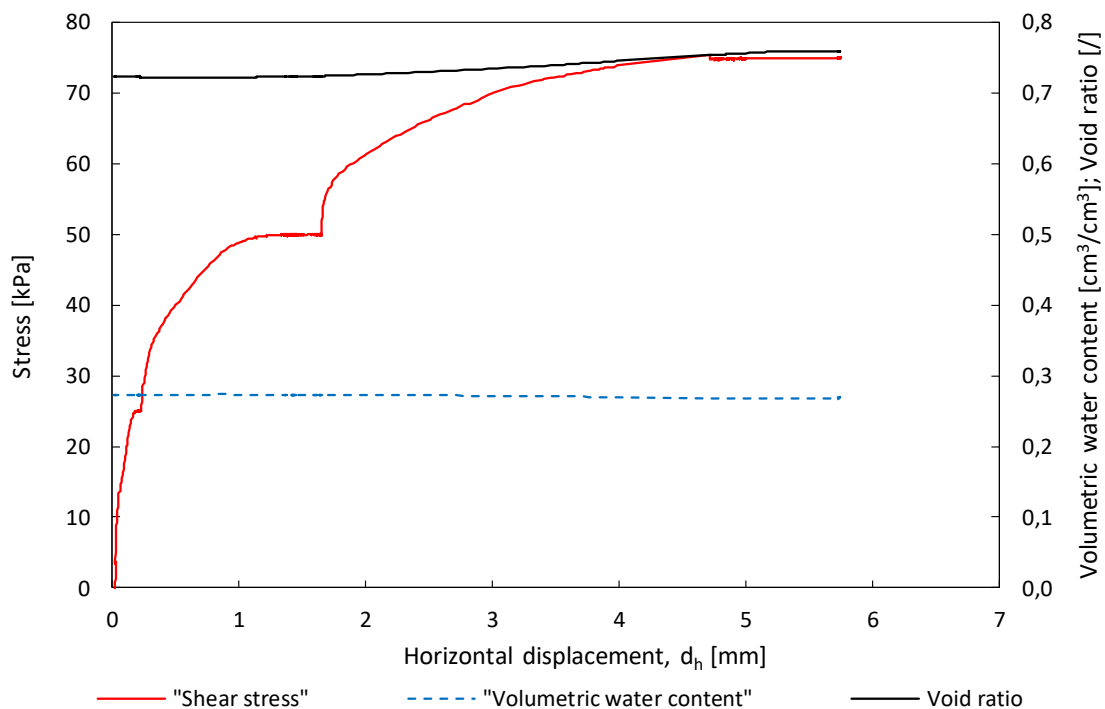


**Figure 97:** Change of the void ratio and volumetric water content during the application of shear stress under 50 kPa of net vertical stress in the UVSCDS11 test.

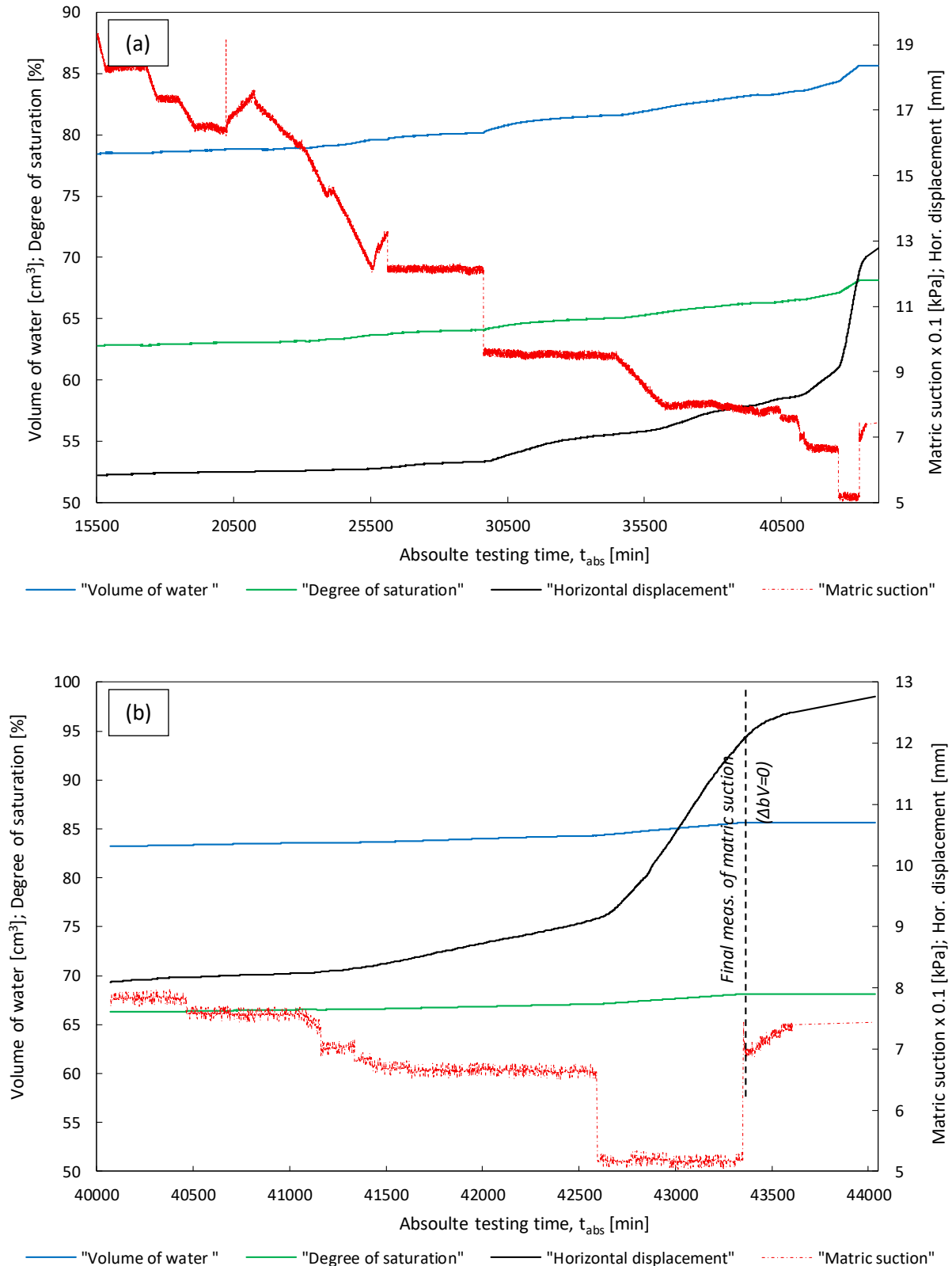


**Figure 98:** Matric suction, horizontal displacement, the degree of saturation and volume of water inside the specimen during the a) wetting stage, and b) yielding of the specimen in the UVSCDS11 test.

After the horizontal displacement reached 12.45 mm, the shear actuator was stopped and 74 kPa of matric suction was measured. Change of the volumetric water content, void ratio and degree of saturation vs. horizontal displacement are presented in Figure 99 for the wetting part of the test.

Similar behavior was observed for the UVSCDS12 tests during the application of initial loading conditions. The sample had a slightly lower initial water content of 14.1 %, for which 397 kPa of matric was measured. The degree of saturation equal to 47.1%, volumetric water content of 21% and void ratio of 0.81 were determined for the natural water content. After the consolidation at constant water content under 100 kPa of net vertical stress, 100 kPa of shear stress was applied in a single step through 2 min time interval. The specimen behavior changed from compressive to dilative after 1 mm of horizontal displacement was exceeded. In order to reach equilibrium conditions at lower horizontal displacement, shear stress was reduced for 10 kPa after a ramp stage was completed. Shear stress of 90 kPa was kept constant through the rest of the test. Application of the shear stress with measured void ratio and volumetric water content vs. horizontal displacement for the UVSCDS12 test are shown in Figure 100.

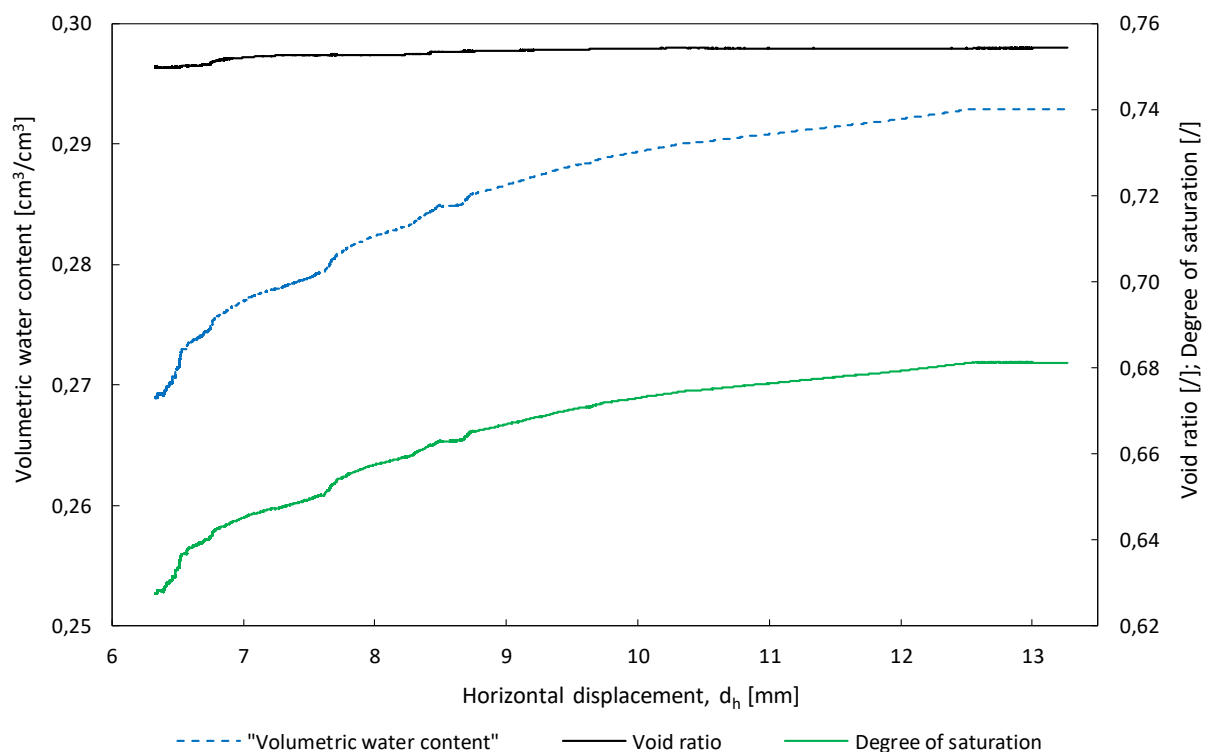


**Figure 99:** Change of the volumetric water content, void ratio and degree of saturation vs. horizontal displacement for the wetting part of the UVSCDS11 test.

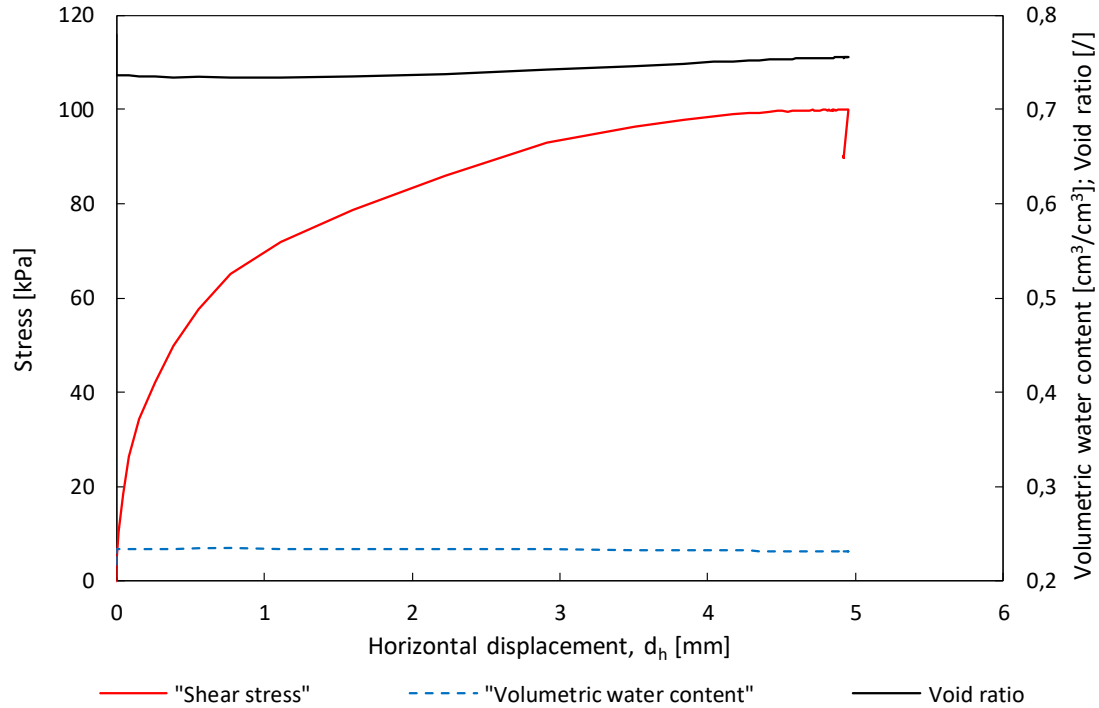


**Figure 100:** Change of the void ratio and volumetric water content during the application of shear stress under 100 kPa of net vertical stress in the UVSCDS12 test.

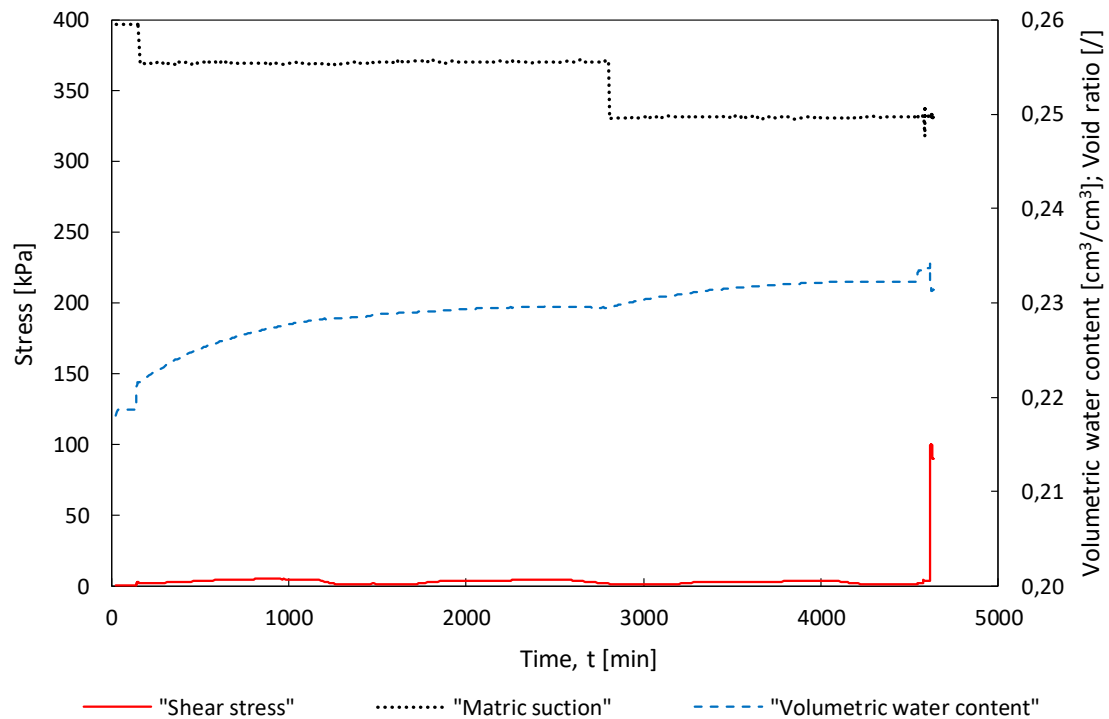


**Figure 101:** Initial suction measurement, consolidation, equilibration at 370 and 331 kPa of matric suction and application of shear stress vs. time for the UVSCDS12 test.

In the following part of the UVSCDS12 test, imposed normal and shear loads were kept constant, while the water content of the tested specimen was slowly increased by reducing the matric suction value. Change of the matric suction, horizontal displacement, volume of water inside the specimen, and degree of saturation during the time are summarized in Figure 102 a). Figure 102 b) shows a change of the volumetric water content, degree of saturation and void ratio with horizontal displacement.

The final part of the experiment, in which the specimen started to yield at an increased rate is indicated in Figure 103. The results show that the specimen was equilibrated at 33 kPa ( $t_{\text{abs}} = 30250$  min in Figure 103) with no horizontal displacements or change in water content occurring. Then, the matric suction was decreased in two steps. The first decrease of matric suction to around 22 kPa did not cause excessive horizontal deformation while the degree of saturation started to increase. A more rapid increasing of the degree of saturation was observed when the matric suction value was decreased to 10.5 kPa and held constant. The steady increase of shear displacement between time intervals of 31470 to 33120 min changed to a rapid yielding when the degree of saturation value increased above 77 % ( $t_{\text{abs}} = 33120$  min in Figure 103). During the whole stage of equilibration under the constant matric suction of 10.5 kPa, which lasted for around 43 hours, the degree of saturation was increasing at a constant rate.

When the horizontal displacement reached 12.45 mm, matric suction was increased up to around 90 kPa. As a result, shear displacement was stopped immediately, while 30 hours were needed for the excess of water to outflow from the specimen and volumetric water content to become constant. In the final stage, matric suction was lowered until the maximum horizontal displacement was reached. Again, matric suction was measured before dismantling of the device to check the actual matric suction value inside the specimen at the end of the test.

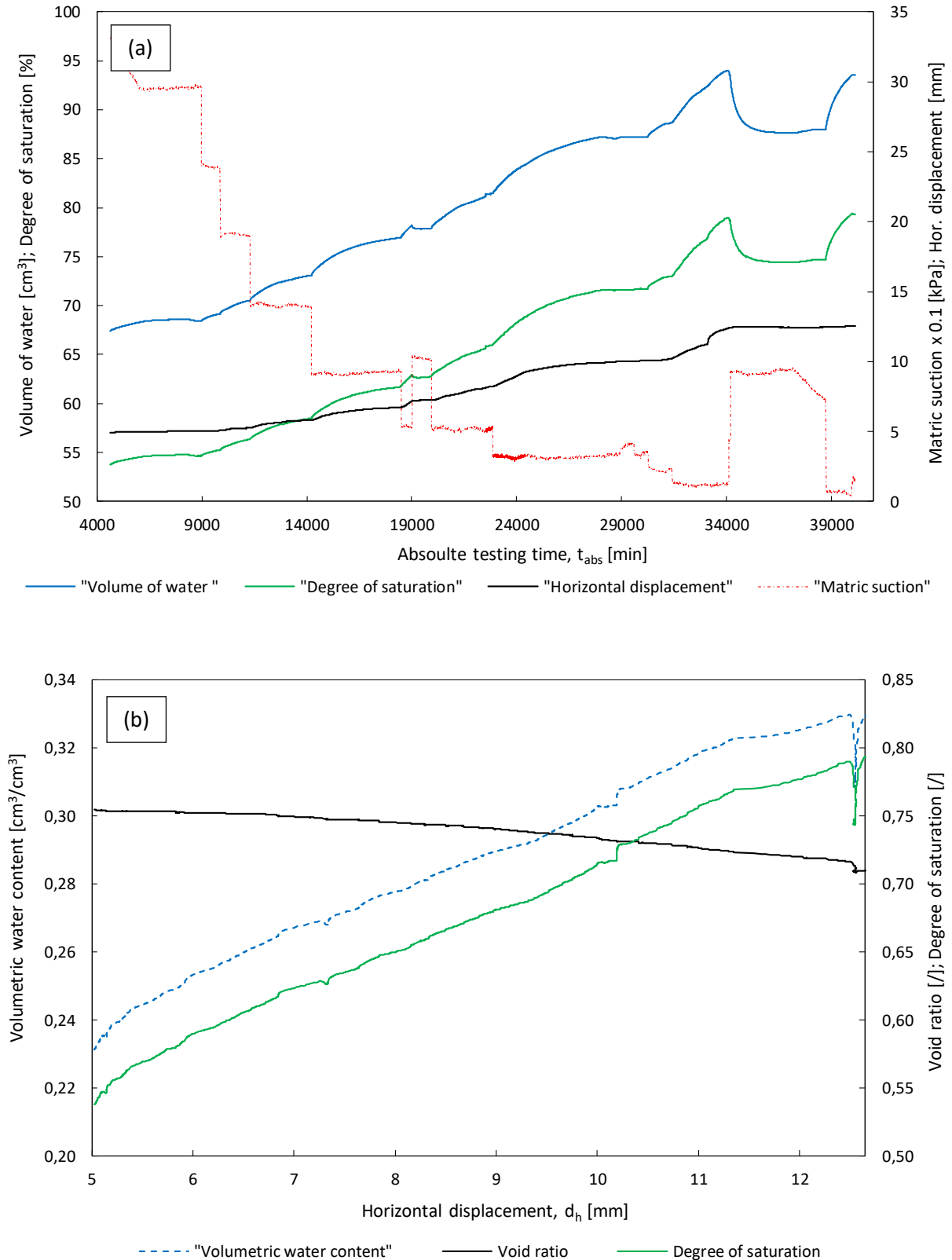


**Figure 102:** Reduction of the matric suction, horizontal displacement, degree of saturation and volume of water inside the specimen during the wetting stage vs. a) absolute duration of the test, and change of the void ratio, volumetric water content and degree of saturation vs. b) horizontal displacement in the UVSCDS11 test.



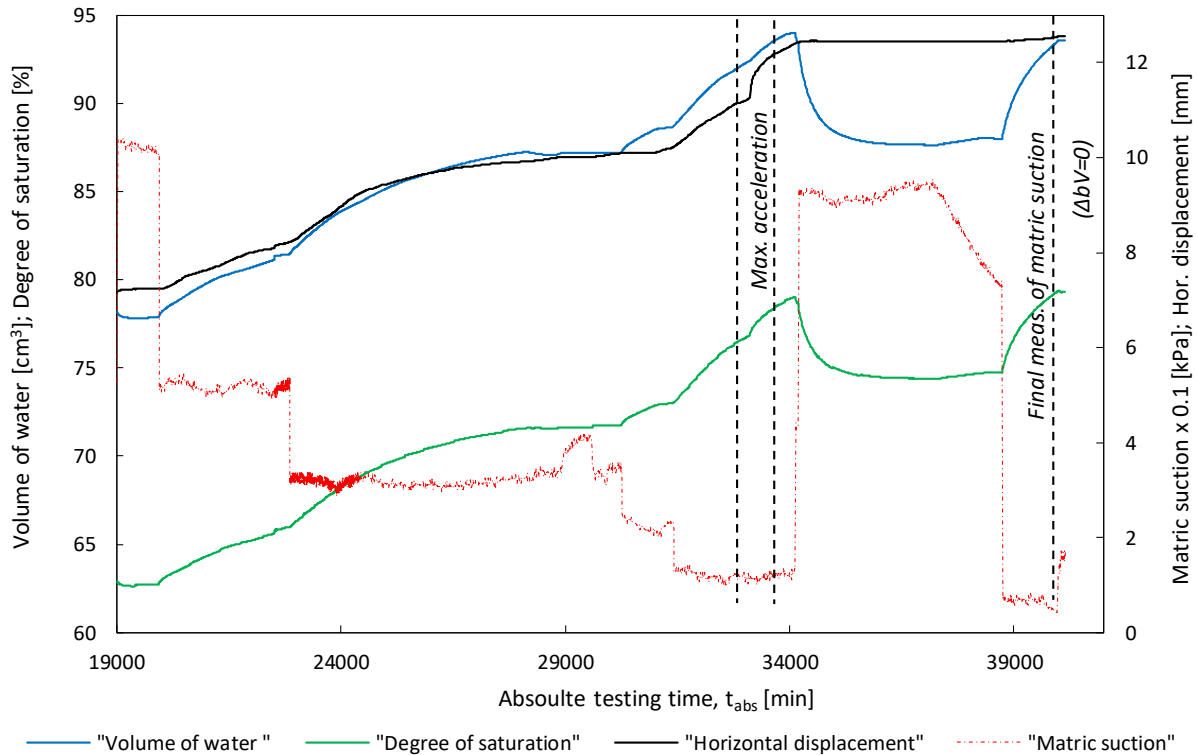


**Figure 103:** Matric suction, horizontal displacement, degree of saturation and volume of water inside the specimen during the yielding of the specimen in the UVSCDS12 test.

#### 6.4.2.1. Interpretation of the wetting test results

Stress paths for both conducted wetting tests are presented in Figure 104. The calculated degree of saturation and matric suction values during the tests were used to express the effective stress by using Bishop's formulation. The obtained values were used to represent the stress path that specimens underwent during the wetting tests. Results show that the gradual decreasing of matric suction under imposed normal and shear stress conditions led to an increasing in water content of tested specimens. Consequently, strength and stiffness reduced due to the decrease of matric suction value. At some point, acceleration of shear displacement was observed, leading to failure of the specimen. However, when the matric suction was increased in the UVSCDS12 test, equilibrium conditions were restored and yielding stopped. Again, further decrease of matric suction caused further horizontal deformations and yielding of the specimen. Although the previously determined SWRC was obtained without the application of the shear stress, initial and final water contents measured in wetting tests fall exactly on the main wetting branch (see Figure 105). The latter value was used to calculate the effective stress at failure.

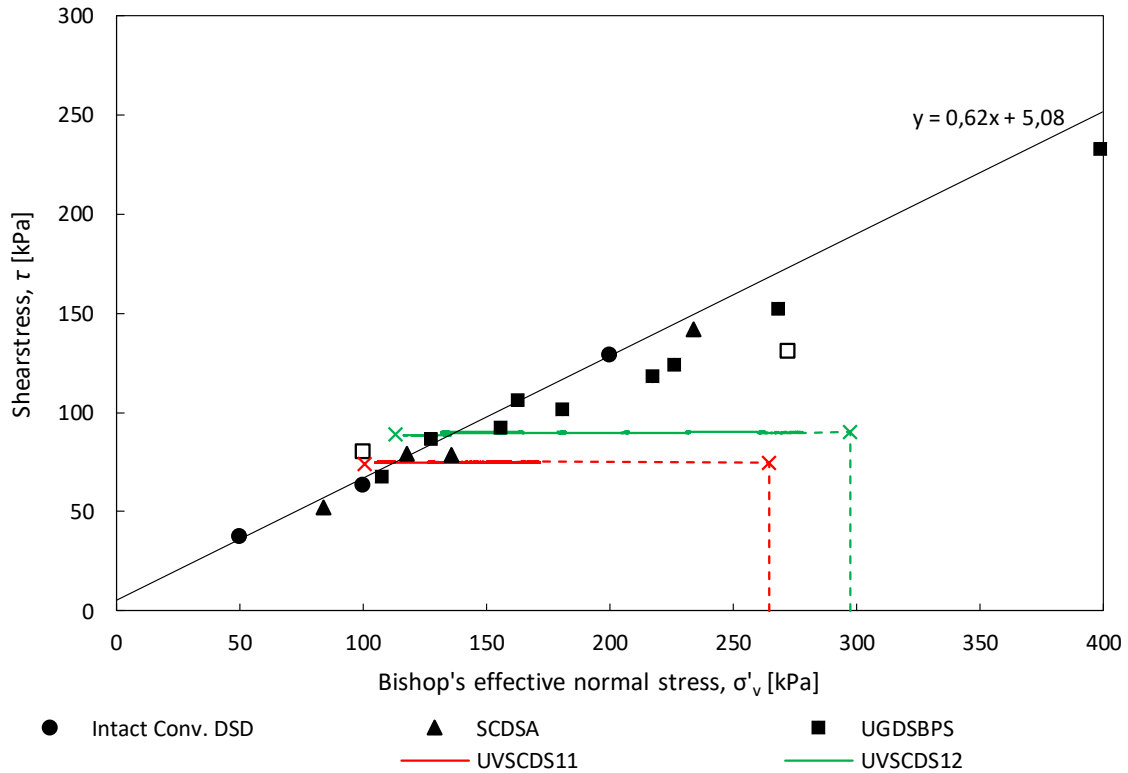


**Figure 104:** Stress paths from UVSCDS11 and UVSCDS12 wetting test with saturated envelope and shear strength test results obtained by using different direct shear devices.

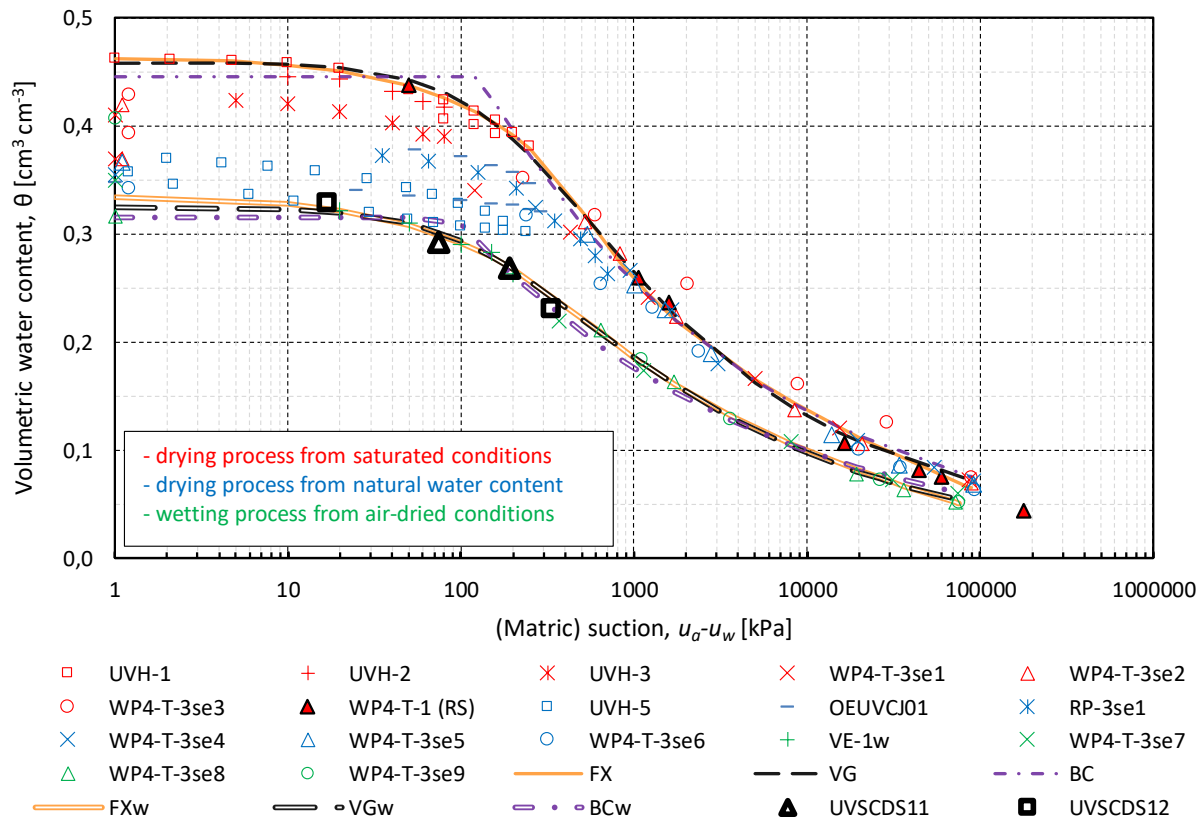


**Figure 105:** Initial and final volumetric water contents from UVSCDS11 and UVSCDS12 wetting tests plotted on derived SWRC curve in  $\theta - (u_a - u_w)$  form.



## **7. NUMERICAL SIMULATIONS**

All of the findings delivered through previous chapters are utilized to build a numerical model and perform different types of analyses in this chapter. Results of the rainfall infiltration analysis are coupled with the slope stability analysis to determine the influence of rainfall infiltration and geotechnical cross-section unsaturated zone on the state of slope stability in flysch slope over time.

## 7.1. Literature overview

To lower the impact of rainfall-induced landslides, which have become a widespread hazard that frequently results in considerable economic loss and human casualties, many efforts have been made throughout the last couple decades regarding the assessment of factors that cause the landslide events, predicting possible locations and explaining mechanisms that cause the landslide phenomena. A number of input parameters and variables that affect the solution make physically based modeling inappropriate for application on large and complex areas. Reliable mathematical models can include numerous variables involved in the triggering process, such as slope morphology, spatial and temporal rainfall variability, mechanical and hydraulic soil properties, initial conditions such as distribution of pore water pressures or moisture content, different boundary conditions, vegetation coverage, loading conditions, etc. (Greco et al. 2010). Given the extreme challenges to comprehensively account for all of these factors, even for a single specific location, studies usually focus only on those factors that have a major influence on the stability of the considered slope, in this case, rainfall. For example, various statistical approaches are commonly used to relate the occurrence of landslides and the rainfall characteristics without considering the influence of geological, hydrological and the physical process of rainfall infiltration in a slope (e.g., Guzzetti et al. 2007, 2008; Dahal and Hasegawa 2008; Brunetti et al. 2010; Peruccacci et al. 2017; Segoni et al. 2018, etc.). Conventional slope stability analyses, which are still most frequently employed in geotechnical engineering practice, account for rainfall influence on slope stability by changing the groundwater flow conditions, where the rising of the groundwater level increases pore water pressures and reduces the shear strength. This type of analysis assumes saturated, steady-state water flow, where for the worst-case scenario, the phreatic surface is often assumed to coincide with the soil surface (Collins and Znidarcic 2004). In this case, further infiltration is not possible, and further rainfall does not affect the stability of the slope. However, depending on the infiltration characteristics of the soil, other pore water pressure profiles are possible within the slope while the pore water pressure change occurs as a transient process, as the rainfall infiltrates into the soil (Collins and Znidarcic 2004; Zhang et al. 2011). Being mostly based on a wetting front concept, conceptual infiltration models (e.g., Green and Ampt 1911; Lumb 1962; Leach and Herbert 1982; Sun et al. 1998) generally have some serious limitation: material properties (USPFs) such as shear strength, water retention or permeability are not considered as a function of matric suction,

slope geometry and variation of rainfall are not considered, etc. Also, in certain types of soils, generally with low hydraulic conductivity, the wetting front concepts are not effective. Low infiltration rates result in a transition zone which is not sharp and distinguishable. Infiltration and evaporation are considered transient processes, which respond to the moisture flux boundary conditions (Fredlund et al. 2012). If a more rigorous distribution of pore water pressure in a slope under complex boundary conditions is to be obtained, the equation describing water flow through an unsaturated–saturated soil system must be solved (Zhang et al. 2011). The main difference in water flow through unsaturated soil, relative to the case of saturated soil, is in the coefficient of permeability, which is assumed not to be a constant value, but rather a function of matric suction or water content. Unlike for the unsaturated soils which are characterized by the presence of negative pore water pressure values, only positive pore water pressure values can exist in saturated soils. Although there are significant differences between the two cases, the formulation of differential equations describing water flow is derived in a similar manner (Fredlund et al. 2012), providing a smooth transition when switching from the unsaturated to the saturated case (Fredlund 1981). Aside from general heterogeneities of soil, the coefficient of water permeability can differ in various points of unsaturated soil due to different water content (or matric suction) values. In this case, the relationship between the coefficient of permeability respective to the water phase and matric suction (or water content) is defined by the UHCF. Anisotropy of soil can cause the coefficient of permeability to vary with the direction. In this case, the major and minor coefficients of permeability, corresponding to directions with the highest and lowest permeability have to be defined. The water storage property of soil has to be defined if transient flow process is considered. Part of the partial differential equation describing a transient process is denoted by the symbol  $m_2^w$  and is equal to the arithmetic slope of the SWRC expressed in terms of the volumetric water content, SWRC- $\theta$  (Fredlund et al. 2012). Fredlund and Morgenstern (1976) proposed the following water phase constitutive relationship for unsaturated soil

$$d\theta_w = m_1^w d(\sigma - u_a) + m_2^w d(u_a - u_w) \quad (81)$$

where  $\sigma$  is the total stress,  $m_1^w$  is the slope of the water volume vs.  $(\sigma - u_a)$  relationship when  $d(u_a - u_w)$  is zero, and  $m_2^w$  is the water storage coefficient, which is the slope of the water volume vs.  $(u_a - u_w)$  relationship when  $d(\sigma - u_a)$  is zero. If under transient water flow the total stress acting on an element of soil remains constant, and pore-air pressure is assumed to remain equal to the atmospheric pressure ( $u_a = p_{atm}$ ), then a change in volumetric water

content is a function only of a change in pore-water pressure, and the following relation is obtained (Fredlund and Morhenstern 1976; Zhang et al. 2004)

$$d\theta_w = m_2^w d(-u_w) . \quad (82)$$

In the case of unsaturated soil with isotropic hydraulic conductivity, ( $k_{w1} = k_{w2} = k_w(u_a - u_w)$ ), a 2D transient seepage equation can be expressed based on continuity considerations and Darcy's law as

$$\frac{\partial}{\partial x} \left( k_w \frac{\partial h_w}{\partial x} \right) + \frac{\partial}{\partial y} \left( k_w \frac{\partial h_w}{\partial y} \right) = m_2^w \rho_w g \frac{\partial h_w}{\partial t} = \frac{\partial \theta_w}{\partial t} \quad (83)$$

where  $m_2^w$  represents the water storage modulus obtained by differentiation of the SWRC- $\theta$  on an arithmetic scale (Fredlund et al. 2012).

Iverson (2000) proposed a model of the transient process of landslide response to rainfall that links slope failure and landslide motion to groundwater pressure heads that change in response to rainfall. By approximating the governing equation for rainfall infiltration in a local rectangular Cartesian coordinate system, he obtained an analytical solution for pressure head. In his work, Iverson (2000) considered only shallow and initially wet soil ( $k_w \approx k_{sat}$ ), exposed to short rainfall duration. Zhan and Ng (2004) performed an analytical analysis to study the rainfall infiltration mechanism and pore-water pressure distribution in single and two-layer unsaturated soil systems. By using the governing equation of 1D vertical transient infiltration, they applied various constant infiltration rates to study the effect of coefficient of saturated permeability, desaturation coefficient, water storage capacity, soil heterogeneity and others. They concluded that, among the three hydraulic parameters, the effects of  $\alpha$  and  $k_s$  on the pore-water pressure response are much more significant than the soil retention capabilities ( $\theta_s - \theta_r$ ). The advantage of numerical analysis is that it can incorporate more sophisticated and advanced models of soil hydraulic properties or advanced boundary conditions that can change in time. Rahardjo et al. (2007) performed parametric numerical studies to investigate controlling factors for slope instability under rainfall conditions. The relative importance of hydraulic soil properties, rainfall intensity, initial water table location and slope geometry in inducing instability of a homogenous soil slope under varied rainfall conditions was investigated through a series of parametric studies. They found that the primary factors controlling the stability of slope under rainfall are soil properties and rainfall intensity, while the initial water table location and slope geometry only played a secondary role (Rahardjo et al. 2007). Also, the results indicated that the instability of slopes with high  $k_s$  values is more likely to be affected by short-

duration rainfall, while only long-duration rainfall and antecedent rainfall are closely related with the failure of slopes with low hydraulic conductivity. They suggested that, for a given rainfall duration, a threshold rainfall intensity exists, which results in the minimum global factor of safety. The applied hydro-mechanical soil parameters, boundary and initial conditions, as well as considered slopes geometry, are typical for residual soils in Singapore. Ng and Pang (2000) performed the series of finite-element transient seepage and limit-equilibrium analyses to study the influence of various rainfall characteristics and stress-dependent SWRCs on the stability of an unsaturated cut slope. In the case of slopes built in volcanic soil in Hong Kong, they showed that wetting stress-dependent SWRCs resulted in substantially higher initial steady-state pore-water pressure distributions with depth than in the case of using conventional drying SWRCs. Zhang et al. (2004) performed the steady-state and transient finite element seepage analyses to show the dependency between pore-water pressure profile and rainfall intensity, the saturated coefficient of permeability and the water storage function. They showed that under steady state conditions, the most important factor affecting the matric suction near ground surface is the ratio between the magnitude of the ground surface moisture flux and the saturated coefficient of permeability  $q/k_s$ . If the steady-state rainfall fluxes  $q$  are two or more orders of magnitude lower than the  $k_s$ , the long-term matric suction does not disappear and remains essentially close to the hydrostatic profile. An increase of the  $q/k_s$  ratio and decrease of the soil AEV caused reduction of matric suction in the vertical soil profile. For the transient seepage conditions, Zhang et al. (2004) showed that the pore-water pressure profile after a rainfall depends on the water storage properties, as well, with the wetting front progress being reduced as the water storage of soil increases. Cascini et al. (2010) proposed an approach for geomechanical modeling of failure and post-failure stages of the shallow landslides of the flow-type. By performing various numerical analyses for the relevant case study of Southern Italy, Sarno - Quindici event which occurred between 4 and 5 May 1998, they showed that localized pore-water pressure values induced by spring from the bedrock played the key role in the failure onset. The same event was modeled combining the limit equilibrium method with computed pore water pressures from the governing transient equation, by using the uncoupled stress-strain analyses, and fully coupled 2D and 3D stress-strain analysis approach of both failure and post-failure stages. Again, stress-strain analyses indicated that rainfall infiltration from the ground surface induces low deformation rates in the slope, while by considering the spring from bedrock, higher pore-water pressures, stress ratios and deformation rates were simulated in the portion of the slope corresponding to the spring zone. Results highlighted that the 3D coupled analyses agree with the slope instability scenarios obtained with simplified models and that



more conventional 2D analyses can be safely referred (Casini et al. 2010). Rahimi et al. (2011) performed parametric numerical studies by using three typical rainfall patterns for Singapore and two different soil types to represent high- and low-conductivity residual soils of Singapore. By applying antecedent rainfall patterns and performing a transient seepage analysis, the obtained pore water pressures were used to calculate factor of safety to analyze the slope stability results. They found that the antecedent rainfall affected the low-conductivity slope more significantly than the high-conductivity slope, while rainfall patterns controlled the time corresponding to a minimum factor of safety value, the rate at which the factor of safety decreased and its value also. Delayed rainfall pattern resulted in the lowest minimum factor of safety, for the high-conductivity slope, while advanced rainfall pattern resulted in a lowest minimum factor of safety for low-conductivity slope (Rahimi et al. 2011). The minimum factor of safety value was found to correspond to the amount of infiltrated water: the delayed rainfall pattern resulted in the highest amount of infiltrated water for the high-conductivity slope, causing the minimum factor of safety value. A minimum factor of safety value and the highest quantity of infiltrated water was obtained for the advanced rainfall pattern in the case of the low-conductivity pattern (Rahimi et al. 2011). By performing numerical parametric analysis, Cuomo and Della Sala (2013) showed that time to runoff, time to failure and runoff rates are strongly affected by SWRCs, initial soil conditions, rainfall intensity, and slope angle. The adopted hydro-mechanical soil properties and geometrical conditions were representative for soils and slopes from different parts of the world. Cuomo and Della Sala (2013) outlined that simplified standard procedures provide only a poor estimation of the time to runoff and runoff discharge, which can be improved through the application of the proposed procedure. Zhang et al. (2014) performed a study by using the two-dimensional slope stability analysis along with an estimated nonlinear shear strength equation. Results showed that the effect of matric suction on the calculated factor of safety is trivial for soils with AEV less than 1 kPa, and that the  $\phi^b$  value equal to zero can be assumed. For AEV ranging from 1 to 20 kPa, the nonlinear equations of unsaturated shear strength should be adopted. For soils with an AEV value between 20 and 200 kPa, an assumed  $\phi^b$  value of  $15^\circ$  provides a reasonable estimation of the effects of unsaturated shear strength in most cases. For soils with an AEV greater than 200 kPa, it can be generally assumed that  $\phi^b = \phi'$ , in applications where geotechnical structures have matric suctions around 100 kPa (Zhang et al. 2014). Numerical modeling of rainfall infiltration coupled with slope stability analyses has been used to assess the impact of Earth's climate change. For example, one aspect of climate change are the variations in rainfall patterns, which affect flux boundary condition across the ground surface – input parameter for numerical

modeling of transient rainfall infiltration process. Kristo et al. (2017) investigate the variations in rainfall patterns in Singapore and its effect on slope stability. Linear regression was used to analyze historical rainfall data (1985-2009) from Seletar and Paya Lebar weather stations. Using the derived trends, which indicated generally increasing trend of rainfall intensity, Kristo et al. (2017) projected rainfall intensities in 2050 and 2100, which were used in the seepage and slope stability analyses performed on a typical residual soil slope in Singapore. The performed slope stability analysis indicated a significant reduction in the factor of safety, especially from 2003 – 2050 due to increase in rainfall intensity, suggesting that climate change might have existed beyond 2009 with possibly detrimental effects to slope stability (Kristo et al. 2017). A similar study was performed by Yeh and Tsai (2018), who analyzed the effects of climate change on rainfall patterns from the perspective of rainfall intensity, and combined the obtained intensity trends with numerical model analysis to examine the rainfall patterns of the Zengwen reservoir catchment area and its effects on slope stability. A qualitative analysis of seepage and slope stability showed that increasing amount of seepage would significantly change pore water pressure in the soil, leading to the quicker occurrence of slope instability after the start of rainfall (Yeh and Tsai 2018).

Shallow flow-type landslides triggered by rainfall in pyroclastic soils frequently affect the region of Campania (southern Italy). Several papers have dealt with modeling of flow-type landslides in carbonate and volcanic contexts (e.g., Pagano et al. 2010; Cascini et al. 2010; Cascini et al. 2013; Pirone et al. 2016). However, only a few studies have focused on landslides in pyroclastic soils resting on flysch bedrock. Santo et al. (2018) performed uncoupled hydro-mechanical analyses on the Bosco de' Preti landslide (Avellino, Italy). This study constitutes a case study of a complex landslide affecting pyroclastic soils on flysch bedrock. In this study, rainfall infiltration was modeled as the transient process only through the pyroclastic soil, for which UHCF and SWRC were known. Flysch bedrock was modeled only as a saturated material, with an adopted value of  $k_s = 1.0\text{E-}09$  m/s according to site measurements in similar flysch deposits of the southern Apennines (Urciuoli et al. 2016). Numerical analysis, in which pore-water pressures obtained from the rainfall infiltration analysis were introduced into slope stability analysis, demonstrated that the rainfall during the two months preceding the event was able to fully saturate the pyroclastic cover and to establish positive pore water pressure at a depth of the surface of rupture, a soil condition never witnessed in carbonatic contexts.

Very few studies concerning rainfall infiltration process through flysch deposits exist. For example, Berti and Simoni (2012) presented the results of monitoring activities carried out on two slopes prone to sliding, built of clay-shales in the Northern Apennines of Italy. They

used descriptive statistics and simple, physically based theories for infiltration and groundwater flow to analyze and interpret the collected field data. They concluded that shallow weathered soils, or clayey cover, and unaltered material at some depth exhibit much different behavior. The responses to single rainfalls are identifiable as pressure pulses in the clay cover, but are never observed in the underlying parental clay-shales where downward gradients indicate recharge and only long-term seasonal fluctuations are recorded. They concluded that short-term variations of pressure head in the clayey cover are ruled by downward propagation of a pressure wave in saturated conditions. By addressing slope stability regarding the presented hydrological framework, they discuss that shallow weathered soils, being the only portion of the profile manifesting abrupt responses to rainfall, are associated with worse conditions (Berti and Simoni 2012). Berti et al. (2017) performed a conventional numerical back analysis of a large landslide in a Cretaceous flysch rocks which occurred in the Savena River basin (Northern Apennines of Italy) on 6 April 2013. LEM and FDM analysis were performed to compare the mobilized strength at failure with those predicted by the modified GSI method (Marinos and Hoek 2001). Completely dry to fully saturated conditions were simulated simply by changing the groundwater level. Analysis results indicate that the combination of a high groundwater level and low rock mass cohesion ( $c'=20-40$  kPa) is most probably responsible for the landslide, while the modified GSI method generally overestimates the strength of the Monghidoro flysch, and can predict the in situ strength only if the disturbance factor,  $D$ , is assumed to be equal to 1 (Berti et al. 2017). However, they emphasize that much of the discrepancy is related with the approximation introduced by the linearization process of the Hoek-Brown envelope to obtain Mohr-Coulomb parameters. Li et al. (2011) and Berisavljević et al. (2015) came to the similar conclusion, suggesting consideration of a different set of parameters in the stress range of interest to overcome the overestimate of the shear strength provided at low stress. Mišćević et al. (2009) performed back-analysis of a landslide which occurred in February 2005 at Bol on the Island of Brač, Croatia, in a geological structure of weakly bounded conglomerates lying above flysch. Field investigation results showed that the landslide surface was formed, not in contact between the conglomerates and marl, but deeper in the flysch, caused by the penetration of the weathering front into the flysch. Numerical modeling was performed using the 2D FEM by performing two types of analysis. In the first, a completely dry up to completely saturated slope was considered simply by raising the groundwater table. The second type of analysis included a combination of change in groundwater table and gradual reduction of shear strength parameters to account for the weathering effects. Numerical modeling results suggest that yielding and initiation of failure is reproduced by incorporating shear strength degradation into

the weathered zone. Models that were focusing on a failure mechanism restricted to plane failure along the contact of two layers due to increased pore pressure failed to reproduce the determined slide surface (Mišćević et al. 2009). Maček et al. (2016) investigated the Slano blato, one of the oldest and largest landslides in Slovenia where the last instability occurred in November 2000, in the form of a large earthflow. The slope was instrumented with suction probes and the results of 6-year monitoring programme indicated that only prolonged wet periods change suction in the earthflow body, while an observed sudden decrease in matric suction during dry periods caused by rainfall events was attributed to the formation of desiccation cracks. SWRC and hydraulic permeability were determined by using only a fine-grained portion of samples obtained by sieving, drying and again wetting of material. For tested material, which could be classified as fat clay (CH), an AEV of 1300 kPa was measured by means of the axis translation technique and WP4-T dew-point potentiometer (Decagon Devices Inc.). Green and Ampt equation (1911) modified by Chen and Young (2006) for an inclined slope was used along with the permeability coefficient obtained in the laboratory of about  $5.0\text{E-}10$  m/s. They calculated that it takes approximately four months for the wetting front to reach 1.2 m of depth, confirming the existence of a long delay between the lowest suction values and the start of the wet rainy periods obtained from the field measurements (Maček et al. 2016). They concluded that the Slano blato is essentially always saturated, except on the top few centimeters where soil can be dried due to excessive evaporation, and that matric suction measurements cannot be used as an indicator of potential future earthflow occurrences, but rather just as an indicator of the periods with the lowest factor of safety, and thus also with the highest probability of instability events. However, none of the studies investigate the influence of rainfall on triggering a flysch slope by considering the rainfall infiltration as a transient process, redistribution of water content and pore-water pressure, and influence of the USPFs on the change of the slope stability. These kinds of studies are completely absent in the literature for landslides occurring in the flysch slopes.

The GeoStudio (GEO-SLOPE International, Ltd.) software suite was used in this study to perform numerical analysis of rainfall infiltration and slope stability in this study. The GeoStudio is an integrated, multi-physics, multi-dimensional, platform of numerical analysis tools developed by GEO-SLOPE International, Ltd. for geo-engineers and earth scientists. The multi-disciplinary nature of GeoStudio is reflected in its range of products: four finite element flow products (heat and mass transfer); two finite element stress-strain products; and a slope stability product that employs limit equilibrium and stress based strategies for calculating

margins of safety. The software package is formulated to support one-dimensional, two-dimensional, axisymmetric, and “plan” view analyses (GEOSLOPE International 2017).

## 7.2. Rainfall infiltration modeling

The commercially available software allows combining multiple analyses into a single modeling project. SEEP/W is a 2D finite-element software product for groundwater flow modeling in porous media. It is capable of modeling a wide range of problems, by performing simple saturated steady-state or more advanced saturated/unsaturated transient analysis with atmospheric coupling at the ground surface (GEOSLOPE International 2017).

### 7.2.1. Theoretical background

The conservation of mass statement requires that the difference in the rate of mass flow into and out of the REV must be equal to the rate of change in mass within the REV, which is equal to the sum of the rate of change of liquid water and water vapor (e.g., Domenico and Schwartz 1998), as follows

$$\dot{M}_{st} \equiv \frac{dM_{st}}{dt} = \dot{m}_{in} - \dot{m}_{out} + \dot{M}_s = \dot{M}_w + \dot{M}_v \quad (84)$$

where  $\dot{M}_{st}$  is the stored mass, the mass transported across the REV surface (inflow and outflow) is represented with  $\dot{m}_{in}$  and  $\dot{m}_{out}$  terms, while mass source or sink within the REV is represented with  $\dot{M}_s$ .  $\dot{M}_w$  and  $\dot{M}_v$  represent the rate of change of liquid water and water vapor, respectively. The rate of change in the stored liquid water is given with

$$\begin{aligned} \dot{M}_w &= \frac{\partial(\rho_w \theta_w)}{\partial t} dxdydz \\ &= \rho_w \left( \rho_w \beta_w \frac{\partial u_w}{\partial t} + \beta \frac{\partial u_w}{\partial t} + m_w \frac{\partial \varphi}{\partial t} \right) + \rho_w \theta_w \alpha_w \frac{\partial T}{\partial t} \end{aligned} \quad (85)$$

where  $\beta_w$  is isothermal compressibility of water,  $\beta$  is the soil structure compressibility,  $m_w$  is the slope of the SWRC- $\theta$ ,  $\alpha_w$  is the volumetric coefficient of thermal expansion at constant pressure, and matric suction is denoted with  $p = (u_a - u_w)$  (GEOSLOPE International 2017).

By using the ideal gas law, the rate of change in the water vapor stored in the REV can be expressed as

$$\dot{M}_v = \frac{\partial M_v}{\partial t} = \frac{M}{R} \frac{\partial}{\partial t} \left( \frac{p_v \theta_a}{T} \right) dx dy dz \quad (86)$$

where  $p_v$  is the vapor pressure and  $\theta_a$  is the volumetric air content, used to calculate the volume of air inside the REV.

SEEP/W considers only liquid water flow due to mechanical energy gradients, while electrical, thermal and chemical energy gradients are ignored. The physical process of vapor flow, which can occur due to partial vapor pressure gradients or gradients in total pressure and density in the bulk air phase, is integrated with AIR/W software module (GEO-SLOPE International 2017). The mass flow rate of liquid water in response to mechanical energy gradients only can be described using Darcy's law (e.g., Bear 1988) while Fick's law can be used to describe the mass flow rate of water vapor (e.g., Saito et al. 2006). The groundwater flow equation implemented in SEEP/W described earlier by (83) is obtained by ignoring the vapor transfer and thermal expression. Total stresses within a domain are assumed constant in the SEEP/W. Therefore, changes in storage due to soil structure compressibility, described by material model input parameter  $\beta$ , are only due to pore-water pressure changes. SEEP/W can be coupled with AIR/W to simultaneously model air transfer and its effect on water transfer and storage. In the absence of an air flow analysis, such as those considered in this study, the pore-air pressure within an unsaturated soil is assumed to be at zero gauge pressure, while the matric suction is equal to the negative water pressure (GEO-SLOPE International 2017).

### 7.2.2. Key-in material properties

The saturated-unsaturated material model was used for analyzing the rainfall infiltration process since the material in few upper meters of slope exists in the essentially unsaturated state. For material that can become unsaturated at any point of the numerical simulation, hydraulic properties, SWRC and UHCF have to be defined to obtain a solution to the problem. SEEP/W provides a few methods for defining the SWRCs and UHCFs. For example, methods such as Modified Kovacs (Aubertin et al. 2003), can be used to estimate SWRC from basic geotechnical properties. Another available method is to choose sample functions, which are already implemented in SEEP/W code with parameters values that are common for certain textures of soil. Generally, this mode is rarely used, for example in the case of preliminary analysis when the influence of SWRC shape and parameters is assessed in some specific engineering situation. Engineering judgment and knowledge about the in-situ conditions are then usually used to define saturated and residual water content conditions. Two closed-form equations can be used

to describe the relationship between the volumetric water content and matric suction of analyses soil. Van Genuchten (1980) or Fredlund and Xing (1994) equation can be used to estimate the SWRC, given that values of equation parameters are known.

Relevant equation parameters obtained by fitting procedure on experimentally obtained results (Peranić et al. 2018) were used to simulate retention properties of soil undergoing wetting process during rainfall infiltration. SWRC equation was combined with the determined saturated coefficient of permeability value  $k_s = 4.6\text{E-}08$  m/s to estimate the UHCF for modeling purposes, as outlined in the previous part of the thesis.

Most of the estimation procedures that combine SWRC equation and  $k_s$  to estimate the UHCF predict an unbounded decrease of the coefficient of permeability with increasing matric suction. There is, however, a “shutoff” of liquid water flow at some relatively high value of matric suction, where there is a transfer from liquid water flow to predominantly vapor water flow (Fredlund et al. 2012). Measurements of water flow at residual water conditions are extremely rare due to the complexity of experimental set-ups that test procedures should include. A study performed by Ebrahimi-Birang et al. (2004) on soil textures ranging from sand to silt, yielded in conclusion that even at residual conditions, where the vapor coefficient of permeability  $k_v$  reaches its maximum value,  $k_w$  still dominates over the  $k_v$  value (Figure 106). They suggested that a reasonable lower limit of the  $k_w$  should be around  $1.0\text{E-}14$  m/s. Extremely low values of the coefficient of permeability can cause significant problems when water flow through unsaturated soil is numerically modeled. However, the soil under consideration and maximum matric suction values appearing in performed analyzes, estimated UHCF for the wetting path suggests that approximately  $3.2\text{E-}11$  m/s should be the lowest  $k_w$  value appearing in the performed analysis. Although around three orders of magnitude lower than the  $k_s$  value, the value is still far higher than the critical value proposed by Ebrahimi-Birang et al. (2004).

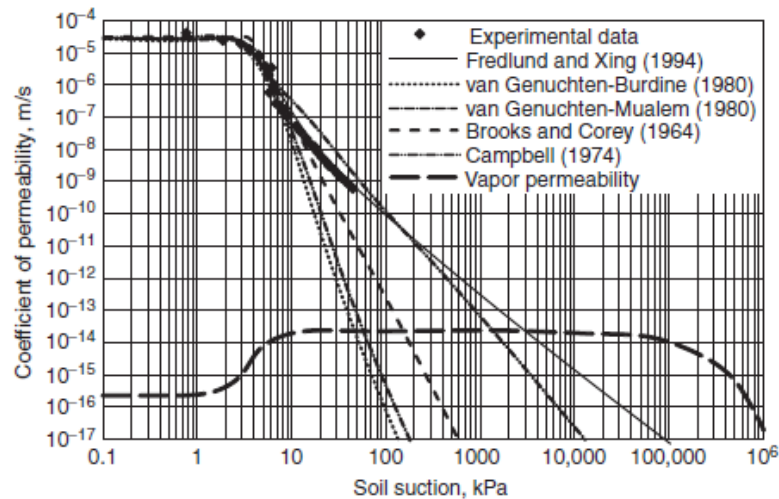


**Figure 106:** Liquid water, vapor, and overall permeability coefficients with respect to soil suction for silty sand (from Fredlund et al. 2012 after Ebrahimi-Birang et al. 2004).

According to suction measurements described earlier, maximum matric suction values that could be expected in the calculation process are well-below 1,000 kPa. For this matric suction range, previously derived UHCFs are shown in Figure 107.

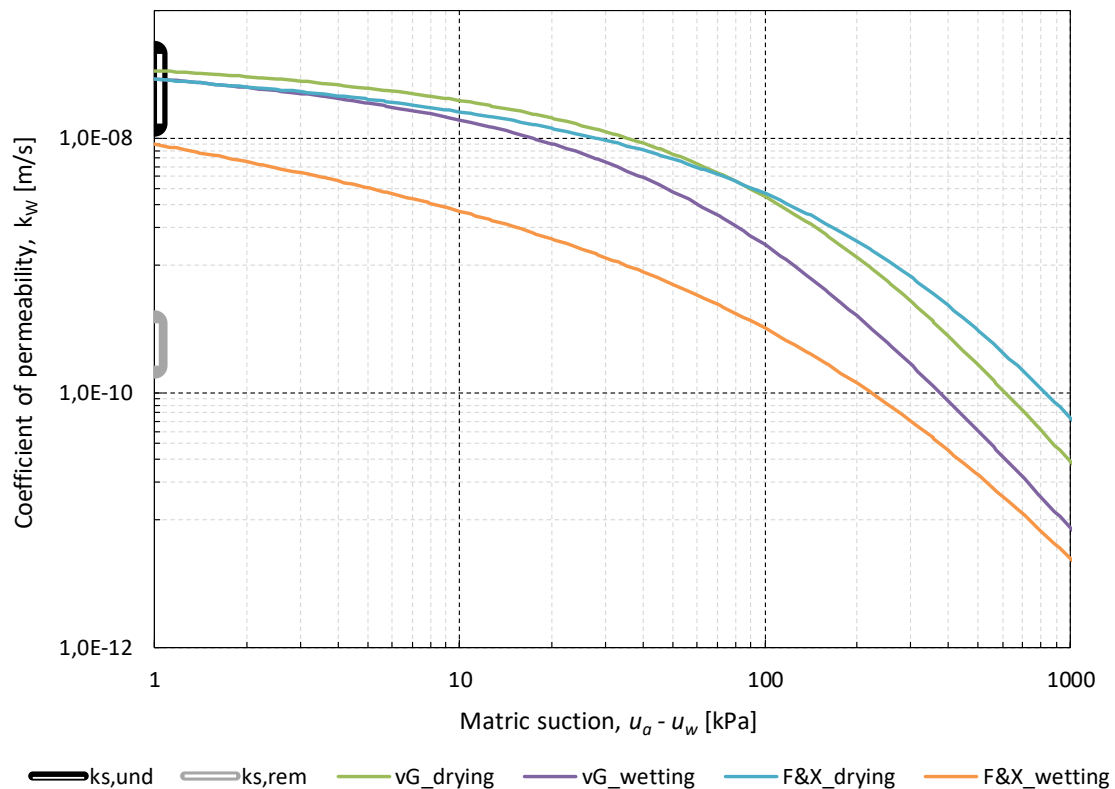


**Figure 107:** Estimated UHCFs for the suction range considered in performed analyses.



### 7.2.3. Initial and boundary conditions

As in any other code implementing the FEM to obtain results numerically, the solution of the FEM equations is constrained by the boundary conditions defined across the domain. The FEM for a seepage analysis basically has the form

$$[K]\{H\} = \{Q\} \quad (87)$$

where  $[K]$  represents a matrix of coefficients related to geometry and material properties, and vectors of the total hydraulic heads and flow quantities at the nodes are represented with  $\{H\}$  and  $\{Q\}$ , respectively (GEO-SLOPE International 2012). Respective to the defined boundary conditions, the above equation is used to obtain the primary unknowns: total head values at each node. Boundary conditions can be specified in terms of the dependent variable ( $H$ ), so-called 1<sup>st</sup> type or Dirichlet boundary conditions, or the gradient of the dependent variable (flux), which are often referred to as 2<sup>nd</sup> type or Neumann boundary conditions. In this study, influence of the rainfall infiltration on the slope stability was analyzed by applying various values of water flux across the soil surface in the model. Collected rainfall data presented in Chapter 2 were used to define the function of water flux vs. time and applied across the slope surface in SEEP/W. Positive pore-water pressure can be generated if the applied water flux boundary condition exceeds the infiltration capacity of the soil. Since the slope is considered in this analysis and geometry and field conditions are such that ponding of water due to excessive precipitation and low hydraulic permeability of the soil is unrealistic, generation of positive pore water pressure along the slope surface was eliminated by using the potential seepage face review option. This special case of the boundary condition reviews that the maximum pore-water pressure along the discharge surface or infiltration boundary is zero (GEO-STUDIO International 2017). This condition was applied to all nodes at the soil surface, with elevation above 228m asl, which corresponds to the Valići Lake water level.

Collected 10-minute rainfall measurements were used for the definition of the water flux boundary condition (Figure 110). To analyze the influence of the resolution of collected rainfall data, boundary condition was applied in the form of 10', 1h and cumulative daily rainfall. Hourly and daily rainfall data were derived from collected 10' measurements. The precipitation taken into account in the performed analyses corresponds to the period from 1 September 2013 until the day of landslide reactivation, namely 14 February 2014. During these 167 days, cumulative precipitation of 1164 mm was recorded. According to rainfall characteristics described in Chapter 2, the average annual precipitation for the period from 1958

till 2014, was 1579 mm. To study the influence of the rainfall intensity, measured amounts of rainfall were multiplied with 0.25, 0.5, 2, 4, 8, 16 and 32. In that case, artificial rainfall data was created with a pattern corresponding to that which caused the landslide reactivation, but with varied intensities (Figure 111).

The water level of 231.80 m above sea level (asl) corresponds to full Valići Reservoir (top of the Valići Dam), while the water level 229.50 m asl corresponds to maximum overflow level (Arbanas et al. 2017). The average working water level of the Valići Reservoir was considered in the numerical analysis by applying a constant total head equal to 228m on the right side of the model. Constant water total head of 301.8 m was defined at the left side of the numerical model according to inverse analysis results shown in Figure 108 and field observations. With the average value of effective friction angle value of  $\phi' = 29^\circ$ , and effective cohesion  $c = 0$  kPa, the landslide becomes unstable only when the sliding mass is completely saturated, with the groundwater table reaching the slope surface almost at entire sliding mass. Similar results were obtained from the shear strength reduction method by Arbanas et al. (2017).

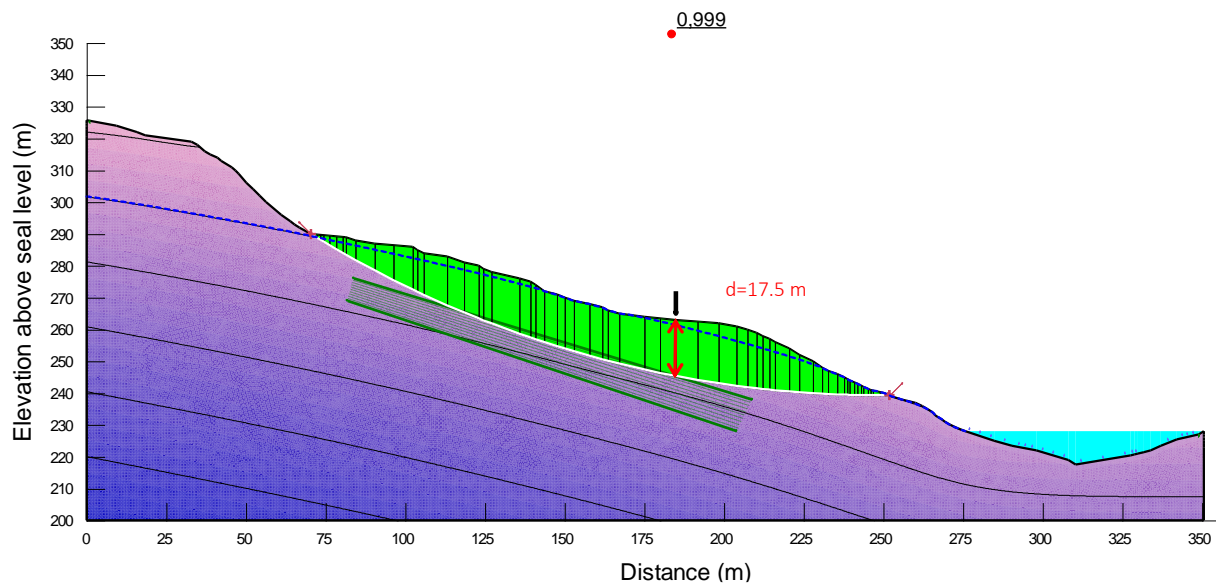


**Figure 108:** Back analysis for determination of critical slip surface with experimentally obtained shear strength parameters.

Field measurements for determination of the water content during different periods of the year, as well as the matric suction values measured by axis translation technique, were used to account for the desiccation effects during the dry summer period. Discretization of the domain was performed by using an automatically generated unstructured pattern of quadrilateral and triangular elements, with an approximate global element size of 1m. Several additional regions were created in the near-surface zone to obtain finer discretization in part of the domain where imposed boundary conditions cause changes to occur more rapidly. For

example, four regions parallel to the slope surface and with 0.5 m of height were added from the soil surface up to 2 m of depth. Additional three zones with a height of 1m were created till the depth of 5 m. This type of discretization was found to ensure numerical fluency, without convergence problems and with reasonable calculation times. The detail of discretization in the near-surface zone is outlined in Figure 109.

Varying values of the matric suction were applied at part of the slope cross-section close to the landslide surface. The constant pore-water pressure was defined to account for desiccation effects that occur during the summer period due to the negative water flux. A close match with observed triggering features was obtained when matric suction value of 300 kPa was applied in the most upper part of the slope, along with previously defined BC's. Groundwater level at the location of piezometer in the upper part of the slope closely matches with that obtained by selected boundary and initial conditions. Matric suction value of 300 kPa is close to that measured by the axis translation technique on relatively dry soil samples collected during July 2017 (e.g., UVSCDS11 and UVSCDS12 tests). However, in order to analyze the influence of the initial pore-water pressure distribution, various initial pore-water pressure profiles were applied as well. Figure 109 shows the FEM model built in SEEP/W with applied initial and boundary conditions, mixed quadrilateral and unstructured triangular mesh for discretization, and with an indicated location of the sampling pit and borehole B1 where inclinometer was installed and borehole B2 where groundwater level is being monitored. Figure 112 shows initial pore-water pressure distribution and associated FoS for defined ICs and BCs.

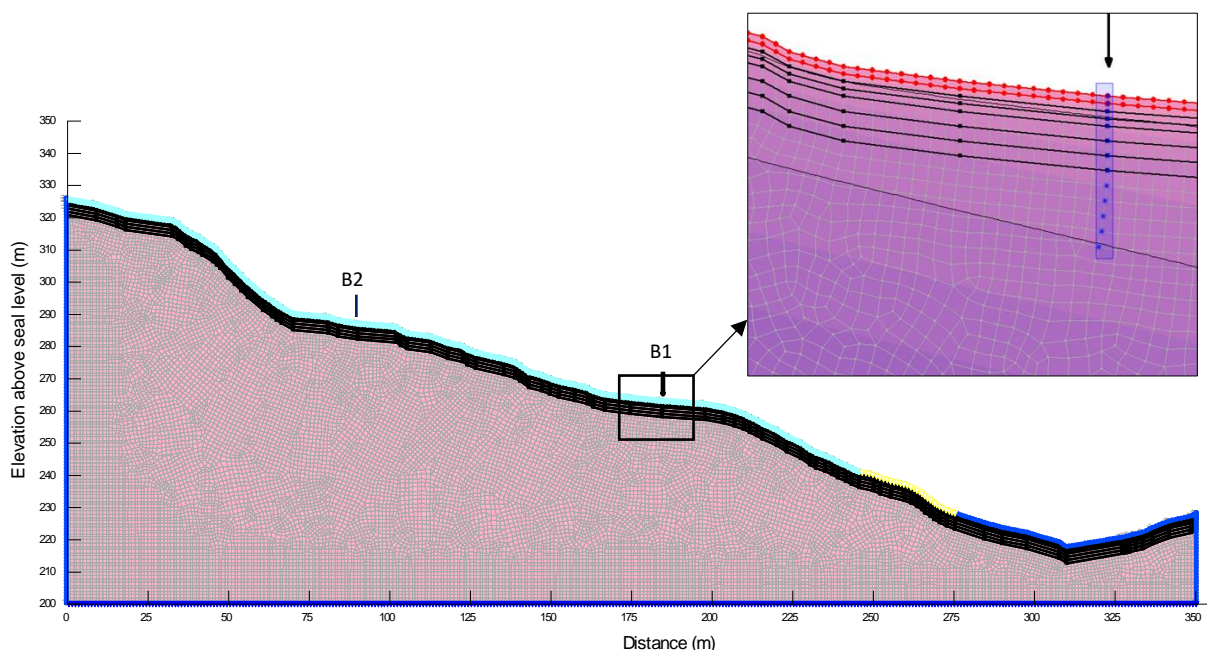


**Figure 109:** Initial and boundary conditions, and discretization with mixed unstructured finite element mesh for calculation of infiltration process using SEEP/W (GEO-SLOPE International, Ltd).

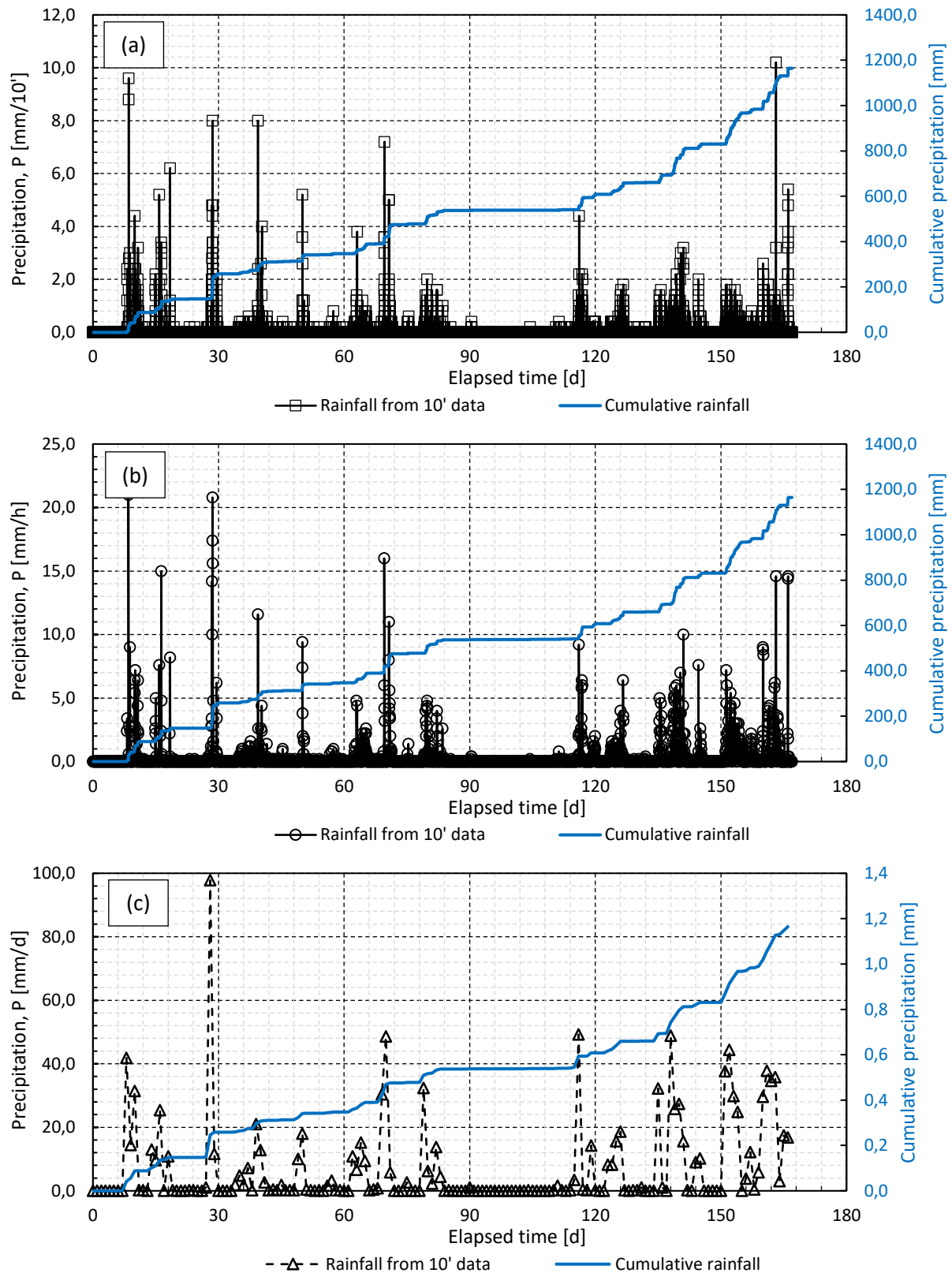


**Figure 110:** Measured and derived precipitation data used for determination of a flux boundary condition for seepage analysis in form of: a) ten-minute; b) hourly; and c) daily rainfall with cumulative amount of precipitation in the period from 1 September 2013 until landslide reactivation on 13 February 2014.

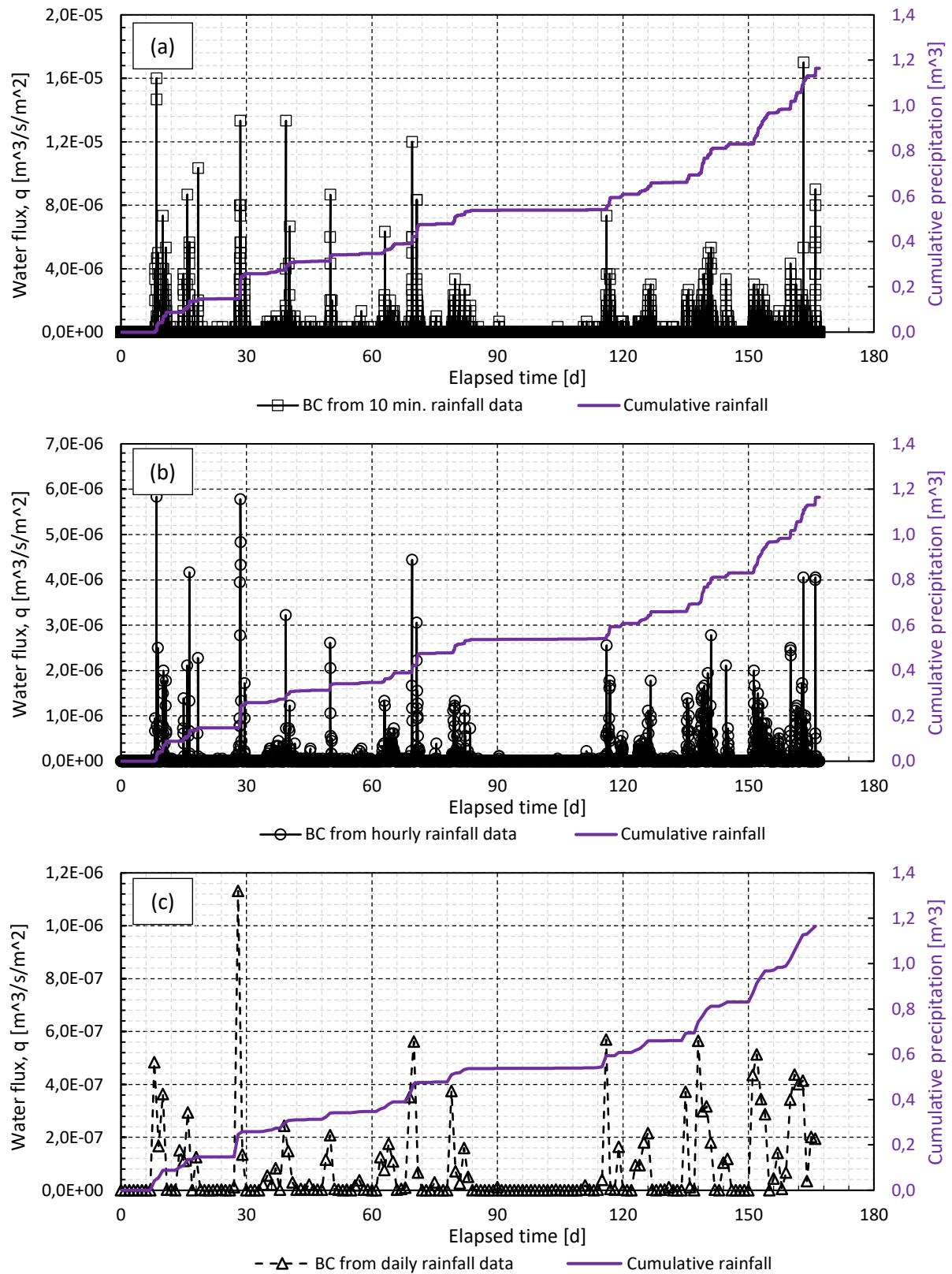


**Figure 111:** Water flux boundary condition used in infiltration analysis with SEEP/W in form of: a) ten-minute; b) hourly; and c) daily rainfall with cumulative amount of precipitation in the period from September 2013 until landslide activation, 13 February 2014.



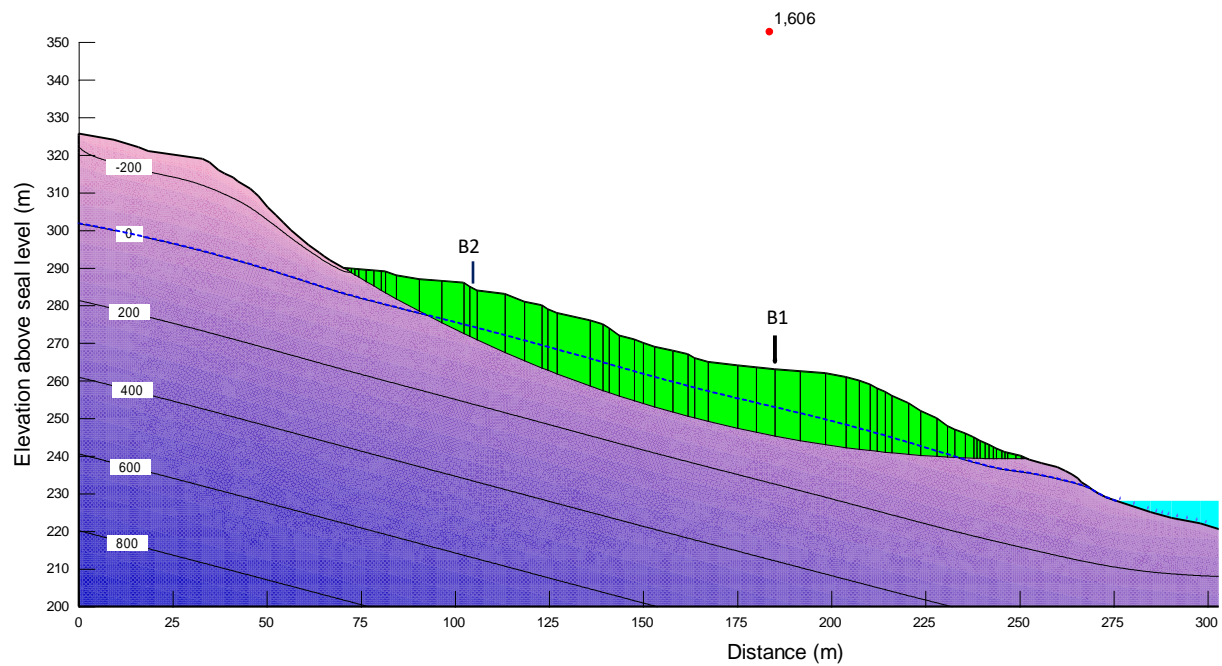


**Figure 112:** Initial pore-water pressure distribution in analyzed cross-section of geotechnical profile with imposed 300 kPa of constant matric suction in the uppermost region ( $d=0.5$  m) and the initial FoS for the relevant sliding surface.

### 7.3. Slope stability modeling

SLOPE/W is a component of the GeoStudio (GEO-SLOPE International, Ltd.) software suite, used to perform slope stability analysis of soil and rock slopes. Implementing the well-known limit equilibrium method (LEM), the software enables analyzing complex slope stability problems by choosing among numerous analysis methods, considering various shapes of slip surface, soil properties, and shear strength models, pore-water pressure and loading conditions, different reinforcement elements, etc. Being a component of the GeoStudio software suite, SLOPE/W can be used as stand-alone software, or integrated with some other GeoStudio products. For example, SEEP/W offers several ways for defining pore-water pressure distribution in order to calculate the effective stress acting on the slip surface. Piezometric line (single or multiple),  $R_u$  and B-bar coefficient approach, or spatial function of pore-water pressures head can be used for defining pore-water pressure distribution directly in SEEP/W. Otherwise, results obtained from any finite element based products available in GeoStudio can be introduced in SEEP/W (GEO-SLOPE International 2017b). Pore water pressure distribution can come from any steady-state seepage analysis or any particular time step of transient analysis performed in SEEP/W software. Generation of excess pore-water pressure due to external loadings or transient consolidation analysis results obtained in SIGMA/W, earthquake-induced inertial forces causing different excess pore-water pressures at different time steps calculated in QUAKE/W, or ground surface evaporative flux analysis performed in VADOSE/W software, can all be used as input data when defining pore-water pressures for slope stability analysis (GEO-SLOPE International 2017b). Transient pore-water pressures obtained from finite-element based software provide insight into slope stability change over time. One of the drawbacks of the LE formulation is that computed stress distribution can differ from actual stress conditions existing in-situ. More realistic stress distribution can be obtained from finite-element stress formulation in SIGMA/W, especially for the case where reinforcement elements are included, and introduced into SLOPE/W analysis for a more precise definition of stress distribution along the sliding surface as well. Various slip surface search techniques, capabilities of performing probabilistic and sensitivity analysis, reinforcement, surcharge and seismic load functionality, support for limit state design according to Eurocode and application of partial factors of safety, staged pseudo-static and rapid drawdown formulations are some of the features that SLOPE/W slope stability software offers.

### 7.3.1. Theoretical background

Stability analysis of earth structures is among the oldest types of numerical analysis performed in geotechnical engineering practice. Development of the idea that a potential sliding mass can be discretized into a certain number of slices dates back to the early 20<sup>th</sup> century when in 1916 Petterson (1955) presented stability analysis of the Stigberg Quay in Gothenburg (Sweden). This work introduced the use of circular sliding surfaces in the analysis of stability problems in clay: an approach that became very popular and widely adopted, both to geotechnical and civil engineers (Petterson 1955). In the following decades, the limit equilibrium method was developed rapidly by many researchers. For example, Fellenius (1936) divided the sliding soil mass into slices to analyze their static equilibrium by equating forces and moments to zero. Janbu (1954), Bishop (1955), Bishop and Morgenstern (1960) improved work of Fellenius by introducing more realistic assumptions. Development of the electronic computer made it possible to include noncylindrical failure surfaces and made calculation procedures that are iterative in nature easier to handle, so more rigorous mathematical formulations that include all interslice forces and satisfy both force and momentum static equations were developed by, for example, Morgenstern and Price (1965), Spencer (1967, 1973), etc. While Spencer (1967) adopted a constant relationship between the interslice shear and normal forces for all slices, which is altered through iterative procedure until a factor of safety respective to moment equilibrium and a factor of safety with respect to horizontal force equilibrium become equal, Morgenster and Price (1965) proposed a similar procedure but allowed various interslice force functions. Besides these, SLOPE/W offers calculation according to Corps of Engineers #1 and #2 methods (U.S. Army Corps of Engineers 2003), Lowe-Karafiath method (1960), Sarma method (1973) and others. The main characteristics of limit equilibrium methods that are most widely used in engineering practice for slope stability analyses are summarized in, for example, Duncan and Wright (1980) and Duncan (1996). Duncan (1996) discussed state of the art for LEMs and finite-element analysis for addressing the slope stability problems. Although the LEM has the obvious limitation that they rely purely on the principle of statics while stress-strain constitutive relationship ensuring displacement compatibility does not exist, it is still the most widely used tool for slope stability analysis in everyday engineering practice.

All of the methods that are available in SLOPE/W with an indication of satisfied static equations, characteristics, and the relationship of interslice forces are summarized in Table 20. Methods satisfying normal and shear interslice force equation usually differ in an assumption of inclination of resultant force, which can be assumed horizontal when only the normal



component of interslice force is considered, constant, variable, equal to ground surface inclination, or some other assumption is made.

**Table 20:** LEMs available in SLOPE/W with an indication of satisfied static equations and interslice force characteristics (modified form GEOSLOPE International 2017).

Method	Moment equil.	Force equil.	Interslice force	
			<u>Normal</u>	<u>Shear</u>
Ordinary (Swedish) or Fellenius	Yes	No	No	No
Bishop's Simplified	Yes	No	Yes	No
Janbu's Simplified	No	Yes	Yes	No
Spencer	Yes	Yes	Yes	Yes
Morgenstern-Price	Yes	Yes	Yes	Yes
Corps of Engineers #1 and #2	No	Yes	Yes	Yes
Lowe-Karafiath	No	Yes	Yes	Yes
Janbu Generalized	Yes	Yes	Yes	Yes
Sarma (vertical slices only)	Yes	Yes	Yes	Yes

The Morgenstern-Price and the Spencer methods are recognized as general limit equilibrium methods of slices, and the factors of safety are computed by the converging technique of the Newton-Raphson method (Furuya 2004). A general limit equilibrium (GLE) formulation was developed by Fredlund (Fredlund 1974, 1975; Fredlund and Krahn 1977; Fredlund et al. 1981) and only basic concepts of the LEM are summarized in the following part. The idea of using two factors of safety equations, one with respect to moment equilibrium ( $F_m$ ) and one with respect to force equilibrium ( $F_f$ ) was first published by Spencer (1967). The Morgenstern-Price method with half-sine interslice force function was used in stability analysis performed in this study, so this equation was used in the GLE formulation:

$$X = E\lambda f(x) \quad (88)$$

where  $f(x)$  is a interslice force function,  $\lambda$  is a percentage of the function used expressed in decimal form, while  $X$  and  $E$  are the interslice shear and normal forces (GEOSLOPE International 2017). The two above mentioned equations have the following form:

$$F_m = \frac{\sum [c' \beta R + (N - u_w \beta) R \tan \phi']}{\sum W_x - \sum N_f \pm \sum D_d} \quad (89)$$

and

$$F_f = \frac{\sum [c' \beta \cos \alpha + (N - u \beta) \tan \phi' \cos \alpha]}{\sum N \sin \alpha - \sum D \cos \omega} \quad (90)$$

where  $N$  is normal force at the slice base,  $W$  denotes weight of the slice,  $D$  is concentrated point load,  $\alpha$  is angle between the tangent to the center of the base of slice and the horizontal,  $\beta, R, x, f, d$  and  $\omega$  are geometric parameters (Fredlund and Krahn 1977; GEO-SLOPE International 2017). Vertical force equilibrium provides the normal force at the base of each slice  $N$ , one of the key variables in both equations:

$$N = \frac{W + (X_R - X_L) - \frac{(c' \beta \sin \alpha + u_w \beta \sin \alpha \tan \phi')}{F}}{\cos \alpha + \frac{\sin \alpha \tan \phi'}{F}}. \quad (91)$$

When  $N$  is substituted into the (89) equation,  $F$  becomes  $F_m$ , while  $F$  becomes  $F_f$  when  $N$  is substituted into the (90) equation. Since the normal force at the slice base depends on the interslice shear forces from both the left,  $X_L$ , and right side,  $X_R$ , different methods will provide different  $N$  values, depending on how interslice shear forces are treated (GEO-SLOPE International 2017). GLE formulation is not restricted by the slip surface shape and only one factor of safety is obtained for the entire slope.  $F_m$  and  $F_f$  are equal when both equation (89) and equation (90) are satisfied. The same value appears in the equation (91) for the normal force at slice's base. The latter can affect computed stress distribution along the slip surface (GEOSLOPE International 2017). Again, one possibility for improvement of stress calculation could be coupling stress analysis performed using the FEM, for example, rather than only static considerations from LEM.

Another essential feature affecting the FoS values in the performed analysis is dealing with matric suction. SEEP/W was used to perform transient seepage analysis for applied boundary head, and flux conditions described earlier. Irrespective of used time step or properties of the applied flux boundary condition, calculation results were saved after every 24h of transient seepage simulation. Consequently, 167 pore-water pressure distribution profiles were obtained for 167 days of numerical simulation. Transient seepage analysis performed in SEEP/W was defined as parent analysis for the slope stability calculations in SLOPE/W and the factor of safety was calculated for each simulation result. Finally, changes of FoS through 167 days were plotted to assess the influence of rainfall infiltration on slope stability in time. Initial FoS value corresponding to applied ICs and BCs defined earlier was obtained from the initial SEEP/W analysis. These results represent conditions that could have existed on 1 September 2013. Due to the desaturation of the residual soil in the near-surface zone of the cross section, negative pore water pressures were obtained above the phreatic line. Although the SLOPE/W can accommodate equally positive and negative pore water pressure

values, increase in shear strength due to matric suction is considered only if  $\phi^b$  value is specified for the material in which matric suction develops during simulation. If necessary, GeoStudio offers to set the maximum matric suction value which can occur in each type of material included in the analysis. In this way, unrealistically high matric suction values are avoided and usually the matric suction profile becomes straight line up to the soil surface if flux boundary conditions allow this type of pore-water pressure distribution.

### 7.3.2. Key-in material properties

One type of material representing the residual soil from a flysch rock mass was defined in SLOPE/W analysis. Shear strength of the material was described by using the extended Mohr-Coulomb failure criterion with  $\phi^b$  value set equal to  $\phi'$  in the preliminary analysis, or obtained from SWRC- $\theta$  or set equal to constant values of  $1/2 \phi'$  and  $2/3 \phi'$  in the following analysis. Saturated unit weight was considered in the preliminary analysis and a later option to calculate unit weight from defined SWRC- $\theta$  was used as well. Values were changed in order to assess the influence of different variables on slope stability during rainfall infiltration. The grid and radius option was used to define a slip surface in the preliminary analysis. Since the back-analysis results were similar to those obtained by shear strength reduction method (Arbanas et al. 2017) and geometry and landslide conditions corresponded to those that were observed by in-situ investigations, entry and exit option with specified radius tangent lines was used in a more advanced analysis performed subsequently.

It was found that the influence of the matric suction on shear strength has little effect on the landslide occurrence itself since the FoS approaches critical values only when matric suction is almost completely eliminated from the sliding mass. In that sense, higher starting values of FoS are obtained for higher  $\phi^b$  values, but the time required for the slope to fail remained basically unaffected by the chosen  $\phi^b$  value. The time required to reach failure was found to be affected by the initial water content of the slope (or pore-water pressure distribution), which significantly reduces infiltration capabilities of topsoil and provides greater storage for infiltrated water, delaying the time for waterfront to reach the groundwater table, when a sudden increase in pore-water pressure induces the slope failure. Material properties used in slope stability analysis are summarized in Table 21.

**Table 21:** Material properties for slope stability analysis in SLOPE/W.

Material	Unit weight, $\gamma$ [kN/m <sup>3</sup> ]	Shear strength parameters			Failure envelope
		$c'$ [kPa]	$\phi'$ [°]	$\phi^b$ [°]	
Residual soil	19*	0	29	$\phi'^{**}$	Mohr-Coulomb

\* For analysis in which impact of unit weight change due to desaturation on slope stability was analyzed, unit weight was calculated from SWRC- $\theta$ ;

\*\* For analysis in which impact of  $\phi^b$  value on slope stability was analyzed,  $\phi^b$  values were defined as constants equal to  $1/2 \phi'$ ,  $2/3 \phi'$ , or obtained from the Vanapalli (1996) estimation equation implemented in SEEP/W.

## 7.4. Results of numerical simulations

In the following part results obtained from numerical analysis are presented. First, rainfall infiltration and slope stability analysis were performed by using 10' collected rainfall data in the period from 1 September 2013 until 14 February 2014, day after the landslide event was reported. In this analysis, BC consisted of 24,047 input data of measured rainfall quantity in 10 minute periods. In order to study the influence of recording interval at which rainfall data are collected, hourly and daily rainfall measurements were derived from 10-minute measurements. In this way, the same cumulative amount of rainfall (1,164 mm) was applied through flux BCs with 4,008 and 167 input data, respectively. It was expected that, since the permeability is averaged over the time interval, with increasing time interval the infiltrated amount of rainfall should increase, apparently decreasing the amount of rainfall included in the runoff process. After this, the same type of analysis was performed by using 10 minute, hourly and daily rainfall quantities but with a different number of time steps. In this way, the influence of the employed time increment was analyzed on possible rainfall infiltration and slope stability results.

The influence of the matric suction on the shear strength was analyzed by applying different  $\phi^b$  values. It was expected that this value should only control the absolute FoS value, while the time required to reach the instability conditions would be controlled rather by retention and permeability features of the soil. Finally, to investigate the possible influence of the soil weight change in the near-surface zone, SWRC was used to calculate the unit weight through time, instead of using constant (saturated) value.

In the following type of numerical analysis, the artificial rainfall was created and applied as a flux boundary condition to assess the influence on slope stability in time with respect to actually measured quantities. Recorded quantities of rainfall were simply multiplied with  $n = 0.5, 2, 4, 8$ , and  $16$ , and were applied as a flux BC. In this case, the rainfall pattern remained unchanged while the rainfall intensities were altered to produce cumulative rainfall amounts equal to  $582.2, 2,328.8, 4,657.6$ , and  $9,315.2$  mm over a period of 167 days.

Another type of analysis was performed for the same initial and boundary conditions, but constant flux boundary condition applied at the soil surface. Instead of using real rainfall measurements, the last numerical analysis was performed by applying constant flux BC equal to  $q = n * k_s$ , with  $n = 0.5, 0.75, 1, 2, 4, 8$ , and  $16$ . Change of slope stability with time was analyzed by plotting the FoS value vs. elapsed time. Results show that there is a critical value of rainfall intensity, above which the time required for the slope to fail remains unchanged.

Finally, to account for various antecedent rainfall or evaporation conditions that could result in different initial pore-water pressure distributions and moisture contents along the geotechnical cross-section, various values of the matric suction were applied in the first 0.5 m of the slope. Starting values of 100, 200 and 400 kPa were considered. Results showed that higher matric suction in the soil profile results in higher starting FoS value due to the increase of shear strength component associated with it, while lower initial water content resulted with reduced hydraulic permeability and larger storage capacity, finally leading to a reduction of slope stability at a lower rate and vice versa.

Figure 113 a) shows an initial degree of saturation along the profile B1 (indicated in Figure 112) and its change over a period of 167 days of simulation for applied 10' recorded rainfall. Figure 113 b) shows calculated pore-water pressure distributions for the relevant time steps. Pore-water pressure distributions along the cross-section of the landslide and the corresponding FoS value for considered slip surface for the 110<sup>th</sup>, 140<sup>th</sup> and 160<sup>th</sup> day of the simulation are shown in Figure 114 a), b), and c), respectively. Figure 115 shows starting a) frictional strength component and b) strength component associated with matric suction, and their decrease during the time caused by the rainfall infiltration process. Effective cohesion value was set to zero. Results indicate that frictional strength component associated with the effective stress provides stability when matric suction is eliminated from the profile cross-section, while suction strength component is high only for the initial part of the analysis corresponding to higher matric suction levels in the area of the landslides crown and toe. For high groundwater levels, it seems that all of the strength associated with the matric suction is eliminated along the failure surface and the landslide stability relies on the effective stress associated with the angle of internal friction.

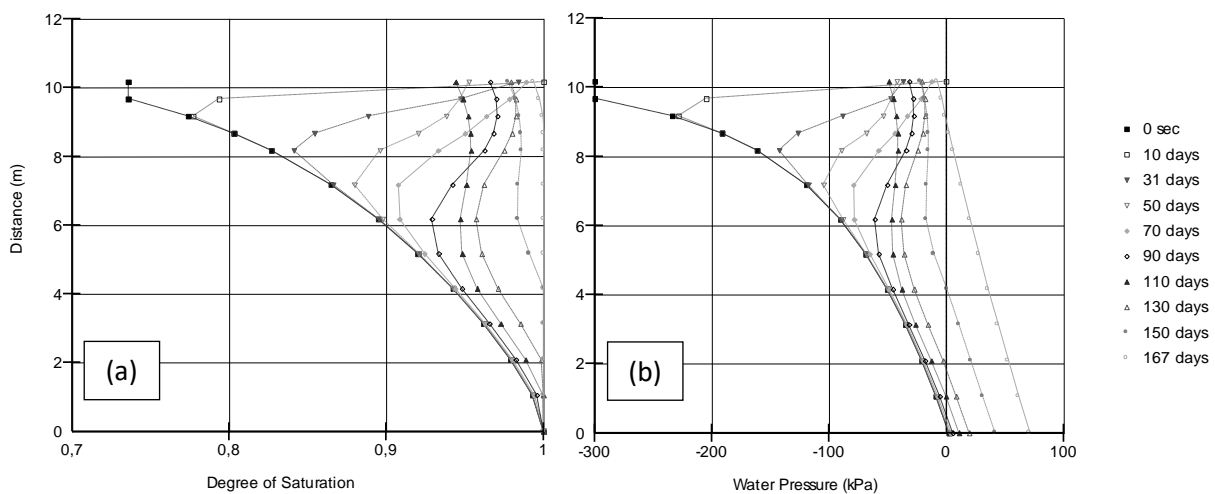


**Figure 113:** Results for initial and changing values of a) degree of saturation, and b) pore-water pressure distribution along the profile B1 during 167 days of simulation.

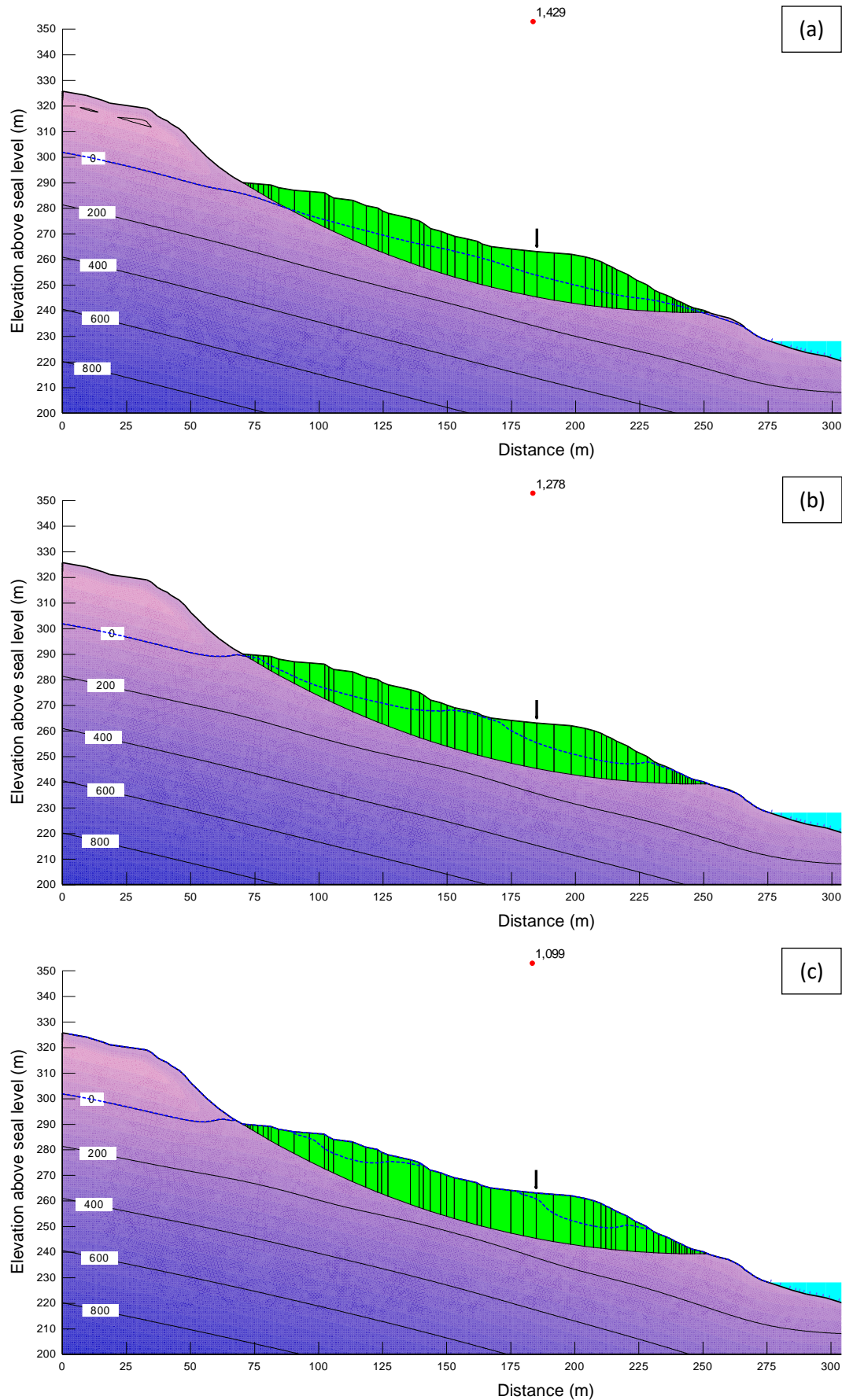


**Figure 114:** Pore-water pressure distributions along the cross-section of the landslide and the corresponding FoS value after a) 110; b) 140; and c) 160 days of simulation.

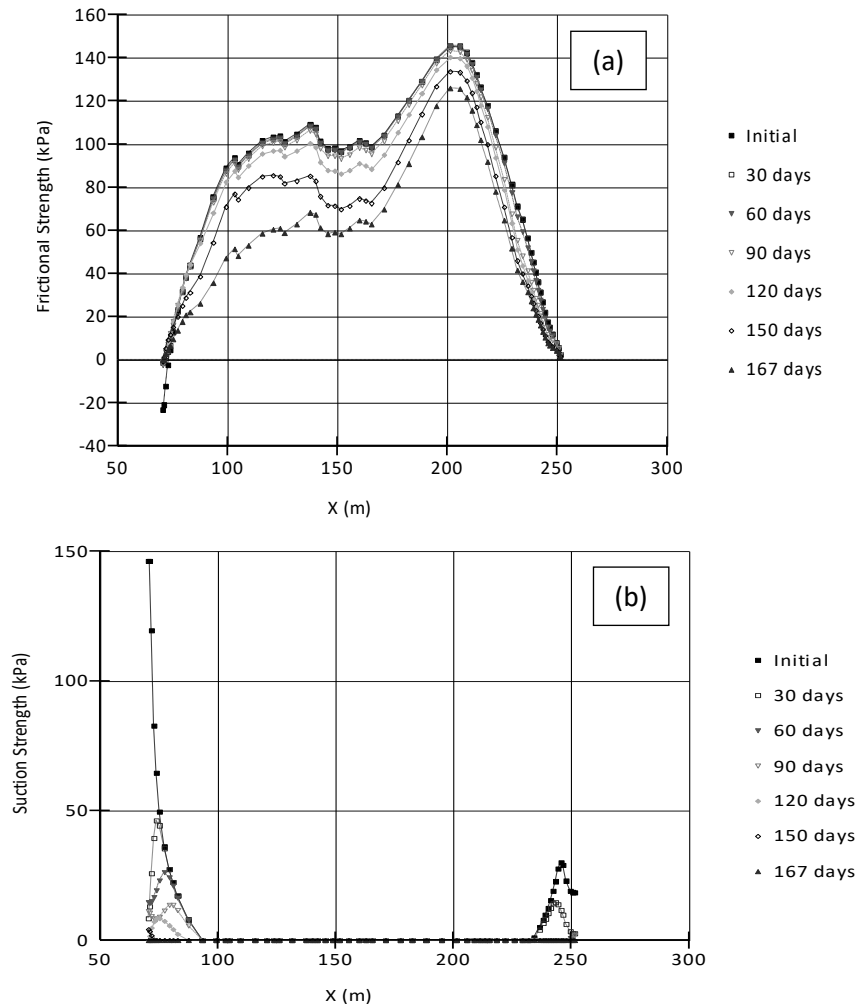


**Figure 115:** Change of shear strength components along the sliding surface due to rainfall infiltration. Starting values and decrease of a) frictional and b) strength component associated with matric suction.

#### 7.4.1. Influence of the rainfall input data (10', 1h and daily rainfall)

Figure 116 presents the results obtained for 10' input rainfall data and derived hourly and daily quantities. In the case of flux BC with 10' data, the time increment was set to 10 minutes. In two other cases, time intervals of 1 hour and 1 day were used, respectively. Results show that in the case when daily rainfall data is used to define flux BC, averaging permeability and rainfall data on a daily base result in a reduction of FoS at a much higher rate. With the time required for the slope to fail equal to 167 and 164 days, there is no significant difference when 10' or hourly rainfall is used. On the other hand, only 142 days are required to reach the failure if daily rainfall is used. The obtained results indicate that, for analyzing the rainfall infiltration into the slope of low permeability, input boundary conditions representing the rainfall should be defined from high-resolution measurements. Although 10' measurement interval presumably provides the most realistic input data, respective to computational requirements and the accuracy of obtained results when compare to those obtained from 10' input data, hourly measurements have proven to be the optimum form of input data.

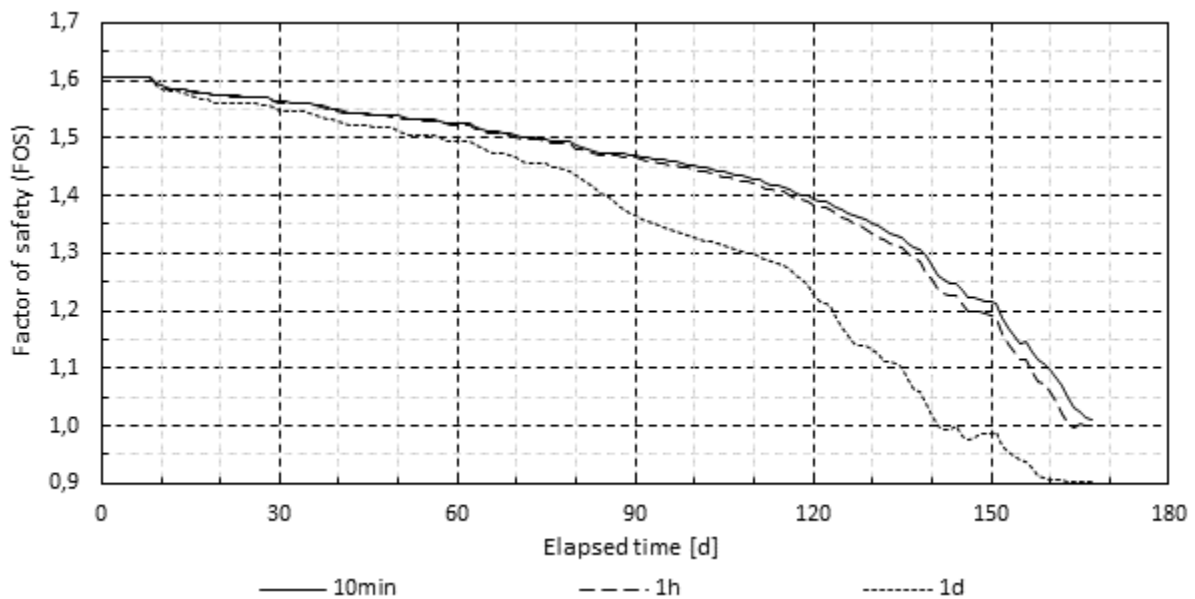


**Figure 116:** Factor of safety vs. time for constant (saturated) unit weight and unit weight calculated from the SWRC- $\theta$ .

#### 7.4.2. Influence of material properties: shear strength and unit weight

Results shown in Figure 117 show that adopted  $\phi^b$  value has little influence on the absolute value of the calculated FoS in the initial part of the analysis when a substantial portion of the



sliding mass above the groundwater level has higher matric suction values. However, in the latter part (i.e., after 80 days of simulation) due to the gradual elimination of the matric suction in the cross-section, the effect becomes negligible and results become basically independent of the chosen expression for quantification of  $\phi^b$  value. With time rainfall infiltration saturates the sliding mass above the phreatic line, reducing the matric suction and, thus, eliminating the shear strength component associated with it.

Since only a small portion of the slope is unsaturated, change of unit weight during the rainfall infiltration has even less influence on calculation results, as summarized in Figure 118.

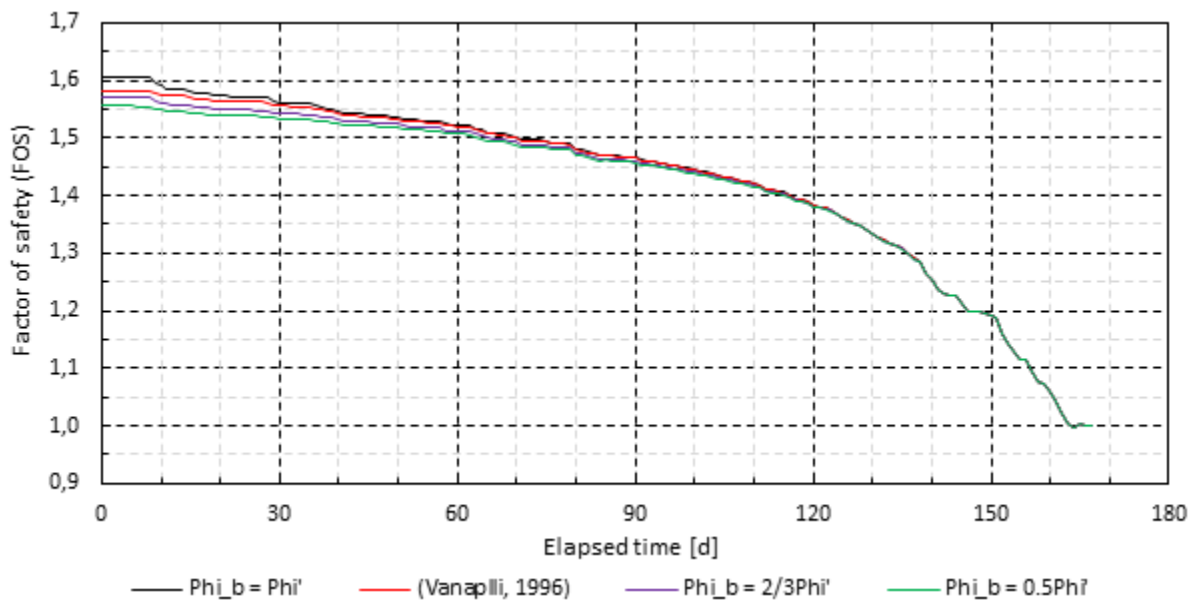


**Figure 117:** Factor of safety vs. time for different  $\phi^b$  values.

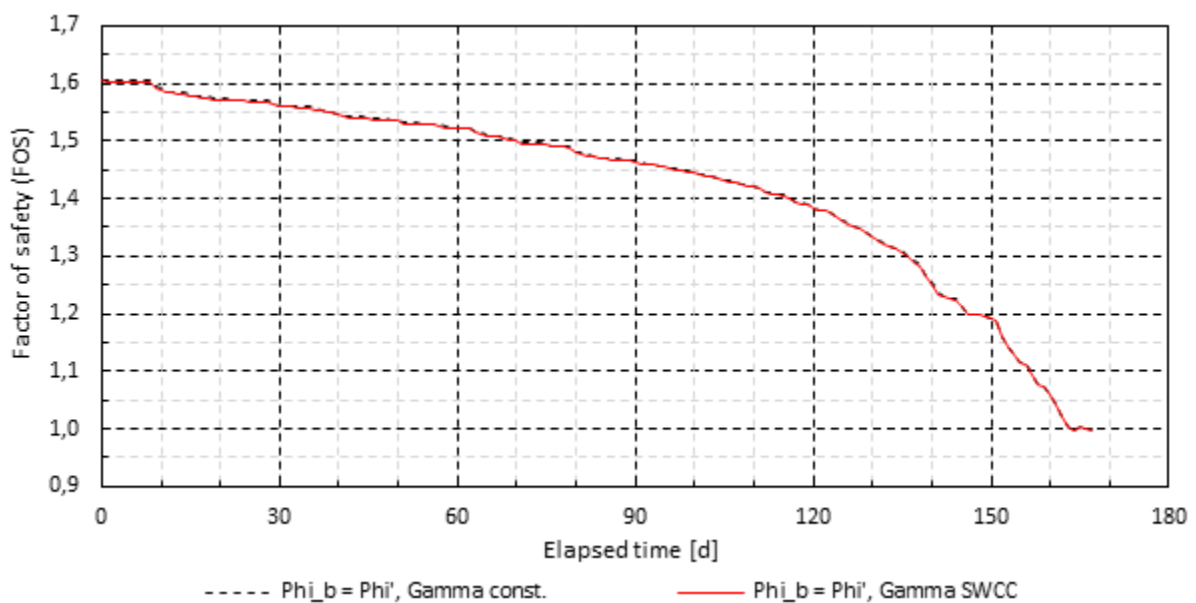


**Figure 118:** Factor of safety vs. time for a constant (saturated) unit weight and unit weight calculated from the SWRC- $\theta$  with  $\phi^b = \phi'$ .

### 7.4.3. Artificial rainfall data: influence of the rainfall intensity

Figure 119 shows results of the numerical analysis performed for measured 10' precipitation data applied as a flux boundary condition and artificially generated BC where recorded quantities were multiplied with  $n=0.5, 0.75, 2, 4, 8, 16$  and  $32$ . Results show that if half of the measured precipitation is applied as the flux BC, the slope remains stable after 167 days of simulation, however, with FoS value being reduced to only 1.1. On the other hand, 154 and 151 days are required for the slope to fail when measured quantities are doubled or multiplied with  $n=4$ , respectively. FoS drops below unity after 145 days of simulation for  $n=8$ , and 141 day is required for the slope to become unstable when  $n$  becomes equal to or higher than 16.

The same conclusion is obtained if the artificial rainfall is generated from hourly measurements, with the only difference being that time required for the slope to fail is somewhat shorter due to averaging of the permeability of the soil. In that case, the time to failure is equal to 164, 156, 145, 140 days for  $n = 1, 2, 4$ , and  $8$ , while 137 days are required when  $n \geq 16$ .

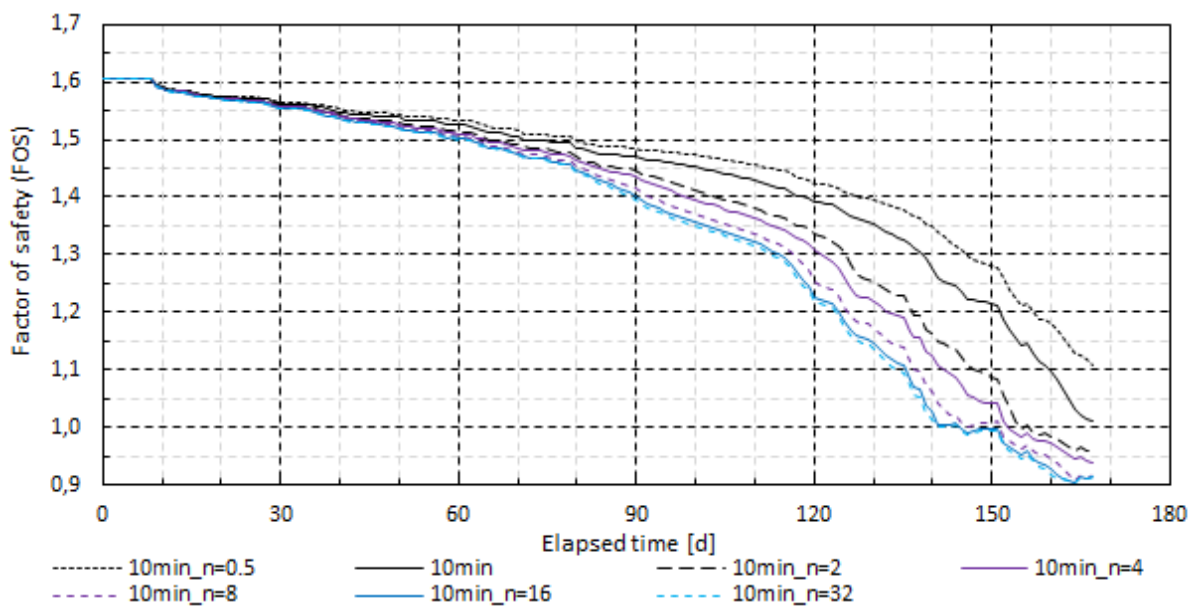
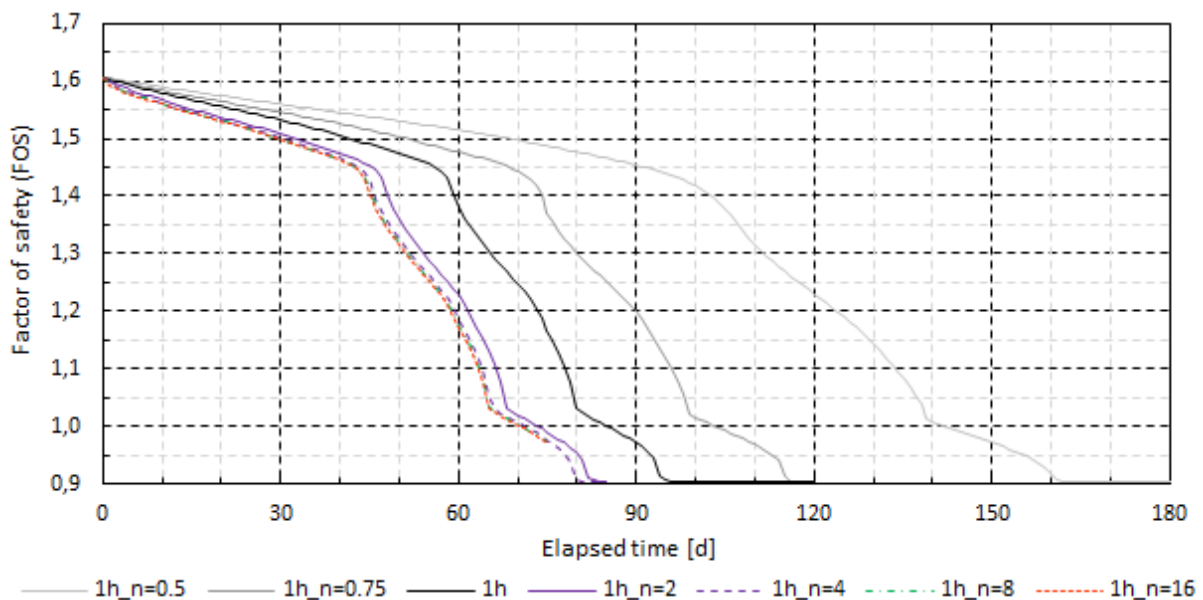


**Figure 119:** Change of slope stability with time for measured 10' precipitation data applied as a flux boundary condition and artificially generated precipitation data with the same pattern as recorded precipitation and flux quantities equal to  $q = q_{measured} * n$ , with  $n = 0.5, 0.75, 2, 4, 8, 16$  and  $32$ .

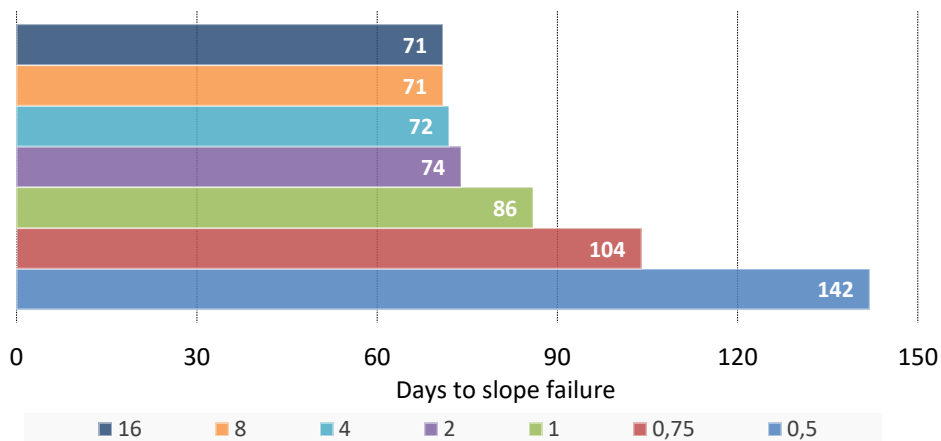
### 7.4.4. Results for different values of constant flux boundary conditions

Figure 120 shows the results of analysis with applied constant flux BC with  $q = n * k_s$ , with  $n = 0.5, 0.75, 1, 2, 4, 8$ , and  $16$ . Translated to rainfall intensity, saturated coefficient of hydraulic permeability  $k_s = 4.6E-08$  m/s corresponds to 0.17 mm/h or 3.97 mm/d. The obtained

results show that the time required for slope failure only slightly changes if the rainfall intensity is higher than  $2k_s$ , which corresponds to 0.33 mm/h or 7.95 mm/d, while intensities higher than  $4k_s$ , which correspond to 0.66 mm/h or 15.9 mm/d, practically do not affect the rate at which FoS reduces. For a large number of simple rainfall measuring devices, such as tipping bucket rain gauge, 0.5 mm is usually the minimum quantity of rain required for tip generation. The obtained data confirm that long duration of rainfall is a crucial factor for landslide triggering in flysch slopes. On the other hand, high precipitation intensities cause excessive runoff, while the high quantity of precipitation has only a minor influence on slope stability through time. Same results are shown regarding the number of days required for the slope to become unstable in Figure 121.



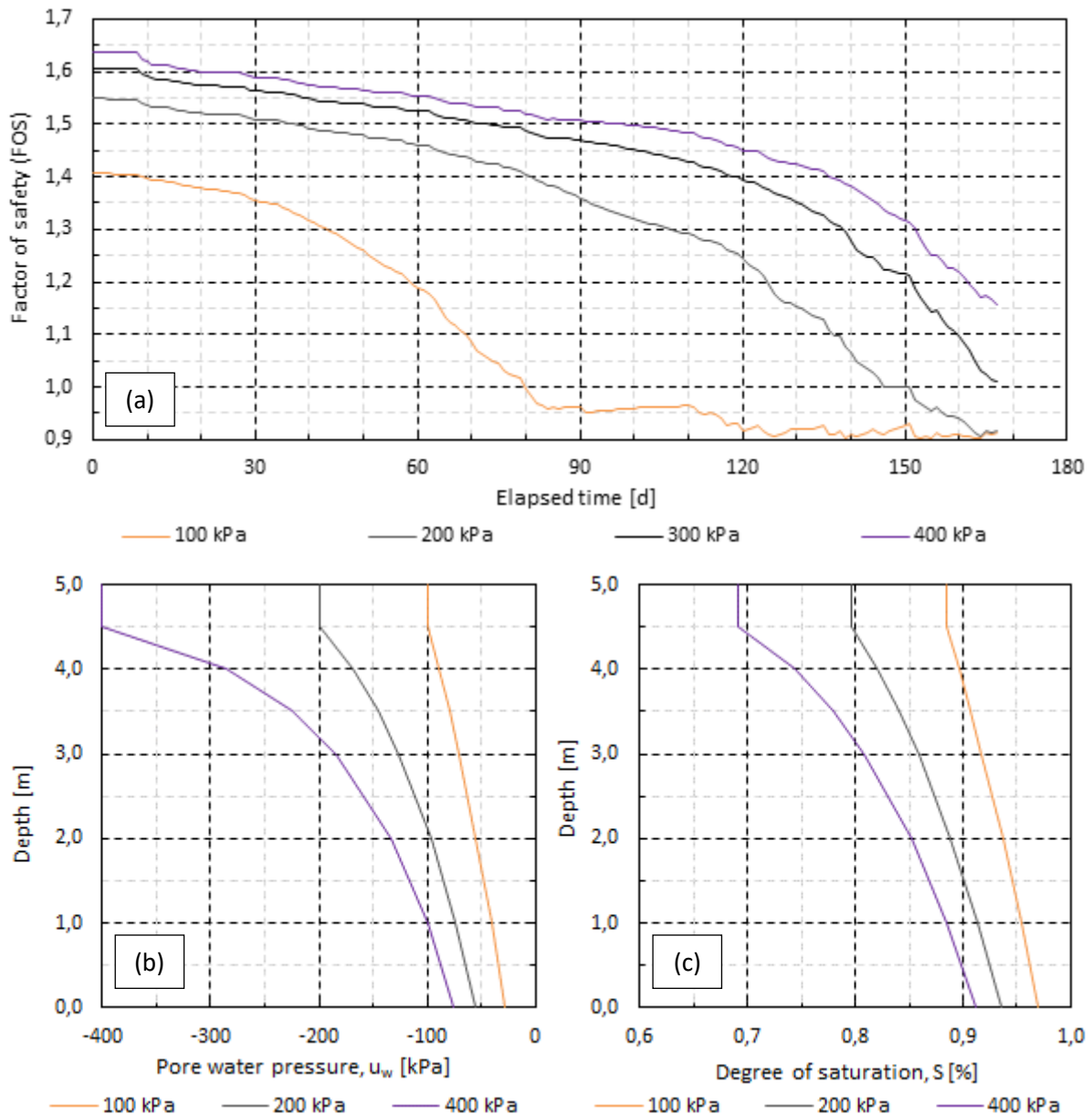
**Figure 120:** Factor of safety vs. time for constant flux boundary condition equal to  $q = n * k_s$ , with  $n = 0.5, 0.75, 1, 2, 4, 8$ , and  $16$ .



**Figure 121:** Number of days required for the slope to become unstable for different constant flux boundary conditions  $q = n * k_s$ , with  $n = 0.5, 0.75, 1, 2, 4, 8$ , and  $16$ .

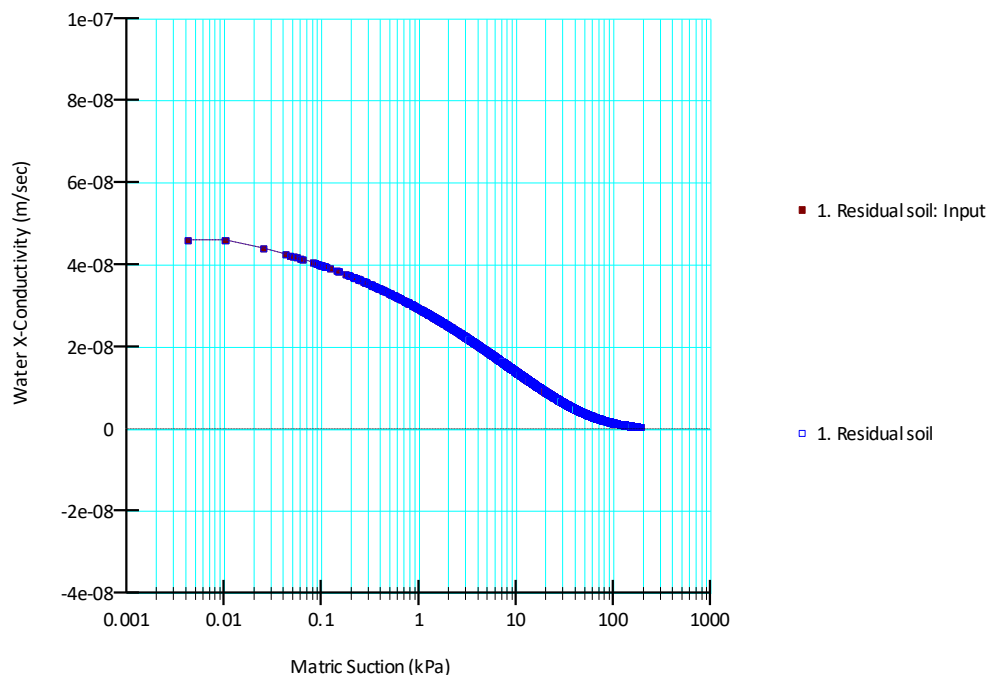
#### 7.4.5. Results for different initial pore-water pressure distributions

Figure 122 shows results for simulations performed with different initial pore-water pressure distributions obtained by applying constant matric suction values equal to 100, 200, 300 and 400 kPa in the uppermost region. For 10' rainfall data used to define flux BC, time required for slope to fail increased from 81 days in case of 100 kPa of imposed matric suction value, up to 147 and 167 days in case of imposed matric suction values of 200 and 300 kPa, respectively. In case of 400 kPa, the slope remained stable after 167 days of simulation ( $FoS=1.16$ ). The obtained results indicated the importance of the initial pore-water pressure conditions.



**Figure 122:** Influence of different initial pore-water pressure distributions obtained for applied matric suction values of 100, 200 and 400 kPa in the uppermost region ( $d=0.5$  m): a) change of slope stability with time; b) initial pore-water pressure profile; and c) initial degree of saturation along first 5 m of depth.

Convergence for each time step was checked by plotting the calculated permeability along with the input UHCF. Larger discrepancies between the two would indicate possible calculation errors. For initial matric suction value of 300 kPa applied in the uppermost region of the slope, 24,048 calculation steps to simulate 167 days of rainfall infiltration, and ten-minute time increment (0.0069439 days), conductivity vs. matric suction plot shown in Figure 123 suggests the convergence criteria was met for all of the calculated time steps. Calculated results were saved after every 24 hours of simulation (144 steps).



**Figure 123:** Review of the convergence conditions by plotting the input UHCF and calculated permeability values for each time step of a transient simulation.

## **8. DISCUSSION AND CONCLUSION**

This chapter concludes the thesis by stating the most important findings and scientific contributions. Suggestions for possible further research are provided.

To test a stated hypotheses, research included field investigations and surveys, laboratory testing and measurements, and numerical modeling. Since the behavior of the residual soil from a flysch rock mass from the Rječina River Valley was never investigated under negative pore-water pressure conditions, or generally in terms of the unsaturated soil mechanics, one of the aims of this study was the determination of the unsaturated soil property functions (USPFs): soil-water retention curves, permeability functions, and unsaturated shear strength. Although it required a significant effort, determination of the USPFs was an essential objective, since it provided necessary input data for performing the rainfall infiltration and slope stability analysis. Previous observations and experiences have already indicated that the crucial part for the landslide triggering in the investigated area is long-lasting precipitation. However, results presented in this study made it possible to quantitatively examine the triggering of rainfall-induced landslides in flysch deposits considering, for the first time, the transient rainfall infiltration process through the unsaturated zone of a geotechnical cross-section, and all of the effects on the slope stability state that it causes over time. Determination of the UHCFs ensured achieving the second aim of the study, as well: to perform the analysis which determined the influence of the geotechnical cross-section unsaturated zone and rainfall characteristics on the landslide triggering.

Laboratory tests conducted to determine the basic soil properties showed that the superficial slope deposits mainly consist of fine-grained material with silty particles prevailing in all of the tested samples. Similar granulometric composition and Atterberg's limits (see Figure 5 and Figure 6) of the material present at the landslide body surface indicate presumably similar water retention and conductivity features. Unlike in the case of completely remolded and consolidated samples prepared in laboratory conditions, undisturbed samples used in successive tests for different purposes are characterized by high heterogeneity on the macroscale. Heterogeneity arises from the presence of macroscale voids caused by the biological activity of worms and roots in soil close to the surface or arises from the presence of siltstone grains that vary in size and weathering degrees (for example, see Figure 3 b) and Figure 7). Such heterogeneity can create difficulties when performing laboratory tests on small specimens and cause inconsistencies in the obtained results. However, in the sense of the granulometric composition and plasticity limits, the material located near the ground surface seems to be very homogeneous. Granulometric composition and plasticity limits have shown to reflect water retention capabilities and hydraulic conductivity features of a material. Therefore, the identification test results indicated that the superficial residual soil should have similar USPFs.

Similar results obtained from the grain size distribution tests performed on samples collected from different parts of the landslide surface indicate similar conditions in material origin due to the weathering process of the bedrock siltstone, as well. The only sample with a slightly higher content of sand particles (28.2%) was sample no. 10, collected below the landslide toe. Samples collected from the central part of the landslide body (points 2, 8 and 9 in Figure 4) had the greatest quantity of particles larger than 2 mm, with the highest content obtained for the sample collected at the location no. 9 (9.5% by weight). Overall, tested samples consisted of 53 % of silt particles and around 30 % of clay particles (Table 1). According to determined Atterberg's limits, most of the materials could be classified as lean clay (CL). Only samples collected at locations no. 8 and 10 are plotted beneath the A-line in the plasticity chart. Again, the clustering of obtained results in the plasticity chart indicated uniform material properties of the near-surface soil along the landslide body.

The soil-water retention curves (SWRCs) of residual soil formed by the weathering process of a flysch rock mass have been determined. A wide range of pore sizes present in the material results in gentle slopes of the SWRC covering a wide range of suctions. As a result, a total of six different devices and two measurement techniques were used to perform measurements on the undisturbed samples in all three characteristic SWRC zones. The measurements performed on air-dried specimens indicated suction values higher than 90 MPa for undisturbed and 175 MPa for remolded specimens. The AEV of 210 kPa and the AExV of 56 kPa were determined for the drying and wetting paths respectively with the pore-size distribution index value of 0.26, which seems to be unaffected by the ongoing process type. The results obtained from remolded specimens undergoing desorption process show higher AEV (450 kPa) and higher desaturation rate ( $\lambda = 0.33$ ). The water retention characteristics were determined using undisturbed specimens undergoing drying and wetting processes, under varying vertical stress values, and starting from different water contents. Due to the observed volumetric changes caused by the suction variation, all the tests were performed in a way that allowed both the total volume and water volume to be measured. The effects of the overburden pressure on the soil-water characteristics were analyzed using the suction-controlled oedometers for the drying and wetting process. The density measurements collected by using the wax dipping and water displacement technique and standard null-type pressure plate devices provided the SWRC- $\theta$  measurements for the undisturbed specimens for up to 700 kPa of matric suction. The density measurements combined with the WP4-T device provided the water retention characteristics of the undisturbed specimens undergoing the drying or wetting processes for suction values lower than 1 MPa and higher than 175 MPa. The obtained results



showed a agreement with the measurements performed by using the axis translation technique for suction values as low as 300 kPa, suggesting that the use of undisturbed samples should be preferred in this case. The measurements performed with the WP4-T device from the remolded specimens converge with the measurements obtained from the undisturbed specimens at suction values higher than 1 MPa during the drying process and 6 MPa during the wetting process, indicating the range where soil structure possibly affects the retention properties of soil. A non-linear regression analysis was performed on the results obtained during the drying and wetting processes to obtain the best-fit equation and parameters of three of the most commonly used SWRC equations: Brooks and Corey (1964), van Genuchten (1980) and Fredlund and Xing (1994). Volume changes measured in SWRC tests and conventional oedometer tests results were used to assess the influence of soil suction on the effective stress. The Khalili and Khabbaz (1998) effective stress parameter seems to reasonably predict the effective stress for suctions up to 8,000 kPa. Using the constant value of the fitting parameter (-0.55) seems to overestimate the increase in effective stress due to the increase in soil suction for soil suction values higher than 8 MPa. A different pattern of behavior was obtained for undisturbed and remolded samples. Remolded samples behaved as a normally consolidated from the beginning of the drying process, undergoing a large volume deformations (for example, see Figure 37). However, in the case of the wetting path, both the undisturbed and remolded specimens act as over-consolidated material. Mechanical properties of the investigated soil are such that a large portion of deformation is irretrievable, causing relatively small swelling effects during the wetting process (Figure 36). Air-dried undisturbed specimen OEUV CJ03 manifested over-consolidated behavior due to exposure to high matric suction values, both during the wetting and drying path. Undisturbed specimens starting from the natural water content follow the similar pattern of behavior when exposed to the drying and wetting cycle. First, samples behaved as over-consolidated material following the slope of the swelling curve. Then, when soil suction was increased up to certain value, normally-consolidated behavior was observed with the further increase of matric suction, following the slope of the virgin compression line. Finally, during the decrease of matric suction, the slope of the swelling curve is followed during the wetting path. According to the above observations, it can be concluded that, if the overburden pressure could be estimated, the effective stress value at the inflection point along the drying path indicates the maximum matric suction to which the sample was exposed in its history. For that purpose, high-quality undisturbed samples should be used. The correlation model proposed by Zapata (1999) performed surprisingly well, both for the drying and wetting process, while the model proposed by Perera et al. (2005) failed to predict obtained SWRC

accurately. However, the latter model was found to perform much better when the percentage of clay particles was used instead of  $P_{200}$  value. Finally, comparing to average features of different soil texture groups, it is clear that the complex origin process generates interesting hydro-mechanical features of the investigated material, where the saturated and residual water contents are characteristic for silts, and retention parameters regarding desaturation rate and the AEV are commonly measured for silty clay and clay loam textures. On the other hand, determined shear strength parameters are commonly obtained for soil with much coarser grains.

The saturated coefficient of permeability was measured with constant (triaxial cell) and falling (oedometer) head methods on undisturbed and completely remolded and consolidated samples. The obtained results were combined with the determined SWRC to predict the unsaturated hydraulic conductivity function (UHCF). The results obtained with the HYPROP device on undisturbed samples starting from different initial water contents were used to calculate the hydraulic permeability under increasing matric suction values. The obtained results (Figure 48 and Figure 49) showed that for the same value of effective stress or void ratio, the saturated permeability of completely disturbed samples is around two orders of magnitude lower than of undisturbed specimens ( $k_s = 4.6\text{E-}08$  m/s). According to this and findings from SWRC measurements, it can be concluded that hydraulic properties of residual soil from a flysch rock mass should be determined on undisturbed samples since the soil structure and history significantly affect the hydro-mechanical properties of the investigated soil. UHCF calculated from the results obtained with the HYPROP device according to the Darcy-Buckingham law (Figure 50) showed that the specimen installed at the natural water content, although it had the highest void ratio among tested samples, had the lowest hydraulic permeability due to a lower degree of saturation value, relative to initially saturated samples (Table 9). It is interesting that measured suction values with mini-tensiometers in HYPROP device were not high: for the obtained degree of saturation, it would be expected to measure higher matric suction values that would cause instant cavitation of tensiometers. It seems that lower value of the measured degree of saturation exists due to the presence of larger voids in a complex specimen matrix, resulting with relatively low average values of matric suction since high matric suction values could not exist in pores with a large diameter. On the other hand, the presence of air in large pores would decrease permeability respective to the water phase on a specimen scale.

According to the test results obtained with conventional direct shear test apparatus in saturated conditions, shear strength characteristics seem not to be affected by specimen preparation technique and disturbance effects to such an extent as it is the case for the hydraulic

features (Figure 71 and Figure 72). For considered stress range, the results obtained on undisturbed specimens always plotted slightly higher than those obtained for remolded specimens, resulting with a slightly higher value of the effective angle of internal friction  $31.7^\circ$  vs.  $28.6^\circ$ , and low effective cohesion values of 5.1 and 5.8 kPa, respectively. The influence of the disturbance on shear stiffness seems to be negligible (Figure 71). Shear strength test results obtained on undisturbed samples with modified, axis-translation based direct shear apparatuses, reveal that matric suction affects both the shear strength and stiffness characteristics of the investigated soil. Although the obtained results were not always perfectly consistent, which might be due to the use of various testing devices, sample heterogeneity, and hysteresis effects caused by different saturation conditions, some general conclusions could be drawn. In all tests, the increase of matric suction resulted with an increase of the shear strength and stiffness of tested specimens during the shearing. Compressive behavior during the shearing in saturated conditions changed to dilative as the matric suction was increased during shear. On the other hand, as the matric suction value increased, so did the rate at which water drains out from the specimen. Consequently, the degree of saturation decreases during the shear as the matric suction is increased at increasing rate due to, both, dilation effects and water outflow from the specimen. Compression and flow of water inside the specimen during the shear at low suction values resulted in an increased value of the degree of saturation. The threshold matric suction value separating the two patterns of behavior was determined to be around 36 and 72 kPa (e.g., see Figure 89, Figure 90, and Figure 91) and was found to increase with the increase of the net vertical stress value applied during the shear stage. Since the AEV generally increases with the increase of net vertical stress, which reduces the void ratio of the tested specimen, the obtained results provide insight into the interconnection between the SWRC and behavior of fine-grained soil during the shear in unsaturated conditions. By plotting the obtained results in two planes of the extended Mohr-Coulomb's failure envelope, it was found that for matric suction values up to around 75 kPa, the angle of internal friction related to the matric suction,  $\phi^b$ , is close to or equal to the value of the effective friction angle  $\phi^b \approx \phi'$  (approximately  $30^\circ$ ). Then, there is a narrow range of matric suction for which the relationship  $\phi^b$  vs.  $\phi'$  is non-linear, following by a sharp reduction of  $\phi^b$  value. As the matric suction is increased above 100 kPa,  $\phi^b$  value was found to be equal to a constant value of approximately  $1/3 \phi'$  ( $9^\circ$ ) (Figure 94 a). It can be concluded that the obtained results confirmed observations from Sheng et al. (2011) that further investigation of the unsaturated shear strength properties should be performed on undisturbed samples collected in-situ, rather than in laboratory produced conditions. The obtained results

depart to a certain extent from the behavior patterns described in the literature, obtained mostly on slurry samples prepared and consolidated in the laboratory. According to the SWRC measurements, the increase of shear strength due to the increase of matric suction should be extended to higher matric suction values. The unsaturated shear strength tests indicate that the matric suction value at which the relationship between  $\phi^b$  vs.  $\phi'$  becomes nonlinear is much lower than the AEV of soil determined from the SWRC tests, and is closer to the AExV. The results provide a motivation to further explore the hysteresis effects on shear strength properties of undisturbed samples. Although the disturbance effects did not affect shear strength characteristics significantly in case of the tests in saturated conditions, the same may not be true for the unsaturated conditions.

The experimentally obtained shear strength results enabled determination of suction-stress values according to the outlined procedure. The latter was used to verify the closed-form suction stress characteristic curve equation predicted by the expression (68). Agreement between experimentally obtained and predicted suction stress values was obtained, indicating that the investigated soil fits in the suction-stress concept reasonably well. However, Bishop's formulation for the effective stress was found to fit results obtained on undisturbed samples in saturated and unsaturated conditions, both for tests with control of matric suction performed at a constant shear rate, and stress-controlled wetting tests equally well. The reason for this are specific retention properties of the investigated soil. Obtained SWRCs showed that residual conditions could not be distinguished but, rather, water content was found to always decrease as the matric suction is increased, even for the high-suction range. Thus, there is practically no difference between Bishop's effective stress parameter (degree of saturation), and the effective degree of saturation (9) which normalizes the degree of saturation between saturated and residual conditions. Wetting tests performed on specimens collected during the dry summer period, starting from natural water content, showed that the gradual decrease of matric suction under imposed normal and shear stress conditions leads to an increase in water content and can lead to a failure of tested specimens. Strength and stiffness were reduced due to a decrease of matric suction. At some point, the acceleration of shear displacement was observed, which was considered as an indication of failure. However, if the matric suction was increased, such as was the case for the UVSCDS12 test, equilibrium conditions were restored, and the yielding was stopped. Again, a further decrease of matric suction resulted in yielding of tested specimen and accumulation of horizontal deformations. Although the defined SWRC was obtained without application of shear stress, initial and final water contents measured in wetting tests fell exactly on the main wetting branch (Figure 105). Imposed matric suction values and calculated

degree of saturation were used to define stress path in terms of Bishop's effective stress formulation. Since it took approximately one month for conduction of each test, only two wetting tests were performed in this study. Nevertheless, from the stress paths shown in Figure 104, it can be concluded that the failure envelope defined in terms of Bishop's effective stress formulation was able to predict failure under the wetting conditions accurately. Matric suction values higher than 350 kPa were measured on undisturbed samples that were collected during the dry summer period and installed at natural water content (e.g., see Table 16 and tests UVSCDS04, UVSCDS11, and UVSCDS12).

Climate conditions relevant to the investigation area were presented. According to field investigations, natural water content determination and measurement of matric suction for natural water content, it was found that the interaction between the soil and atmosphere at the investigation site, or more precisely reduced amount of rainfall, increased evaporation or evapotranspiration along with hydro-mechanical features of the material are such that can cause a significant desaturation of the uppermost material covering the landslide body up to several meters of depth. During the dry summer periods, the degree of saturation as low as 50% was measured on several occasions (Table 2) while the high-intensity short-term rainfall during September and October 2017 were able to significantly increase water content only in the very-top material, while the degree of saturation remained practically unchanged after approximately 1 m of depth. Determination of the natural water content during machine borehole drilling at sampling pit location (borehole B1) was performed during May 2018. Again, the superficial material was not completely saturated up to the depth of 2.5 m (Table 3). At the same time, axis-translation laboratory tests for determination of SWRC performed on undisturbed samples undergoing wetting process showed that, even when matric suction was reduced to 0 kPa (pore air pressure equal to the atmospheric pressure), tested specimens did not achieve fully-saturated conditions. Instead, depending on various conditions such as initial moisture content, applied stress etc., the degree of saturation remained in a range from 80% to 95%, (Figure 34). At the same time, hydraulic permeability measurements performed with the HYPROP device starting from different initial water content conditions, and obtained UHCF which was determined by combining the saturated coefficient of permeability and SWRC, reveal that even slight reduction in degree of saturation can cause a decrease of hydraulic permeability for few orders of magnitude, respective to  $k_s$  obtained under positive pore-water pressure values and fully saturated conditions (Figure 51). These findings should not be ignored since they indicate complex hydraulic features of the investigated material, which could have an important role in ensuring the stability of slopes built in flysch deposit under extreme precipitation conditions.

The effect seems to be two-sided. Low hydraulic conductivity ensures low rates of infiltration and results in excessive runoff during high rainfall intensities. Performed analysis shows that any rainfall intensity higher than approximately  $2k_s$ , which is equivalent to 8 mm of rain equally distributed per day, do not affect calculation outcome since these quantities cannot be infiltrated into the slope and cause an increase of water content in the slope cross-section, or elevation of the groundwater level, if the storage capacity is surpassed. On the other hand, although the degree of saturation value can be close to unity, and corresponding matric suction values very low (e.g., see DSUVCJ01 test in Figure 76) the weight of water inside soil pores is still being held by the capillary forces inside the soil and this doesn't cause a significant positive pore-water pressure increase on the sliding surface. Only after the infiltration has lasted long enough so that all of the voids above the phreatic line are filled with water and the whole sliding mass is completely saturated with the matric suction being completely eliminated from the landslide cross-section, does the weight of water column generate rapid pore-water pressure increase along the sliding surface causing the slope failure. Numerical analysis results demonstrated this type of mechanism: Figure 113 b) shows that a significant increase in groundwater level occurs at a progressive rate during the last 30 days of simulation. In the period before, large storage capacity delays build-up of positive pore-water pressure along the sliding surface. Periodical inclinometer surveys confirmed that shearing occurs at a depth of around 18 m at the B1 location. Previous slope stability analysis performed with the shear strength reduction method (Arbanas et al. 2017) and back-analysis results performed with the limit equilibrium method in this study confirmed that failure occurs when the groundwater level almost entirely reach the ground surface, with the depth of the sliding surface of 17.5 m at a relevant location. Groundwater level observations at the B2 location show that in the upper part of the landslide, the groundwater level is somewhat deeper, with a phreatic line around 8 m below the ground surface.

Numerical analysis results provided answers to some important questions regarding the rainfall-induced landslides in flysch deposits and ensured the information for the verification of research hypothesis. Simulations have confirmed that the key factor inducing slope failure is persistent rainfall. For the applied boundary conditions defined according to in-situ measurements and laboratory test results, and by using the 10 minute rainfall data collected at the investigation site during the six month period preceding the reactivation of the Valići Landslide, results showed that the slope becomes unstable after 167 days of simulation. The influence of several factors was analyzed by performed numerical analysis. At the start of the simulation, when the influence of soil desiccation during the dry summer period was simulated

by applying various initial matric suction values in the most upper region of the slope up to the depth of 0.5 m, the matric suction was found to increase the absolute FoS value by providing the increased shear strength along the shallow part of the sliding surface, where matric suction exists (Figure 113). However, matric suction is reduced and finally eliminated from the area of the landslide crown and toe (Figure 117) during the persistent rainfall infiltration process, with only a frictional component of shear strength associated with the effective stress remaining to ensure the stability of the slope. During the landslide triggering, only positive pore-water pressure exists along the entire sliding surface, and shear strength component associated with the matric suction does not affect the failure occurrence itself. However, matric suction associated with the hydraulic features of the soil, UHCF, and SWRC was found to play an important role when analyzing the rate at which FoS value is reduced during the time and how state of slope stability changes with time. For the flux BC applied in the form of ten-minute, hourly and daily rainfall, it was found that for a slope with low hydraulic permeability, the higher the resolution of the rainfall data, the results of transient rainfall infiltration analysis should be more realistic. Use of daily rainfall measurements to define flux BC and averaging of rainfall respective to hydraulic permeability, resulted in apparently higher amounts of infiltrated water and faster saturation of the sliding mass, causing the instability to occur after only 142 days of simulation (Figure 116). Although 10' measurement interval presumably provides the most realistic results, relative to computational requirements and the accuracy of obtained results when compare to those obtained from 10' input data, hourly measurements have proved to be the optimum form of input data in this case. Higher starting values of FoS are obtained for higher  $\phi^b$  values, but the time required the slope to fail remained unaffected by the chosen  $\phi^b$  (Figure 117). The same conclusion was drawn regarding the use of constant (saturated) unit weight or calculated from the SWRC- $\theta$  during the rainfall infiltration. The time required to reach failure was found to be significantly affected by the initial water content (or pore-water pressure) distribution (Figure 122). Higher matric suction values and associated lower water contents along the cross-section significantly reduce the infiltration rates in the unsaturated zone and provide greater storage capacity for the infiltrated water, thus delaying the slope failure. The initial pore-water pressure distribution and water content along the geotechnical cross-section reflect the antecedent meteorological conditions. In case of a dry period with a reduced amount of rainfall and increased evaporation, negative water flux occurs in a slope. Starting from the surface, the latter causes a non-linear increase of matric suction and reduction of water content respectively. During the wet season with abundant rainfall and negligible evaporation, a positive water flux from the soil surface causes an increase in water

content and reduction of matric suction along the cross-section. The obtained results suggest that the antecedent (rainfall) conditions, along with the rainfall duration play the crucial role in landslide occurrence in flysch deposits. Analysis of cumulative annual precipitation for the period from 1957 to 2015 shown in Chapter 2 suggests that, despite some periodic fluctuations, cumulative annual quantity remained unaltered through the entire period. On the other hand, by summarizing the cumulative monthly precipitation into two parts of the year with distinct amounts of rainfall (start of March till the end of August for the dry period and the start of September till the end of February for the wet part of the year), a marked change in rainfall distribution on annual basis was found (e.g., see Figure 18). With the steadily increasing amount of rainfall during the wet part of the season and, at the same time, the amount of rainfall during the dry period of the season being equally reduced, the influence of changing rainfall characteristics on slope stability of flysch deposits yet remains to be determined. Findings from this research should provide a solid basis for the start.

Although many of the rainfall-triggered landslides in past few decades were found to be a reactivation or partial reactivation of some old, larger dormant landslides, little is known about the slope processes that were occurring in the past in the Rječina River Valley. Under which conditions and what was the triggering factor, such as inertial forces caused by the dynamics in the Earth's crust, the weathering process, erosion and activity of the Rječina river, excessive precipitation, anthropogenic influences, etc. or combination of all, remains a great unknown. However, it is clear that historical events in combination with material features which are greatly defined by the high potential to the weathering and change in physical and chemical conditions of the original bedrock, presence of the low-conductivity unsaturated residual soil at the surface of the slopes with specific hydraulic features, the presence of the Rječina river at lower part of the slopes, in combination with the climate conditions characterized by extensive rainfall during the autumn and winter period, and very dry summers, have all resulted in slopes that are marginally stable. The described mechanism of delayed landslide triggering under excessive precipitation, which is mainly attributed to the presence of the near-surface unsaturated zone and its specific hydro-mechanical features with low permeability and water storage capacity that retard the groundwater table rise, could be the mechanism credited for landslides generated in this area.



## Reflections on further research

Probably any of the activities that were performed to fulfill the research objectives could be improved to some extent or have generated some additional questions that seek for the answers.

For example, numerous laboratory experiments showed that high plasticity fine-grained soils undergo significant volume changes when matric suction is changed. The above volume changes associated with the change of the effective stress are especially pronounced for specimens prepared from a slurry. At the same time, SWRC tests performed on undisturbed specimens are very rare, especially for residual soils. Thus, when the matric suction is increased, water can be expelled from the soil because of two reasons: i) volumetric deformations occur due to increased effective stress caused by increased matric suction, where the soil remains still in saturated state but with negative pore-water pressures; or ii) due to exceeded AEV in the largest pore when degree of saturation drops below 100%, the water phase becomes discontinuous, and the soil becomes unsaturated. However, measurements performed in this study using the undisturbed samples indicate that a transient stage exists, where both of the processes occur simultaneously. Since the adsorption process was the primary focus of the study, for which it was found that total volume changes, under the matric suction range relevant for performed analysis should have negligible effects on UHCF, this effect was not investigated further. To investigate a described problem, more precise measurement techniques could be required. For example, the total volume change of the specimen could be underestimated if the effective lateral stress caused by increased matric suction under imposed net vertical stress value results in specimen detachment from the rigid wall inside the modified, axis-translation based oedometer apparatus. The wax dipping and water displacement technique was found to be very useful when combined with some SWRC measurement techniques but, in some cases, could not yield enough accurate results. However, advanced laboratory equipment, such as modified, axis translation double-cell triaxial apparatus could be used to simultaneously measure changes of water content at imposed matric suction values and total sample deformations from fluid displacements inside the inner cell. The obtained results could provide more detailed insight into water retention characteristics of undisturbed samples of residual soil from a flysch rock mass, and possibly provide more accurate SWRC and UHCF.

The unsaturated hydraulic conductivity was determined from direct measurements of the saturated coefficient of permeability and SWRC. The Extended Evaporation Method (Schindler et al. 2015) was used to get insight into hydraulic permeability under matric suction

values up to 130 kPa as well. However, parameter estimation techniques or some other regression-based indirect method could be used on observations from conducted laboratory tests to investigate the hydraulic features of the investigated material further. Since all of the measurements were performed on small samples in the laboratory, double ring infiltrometer or some other technique could be used to perform field measurements for hydraulic characterization of the investigated soil.

The study aimed to determine the influence of the unsaturated zone on the landslide occurrence. Occasional field measurements, information about the reservoir levels, precipitation data and measurements on undisturbed samples collected at the natural water content were used to define the required initial and boundary conditions, and material properties. However, some continuous in-situ monitoring of relevant variables, such as matric suction and water content along several profiles, groundwater table or positive pore-water pressures at several additional locations would ensure additional information and input-parameters that could be incorporated in the defined numerical model to improve its accuracy and to assess the state of the slope stability more realistically. Measured pore-water pressure distribution and moisture content changes could be used for model calibration purposes, if required. In the case of remote data transfer from the monitoring system, measured values could be used to calculate the slope stability state in real-time. In the case of extreme meteorological conditions, weather forecast or radar precipitation data could be used to perform slope stability analysis according to existing ground conditions on the site and anticipated rainfall, even before the rainfall has arrived on the site. Experiences could be valuable for different applications, such as the landslide early warning systems.

Due to the spherical shape of the sliding surface, 3D stability analysis results could differ from those obtained from the 2D analysis, especially in the case of landslides involving stability analysis in partially saturated conditions. A portion of the sliding surface included inside the unsaturated zone becomes greater if landslide geometry is defined in 3D. Consequently, more of the sliding plane becomes exposed to the negative pore-water pressure conditions and, in general, a 3D analysis should provide more accurate slope stability results. 3D surface scans of the landslide body could enable more advanced infiltration analysis. It is probable that depressions and irregularities existing at the landslide surface, which cannot be captured by the two-dimensional analysis, would have an influence on the rainfall infiltration analysis, especially considering the occasional water ponding conditions which should be included for locations with such geometrical conditions. Generally, a 3D DEM of the landslide

should ensure more realistic calculations of the infiltration and runoff quantities, and provide more realistic slope stability results.

Since the long-term rainfall was considered in this study, the applied flux boundary condition representing the precipitation was simplified, accounting only for the rainfall component. The evapo(transpi)ration effects were assumed to have a negligible effect in this case and were not considered. To define a more precise ground surface moisture flux BCs, the actual evaporation should be quantified for the investigated location. However, the latter step implies a determination of how different matric suction values (or soil water contents) affect the evaporation process, among the other quantities that are usually provided by the commercially available automated weather stations such as temperature, wind conditions, solar radiation, etc. Due to the vegetation present at the landslide location, water intake from the plants and its influence on the matric suction and water content along the landslide cross-section should be considered as well.

A performed numerical analyses are rather simple. The equation describing water flow through unsaturated soil is solved first. Calculated volumetric water content values are used to define pore-water pressure values according to defined SWRC for the ongoing process. Finally, the obtained pore-water pressure profiles are introduced into the slope stability model based on LEM to calculate the factor of safety value. A more advanced, fully coupled approach would imply obtaining the solution of two PDEs simultaneously: one for the hydraulic part of the problem and another for the mechanical part. In that way, change of matric suction (or water content) in the REV would cause a change of the effective stress and generate associated deformations which would, again, modify hydraulic features of the soil. Although the SWRC measurements performed during the wetting process, which is relevant for the performed analysis of rainfall infiltration, indicated that volumetric deformations should have negligible effects on the hydraulic features of the investigated soil, the more advanced formulation should provide more accurate simulation results, especially if the simulation would account both for the drying and wetting process. However, the latter would require additional experimental and numerical efforts due to the hysteresis effects and associated problems with shifting from the drying to the wetting branch, or along some of the possible scanning curves. Another motivation for this type of analysis is the obvious shortcomings of the LEM, especially regarding the calculation procedure for the determination of the FoS value and stress distribution along the sliding plane. The stress-strain constitutive relationship would ensure a more advanced investigation of the triggering mechanism.

Finally, much of the research should be performed to assess the influence of various rainfall patterns and changing rainfall trends on the slope stability in flysch deposits. Redistribution of the annual rainfall amount should affect the landslide occurrence in flysch deposits favorably or unfavorably. Precise rainfall measurements from the last one or two decades could provide some input data to obtain the insights into the possible direction of change. Obtained UHCF provides insight into rainfall patterns that are unfavorable for the flysch slopes. Different time-dependent artificial rainfall patterns could be used in numerical simulation to gather the information on how each of the considered rainfall patterns affects the state of slope stability over time.



## Bibliography

- Agus, S. S., Leong, E. C., and Schanz, T. 2003. Assessment of statistical models for indirect determination of permeability functions from soil–water characteristic curves, *Geotechnique*, 53(2): 279-282. doi:10.1680/geot.2003.53.2.279
- Agus, S. S., and Schanz, T. 2005. Comparison of Four Methods for Measuring Total Suction, *Vadose Zone Journal*, 4(4): 1087-1095. doi:10.2136/vzj2004.0133
- Aitchison, G. D. 1964. Engineering concepts of moisture equilibria and moisture changes in soils. Statement of the Review Panel, in *Moisture Equilibria and Moisture Changes in Soils Beneath Covered Areas*, A Symposium in Print, Butterworths, Sydney: 7-21.
- Aleotti, P., Polloni, G., Casagli, N., and Dapporto, S. 2004. Shallow failures triggered by the November 2002 meteoric event in the Albaredo Valley, Valtellina (Italian Central Alps): mechanics and stability analyses, in W. Lacerda, M. Ehrlich, S.A.B. Fontoura, and A.S.F. Sayao (Eds.), *Proceedings of the Ninth International Symposium on Landslides: Evaluation and Stabilization*, June 28 -July 2, 2004 Rio de Janeiro, Brazil, Taylor & Francis Group, London: 971-977.
- Alonso, E. E., Gens, A., and Josa, A. 1990. A constitutive model for partially saturated soils, *Geotechnique*, 40(3): 405-430. doi:10.1680/geot.1990.40.3.405
- Alonso, E. E., Gens, A., Lloret, A., and Delahaye, C. 1995. Effect of rain infiltration on the stability of slopes, in *Proceedings of the first conference on unsaturated soils UNSAT'95*, 6-8 September 1995, Paris, Balkema, Rotterdam, Netherlands, 1: 241-250.
- Alonso, E. E., Pereira, J.-M., Vaunat, J., and Olivella, S. 2010. A microstructurally based effective stress for unsaturated soils, *Geotechnique*, 60(12): 913-925. doi:10.1680/geot.8.P.002
- Arbanas, Ž., Dugonjić Jovančević, S., Vivoda, M., and Mihalić Arbanas, S. 2014. Study of Landslides in Flysch Deposits of North Istria, Croatia: Landslide Data Collection and Recent Landslide Occurrences, in: K. Sassa, P. Canuti, and Y. Yin (Eds.) *Proceedings of the WLF 3, Landslide Science for a Safer Geoenvironment, Volume 1: The International Programme on Landslides (IPL)*, June 2014, Beijing, China, Springer International Publishing, Switzerland, 1: 89-94. doi:10.1007/978-3-319-04999-1\_7

- Arbanas, Ž., Jagodnik, V., Ljutić, K., Vivoda, M., Dugonjić Jovančević, S., Peranić J. 2014. Remote Monitoring of a Landslide Using an Integration of GPS, TPS and Conventional Geotechnical Monitoring Methods, in: S. Mihalić Arbanas, Ž. Arbanas (Eds.) *Proceedings of the 1st Regional Symposium on Landslides in the Adriatic-Balkan Region*, 7-9 March 2013, Zagreb, Croatia: 39-44.
- Arbanas, Ž., Mihalić Arbanas, S., Vivoda, M., Peranić, J., Dugonjić Jovančević, S., Jagodnik, V. 2014. Identification, monitoring and simulation of landslides in the Rječina River Valley, Croatia, in: K. Sassa, and Q. Dang Khang (Eds.) *Proceedings of the SATREPS Workshop on Landslide Risk Assessment Technology*, 29-30 July 2014, Hanoi, Vietnam: 200-213.
- Arbanas, Ž., Sassa, K., Nagai, O., Jagodnik, V., Vivoda, M., Dugonjić Jovančević, S., Peranić, J., Ljutić K. 2014. A landslide monitoring and early warning system using integration of GPS, TPS and conventional geotechnical monitoring methods, in: K. Sassa, P. Canuti, and Y. Yin (Eds.) *Proceedings of the WLF3, Landslide Science for a Safer Geoenvironment, Volume: 2: Methods of Landslide Studies*, June 2014, Beijing, China, Springer International Publishing, Switzerland, doi:10.1007/978-3-319-05050-8\_98
- Arbanas, Ž., Mihalić Arbanas, S., Vivoda Prodan, M., Peranić, J., Sečanj, M., Bernat Gazibara, S., Krkač, M. 2017. Preliminary investigations and numerical simulations of a landslide reactivation, in: M. Mikoš, B. Tiwari, Y. Yin, K. Sassa (Eds.) *Advancing culture of living with landslides, WLF2017*, 29 May – 2 June 2017, Ljubljana, Slovenia, Springer International Publishing AG, Switzerland, Cham: 649-657. doi:10.1007/978-3-319-53498-5\_75
- Arbanas, Ž., Vivoda, M., Mihalić Arbanas, S., Peranić, J., Sečanj, M., Bernat, S., Krkač, M. 2017. Analysis of a reservoir water level impact on landslide reactivation, in: B. Abolmasov, M. Marjanović, M., and U. Đurić (Eds.) *Proceedings of the 2nd Regional Symposium on Landslides in the Adriatic-Balkan Region*, 14-16 May 2015, Belgrade, Serbia: C1-C6.
- Arifin, Y. F., and Schanz, T. 2009. Osmotic suction of highly plastic clays, *Acta Geotechnica*, 4(3): 177-191. doi:10.1007/s11440-009-0097-0
- ASTM D1140-17, Standard Test Methods for Determining the Amount of Material Finer than 75- $\mu\text{m}$  (No. 200) Sieve in Soils by Washing, ASTM International, West Conshohocken, PA, 2017. doi:10.1520/D1140-17
- ASTM D2435-96, Standard Test Method for One-Dimensional Consolidation Properties of Soils, ASTM International, West Conshohocken, PA, 1996. doi:10.1520/D2435-96

- ASTM D2487-11, Standard Practice for Classification of Soils for Engineering Purposes (Unified Soil Classification System). ASTM International, West Conshohocken, PA, 2011. doi:10.1520/D2487-11
- ASTM D3080/D3080M-11, Standard Test Method for Direct Shear Test of Soils Under Consolidated Drained Conditions, ASTM International, West Conshohocken, PA, 2011. doi:10.1520/D3080\_D3080M-11
- ASTM D4318-17, Standard Test Methods for Liquid Limit, Plastic Limit, and Plasticity Index of Soils, ASTM International, West Conshohocken, PA, 2017. doi:10.1520/D4318-17E01
- ASTM D5084-03, Standard Test Methods for Measurement of Hydraulic Conductivity of Saturated Porous Materials Using a Flexible Wall Permeameter, ASTM International, West Conshohocken, PA, 2003. doi:10.1520/D5084-03
- ASTM D6836-02, Standard Test Methods for Determination of the Soil Water Characteristic Curve for Desorption Using a Hanging Column, Pressure Extractor, Chilled Mirror Hygrometer, and/or Centrifuge, ASTM International, West Conshohocken, PA, 2002. doi:10.1520/D6836-02
- ASTM D7263-09, Standard Test Methods for Laboratory Determination of Density (Unit Weight) of Soil Specimens, ASTM International, West Conshohocken, PA, 2009. doi:10.1520/D7263-09
- ASTM D7664-10, Standard Test Methods for Measurement of Hydraulic Conductivity of Unsaturated Soils, ASTM International, West Conshohocken, PA, 2010. doi:10.1520/D7664-10
- ASTM D7928-17, Standard Test Method for Particle-Size Distribution (Gradation) of Fine-Grained Soils Using the Sedimentation Analysis, ASTM International, West Conshohocken, PA, 2017. doi:10.1520/D7928-17
- ASTM D854-14, Standard Test Methods for Specific Gravity of Soil Solids by Water Pycnometer, ASTM International, West Conshohocken, PA, 2014. doi:10.1520/D0854-14
- Aubertin, M., Mbonimpa, M., Bussière, B., and Chapuis, R.P. 2003. A model to predict the water retention curve from basic geotechnical properties, *Canadian Geotechnical Journal*, 40(6): 1104-1122. doi:10.1139/t03-054
- Aversa, S., and Nicotera, M. 2002. A triaxial and oedometer apparatus for testing unsaturated soils, *Geotechnical Testing Journal*, 25(1): 3-15. doi:10.1520/GTJ11075J



- Barbour, S.L., and Yang, N., 1993. A review of the influence of clay–brine interactions on the geotechnical properties of Ca-montmorillonitic clayey soils from western Canada, *Canadian Geotechnical Journal*, 30(6): 920-934. doi:10.1139/t93-090
- Bear, J. 1988. Dynamics of Fluids in Porous Media. New York: American Elsevier Publishing Company, Inc.
- Benac, Č., Arbanas, Ž., Jardas, B., Kasapović, S., Jurak, V. 1999. Complex landslide in the Rječina river valley, *Rudarsko-geološko-naftni zbornik*, 11: 81-90 (in Croatian).
- Benac, Č., Arbanas, Ž., Jurak, V., Oštrić, M., Ožanić, N. 2005. Complex landslide in the Rječina valley (Croatia): origin and sliding mechanism, *Bulletin of Engineering Geology and the Environment*, 64(4): 361-371. doi:10.1007/s10064-005-0002-5
- Benac, Č., Dugonjić, S., Arbanas, Ž., Oštrić, M., Jurak, V. 2009. Origin of instability phenomena along the karst-flysch contacts. Cavtat, Croatia, CRC Press: 757-761.
- Benac, Č., Dugonjić, S., Vivoda, M., Oštrić, M., Arbanas, Ž. 2011. A Complex landslide in the Rječina Valley: results of monitoring from 1998-2010, *Geologica Croatica*, 64(3): 239-249. doi:10.4154/GC.2011.20
- Benac, Č., Oštrić, M., and Dugonjić Jovančević, S. 2014. Geotechnical properties in relation to grain-size and mineral composition: The Grohovo landslide case study (Croatia), *Geologia Croatica*, 67(2): 21-30.
- Berisavljević, Z., Berisavljević, D., and Čebašek, V. 2015. Shear strength properties of Dimitrovgrad flysch, Southeastern Serbia, *Bulletin of Engineering Geology and the Environment*, 74(3): 759-779. doi:10.1007/s10064-014-0678-5
- Berti, M., and Simoni, A. 2012. Observation and analysis of near-surface pore-pressure measurements in clay-shales slopes, *Hydrological Processes*, 26: 2187-2205. doi:10.1002/hyp.7981
- Berti, M., Bertello, L., Bernardi, A.R., Caputo, G. 2017. Back analysis of a large landslide in a flysch rock mass, *Landslides*, 14(6): 2041-2058. doi:10.1007/s10346-017-0852-5
- Bishop, A. W. 1954. The use of pore pressure coefficients in practice, *Geotechnique*, 4(4): 148-152. doi:10.1680/geot.1954.4.4.148
- Bishop, A. 1955. The use of slip circle in the stability analysis of slopes, *Geotechnique*, 5(1): 7-17. doi:10.1680/geot.1955.5.1.7
- Bishop, A. 1959. The principle of effective stress. Teknisk Ukeblad. doi:106(39): 859-863.
- Bishop, A., and Morgenstern, N. 1960. Stability coefficients for earth slopes, *Geotechnique*, 10(4): 164-169 doi:10.1680/geot.1960.10.4.129

- Bishop, A., and Blight, G. 1963. Some aspects of effective stress in saturated and unsaturated soils, *Geotechnique*, 13(3): 177-197. doi:10.1680/geot.1963.13.3.177
- Bocking, K., and Fredlund, D. G. 1980. Limitations of the axis translation technique. New York, ASCE: 117–135
- Bolt, G. H. 1956. Physicochemical analysis of the compressibility of pure clays, *Geotechnique*, 6: 86–93. doi:10.1680/geot.1956.6.2.86
- Bosen, J.F. 1958. An approximation formula to compute relative humidity from dry bulb and dewpoint temperature, *Monthly Weather Review*, 86(12): 486.
- Bouchemella, S., Ichola, I.A., and Seridi, A. 2016. Estimation of the empirical model parameters of unsaturated soils, in: P. Delage, Y.-J. Cui, S. Ghabezloo, J.-M. Pereira and A.-M. Tang (Eds.) *Proceedings of the 3rd European Conference on Unsaturated Soils "E-UNSAT 2016"*, 12-14 September 2016, Paris, France. doi:10.1051/e3sconf/20160916007
- Brooks, R. H., and Corey, A. T. 1964. Hydraulic properties of porous media, *Colorado State University Hydrology Papers*, No. 3, Fort Collins, Colorado.
- Brooks, S. M., Spencer, T., and Boreham, S. 2012. Deriving mechanisms and thresholds for cliff retreat in soft-rock cliffs under changing climates: Rapidly retreating cliffs of the Suffolk coast, UK, *Geomorphology*, 153-154: 48-60. doi:10.1016/j.geomorph.2012.02.007
- Brunetti, M. T., Peruccacci, S., Rossi, M., Luciani, S., Valigi, D., Guzzetti, F. 2010. Rainfall thresholds for the possible occurrence of landslides in Italy, *Natural Hazards and Earth Systems Sciences*, 10(3): 447-458. doi:10.1016/j.geomorph.2017.03.031
- Buma, J., and Dehn, M. 2000. Impact of climate change on a landslide in South East France, simulated using different GCM scenarios and downscaling methods for local precipitation, *Climate Research*, 15(1): 69-81. doi:10.3354/cr015069
- Burdine, N.T. 1953. Relative Permeability Calculations From Pore Size Distribution Data. *Transactions of the Metallurgical Society of AIME*, 198: 71-78. doi:10.2118/225-G
- Cai, G., Zhou, A., and Sheng, D. 2014. Permeability function for unsaturated soils with different initial densities, *Canadian Geotechnical Journal*, 51: 1456-1467. doi:10.1139/cgj-2013-0410
- Campbell, G., Smith, D., and Teare, B. 2007. Application of a dew point method to obtain the soil-water characteristics, in: T. Schanz (Eds.) *Experimental Unsaturated Soil Mechanics, Springer Proceedings in Physics, vol 112*, Springer, Berlin, Heidelberg: 71-77. doi:10.1007/3-540-69873-6\_7

- Cannon, S., and DeGraff, J. 2009. The Increasing Wildfire and Post-Fire Debris-Flow Threat in Western USA, and Implications for Consequences of Climate Change, in: K. Sassa , P. Canuti (Eds.) *Landslides – Disaster Risk Reduction*, Springer, Berlin, Heidelberg: 177-190. doi:10.1007/978-3-540-69970-5\_9
- Cardoso, R., Romero, E., Lima, A., and Ferrari, A. 2007. A comparative study of soil suction measurement using two different high-range psychrometers, in: T. Schanz (Eds.) *Experimental Unsaturated Soil Mechanics, Springer Proceedings in Physics, vol 112*. Springer, Berlin, Heidelberg: 79-93. doi:10.1007/3-540-69873-6\_8
- Carretero, S., Rapaglia, J., Bokuniewicz, H., and Kruse, E. 2013. Impact of sea-level rise on saltwater intrusion length into the coastal aquifer, Partido de La Costa, Argentina, *Continental Shelf Research*, 61-62: 62-70. doi:10.1016/j.csr.2013.04.029
- Carsel, R.F, and Parrish, R.S. 1988. Developing joint probability distributions of soil water retention characteristics, *Water Resources Research*, 24(5): 755-769. doi:10.1029/WR024i005p00755
- Casagli, N., Dapporto, S., Ibsen, M.L., Tofani, V., Vannocci, P. 2006. Analysis of the landslide triggering mechanism during the storm of 20th–21st November 2000, in Northern Tuscany, *Landslides*, 3: 13-21. doi:10.1007/s10346-005-0007-y
- Cascini, L., Cuomo, S., Pastor, M., and Sorbino, G. 2010. Modeling of rainfall-induced shallow landslides of the flow-type, *Journal of Geotechnical and Geoenvironmental Engineering*, 136(1): 85-98. doi:10.1061/(ASCE)GT.1943-5606.0000182
- Cascini, L. Cuomo, S., Della Sala M. 2011. Spatial and temporal occurrence of rainfall-induced shallow landslides of flow type: a case of Sarno-Quindici, Italy, *Geomorphology*, 126(1-2): 148-158. doi:10.1016/j.geomorph.2010.10.038
- Cascini, L., Cuomo, S., Pastor, M., and Sacco, C. 2013. Modelling the post-failure stage of rainfall-induced landslides of the flow type, *Canadian Geotechnical Journal*, 50: 924-934. doi:10.1139/cgj-2012-0375
- Cascini, L., Sorbino, G., Cuomo, S., and Ferlisi, S. 2014. Seasonal effects of rainfall on the shallow pyroclastic deposits of the Campania region (southern Italy), *Landslides*, 11(5): 779-792. <https://doi.org/10.1007/s10346-013-0395-3>
- CEN ISO/TS 17892-10:2004(E): Geotechnical investigation and testing — Laboratory testing of soil — Part 10: Direct shear tests.
- Chae, B.-G., Lee, J.-H., Park, H.-J., and Choi, J. 2015. A method for predicting the factor of safety of an infinite slope based on the depth ratio of the wetting front induced by rainfall

- infiltration, *Natural Hazards and Earth System Sciences*, 15: 1835-1849. doi:10.5194/nhess-15-1835-2015
- Chen, G., Jiao, L., and Li, X. 2016. Sensitivity analysis and identification of parameters to the Van Genuchten equation, *Journal of Chemistry*, 2016: 8. doi:10.1155/2016/9879537
- Chen, L., and Young, M.H. 2006. Green-Ampt infiltration model for sloping surface, *Water Resources Research*, 42: 1-9. doi:10.1029/2005WR004468
- Chen, P., Wei, C., Liu, J., and Ma, T. 2013. Strength theory model of unsaturated soils with suction stress concept, *Journal of Applied Mathematics*, 2016: 10 pages. doi:10.1155/2013/756854
- Chiang, S.-H., and Chang, K.-T., 2011. The potential impact of climate change on typhoon-triggered landslides in Taiwan, 2010–2099, *Geomorphology*, 133(3-4): 143-151. doi:10.1016/j.geomorph.2010.12.028
- Chidichimo, F., De Biase, M., Rizzo, E., Masi, S., Straface, S. 2015. Hydrodynamic parameters estimation from self-potential data in a controlled full scale site, *Journal of Hydrology*, 522: 572-581. doi:10.1016/j.jhydrol.2015.01.022
- Childs, E., and Collis-George, G. 1950. The permeability of porous materials, *Proceedings of the Royal Society of London. Series A. Mathematical and Physical Sciences*, 201A: 392-405. doi:10.1098/rspa.1950.0068
- Chiu, T., and Shackelford, C. 1998. Unsaturated hydraulic conductivity of compacted sand-kaolin mixtures, *Journal of Geotechnical and Geoenvironmental Engineering*, 124 (2): 160-170. doi:10.1061/(ASCE)1090-0241(1998)124:2(160)
- Cho, G.C., and Santamarina, J.C. 2001. Unsaturated particulate materials—Particle-level studies, *Journal of Geotechnical and Geoenvironmental Engineering*, 127(1): 84–96. doi:10.1061/(ASCE)1090-0241(2001)127:1(84)
- Cho, S.E., and Lee, S.R. 2001. Instability of unsaturated soil slopes due to infiltration, *Computers and Geotechnics*, 28(3): 185-208. doi:10.1016/S0266-352X(00)00027-6
- Clarizia, M., Gulla, G., and Sorbino, G. 1996. Sui meccanismi di innesco dei soil slip, in: *Proceedings of Convegno Internazionale "La prevenzione delle catastrofi idrogeologiche: il contributo della ricerca scientifica"*, 5-7 November 1996, Alba, Italia, 1: 585–597 (in Italian).
- Coe, J.A. 2012. Regional moisture balance control of landslide motion: Implications for landslide forecasting in a changing climate, *Geology*, 40(4): 323-326. doi:10.1130/G32897.1

- Coe, J. 2016. Landslide hazards and climate change: A perspective from the United States, in: K. Ho, L. Suzanne, and L. Picarelli (Eds.) *Slope safety preparedness for impact of climate change*. London: CRC Press: 479-523. doi:10.1201/9781315387789-16
- Coleman, J. D. 1962. Stress/strain relations for partly saturated soils, *Geotechnique*, 12(4): 348–350.
- Collins, B. D., and Znidarcic, D. 2004. Stability analyses of rainfall induced landslides, *Journal of Geotechnical and Geoenvironmental Engineering*, 130(4): 362–372. doi:10.1061/(ASCE)1090-0241(2004)130:4(362)
- Collins, B., Kayen, R., and Sitar, N. 2007. Process-based empirical prediction of landslides in weakly lithified coastal cliffs, San Francisco, California, USA, in: R. McInnes, J. Jakeways, H. Fairbank, and E. Mathie (Eds.) *Landslides and Climate Change - Challenges and Solutions*, Taylor & Francis, London, UK: 175-184.
- Comegna, L., Picarelli, L., Buccignani, E., and Mercogliano, P. 2013. Potential effects of incoming climate changes on the behaviour of slow active landslides in clay, *Landslides*, 10(4): 373-391. doi:10.1007/s10346-012-0339-3
- Corey, A. T. 1954. The interrelation between gas and oil relative permeabilities, *Producer's Monthly*, 19(1):38-41.
- Crosta, G.B., and Fratini, P. 2001. Rainfall thresholds for triggering soil slips and debris flow, in: A. Mugnai, F. Guzzetti, G. Roth (Eds.) *Proceedings of the 2nd EGS Plinius Conference on Mediterranean Storms*, 16-18 October 2000, Siena, Italy: 463-487.
- Crosta, G.B., and Dal Negro, P. 2003. Observations and modelling of soil slip-debris flow initiation processes in pyroclastic deposits: the Sarno 1998 event, *Natural Hazards and Earth System Sciences*, 3: 53-69. doi:10.5194/nhess-3-53-2003
- Crozier, M.J. 2010. Deciphering the effect of climate change on landslide activity: a review, *Geomorphology*, 124(3-4): 260-267. doi:10.1016/j.geomorph.2010.04.009
- Cruden, D., and Varnes, D. 1996. Landslide types and processes, in: A.K. Turner, and R.L. Schuster (Eds.) *Landslides: investigation and mitigation (Special Report)*, National Academy Press, Washington, DC, USA, 247: 36–75.
- Cui, Y. J., Tang, A. M., Loiseau, C., and Delage, P. 2008. Determining the unsaturated hydraulic conductivity of a compacted sand-bentonite mixture under constant-volume and free-swell conditions, *Physics and Chemistry of the Earth*, 33: S462–S471.
- Cunningham, M. R., Ridley, A. M., Dineen, K., and Burland, J. B. 2003. The mechanical behaviour of a reconstituted unsaturated silty clay, *Geotechnique*, 53(2): 183-194. doi:10.1680/geot.2003.53.2.183

- Cuomo, S. 2006. Geomechanical modelling of triggering mechanisms for flow-like mass movements in pyroclastic soils. PhD thesis. Universita di Salerno.
- Cuomo, S., and Della Sala, M. 2013. Rainfall-induced infiltration, runoff and failure in steep unsaturated shallow soil deposits, *Engineering Geology*, 162(25): 118-127. doi:10.1016/j.enggeo.2013.05.010
- Dahal, R.K., and Hasegawa, S. 2008. Representative rainfall thresholds for landslides in the Nepal Himalaya, *Geomorphology*, 100(3): 429-443. doi:10.1016/j.geomorph.2008.01.014
- De Graff, J. 2018. A rationale for effective post-fire debris flow mitigation within forested terrain, *Geoenvironmental Disasters*, 5(7): 9 pages. doi:10.1186/s40677-018-0099-z
- Department of the army U.S. Army Corps Of Engineers Washington, D. 2.-1., 2003. Engineering and Design SLOPE STABILITY Manual. Washington, DC: U.S. Army Corps of Engineers.
- Dilley, M., Chen, R.S., Deichmann, U., Lerner-Lam, A.L., Arnold, M., Agwe, J., Buys, P., Kjekstad, O., Lyon, B., and Yetman, G. 2005. Natural disaster hotspots: a global risk analysis, *World Bank Disaster Risk Management Series*, 5: 1-132. doi:10.1007/978-3-322-82113-3\_1
- Di Mariano, A. 2000. Le argille a scaglie e il ruolo della suzione sulla loro deformibilita, PhD Thesis, Universita di Palermo e di Catania.
- Domenico, P.A., Schwartz, F.W. 1998. Physical and chemical hydrogeology (2nd edition). New York: John Wiley & Sons, Inc.
- Dugonjić Jovančević, S., and Arbanas, Ž. 2012. Recent landslides on the Istrian Peninsula, Croatia, *Natural hazards*, 62(3): 1323-1338. doi:10.1007/s11069-012-0150-4
- Dugonjić Jovančević, S., Peranić, J., Ružić, I., and Arbanas, Ž. 2016. Analysis of a historical landslide in the Rječina River Valley, Croatia, *Geoenvironmental Disasters*, 3(26): 9 doi:10.1186/s40677-016-0061-x
- Duncan, J.M., and Wright, S.G. 1980. The accuracy of equilibrium methods of slope stability analysis, *Engineering Geology*, 16(1): 5-17. doi:10.1016/0013-7952(80)90003-4
- Duncan, J.M. 1996. State of the Art: Limit equilibrium and Finite\*Element analysis of slopes, *Journal of Geotechnical Engineering*, 122(7): 577-596. doi:10.1061/(ASCE)0733-9410(1996)122:7(577)
- Ebrahimi-Birang, N., Gitirana, G.F.N., Fredlund, D. G., Fredlund, M. D., and Samarasekera, L. 2004. A lower limit for the water permeability coefficient, in: *Proceedings of 57th Canadian Geotechnical Conference*, 24-26 October 2004, Quebec: 12-19.

- Eching, S.O., and Hopmans, J.W. 1993. Optimization of Hydraulic Functions from Transient Outflow and Soil Water Pressure Data, *Soil Science Society of America Journal*, 57(5): 1167-1175.
- Escario, V., and Saez, J. 1986. The shear strength of partly saturated soils, *Géotechnique*, 36(3): 453-456. doi:10.1680/geot.1986.36.3.453
- Escario, V., and Juca, J.F.T. 1989. Strength and deformation of partly saturated soils, in: *Proceedings of the Twelfth International Conference on Soil Mechanics and Foundation Engineering*, 13-18 August 1989, Rio de Janeiro, 1: 43-46.
- Fatehnia, M., and Tawfiq, K. 2014. Comparison of the methods of hydraulic conductivity estimation from mini disk infiltrometer, *Electronic Journal of Geotechnical Engineering*, 19(E): 1047-1063.
- Fellenius, W. 1936. Calculation of the Stability of Earth Dams. Washington: 445-463.
- Fischer, L., Huggel, C., Kääh, A., and Haeberli, W. 2013. Slope failures and erosion rates on a glacierized high-mountain face under climatic changes, *Earth Surface Processes and Landforms*, 38(8): 836-846. doi:10.1002/esp.3355
- Fischer, L., Purves, R.S., Huggel, C., Noetzli, J., and Haeberli, W. 2012. On the influence of topographic, geological and cryospheric factors on rock avalanches and rockfalls in high-mountain areas, *Natural Hazards and Earth System Sciences*, 12: 241-254. doi:10.5194/nhess-12-241-2012
- Francani, V., Gattinoni, P., and Rampazzo, R. 2011. Slope instability triggered by climate change in periglacial areas, *Italian Journal of Engineering Geology and Environment*, 2(1): 39-62. doi:10.4408/IJEGE.2011-02.O-03
- Fredlund, D. G. 1974. Slope stability analysis. User's Manual CD-4. Department of Civil Engineering, University of Saskatchewan. Saskatoon, Sask.
- Fredlund, D. G. 1975. A comprehensive and flexible slope stability program. Calgary, Alta, 3: 109-142.
- Fredlund, D. G., and Morgenstern, N. 1976. Constitutive relations for volume change in unsaturated soils, *Canadian Geotechnical Journal*, 13: 261-276. doi:10.1139/t76-029
- Fredlund, D. G., and Krahn, J. 1977. Comparison of slope stability methods of analysis, *Canadian Geotechnical Journal*, 14(3): 429-439. doi:10.1139/t77-045
- Fredlund, D. G., and Morgenstern, N. 1977. Stress state variables for unsaturated soils, *Journal of the Geotechnical Engineering Division*, 103(5): 447-466.
- Fredlund, D. G., Morgenstern, N. R., and Widger, R. A. 1978. The shear strength of unsaturated soils, *Canadian Geotechnical Journal*, 15(3): 313-321. doi:10.1139/t78-029.

- Fredlund, D. G. 1981. Seepage in saturated soils. Session 3 on Groundwater and Seepage Problems, in: *Proceedings of the Tenth International Conference on Soil Mechanics and Foundation Engineering*, 15-19 June, Stockholm, Sweden, 4:629-641.
- Fredlund, D. G., Krahn, J., and Pufahl, D.E. 1981. The relationship between limit equilibrium slope stability methods, in: *Proceedings of the Tenth International Conference on Soil Mechanics and Foundation Engineering*, 15-19 June, Stockholm, Sweden, 3: 409-416.
- Fredlund, D. G., and Rahardjo, H. 1993. Soil mechanics for unsaturated soils. New York: John Wiley & Sons Inc. doi:10.1002/9780470172759
- Fredlund, D. G., and Xing, A. 1994. Equations for the soil-water characteristic curve, *Canadian Geotechnical Journal*, 31: 521-532. doi:10.1139/t94-061
- Fredlund, D. G., Xing, A., and Huang, S. 1994. Predicting the permeability function for unsaturated soils using the soil-water characteristic curve, *Canadian Geotechnical Journal*, 31(4): 533-546. doi:10.1139/t94-062
- Fredlund, D. G., Xing, A., Fredlund, M.D., and Barbour, S.L. 1996. The relationship of the unsaturated soil shear to the soil-water characteristic curve, *Canadian Geotechnical Journal*, 33(3): 440-448. doi:10.1139/t96-065
- Fredlund, D. G., Rahardjo, H., Leong, E., and Ng, C. 2001. Suggestions and recommendations for the interpretation of soil–water characteristic curves, in: *Proceedings of the Fourteenth Southeast Asian Geotechnical Conference*, 10-14 December 2001, Hong Kong, 1: 503–508.
- Fredlund, D. G., Sheng, D., and Zhao, J. 2011. Estimation of soil suction from the soil-water characteristic curve, *Canadian Geotechnical Journal*, 48: 186-198. doi:10.1139/T10-060
- Fredlund, D. G., Rahardjo, H., and Fredlund, M. D. 2012. Unsaturated Soil Mechanics in Engineering Practice. New Jersey: John Wiley & Sons, Inc., Hoboken.
- Fredlund, D. G., and Houston, S. L. 2013. Interpretation of soil-water characteristic curves when volume change occurs as soil suction is changed, in: *Advances in Unsaturated Soils - Proceedings of the 1st Pan-American Conference on Unsaturated Soils, PanAmUNSAT 2013*, 20-22 February 2013, Cartagena de Indias, Colombia: 15-31.
- Fredlund, D. G. 2017. Role of the Soil-Water Characteristic Curve in Unsaturated Soil Mechanics, in: *Proceedings of the 19th International Conference on Soil Mechanics and Geotechnical Engineering*, 17-22 September 2017, Seoul, Korea: 57-79.
- Fujimaki, H., and Inoue, M. 2003. A flux-controlled steady-state evaporation method for determining unsaturated hydraulic conductivity at low matric pressure head values, *Soil Science*, 85(4): 228-232. doi:10.1097/01.ss.0000075284.87447.cf



- Fukuoka, H., Sassa, K., Wang, G., and Sasaki, R. 2006. Observation of shear zone development in ring-shear apparatus with a transparent shear box, *Landslides*, 3: 239–251. doi:10.1007/s10346-006-0043-2
- Furuya, T. 2004. Review and Comparison of Limit Equilibrium Methods of Slices for Slope Stability Analysis, *Bulletin of the national institute for rural engineering*, 43: 1-21.
- Gili J. A, Corominas J, and Rius J. 2000. Using Global Positioning System techniques in landslide monitoring, *Engineering Geology*, 55(3): 167-192 doi:10.1016/S0013-7952(99)00127-1
- Gallage, C., Kodikara, J., and Uchimura, T. 2013. Laboratory measurement of hydraulic conductivity functions of two unsaturated soils during drying and wetting process, *Soils and Foundations*, 53(3): 417-430. doi:10.1016/j.sandf.2013.04.004
- Gan, J. K.-M., and Fredlund, D. G. 1988. Multistage direct shear testing of unsaturated soils, *Geotechnical Testing Journal*, 11(2): 132-138. doi:10.1520/GTJ10959J
- Gan, J. K.-M., Fredlund, D. G., and Rahardjo, H. 1988. Determination of the shear strength parameters of an unsaturated soil using the direct shear test, *Canadian Geotechnical Journal*, 25(3): 500-510. doi:10.1139/t88-055
- Gariano, S. L., and Guzzetti, F. 2016. Landslides in a changing climate, *Earth-Science Reviews*, 162: 227-252. doi:10.1016/j.earscirev.2016.08.011
- GDS Instruments, 2013. Instruction Manual: Unsaturated Back Pressured Shear Box.
- Gee, G. W., Campbell, M. D., Campbell, G. S., and Campbell, J. H. 1992. Rapid measurement of low soil water potentials using a water activity meter, *Soil Science Society of America*, 56(4): 1068-1070. doi:10.2136/sssaj1992.03615995005600040010x
- Geertsema, M., Clague, J. J., Schwab, J. W., and Evans, S. G. 2006. An overview of recent large catastrophic landslides in northern British Columbia, Canada, *Engineering Geology*, 83(1-3): 120-143. doi:10.1016/j.enggeo.2005.06.028
- GEO-SLOPE International, Ltd. 2012. Stability Modelling with SLOPE/W, An Engineering Methodology. Calgary, Alberta, Canada.
- GEO-SLOPE International, Ltd. 2017. Heat and mass transfer modeling with GeoStudio 2018 (Second Edition). Calgary, Alberta, Canada.
- GEOSLOPE International, L. 2017. Stability Modelling with GeoStudio. Canada: Calgary, AB, Canada.
- Gil, E., and Dlugosz, M. 2006. Threshold values of rainfalls triggering selected deep-seated landslides in the Polish flysch Carpathians, *Studia Geomorphologica Carpatho-Balcanica*, 40: 21-43.

- Gofar, N., and Lee, L., 2008. Extreme rainfall characteristics for surface slope stability in the Malaysian Peninsular, *Journal of Assessment and Management of Risk for Engineered Systems and Geohazards (Georisk)*, 2(2): 65-78. doi:10.1080/17499510802072991
- Greco, R., Guida, A., Damiano, E., and Olivares, L. 2010. Soil water content and suction monitoring in model slopes for shallow flowslides early warning applications, *Physics and Chemistry of the Earth Parts A/B/C*, 35(3-5): 127-136. doi:10.1016/j.pce.2009.12.003
- Greco, R., and Gargano, R. 2015. A novel equation for determining the suction stress of unsaturated soils from the water retention curve based on wetted surface area in pores, *Water Resources Research*, 51: 6143–6155. doi:10.1002/2014WR016541
- Green, W. H., and Ampt, G.A. 1911. Studies on soil physics: flow of air and water through soils, *Journal of Agricultural Science*, 4: 1-24. doi:10.1017/S0021859600001441
- Gribb, M. 1996. Parameter estimation for determining hydraulic properties of a fine sand from transient flow measurements, *Water Resources Research*, 32(7): 1965-1974. doi:10.1029/96WR00894
- Guha, S., Below, R., Ph. Hoyois, Ph. (2015) EM-DAT: International Disaster Database – [www.emdat.be](http://www.emdat.be) – Université Catholique de Louvain – Brussels – Belgium.
- Guzzetti, F., Peruccacci, S., Rossi, M., and Stark, C. P. 2007. Rainfall thresholds for the initiation of landslides in central and southern Europe, *Meteorology and Atmospheric Physics*, 98(3-4): 239-267. doi:10.1007/s00703-007-0262-7
- Guzzetti, F., Peruccacci, S., Rossi, M., and Stark, C. P. 2008. The rainfall intensity–duration control of shallow landslides and debris flows: an update, *Landslides*, 5(1): 3-17. doi:10.1007/s10346-007-0112-1
- Haeberli, W. 2013. Mountain permafrost—research frontiers and a special long-term challenge, *Cold Regions Science and Technology*, 96: 71-76. doi:10.1016/j.coldregions.2013.02.004
- Haque, U.; Blum, P.; da Silva, P.F.; Andersen, P.; Pilz, J.; Chalov, S.R.; Malet, J.-P.; Jemec Auflič, M.; Andres, N.; Poyiadji, E.; Lamas, P.C.; Zhang, W.; Peshevski, I.; Pétursson, H.G.; Kurt, T.; Dobrev, N.; García-Davalillo, J.C.; Matina, H.; Ferri, S. 2016. Fatal landslides in Europe, *Landslides*, 13(6): 1545-1554. doi:10.1007/s10346-016-0689-3
- Harrison, I. 1965. Fundamental concepts and definitions relating to humidity. New York, Reinhold Publishing Company: 3-69.
- Hayek, M. 2016. Analytical solution to transient Richards' equation with realistic water profiles for vertical infiltration and parameter estimation, *Water Resources Research*, 52(6): 4438-4457. doi:10.1002/2015WR018533

- Heyerdahl, H., and Pabst, T. 2018. Comparison of experimental and predictive approaches for determination of water retention curves of intact samples of quaternary soils, *Geotechnical and Geological Engineering*, 36 (2): 1365-1385. doi:10.1007/s10706-017-0398-2
- Hilf, J. W. 1956. An investigation of pore-water pressure in compacted cohesive soils, PhD Thesis, *Technical Memorandum. No. 654.*, Denver, CO.: U.S. Department of the Interior, Bureau of Reclamation, Design and Construction Division.
- Hornung, U. 1983. Identification of nonlinear soil physical parameters from an input-output experiment, in: P. Deufhard, E. Hairer (Eds.) *Numerical treatment of inverse problems in differential and integral equations. Progress in Scientific Computing, Vol. 2.* Birkhäuser Boston. doi:10.1007/978-1-4684-7324-7\_16
- Hoyos, L. R., Velosa, C. L., and Puppala, A. J. 2014. Residual shear strength of unsaturated soils via suction-controlled ring shear testing, *Engineering Geology*, 172(8): 1-11. doi:10.1016/j.enggeo.2014.01.001
- Huang, S., Fredlund, D. G., and Barbour, S. 1998. Measurement of the coefficient of permeability for a deformable unsaturated soil using a triaxial permeameter, *Canadian Geotechnical Journal*, 35(3): 426-432. doi:10.1139/t98-011
- Huat, B., Ali, F., and Hasim, S. 2005. Modified shear box test apparatus for measuring shear strength of unsaturated residual soil, *American Journal of Applied Sciences*, 2(9): 1283-1289. doi:10.3844/ajassp.2005.1283.1289
- Hungr, O., Leroueil, S., and Picarelli, L. 2014. The Varnes classification of landslide types, an update, *Landslides*, 11(2): 167-194. doi:10.1007/s10346-013-0436-y
- Hürlimann, M., Abancó, C., and Moya, J. 2012. Rockfalls detached from a lateral moraine during spring season. 2010 and 2011 events observed at the Rebaixader debris-flow monitoring site (Central Pyrenees, Spain), *Landslides*, 3(3): 385-393. doi:10.1007/s10346-011-0314-4
- Ingles, O.G. 1962. Bonding Forces in Soils: Part 3. A theory of tensile strength for stabilized and naturally coherent soils, in: *Proceedings of the 1st Conf. of the Australian Road Research Board*, 1962, Canberra: 1025–1047.
- Inoue, M., Šimuněk, J., Hopmans, J. W., Clausnitzer, V. 1998. In situ estimation of soil hydraulic functions using a multistep soil-water extraction technique, *Water Resources Research*, 34(5): 1035-1050. doi:10.1029/98WR00295.
- Israelachvili, J. 1992. Intermolecular and surface forces, 2nd Ed., Academic, San Diego.

- Iverson, R. M. 2000. Landslide triggering by rain infiltration, *Water Resources Research*, 36(7): 1897-1910. doi:10.1029/2000WR900090
- Jaedicke, C., Van Den Eeckhaut, M., Nadim, F., Hervás, J., Kalsnes, B., Vangelsten, B.V., Smith, J.T., Tofani, V., Ciurean, R., Winter, M.G., Sverdrup-Thygeson, K., Syre, E., Smebye, H. 2014. Identification of landslide hazard and risk ‘hotspots’ in Europe, *Bulletin of Engineering Geology and the Environment*, 73(2): 325–339. doi:10.1007/s10064-013-0541-0
- Janbu, N. 1954. Applications of Composite Slip Surfaces for Stability Analysis, in: *Proceedings of the European Conference on Stability of Earht Slopes*, 20-25 September 1954, Stockholm, Sweden: 39-43.
- Jennings, J. E., and Burland, J. B. 1962. Limitation to the use of effective stress in partley saturated soils, *Geotechnique*, 12(2): 125-144. doi:10.1680/geot.1962.12.2.125.
- Johnson, R.E, and Dettre, R.H. 1969. Wettability and contact angles, in: E. Matijevic (Ed.): *Surface and Colloid Sience, Vol. II*, Wiley Interscience, New York.
- Jommi, C. 2000. Remarks on the constitutive modeling of unsaturated soils, in A. Tarantino and C. Mancuso (Eds.), *Experimental Evidence and Theoretical Approaches in Unsaturated Soils*, 10-12 April 2000, Trento, Balkema, Rotterdam, 139–153.
- Kaye, G.W.C., and Laby, T.H. 1973. Tables of Physical and Chemical Constants, 14th edition, Longman, London.
- Khalili, N., and Khabbaz, M. H. 1998. A unique relationship for  $\chi$  for the determination of the shear strength of unsaturated soils, *Geotechnique*, 48(5): 1-7. doi:10.1680/geot.1998.48.5.681
- Khalili, N., Geiser, F., Blight, G.E. 2004. Effective stress in unsaturated soils: Review with new evidence, *International Journal of Geomechanics* 4(2), 115–126, doi:10.1061/(ASCE)1532-3641(2004)4:2(115).
- Khosravi, A., and McCartney, J. S. 2011. Resonant Column Test for Unsaturated Soils With Suction–Saturation Control, *Geotechnical Testing Journal*, 34(6): 730-739. doi:10.1520/GTJ103102
- Kim, B.-S., Shibuya, S., Park, S.-W., and Kato, S. 2010. Application of suction stress for estimating unsaturated shear strength of soils using direct shear testing under low confining pressure, *Canadian Geotechnical Journal*, 47(9): 955-970. doi:10.1139/T10-007

- Kim, J., Jeong, S., and Regueiro, R. A. 2012. Instability of partially saturated soil slopes due to alteration of rainfall pattern, *Engineering Geology*, 147-148: 28-36. doi:10.1016/j.enggeo.2012.07.005
- Kim, T.-H. 2001. Moisture-induced tensile strength and cohesion in sand, PhD thesis, Univ. of Colorado at Boulder, Boulder.
- Klimeš, J., Baron, I., Panek, T., Kosačik, T., Burda, J., Kresta, F., and Hradecký, J. 2009. Investigation of recent catastrophic landslides in the flysch belt of Outer Western Carpathians (Czech Republic): progress towards better hazard assessment, *Nat Hazards Earth System Sciences*, 9: 119-128. doi:10.5194/nhess-9-119-2009
- Klose, M., Maurischat, P., and Damm, B. 2015. Landslide impacts in Germany: a historical and socioeconomic perspective, *Landslides* 13(1):183–199. doi:10.1007/s10346-015-0643-9
- Kool, J. B., Parker, J.C., and van Genuchten, M. T. 1985. Determining soil hydraulic properties from one-step outflow experiments by parameter estimation: I. Theory and numerical studies, *Soil Science Society of America Journal*, 49: 1348-1354.
- Krahn, J., and Fredlund, D.G. 1972. On total matric and osmotic suction, *Journal of Soil Science Journal*, 114(5): 339-348.
- Kristo, C., Rahardjo, H., and Satyanaga, A. 2017. Effect of variations in rainfall intensity on slope stability in Singapore, *International Soil and Water Conservation Research*, 5(4): 258-264. doi:10.1016/j.iswcr.2017.07.001
- Kunze, R.J., Uehara, G., and Graham, K. 1968. Factors important in the calculation of hydraulic conductivity, *Soil Science Society of America Proceedings*, 32: 760-765. doi:10.2136/sssaj1968.03615995003200060020x
- Lambe, T. W. 1960. A mechanistic picture of the shear strength of clay, in: *Proceedings of the Research Conference on the Shear Strength of Cohesive Soils*, June 1960, Boulder, Colorado, US, ASCE, New York, 437.
- Lancaster, S., Nolin, A., Copeland, E., and Grant, G., 2012. Periglacial debris-flow initiation and susceptibility and glacier recession from imagery, airborne LiDAR, and ground-based mapping, *Geosphere*, 8(2): 417-430. doi:10.1130/GES00713.1
- Lambe, T.W., Whitman, R.V. 1969. Soil mechanics. John Wiley and Sons, New York.
- Lan, H. 2004. Rainfall-induced landslide stability analysis in response to transient pore pressure - A case study of natural terrain landslide in Hong Kong, *Science in China Series E Technological Sciences*, 46(7) 52-68. doi:10.1360/03ez0018

- Leach, B., and Herbert, R. 1982. The genesis of a numerical model for the study of the hydrology of a steep hillside in Hong Kong, *Quarterly Journal of Engineering Geology and Hydrogeology*, 15(3): 243-259.
- Lee, E.M. 2011. Reflections on the decadal-scale response of coastal cliffs to sea-level rise, *Quarterly Journal of Engineering Geology and Hydrogeology*, 44(4): 481-489. doi:10.1144/1470-9236/10-063
- Legg, N.T., Meigs, A.J., Grant, G.E., and Kennard, P. 2014. Debris flow initiation in proglacial gullies on Mount Rainier, Washington, *Geomorphology*, 226(1): 249-260. doi:10.1016/j.geomorph.2014.08.003
- Leong, E.C., and Rahardjo, H. 1997. Review of Soil-Water Characteristic Curve Equations, *Journal of Geotechnical and Geoenvironmental Engineering*, 123 (12): 1106-1117. doi:10.1061/(ASCE)1090-0241(1997)123:12(1106)
- Leong, E.-C., Tripathy, S., and Rahardjo, H. 2003. Total suction measurement of unsaturated soils with a device using the chilled-mirror dew-point technique, *Geotechnique*, 53 (2): 173-182. doi:10.1680/geot.2003.53.2.173.
- Leong, E. C., Tripathy, S., and Rahardjo, H. 2004. A modified pressure plate apparatus, *ASTM Geotechnical Testing Journal*, 27(3): 322–331. doi:10.1520/GTJ11053.
- Leong, E., and Abuel-Naga, H. 2018. Contribution of osmotic suction to shear strength of unsaturated high plasticity silty soil, *Geomechanics for Energy and the Environmen*, 15: 65-73. <https://doi.org/10.1016/j.gete.2017.11.002>.
- Li, A.J., Merifield, R.S., and Lyamin, A.V. 2011. Effect of rock mass disturbance on the stability of rock slopes using the Hoek–Brown failure criterion, *Computers and Geotechnics*, 38(4): 546-558. doi:10.1016/j.compgeo.2011.03.003
- Li, A.G., Yue, Z.Q., Tham, L.G., Lee, C.F., Law, K.T. 2005. Field-monitored variations of soil moisture and matric suction in a saprolite slope, *Canadian Geotechnical Journal*, 42(1): 13-26. doi:10.1139/t04-069
- Likos, W. 2014. Effective stress in unsaturated soil: accounting for surface tension and interfacial area, *Vadose Zone Journal*, 13(5): 12. doi:10.2136/vzj2013.05.0095
- Li, X., Zhang, L.M., and Fredlund, D.G. 2009. Wetting front advancing column test for measuring unsaturated hydraulic conductivity, *Canadian Geotechnical Journal*, 46(12): 1431-1445. doi:10.1139/T09-072
- Logar, J., Fifer Bizjak, K., Kočevár, M., Mikoš, M., Ribičič, M., and Majes, B. 2005. History and present state of the Slano Blato Landslide, *Nat Hazards Earth System Sciences*, 5: 447–457. doi:10.5194/nhess-5-447-2005

- Lourenço, S., Toll, D.G., Augarde, C.E., Gallipoli, D., Congreve, A., Smart, T., and Evans, F.D. 2008. Observations of unsaturated soils by Environmental Scanning Electron Microscopy in dynamic mode, in *Proceedings of the 1st European Conference on Unsaturated Soils, E-UNSAT 2008, Unsaturated soils: advances in geo-engineering*, 2-4 July 2008. Durham, United Kingdom, Abingdon, Oxon: Taylor & Francis: 145-150. doi:10.1201/9780203884430.ch15
- Lowe, J., and Karafiath, L. 1960. Stability of earth dams upon draw-down, in: H.Y. Fang (Ed.) *Foundation Engineering Handbook*, Springer, Boston, MA, Mexico City: 537-552. doi:10.1007/978-1-4757-5271-7\_10
- Lowe, P.R. 1977. An approximating polynomial for the computation of saturation vapour pressure, *Journal of Agriculture and Forest Meteorology*, 16: 100–103. doi:10.1175/1520-0450(1977)016<0100:AAPFTC>2.0.CO;2
- Lumb, P. 1962. Effect of rain storms on slope stability, in: P. Lumb (Ed.) *Proceedings of the Symposium on Hong Kong Soils*, Hong Kong: 73-87.
- Lu, N., and Griffiths, D.V. 2004. Profiles of Steady-State Suction Stress in Unsaturated Soils, *Journal of Geotechnical and Geoenvironmental Engineering*, 130(10): 1063-1076. doi:10.1061/(ASCE)1090-0241(2004)130:10(1063)
- Lu, N., and Likos, W. J. 2004. Unsaturated soil mechanics. New Jersey: John Wiley & Sons, Inc., Hoboken.
- Lu, N., Wu, B., Tan, C. 2005. A tensile strength apparatus for cohesionless soils, in: A. Tarantino, E. Romero, Y. J. Cui (Eds.) *Proceedings of an International Symposium on Advanced Experimental Unsaturated Soil Mechanics*, 27-29 June 2005, Trento, Italy, Balkema; London: 105-110.
- Lu, N., and Likos, W.J. 2006. Suction Stress Characteristic Curve for Unsaturated Soil, *Journal of Geotechnical and Geoenvironmental Engineering*, 132(2): 131-142. doi:10.1061/(ASCE)1090-0241(2006)132:2(131)
- Lu, N., Wu, B. and C. P. Tan 2007. Tensile strength characteristics of unsaturated sands, *Journal of Geotechnical and Geoenvironmental Engineering*, 133(2): 144–154. doi:10.1061/(ASCE)1090-0241(2007)133:2(144)
- Lu, N. 2008. Is matric suction stress variable?, *Journal of Geotechnical and Geoenvironmental Engineering*, 134(7): 899–905. doi:10.1061/(ASCE)1090-0241(2008)134:7
- Lu, N., and Godt, J.W. 2008. Infinite slope stability under steady unsaturated seepage conditions, *Water Resources Research*, 44(11): 13 pages. doi:10.1029/2008WR006976

- Lu, N., Kim, T.-H., Sture, S., and Likos, W. J. 2009. Tensile strength of unsaturated sand, *Journal of Engineering Mechanics*, 135(12), 1410–1419. doi:10.1061/(ASCE)EM.1943-7889.0000054
- Lu, N., Godt, J.W., and Wu, D.T. 2010. A closed-form equation for effective stress in unsaturated soil, *Water Resources Research*, 46: 1-14. doi:10.1029/2009WR008646
- Lu, N., and Godt, J.W. 2013. Hillslope Hydrology and Stability. Cambridge University Press. doi:10.1017/CBO9781139108164
- Lu, N., Kaya, M., Collins, B.D., and Godt, J. W. 2013. Hysteresis of hydromechanical properties of a silty soil, *Journal of Geotechnical and Geoenvironmental Engineering*, 139(3):207-510. doi:10.1061/(ASCE)GT.1943-5606.0000786.
- Lu, N., and Khorshidi, M. 2015. Mechanisms for soil water retention and hysteresis at high suction range, *Journal of Geotechnical and Geoenvironmental Engineering*, 141(8). doi:10.1061/(ASCE)GT.1943-5606.0001325
- Ljutić, K., Jagodnik, V., Vivoda, M., Dugonjić Jovančević, S., Arbanas, Ž. 2013. The Grohovo Landslide Monitoring System - Experiences from 18 Months Period of Monitoring System Operating, in: S. Mihalić Arbanas, and Ž. Arbanas (Eds.) *Proceedings of the 1st Regional Symposium on Landslides in the Adriatic-Balkan Region "Landslide and Flood Hazard Assessment"*, 6-9 March 2013, Zagreb, Croatia: 45-50.
- Maček, M., Majes, B., and Petkovšek, A. 2016. Lessons learned from 6 years of suction monitoring of the Slano blato landslide, *Rivista Italiana di Geotecnica*, 50(1): 21-33.
- Marinho, F. A. M., Take, W. A., and Tarantino, A. 2008. Measurement of matric suction using tensiometric and axis translation techniques, *Geotechnical and Geological Engineering*, 26(6): 615-631. doi:10.1007/s10706-008-9201-8
- Marinho, F., Oliveira, O., Adem, H., and Vanapalli, S. 2013. Shear strength behavior of compacted unsaturated residual soil, *International Journal of Geotechnical Engineering*, 7(1): 1-9. doi:10.1179/1938636212Z.000000000011
- Marinos, P., and Hoek, E. 2001. Estimating the geotechnical properties of heterogeneous rock masses such as flysch, *Bulletin of Engineering Geology and the Environment*, 60: 85-92.
- Matyas, E. L., and Radhakrishna, H. S. 1968. Volume change characteristics of partially saturated soils, *Geotechnique*, 18(4): 432–448. doi:10.1680/geot.1968.18.4.432
- McCartney, J. 2007. Determination of the hydraulic characteristics of unsaturated soils using a centrifuge permeameter, PhD Dissertation, The University of Texas at Austin.
- McCartney, J. S., Villar, L., and Zornberg, J. G. 2007. Estimation of the hydraulic conductivity function of an unsaturated clay using an infiltration column test, in: *Proceedings of the*



- Sixth Brazilian Symposium on Unsaturated Soils*, 13- November 2007, Salvador, Brazil, 1: 321-328.
- McCartney, J.S., and Zornberg, J.G. 2010. Centrifuge permeameter for unsaturated soils. II: Measurement of the Hydraulic Characteristics of an Unsaturated Clay, *Journal of Geotechnical and Geoenvironmental Engineering*, 136(8): 1064-1076. doi:10.1061/(ASCE)GT.1943-5606.0000320
- Meerdink, J.S., Benson, C.H., and Khire, M. 1996. Unsaturated hydraulic conductivity of two compacted barrier soils, *Journal of Geotechnical Engineering*, 122(7): 565-576. doi:10.1061/(ASCE)0733-9410(1996)122:7(565)
- Mihalić Arbanas, S., Sećanj, M., Bernat Gazibara, S., Krkač, M., Arbanas, Ž. 2017. in: B. Abolmasov, M. Marjanović, M., and U. Đurić (Eds.) *Proceedings of the 2nd Regional Symposium on Landslides in the Adriatic-Balkan Region*, 14-16 May 2015, Belgrade, Serbia: 197-202.
- Miller, D.J., and Nelson, J.D. 2006. Osmotic suction in unsaturated soil mechanics, in: *Proceedings of the 4th International Conference on Unsaturated Soils*, 2-6 April 2006, Carefree, Arizona, US, 2(147): 1382-1393. doi:10.1061/40802(189)114
- Miščević, P., Števančić, D., and Štambuk-Cvitanović, N. 2009. Slope instability mechanisms in dipping conglomerates over weathered marls: Bol landslide, Croatia, *Environmental Geology*, 56(7): 1417-1426. doi:10.1007/s00254-008-1236-x
- Mitchell, J. K. 1976. Fundamentals of soil behavior, Wiley, New York.
- Morgenstern, N.R., and Price, V.E. 1965. The analysis of the stability of general slip surfaces. *Geotechnique*, 15(1): 79-93. doi:10.7939/R3JS9HF63
- Mualem, Y. 1976. Hysteretical models for prediction of the hydraulic conductivity of unsaturated porous media, *Water Resources Research*, 12(6): 1248-1254. doi:10.1029/WR012i006p01248
- Naik, A.P., Ghosh, B., and Pekkat, S. 2018. Estimating soil hydraulic properties using mini disk infiltrometer, *ISH Journal of Hydraulic Engineering*, 25(1): 9 pages. doi:10.1080/09715010.2018.1471363
- Nakhaei, M., and Šimunek, J. 2014. Parameter estimation of soil hydraulic and thermal property functions for unsaturated porous media using the HYDRUS-2D code, *Journal of Hydrology and Hydromechanics*, 621:7-15. doi:10.2478/johh-2014-0008
- Ng, C.W.W., and Shi, Q. 1998. Influence of rainfall intensity and duration on slope stability in unsaturated soils, *Quarterly Journal of Engineering Geology and Hydrogeology*, 31(2): 105-113. doi:10.1144/GSL.QJEG.1998.031.P2.04

- Ng., C.W.W., and Pang, Y.W. 2000. Influence of stress state on soil-water characteristics and slope stability, *Journal of Geotechnical and Geoenvironmental Engineering*, 126(2): 157-166. doi:10.1061/(ASCE)1090-0241(2000)126:2(157)
- Ng, C.W.W., and Menzies, B. 2007. Advanced Unsaturated Soil Mechanics and Engineering. London: Taylor & Francis.
- Nikooee, E., Habibagahi, G., Hassanizadeh, S., and Ghahramani, A. 2012. Effective stress in unsaturated soils: A thermodynamic approach based on the interfacial energy and hydromechanical coupling, *Transport in Porous Media*, 96(2): 369-396. doi:10.1007/s11242-012-0093-y
- Nott, J.F., Thomas, M.F., and Price, D.M. 2001. Alluvial fans, landslides and Late Quaternary climatic change in the wet tropics of northeast Queensland, *Australian Journal of Earth Sciences*, 48(6): 875-882. doi:10.1046/j.1440-0952.2001.00906.x
- Nuth, M., and Laloui, L. 2008. Effective stress concept in unsaturated soils: Clarification and validation of a unified framework, *International Journal for Numerical and Analytical Methods in Geomechanics*, 32(7): 771-801. doi:10.1002/nag.645
- Oh, S., Lu, N., Kim, Y.K., and Lee, S.J. 2012. Relationship between the Soil-Water Characteristic Curve and the Suction Stress Characteristic Curve: Experimental Evidence from Residual Soils, *Journal of Geotechnical and Geoenvironmental Engineering*, 138(1): 1490-1503. doi:10.1061/(ASCE)GT.1943-5606.0000564
- Oh, S., and Lu, N. 2013. Uniqueness of the Suction Stress Characteristic Curve under Different Confining Stress Conditions, *Vadose Zone Journal*, 13(5): vzj2013.04.0077. doi:10.2136/vzj2013.04.0077
- Okada, Y., Sassa, K., and Fukuoka, H. 2004. Excess pore pressure and grain crushing of sands by means of undrained and naturally drained ring-shear tests, *Engineering Geology*, 75(3-4): 325–343. doi:10.1016/j.enggeo.2004.07.001
- Oštrić, M., Ljutić, K., Krkač, M., Setiawan, H., He, B., and Sassa, K. 2012. Undrained Ring Shear Tests Performed on Samples from Kostanjek and Grohovo Landslide, in: K. Sassa, K. Takara, B. He (Eds.) *Proceedings of the IPL Symposium -10th Anniversary Meeting*, 17-20 January 2012, Kyoto, Japan: 47-52.
- Pagano, L., Picarelli, L., Rianna, G., and Urciuoli, G. 2010. A simple numerical procedure for timely prediction of precipitation-induced landslides in unsaturated pyroclastic soils, *Landslides*, 7(3): 279-289. doi:10.1007/s10346-010-0216-x
- Papa, R., and Nicotera, M.V. 2011. Shear strength of a pyroclastic unsaturated soil from suction-controlled direct shear tests, in: E. E. Alonso, A. Gens (Eds.) *Proceedings of the*

- 5<sup>th</sup> *International Conference on Unsaturated Soils*, 6-8 September 2010, Barcelona, Spain, CRC Press, Taylor & Francis Group, London, 347-352. doi:10.1201/b10526-46
- Pasha, A., Khoshghalb, A., and Khalili, N. 2016. Pitfalls in Interpretation of Gravimetric Water Content–Based Soil-Water Characteristic Curve for Deformable Porous Media, *International Journal of Geomechanics*, 16(6): D4015004. Doi:10.1061/(ASCE)GM.1943-5622.0000570
- Pasuto, A., and Silvano, S. 1998. Rainfall as a trigger of shallow mass movements. A case study in the Dolomites, Italy, *Environmental Geology*, 35(2-3): 184-189. doi:10.1007/s002540050
- Peranić, J., Arbanas, Ž., Cuomo, S., and Maček, M. 2018. Soil-Water Characteristic Curve of Residual Soil from a Flysch Rock Mass, *Geofluids*, Article ID 6297819, 2018:15 pages. doi:10.1155/2018/6297819
- Perera, Y., Zapata, C., Houston, W.N., and Houston, S.L. 2005. Prediction of the Soil-Water Characteristic Curve Based on Grain-Size-Distribution and Index Properties, in: E.M. Rathje (Ed.) *Proceedings of the Geo-Frontiers 2005 Conference (Geotechnical Special Publication)*, 24-26 January 2005, Austin, Texas, United States, American Society of Civil Engineers: 12 pages. doi:10.1061/40776(155)4
- Peruccacci, S., Brunetti, M.T., Gariano, S.L., Melillo, M., Rossi, M., and Guzzetti, F. 2017. Rainfall thresholds for possible landslide occurrence in Italy, *Geomorphology*, 290: 39-57. doi:10.1016/j.geomorph.2017.03.031
- Petterson, K. 1955. The Early History of Circular Sliding Surfaces, *Geotechnique*, 5(4): 275-296. doi:10.1680/geot.1955.5.4.275
- Pham, H. Q., and Fredlund, D. G. 2005. A volume-mass constitutive model for unsaturated soils, in: *Proceedings of the Fifty-Eighth Canadian Geotechnical Conference, GeoSask 2005*, 18-21 September 2005, Saskatoon, SK, Canada, 2: 173–181.
- Philip, J. R. 1977. Unitary approach to capillary condensation and adsorption, *The Journal of Chemical Physics*, 66: 5069–5075. doi:10.1063/1.433814
- Pirone, M., Papa, R., Nicotera, M., and Urciuoli, G. 2016. Analysis of safety factor in unsaturated pyroclastic slope, in: S. Aversa, L. Cascini, L. Picarelli, C. Scavia (Eds.); *Proceedings of the 12<sup>th</sup> International Symposium on Landslides, Landslides and Engineered Slopes: Experience, Theory and Practice*, 12-19 June 2016, Napoli, Italy: 1647-1654. doi:10.1201/b21520-204

- Polemio, M., 1997. Rainfall and Senerchia Landslides, Southern Italy. in: *Proceeding of 2nd Panamerican Symposium on Landslides*, 10-14 November 1997, Rio De Janeiro, Brasil, 1: 175–184.
- Pulido-Leboeuf, P. 2004. Seawater intrusion and associated processes in a small coastal complex aquifer (Castell de Ferro, Spain), *Applied Geochemistry*, 19(10): 1517-1527. doi:10.1016/j.apgeochem.2004.02.004
- Qian, X., Gray, D., and Woods, R. 1991. Resonant Column Tests on Partially Saturated Sands, *Geotechnical Testing Journal*, 14(3): 266-275. doi:10.1520/GTJ10571J
- Rahardjo, H., Li, X.W., Toll, D.G, and Leong, E. 2001. The effect of antecedent rainfall on slope stability, *Geotechnical and Geological Engineering*, 19(3-4): 371-399. doi:10.1023/A:101312972
- Rahardjo, H., Lee, T.T., Leong, E.C., and Rezaur, R.B. 2005. Response of a residual soil slope to rainfall, *Canadian Geotechnical Journal*, 42(2): 340-351. doi:10.1139/t04-101
- Rahardjo, H., Ong, T.H., Rezaur, R.B., and Leong, E.C. 2007. Factors controlling instability of homogeneous soil slopes, *Journal of Geotechnical and Geoenvironmental Engineering*, 133(12): 1532-1543. doi:10.1061/(ASCE)1090-0241(2007)133:12(1532)
- Rahardjo, H. Satyanaga, A., Leong, E.C., Ng, Y.S., Foo, M.D., and Wang, C.L. 2007. Slope failures in Singapore due to rainfall, in: J. Ameratunga, B. Taylor, and M. Patten (Eds.) *10th Australia New Zealand Conference on Geomechanics – Common Ground 2007*, 21-24 October 2007, Brisbane, Queensland, Australia, Institution of Engineers: 704-709.
- Rahardjo, H., Nio, A.S., Leong, E.C., and Song, N.Y. 2010. Effects of groundwater table position and soil properties on stability of slope during rainfall, *Journal of Geotechnical and Geoenvironmental Engineering*, 136(11): 1555-1564. doi:10.1061/(ASCE)GT.1943-5606.0000385
- Rahardjo, H., Satyanaga, A., and Leong, E. 2016. Effects of rainfall characteristics on the stability of tropical residual soil slope, in: P. Delage, Y.-J. Cui, S. Ghabezloo, J.-M. Pereira and A.-M. Tang (Eds.) *Proceedings of the 3rd European Conference on Unsaturated Soils “E-UNSAT 2016”*, 12-14 September 2016, Paris, France, 9, 15004. doi:10.1051/e3sconf/20160915004
- Rahimi, A., Rahardjo, H., and Leong, E.-C. 2011. Effect of Antecedent Rainfall Patterns on Rainfall-Induced Slope Failure, *Journal of Geotechnical and Geoenvironmental Engineering*, 137(5): 483-491. doi:10.1061/(ASCE)GT.1943-5606.0000451

- Rahimi, A., Rahardjo, H., and Leong, E.-C. 2015. Effects of soil–water characteristic curve and relative permeability equations on estimation of unsaturated permeability function, *Soils and Foundations*, 55(6): 1400-1411. doi:10.1016/j.sandf.2015.10.006
- Ramos, T.B. Gonçalves, M.C. Martins, J.C. van Genuchten, M.Th., and Pires F.P. 2006. Estimation of soil hydraulic properties from numerical inversion of tension disk infiltrometer data, *Vadose Zone Journal*, 5: 684-696. doi:10.2136/vzj2005.0076
- Rao, S.M., and Shivananda, P. 2005. Role of osmotic suction in swelling of salt amended clays, *Canadian Geotechnical Journal*, 42(1): 307-315. doi:10.1139/t04-086
- Rao, S.M, and Thyagaraj, T. 2007a. Swell compression behavior of compacted clays under chemical gradients, *Canadian Geotechnical Journal*, 44(5): 520-532. doi:10.1139/t07-002
- Rao, S.M., and Thyagaraj, T. 2007b. Role of direction of salt migration on the swelling behaviour of compacted clays, *Applied Clay Science*, 38(1-2): 113-129. doi:10.1016/j.clay.2007.02.005
- Rao, S., Deepak, G.B., Raghuveer Rao, P., and Anbazhagan, P. 2017. Influence of physico-chemical components on the consolidation behavior of soft kaolinites, *Acta Geotechnica*, 12(2): 441-451. doi:10.1007/s11440-016-0478-0
- Rao, S. 2019. Insight into the Role of Osmotic Suction in Soil Behavior, in: K. Ilamparuthi, R. Robinson (Eds.) *Geotechnical Design and Practice. Developments in Geotechnical Engineering*, Singapore, Springer, Singapore: 33-43. doi:10.1007/978-981-13-0505-4\_3.
- Ravanel, L., and Deline, P. 2011. Climate influence on rockfalls in high-Alpine steep rockwalls: The north side of the Aiguilles de Chamonix (Mont Blanc massif) since the end of the ‘Little Ice Age’, *The Holocene*, 21(2): 357-365. doi:10.1177/0959683610374887
- Rawls, W., Brakensiek, D., and Saxton, K., 1982. Estimating soil water properties, *Transactions of the ASAE*, 25(5): 1316-1320.
- Revil, A. and Lu, N. 2013. Unified water isotherms for clayey porous materials, *Water Resources Research*, 49(9): 1-15. doi:10.1002/wrcr.20426.
- Richards, B.G. 1965. Measurement of the free energy of soil moisture by the psychrometric technique using thermistors, in: *Moisture Equilibria and Moisture Changes in Soils Beneath Covered Areas, A Symposium in Print*, Butterworths, Sydney, 39–46.
- Robinson, J.D., Vahedifard, F., and AghaKouchak, A. 2017. Rainfall-triggered slope instabilities under a changing climate: comparative study using historical and projected precipitation extremes, *Canadian Geotechnical Journal*, 54(1): 117-127. doi:10.1139/cgj-2015-0602

- Romero, E. 1999. Characterisation and thermo-mechanical behaviour of unsaturated boom clay: an experimental study. PhD thesis, BarcelonaTech, Universitat Politècnica de Catalunya(UPC), Barcelona, Spain.
- Romero, E. 2001. Controlled suction techniques, in: W.Y.Y. Gehling, and F. Schnaid (Eds.) *4th National Brazilian Symposium on Unsaturated Soils*, ABMS, Brazil: 535-542.
- Rosen, M. J. 1989. Surfactants and interfacial phenomena, 2nd Ed., Wiley, New York.
- Saito, H., Simunek, J., and Mohanty, B.P. 2006. Numerical analysis of coupled water, vapor, and heat transport in the vadose zone, *Vadose Zone Journal*, 5(2): 784-800. doi:10.2136/vzj2006.0007
- Salager, S., El Youssoufi, M., and Saix, C. 2010. Definition and experimental determination of a soil-water retention surface, *Canadian Geotechnical Journal*, 47(6): 609-622. doi:10.1139/T09-123
- Samingan, A. S., Leong, E.-C., and Rahardjo, H. 2003. A flexible wall permeameter for measurements of water and air coefficients of permeability of residual soils, *Canadian Geotechnical Journal*, 40(3): 559-574. doi:10.1139/t03-015
- Santamarina, J.C., Klein, K.A., and Fam, M.A. 2001. Soils and waves, Wiley, New York.
- Santo, A., Di Crescenzo, G., Forte, G., Papa, R., Pirone, M., and Urciuoli, G. 2018. Flow-type landslides in pyroclastic soils on flysch bedrock in southern Italy: the Bosco de' Preti case study, *Landslides*, 15: 63-82. doi:10.1007/s10346-017-0854-3
- Sarma, S. 1973. Stability Analysis of Embankments and Slopes, *Geotechnique*, 23(3): 423-433. doi:10.1680/geot.1973.23.3.423
- Sassa, K., Wang, G., and Fukoka, H. 2003. Performing undrained shear tests on saturated sands in a new intelligent type of ring shear apparatus, *ASTM Geotech Testing Journal*, 26(3): 257-265. doi:10.1520/GTJ11304J
- Sassa, K., Fukuoka, H., Wang, G., and Ishikawa, N. 2004. Undrained dynamic-loading ring-shear apparatus and its application to landslide dynamics, *Landslides*, 1(1): 7-19. doi:10.1007/s10346-003-0004-y
- Sassa, K., and Canuti, P. 2009. Landslides disaster risk reduction. Springer, Berlin Heidelberg.
- Schindler, U. 1980. Ein Schnellverfahren zur Messung der Wasserleitfähigkeit im teilgesättigten Boden an Stechzylinderproben, *Archiv für Acker- und Pflanzenbau und Bodenkunde*, 24: 1-7.
- Schindler, U. Durner, W. von Unold, G. Müller, L., and Wieland, R. 2010. The evaporation method: Extending the measurement range of soil hydraulic properties using the air entry

- pressure of the ceramic cup, *Journal of Plant Nutrition and Soil Science*, 173(4): 563-572. doi:10.1002/jpln.200900201
- Schindler, U., von Unold, G., Durner, W., and Mueller, L. 2015. Recent Progress in Measuring Soil Hydraulic Properties, in: *International Conference on Environment And Civil Engineering (ICEACE'2015)* 24-25 April 2015, Pattaya, Thailand, 47-52.
- Schuster, R.L. 1996. Socioeconomic significance of landslides, in: Turner AK, Schuster RL (Eds.) *Landslides: investigation and mitigation. Transportation research board, special report 247*. National Academy Press, Washington, pp. 12–35.
- Seboong, O., and Lu, N. 2014. Uniqueness of the suction stress characteristic curve under different confining stress conditions, *Vadose Zone Journal*, 13(5):1-10. doi:10.2136/vzj2013.04.0077.
- Sedaghatdoost, A., Ebrahimian, H., and Liaghat, A. 2017. Estimating soil hydraulic and solute transport parameters in subsurface drainage systems using an inverse modelling approach, *Irrigation and Drainage*. 67(S2): 82-90. doi:10.1002/ird.2189
- Sedano, J., Vanapalli, S., and Garga, V. 2007. Modified ring shear apparatus for unsaturated soils testing, *Geotechnical Testing Journal*, 30(1): 39-47. doi:10.1520/GTJ100002
- Segoni, S., Piciullo, L., and Gariano, S. 2018. A review of the recent literature on rainfall thresholds for landslide occurrence, *Landslides*, 15(8): 1483-1501. doi:10.1007/s10346-018-0966-4
- Shaw, D.J. 1992. Colloid and surface chemistry, 4th Ed., Butterworth and Heinemann, Stoneham, Mass.
- Sheng, D., Zhou, A., and Fredlund, D.G. 2011. Shear Strength Criteria for Unsaturated Soils, *Geotechnical and Geological Engineering*, 29(2): 145-159. doi:10.1007/s10706-009-9276-x
- Singh, D.N., and Kuriyan, S.J. 2002. Estimation of hydraulic conductivity of unsaturated soils using a geotechnical centrifuge, *Canadian Geotechnical Journal*, 39(3): 684-694. doi:10.1139/t02-013
- Sisler, H.H., Vanderwerf, C.A., Davidson, A.W. 1953. General Chemistry—A Systematic Approach. Macmillan, New York.
- Skempton, A. W. 1960. Significance of Terzaghi's concept of effective stress, in: L. Bjerrum, A. Casagrande, R. B. Peck, and A. W. Skempton, (Eds.) *From theory to practice in soil mechanics*, Wiley, New York.
- Spencer, E. 1967. A method of analysis of the stability of embankments assuming parallel inter-slice forces, *Geotechnique*, 17(1): 11-26. doi:10.1680/geot.1967.17.1.11

- Spencer, E. 1973. Thrust line criterion in embankment stability analysis, *Geotechnique*, 23(1): 85-100. doi:10.1680/geot.1973.23.1.85
- Sprenger, M., Volkmann, T.H.M., Blume, T., and Weiler, M. 2015. Estimating flow and transport parameters in the unsaturated zone with pore water stable isotopes, *Hydrology and Earth System Sciences*, 19: 2617-2635. doi:10.5194/hess-19-2617-2015
- Sophocleous, M. 2010. Understanding and explaining surface tension and capillarity: an introduction to fundamental physics for water professionals, *Hydrogeol Journal*, 18(4): 811-821. doi:10.1007/s10040-009-0565-5.
- Sun, H.W., Wong, H.N., and Ho, K.K.S. 1998. Analysis of infiltration in unsaturated ground, in: K. S. Li, J. N. Kay, and K. K. S. Ho. (Eds.) *Slope Engineering in Hong Kong*, Balkema, Rotterdam, the Netherlands, 101–109.
- Sun, J., Liu, Q., Li, J., and An, Y. 2009. Effects of rainfall infiltration on deep slope failure, *Science in China Series G: Physics, Mechanics & Astronomy*, 52(1): 108-114. doi:10.1007/s11433-009-0004-6
- Šimunek, J., Šejna, M., and van Genuchten, M., 1996. The HYDRUS-2D software package for simulating water flow and solute transport in two-dimensional variably saturated media. Version 1.0. *IGWMC-TPS-53*, International Ground Water Modeling Center, Colorado School of Mines, Golden, Colorado.
- Šimunek, J., and van Genuchten, M. 1996. Parameter estimation of soil hydraulic properties from the tension disc infiltrometer experiment by numerical inversion, *Water Resources Research*, 32(9): 2683-2696.
- Šimunek, J., van Genuchten, M., Gribb, M.Th., and Hopmans, J.W. 1998. Parameter estimation of unsaturated soil hydraulic properties from transient flow processes, *Soil & Tillage Research*, 47: 27-36. doi:10.1016/S0167-1987(98)00069-5
- Tarantino, A., and Tombolato, S. 2005. Coupling of hydraulic and mechanical behaviour in unsaturated compacted clay, *Geotechnique*, 55(4): 307–317. doi:10.1680/geot.2005.55.4.307
- Tarantino, A. 2009. A water retention model for deformable soils, *Geotechnique*, 59 (9): 751-762. doi:10.1680/geot.7.00118
- Taylor, D. W. 1948. *Fundamentals of Soil Mechanics*, Wiley, New York.
- Thakur, V.K.S., Sreedeeep, S., and Singh, D.N. 2006. Laboratory investigations on extremely high suction, *Geotechnical and Geological Engineering*, 24: 565-578. doi:10.1007/s10706-005-1147-5



- Toll, D. G., Rahardjo, H., and Leong, E. C., 1999. Landslides in Singapore, in: *Proceedings of the International Conference on Landslides, Slope Stability and the Safety of Infra-Structures*, 27-28 July 1999, Singapore, 269-276.
- Toll, D.G. 2001. Briefing: Rainfall-induced landslides in Singapore, in: *Proceedings of the Institution of Civil Engineers - Geotechnical Engineering*, October 2001, 149(4): 211-216. doi:10.1680/geng.2001.149.4.211
- Tosatti, G., Castaldini, D., Barbieri, M., D'Amato Avanzi, G., Giannecchini, R., Mandrone, G., Pellegrini, M., Perego, S., Puccinelli, A., Romeo, R.W., Tellini, C. 2008. Additional causes of seismical related landslides in the Northern Apennines, Italy, *Revista de geomorfologie*, 10: 5-21.
- Tuller, M., Or, D., and Dudley, L. M. 1999. Adsorption and capillary condensation in porous media: Liquid retention and interfacial configurations in angular pores, *Water Resources Research*, 35: 1949–1964. doi:10.1029/1999WR900098
- Tuller, M., and Or, D. 2001. Hydraulic conductivity of variably saturated porous media: Film and corner flow in angular pore space, *Water Resources Research*, 37: 1257–1276, doi:10.1029/2000WR900328.
- Tuller, M., and Or, D. 2005. Water films and scaling of soil characteristic curves at low water contents, *Water Resources Research*, 41 (9): 1-6. doi:10.1029/2005WR004142
- Urciuoli, G., Comegna, L., Di Maio, C., and Picarelli, L. 2016. The Basento valley: a natural laboratory to understand the mechanics of earthflows, *Rivista Italiana Geotecnica*, 50(1): 79-90.
- Van Asch, Th.W.J., Buma, J., and Van Beek, L.P.H. 1999. A view on some hydrological triggering systems in landslides, *Geomorphology*, 30(1): 25-32. doi:10.1016/S0169-555X(99)00042-2.
- van Dam, J.C., Stricker, J.N.M., and Droogers, P. 1992. Inverse method for determining soil hydraulic functions from one-step outflow experiments, *Soil Science Society of America Jour.*, 56(4): 1042-1050. doi:10.2136/sssaj1992.03615995005600040007x.
- van Dam, J.C., Stricker, J.N.M., and Droogers, P. 1994. Inverse method to determine soil hydraulic functions from multi-step outflow experiments, *Soil Science Society of America Journal*, 58(3): 647-652. doi:10.2136/sssaj1994.03615995005800030002x.
- van Genuchten, M. T. 1980. A closed-form equation for predicting the hydraulic conductivity of unsaturated soils, *Soil Science Society of America Journal*, 44(5): 892-898. doi:10.2136/sssaj1980.03615995004400050002x.

- Vanapalli, S.K., Fredlund, D.G., Pufahl, D.E, and Clifton, A.W. 1996. Model for the prediction of shear strength with respect to soil suction, *Canadian Geotechnical Journal*, 33(3): 379-392. doi:10.1139/t96-060.
- Vanapalli, S.K., Sillers, W.S., and Fredlund, M.D. 1998. The meaning and relevance of residual state to unsaturated soils, in: *Proceedings of 51st Canadian Geotechnical Conference*, 4-7 October 1998, Edmonton, Alberta, Canada: 1-8.
- Vanapalli, S.K., Fredlund, D.G., and Pufahl, D.E. 1999. The influence of soil structure and stress history on the soil-water characteristics of a compacted till, *Geotechnique*, 49 (2): 143-159. doi:10.1680/geot.1999.49.2.143.
- van Olphen, H. 1991. Clay colloid chemistry, 2nd Ed., Krieger, Boca Raton, Fla.
- Verwey, E. J. W., and Overbeek, J. TH. G. 1948. Theory of the stability of lyophobic colloids, Elsevier, New York.
- Vivoda, M., Dugonjić Jovančević, S., and Arbanas, Ž. 2013. Landslide Occurrence Prediction in the Rječina River Valley as a Base for an Early Warning System, in: S. Mihalić Arbanas, Ž. Arbanas (Eds.) *Proceedings of the 1st Regional Symposium on Landslides in the Adriatic-Balkan Region*, 7-9 March 2013, Zagreb, Croatia: 85-90.
- Vivoda Prodan, M., and Arbanas, Ž. 2016. Weathering Influence on Properties of Siltstones from Istria, Croatia. *Advances in Materials Science and Engineering*, 2016: 15. doi:10.1155/2016/3073202.
- Vivoda Prodan, M., Mileusnić, M., Mihalić Arbanas, S., and Arbanas, Ž. 2017. Influence of weathering processes on the shear strength of siltstones from a flysch rock mass along the northern Adriatic coast of Croatia, *Bulletin of Engineering Geology and the Environment*, 76(2): 695-711. doi:10.1007/s10064-016-0881-7.
- Vlastelica, G., Miščečević, P., and Štambuk Cvitanović, N. 2018. Durability of soft rocks in Eocene flysch formation (Dalmatia, Croatia), *Engineering Geology*, 245(1): 207-217. doi:10.1016/j.enggeo.2018.08.015.
- Wassar, F., Gandolfi, C., Rienzner, M., Chiaradia, E.A., and Bernardoni, E. 2016. Predicted and measured soil retention curve parameters in Lombardy region north of Italy, *International Soil and Water Conservation Research*, 4(3): 207-214. doi:10.1016/j.iswcr.2016.05.005.
- Watson, K.K. 1966. An instantaneous profile method for determining the hydraulic conductivity of unsaturated porous materials, *Water Resources Research*, 2(4): 709-715. doi:10.1029/WR002i004p00709.

- Wheeler, S. J., and Sivakumar, V. 2000. Influence of compaction procedure on the mechanical behaviour of an unsaturated compacted clay. Part 2: Shearing and constitutive modelling, *Géotechnique*, 50(4): 369-376. doi:10.1680/geot.2000.50.4.369.
- White, N.F., Duke, H.R., Sunada, D.K., and Corey, A.T. 1970. Physics of desaturation in porous materials, *Journal of Irrigation and Drainage Division*, 96(2): 165–191.
- Wieczorek, G.F. 1996. Landslide Triggering Mechanisms, in: A. K. Turner, and R. L. Schuster (Eds.) *Landslides: Investigation and Mitigation*, Transportation Research Board, National Research Council, Special Report, Washington DC, 76-90.
- Wijaya, M., Leong, E. C., and Rahardjo, H. 2015. Effect of shrinkage on air-entry value of soils, *Soils and Foundations*, 55 (1): 166-180. doi:10.1016/j.sandf.2014.12.013.
- Wykeham Farrance, 2010. Instruction Manual: AUTOSHEAR - Direct and residual automatic shear apparatus.
- Wu, X., Chen, X., Zhan, F.B., and Hong, S. 2015. Global research trends in landslides during 1991–2014: a bibliometric analysis, *Landslides*, 12(6): 1215-1226. doi:10.1007/s10346-015-0624-z.
- Xue, K., Ajmera, B., Tiwari, B., and Hu, Y. 2016. Effect of long duration rainstorm on stability of Red-clay slopes, *Geoenvironmental Disasters*, 3:12. doi:10.1186/s40677-016-0046-9.
- Yeh, H.-F., and Tsai, Y.-J. 2018. Effect of variations in long-duration rainfall intensity on unsaturated slope stability, *Water*, 10(4):479. doi:10.3390/w10040479.
- Zachman, D.W., Duchateau, P.C., and Klute, A. 1981. The calibration of the Richards flow equation for a draining column by parameter identification, *Soil Science Society of America Journal*, 45(6):1012-1015. doi:10.2136/sssaj1981.03615995004500060002x
- Zaninović, K., Gajić-Čapka, M., Perčec Tadić, M., Vučetić, M., Milković, J., Bajić, A., Cindrić, K., Cvitan, L., Katušin, Z., Kaučić, D., Likso, T., Lončar, E., Lončar, Ž., Mihajlović, D., Pandžić, K., Patarčić, M., Srnc, L., and Vučetić, V. 2008. Klimatski atlas Hrvatske / Climate atlas of Croatia 1961–1990., 1971–2000. Zagreb: Državni hidrometeorološki zavod.
- Zapata, C. 1999. Uncertainty in Soil-Water Characteristic Curve and Impacts on Unsaturated Shear Strength Predictions. PhD Dissertation, Arizona State University, Tempe, United States.
- Zapata, C., Houston, W.N., Houston, S.L., and Walsh, K. 2000. Soil–water characteristic Curve variability, *Geotechnical Special Publication*, 287(99): 84-124. doi:10.1061/40510(287)7

- Zhang, F., and Fredlund, D. G. 2015. Examination of the estimation of relative permeability for unsaturated soils, *Canadian Geotechnical Journal*, 52(12): 2077-2087. doi:10.1139/cgj-2015-0043.
- Zhang, L.L., Fredlund, D.G., Zhang, L.M., and Tang, W.H. 2004. Numerical study of soil conditions under which matric suction can be maintained, *Canadian Geotechnical Journal*, 41(4): 569-582. doi:10.1139/t04-006.
- Zhang, L.L., Zhang, J., Zhang, L.M., and Tang, W.H. 2011. Stability analysis of a rainfall-induced slope failure: a review, *Geotechnical Engineering*, 164(5): 299-316. doi:10.1680/geng.2011.164.5.299.
- Zhang, L.L., Fredlund, D.G., Fredlund, M.D., and Wilson, G.W. 2014. Modeling the unsaturated soil zone in slope stability analysis, *Canadian Geotechnical Journal*, 51: 1-15. doi:10.1139/cgj-2013-0394.
- Zhang, M., Ng, C.W.W. 2003. Interim Factual Testing Report I-SG30 & SR30. Hong Kong University of Science & Technology.
- Zhang, X., Mavroulidou, M., and Gunn, M.J. 2017. A study of the water retention curve of lime-treated London Clay, *Acta Geotechnica*, 12(1): 23-45. doi:10.1007/s11440-015-0432-6.
- Zhan, T.L.T., and Ng, C.W.W. 2004. Analytical analysis of rainfall infiltration mechanism in unsaturated soils, *International Journal of Geomechanics*, 4(4): 273-284. doi:10.1061/(ASCE)1532-3641(2004)4:4(273).
- Zhao, N., Hu, B., Yi, Q., Yao, W., and Ma, C. 2017. The Coupling Effect of Rainfall and Reservoir Water Level Decline on the Baijiabao Landslide in the Three Gorges Reservoir Area, China, *Geofluids*, 2017: 12. doi:10.1155/2017/3724867.
- Zornberg, J.G, and McCartney, J.S. 2010. Centrifuge Permeameter for Unsaturated Soils. I: Theoretical Basis and Experimental Developments, *Journal of Geotechnical and Geoenvironmental Engineering*, 136(8): 1051-1063. doi:10.1061/(ASCE)GT.1943-5606.0000319.



## List of figures

<b>Figure 1:</b>	LIDAR-derived bare-earth DTM of the Rječina River Valley with contours of historical (yellow) and more recent (red) landslides. The zones colored in red and yellow represent the areas of the Grohovo Landslide from 1996, and the Valići Landslide reactivated on 13 February 2014, respectively (modified from Arbanas et al. 2017).....	20
<b>Figure 2:</b>	Results of preliminary investigations: a) landslide map; and b) engineering geological cross-section of the historic and reactivated Valići Landslide (modified from Mihalić Arbanas et al. 2017). ....	21
<b>Figure 3:</b>	a) Sampling pit; b) half of the oven-dried specimen from a depth of 0.75 m. ....	22
<b>Figure 4:</b>	Map of the reactivated landslide on a detailed topographic map with sampling locations and borehole B1 and B2 locations (modified from Mihalić Arbanas et al. 2017).....	24
<b>Figure 5:</b>	GSD results for samples collected at ten locations along the landslide body and slope.....	25
<b>Figure 6:</b>	Plasticity chart of the samples. ....	25
<b>Figure 7:</b>	Collection of near-surface soil samples by using the equipment for undisturbed soil sampling (Eijkelkamp Soil&Water, Inc.) for determination of natural water content and basic physical properties. Sampling depths (0.05; 0.25; 0.45; 0.75; and 1.05 m) are indicated below samples in Figure 7 d). ....	26
<b>Figure 8:</b>	Determination of a) natural water content; b) degree of saturation; and c) volumetric water content for superficial soil at sampling pit location (B1) during various field investigations.....	29
<b>Figure 9:</b>	Core samples obtained by machine-drilling at the B1 location with marked depths. ....	30
<b>Figure 10:</b>	Details of a) inclinometer chasing installation at the B1 location; b) portable inclinometer measuring system Digitilt Classic Inclinometer System (Durham Geo-Enterprises, Inc.); and c) measurements in progress. ....	32
<b>Figure 11:</b>	Inclinometer surveys at the B1 location. ....	33

<b>Figure 12:</b> Collection of continuous groundwater pressure measurements at the B2 location: a) Rugged TROLL 100 Data Logger and BaroTROLL Data Logger (In-Situ Inc.), and b) TROLL Docking Station for periodical download of the recorded data with the Win-Situ 5 software (In-Situ Inc.).....	34
<b>Figure 13:</b> Groundwater level and atmospheric pressure measurements expressed as the pressure height.....	34
<b>Figure 14:</b> The mean annual air temperature for Croatia (Zaninović et al. 2008). ....	36
<b>Figure 15:</b> Comparison of the average air temperature in Rijeka for the period from 1948 to 2017 ( <a href="http://meteo.hr/klima_e.php?section=klima_pracenje&amp;param=srednja_temperatura&amp;Grad=ri_en_sred&amp;Godina=2018">http://meteo.hr/klima_e.php?section=klima_pracenje&amp;param=srednja_temperatura&amp;Grad=ri_en_sred&amp;Godina=2018</a> ). ....	37
<b>Figure 16:</b> The mean annual precipitation for Croatia (Zaninović et al. 2008). ....	38
<b>Figure 17:</b> Cumulative annual precipitation analized for the period from 1957 to 2015 for the meteorological station of Kozala, Rijeka (data obtained on request from DHMZ). ....	39
<b>Figure 18:</b> Cumulative precipitation summarized from a) the start of September till the end of February (wet part of the season); and b) from the start of March till the end of August for the period analyzed (1957 to 2015).....	41
<b>Figure 19:</b> Precipitation characteristic of the latest years with extreme quantities during the wet period of the season (September to March): a) cumulative precipitation; b) a number of days with precipitation and number of days with precipitation intensity higher than $ks$ ; c) $2\ ks$ ; and d) $4ks$ of the soil. ....	42
<b>Figure 20:</b> Precipitation measurements in period preceding the landslide event: daily rainfall for the period 1 September 2013 to 14 February 2014.....	42
<b>Figure 21:</b> Average air temperatures in Croatia for a) summer 2013; b) autumn 2013; and c) winter 2013/2014 compared with the corresponding multi-annual average in the period from 1961 to 1990, according to the DHMZ ( <a href="http://meteo.hr/klima_e.php?section=klima_pracenje&amp;param=ocjena">http://meteo.hr/klima_e.php?section=klima_pracenje&amp;param=ocjena</a> ). ....	43
<b>Figure 22:</b> Average precipitation amounts in Croatia for a) summer 2013; b) autumn 2013; and c) winter 2013/2014 compared with the corresponding multi-annual average in the period from 1961 to 1990, according to the DHMZ ( <a href="http://meteo.hr/klima_e.php?section=klima_pracenje&amp;param=ocjena">http://meteo.hr/klima_e.php?section=klima_pracenje&amp;param=ocjena</a> ). ....	43

<b>Figure 23:</b> An element of unsaturated soil consisting of solid particles, water, air, and contractile skin (left), and phase diagram (right) describing volume and mass relations for unsaturated soil (Fredlund et al. 2012). .....	46
<b>Figure 24:</b> Surface tension phenomenon at the air-water interface: intermolecular forces acting in the contractile skin and interior of water, and tension forces associated with a curved two-dimensional surface (modified from Fredlund et al. 2012).....	51
<b>Figure 25:</b> Physical model of capillarity (Fredlund et al. 2012). .....	52
<b>Figure 26:</b> The Environmental Scanning Electron Microscope micrographs of silica spheres with indicated pressures along the air-water interface (water menisci) and measurable contact angle (modified from Lourenço et al. 2008).....	54
<b>Figure 27:</b> Theoretical relationship between relative humidity, $RH$ , and total suction, $\psi$ , according to Kelvin's equation for a constant temperature of 20° C (293.16 K)..	55
<b>Figure 28:</b> Total, matric, and osmotic suction measurements on compacted Regina clay (Krahn and Fredlund 1972). .....	57
<b>Figure 29:</b> Pressure plate extractors and volumetric pressure plate extractors with hysteresis attachments used at the UniSa, Italy. ....	64
<b>Figure 30:</b> Suction-controlled oedometer devices: a) the Hydrocon consolidation cell (Controls S.p.A.) at the UniRi, and b) the suction-controlled oedometer apparatus (SCOED) at the UniSa. ....	65
<b>Figure 31:</b> The HYPROP evaporation method device (Decagon Devices Inc.): a) test performed at UniLj, and b) pre-conditioned mini-tensiometers and saturated undisturbed specimen. ....	66
<b>Figure 32:</b> The WP4-T (Decagon Devices Inc.) potentiometer device used at UniLj: a) soil suction, and b) density measurements performed on undisturbed sample undergoing the wetting process. ....	68
<b>Figure 33:</b> SWRC in terms of a) gravimetric water content; b) volumetric water content for the drying and wetting process. Symbol (RS) indicates remolded samples; all other samples are undisturbed (Peranić et al. 2018). ....	70
<b>Figure 34:</b> Drying and wetting paths of the SWRC-S in the a) semi-log and b) log-log form (Peranić et al. 2018).....	71
<b>Figure 35:</b> $S$ - $\psi$ - $e$ measurements obtained using the WP4-T and pressure plate extractor apparatus (Peranić et al. 2018). ....	73



<b>Figure 36:</b> Results in terms of $\sigma' - e$ compared with the conventional oedometer test results for the a) UVH-1, OEUVCI03w and OEUVCI03; b) RP-3se1 and RP4-se8 tests (Peranić et al. 2018).....	74
<b>Figure 37:</b> Results in terms of $\sigma' - e$ compared with the conventional oedometer test results for the WP4-T-1 and WP4-T-2 tests (Peranić et al. 2018).....	75
<b>Figure 38:</b> Best-fit Brooks and Corey (1964), van Genuchten (1980) and Fredlund and Xing (1994) equations plotted with the measurements in $\psi - \theta$ plane (Peranić et al. 2018). .....	78
<b>Figure 39:</b> Performance of the two prediction models compared with the Fredlund and Xing (1994) equation obtained by using the non-linear regression procedure on the measured data (Peranić et al. 2018).....	80
<b>Figure 40:</b> Measurements on glass beads undergoing drying and wetting process: a) permeability functions, and b) SWRC (Mualem 1976). ....	83
<b>Figure 41:</b> a) The schematic of soil column (McCartney et al. 2007), and b) wetting front advancement process in an initially air-dried soil column during the capillary-rise process (Li et al. 2009). ....	86
<b>Figure 42:</b> a) A schematic of the flexible-wall permeameter for unsaturated soils (ASTM D7664-10); and, b) limitation of the axis translation technique for determination of the UHCF (Fredlund et al. 2012).....	87
<b>Figure 43:</b> Coefficient of permeability respective to the water phase vs. matric suction obtained from flexible-wall permeability tests (Huang et al. 1998). ....	88
<b>Figure 44:</b> Centrifuge permeameter setup: a) testing environment and data acquisition hub; and b) schematic view of a centrifuge permeameter (Zornberg and McCartney 2010). .....	90
<b>Figure 45:</b> Devices used for measurements of the saturated coefficient of permeability $k_s$ in the Geotechnical laboratory at UniRi: a) front-loading oedometer apparatus 26-WF0302 (Controls S.p.A.) ( <a href="http://www.controls-group.com/eng/soil-mechanics-testing-equipment/permeability-system-using-triaxial-cell.php">http://www.controls-group.com/eng/soil-mechanics-testing-equipment/permeability-system-using-triaxial-cell.php</a> ); b) sketch of the permeability system using the triaxial apparatus 28-WF4050 (Controls S.p.A.), and c) undisturbed specimen with side drains after the permeability test.....	101
<b>Figure 46:</b> Samples used for determination of the saturated coefficient of permeability: a) undisturbed, and b) completely remolded and consolidated. ....	102
<b>Figure 47:</b> Schematic illustration of the HYPROP (Hydraulic PROPerTy analyzer) device (Schindler et al. 2015). ....	104

<b>Figure 48:</b> The saturated coefficient of permeability vs. effective (vertical or mean) stress for undisturbed and remolded samples of residual soil from a flysch rock mass. ....	106
<b>Figure 49:</b> The saturated coefficient of permeability vs. void ratio for undisturbed and remolded samples of residual soil from a flysch rock mass.....	106
<b>Figure 50:</b> Coefficient of permeability respective to the water phase calculated from the HYPROP evaporation method device (Decagon Devices Inc.). ....	107
<b>Figure 51:</b> The UHCFs of residual soil from a flysch rock mass estimated from the drying and wetting SWRCs and the saturated coefficient of permeability $k_s$ obtained for undisturbed samples. ....	107
<b>Figure 52:</b> Relationship between shear strength and matric suction for different values of net stress (Kim et al. 2010).....	111
<b>Figure 53:</b> Various forms for the effective stress parameter as a function of the degree of saturation (modified from Lu and Likos 2006). ....	114
<b>Figure 54:</b> Stress state at the point of the unsaturated element of soil and two independent stress tensors: net stress and matric suction (modified from Fredlund et al. 2012). ....	116
<b>Figure 55:</b> Extended Mohr-Coulomb failure envelope for unsaturated soils (from Ng and Menzies 2007 after Fredlund and Rahardjo 1993).....	117
<b>Figure 56:</b> Shear strength results obtained from unsaturated glacial till specimens GT-16-N4 using the modified direct shear apparatus: a) failure envelope on $\tau$ vs. $ua - uw$ plane and b) corresponding $\phi^b$ values (Gan et al. 1988).....	118
<b>Figure 57:</b> Relationship of SWRC to shear strength envelope for different types of soil: a) desaturation zones along the SWRC, and b) variation in shear strength envelopes for different soils in different desaturation zones (Fredlund et al. 2012).....	119
<b>Figure 58:</b> Microscopic representation of interparticle force equilibrium: a) and b) REV for saturated; c) and d) REV for an unsaturated fine-grained soil system (Lu and Likos 2006).....	121
<b>Figure 59:</b> Conceptual behavior and magnitude of the interparticle stress components as a function of a) particle size, and b) degree of saturation (Lu and Likos 2006). ...	123
<b>Figure 60:</b> Conceptual illustration of behavioral regimes for a) SWRC; b) SSCCs for sand and clay in the form $\sigma'_s(\theta)$ ; and c) in the form $\sigma'_s ua - uw$ (Lu and Likos 2006)...	124
<b>Figure 61:</b> Comparison of a) SWRC and b) SSCC ( $ua - uw$ ) of residual soil from a flysch rock mass with varying soils textures represented with common SWRC parameter values.....	127

<b>Figure 62:</b> Sketch of assumed simplified process of emptying and filling of soil pores and corresponding variation of wetted surface area with water potential (Greco and Gargano 2015).	130
<b>Figure 63:</b> Hume Dam clay soil a) SWRC data from Khalili et al. (2004), and b) suction stress results: dots indicate experimentally obtained values, while lines represent the theoretical expression for the suction stress based on the approach proposed by Greco and Gargano (2015).	132
<b>Figure 64:</b> Comparison of different expressions for the SSCC curve: dots represent the values calculated from the experimental data; the solid lines represent the wet area index approach; the dotted lines represent the approach proposed by Khalili and Khabbaz (1998); the dashed lines the relationship proposed by Lu et al. (2010) (Greco and Gargano, 2015).	133
<b>Figure 65:</b> Some details on collection of undisturbed soil specimens from the a) sampling pit by insertion of b) hard plastic tubes or c) steel cutter for testing in direct shear apparatus.	135
<b>Figure 66:</b> The procedure of collecting the undisturbed soil samples for testing in direct shear apparatus by using the steel cutters directly in-situ: a) 60x60 specimen in cutter; b) specimen extrusion into the perforated styrofoam box with removable upper and lower lids; c) sealing of the sample to minimize the water loss due to evaporation; and d) separation of a single specimen for the installation in testing device. ....	136
<b>Figure 67:</b> The AutoShear Machine 27-WF2160 (Controls S.p.A.) used in the Geotechnical laboratory at the UniRi, during the consolidation stage. ....	137
<b>Figure 68:</b> Details of conventional direct shear tests on undisturbed specimens of residual soil: a) installation of undisturbed specimen collected by insertion of circle steel cutter directly in-situ; b) undisturbed specimen with visible weathered grain of siltstone at the shearing plane; and c) undisturbed specimen during the shearing stage in conventional direct shear apparatus. ....	138
<b>Figure 69:</b> Details of the adopted specimen preparation technique: a) collection of the material after testing the undisturbed specimen for water content determination; b) material thoroughly mixed with de-aired water left to rest over-night; c) installation of sample inside the square cutter; and d) remolded specimen ready for the installation in direct shear apparatus. ....	139

<b>Figure 70:</b> Consolidation stage test results for undisturbed (solid line) and remolded (dashed line) specimens. Black, red, and green colors represent 50, 100, and 200 kPa of vertical stress, respectively.....	140
<b>Figure 71:</b> Shear stage test results for undisturbed (solid line) and remolded (dashed line) specimens at different vertical stress values in terms of a) horizontal displacement vs. shear stress and b) horizontal displacement vs. vertical displacement. Black, red, and green colors represent 50, 100, and 200 kPa of vertical stress, respectively. ....	141
<b>Figure 72:</b> Mohr-Coulomb shear strength envelopes for undisturbed (solid line, filled markers) and remolded specimens (dashed line, empty markers), obtained in conventional direct shear apparatus. ....	142
<b>Figure 73:</b> Remolded specimen dismantled from direct shear apparatus after the test with visible highly weathered siltstone particle crushed on the shearing plane.....	143
<b>Figure 74:</b> Suction Controlled Direct Shear Apparatus (SCDSA) (Megaris s.a.s.) used in the Geotechnical laboratory at the UniSa.....	144
<b>Figure 75:</b> Scheme of pressure regulation circuits and transducers used in the suction-controlled direct shear apparatus (Papa and Nicotera 2011). ....	145
<b>Figure 76:</b> Initial suction measurement stage for the natural water content in the DSUVCJ01 test in terms of a) measured stress values with calculated matric suction value; b) measured axial strain and water volume change with calculated variables: void ratio, volumetric water content and degree of saturation. ....	147
<b>Figure 77:</b> Results for the consolidation stage in the DSUVCJ01 test in terms of a) measured stress values with calculated matric suction value; b) measured axial strain and water volume change with calculated variables: void ratio, volumetric water content and degree of saturation. ....	149
<b>Figure 78:</b> Equilibration of the specimen from the DSUVCJ02 tests at 36 kPa of matric suction after the consolidation at 200 kPa of net vertical stress, in terms of a) measured stress values, calculated matric suction value, and volume of water drained from the specimen; b) measured axial strain with calculated variables: void ratio and volumetric water content. ....	150
<b>Figure 79:</b> Some details of Suction Controlled Direct Shear Apparatus used at the UniSa: a) undisturbed sample collected with cutter in-situ; b) disassembled steel chamber with saturated HAEPD; c) installed sample with the attachment for the wetting test	

connected through the top cap; and d) undisturbed specimen after the shearing stage.....	151
<b>Figure 80:</b> Heterogeneity of the undisturbed samples: siltstone grains of different size and weathering degree, along with some roots present at the shear surface of the specimen used in the DSUVCJ01 test. ....	152
<b>Figure 81:</b> Back pressurized direct shear apparatus for soil testing in unsaturated conditions (GDS Instruments Ltd.) in Geotechnical laboratory of Faculty of Civil Engineering, UniRi. ....	153
<b>Figure 82:</b> Schematic of the UGDSBPS fully equipped for testing in unsaturated conditions options ( <a href="http://www.gdsinstruments.com">www.gdsinstruments.com</a> ).....	153
<b>Figure 83:</b> Preparation of undisturbed specimen for testing in the UGDSBPS collected in-situ with dimensions 100x100x20 mm. ....	155
<b>Figure 84:</b> Saturation of undisturbed specimens used in the UGDSBPS a) outside the shearbox by submersion in de-aired water along with the cutter, filter papers and steel plate at the top of specimen; b) inside the shear box by adding water from the top and bottom.....	155
<b>Figure 85:</b> Results from the UVSCDS02 test for the initial suction measurement, consolidation, and equilibration at 174 kPa of matric suction in terms of a) applied and measured net vertical stress, pore air, pore water pressure, and matric suction in semi-log graph; and, b) change of the specimen height, volume of water in the specimen, void ratio, degree of saturation and volumetric water content for all stages in terms of absolute duration of test. ....	159
<b>Figure 86:</b> Detail of suction measurement from UVSCDS04 test for undisturbed specimen at natural water content collected at the end of July 2017. ....	161
<b>Figure 87:</b> Adopted procedure for installation of undisturbed specimens at natural water content a) collected in-situ directly with cutter; and b) extrusion into the UGDSBPS apparatus.....	162
<b>Figure 88:</b> Undisturbed specimen used in the wetting tests installed into the UGDSBPS apparatus at a natural water content. ....	162
<b>Figure 89:</b> Results obtained for shear stage using all three direct shear test devices under 50 kPa of net vertical stress, in terms of a) shear stress; b) vertical displacement; c) degree of saturation; and, d) change of volume of water vs. horizontal displacement. ....	164

<b>Figure 90:</b> Shear stage tests results obtained from conventional and modified direct shear devices under 100 kPa of net vertical stress, in terms of a) shear stress; b) vertical displacement; c) degree of saturation; and d) change of volume of water vs. horizontal displacement.....	166
<b>Figure 91:</b> Shear stage tests results obtained from conventional and modified direct shear devices under 200 kPa of net vertical stress, in terms of a) shear stress; b) vertical displacement; c) degree of saturation; and d) change of volume of water vs. horizontal displacement.....	168
<b>Figure 92:</b> Shear strength test results in terms of the Bishop's effective stress formulation (Bishop 1959), obtained on undisturbed samples of residual soil from a flysch rock mass by using conventional (DSD) and modified (SCDSA and UGDSBPS) direct shear test apparatuses. ....	173
<b>Figure 93:</b> Heterogeneity at the shearing plane of undisturbed samples: a) occasional presence of roots and siltstone fragments of different weathering degree and size, and b) limestone fragment. ....	173
<b>Figure 94:</b> Failure envelope obtained from conventional and modified direct shear tests performed on undisturbed samples, projected onto: a) $\tau$ versus $(u_a - u_w)$ plane; and b) $\tau$ versus $(\sigma - u_a)$ plane. ....	174
<b>Figure 95:</b> Experimentally obtained shear strength test results for quantification of the SSCC (Lu and Likos 2006) of residual soil from a flysch rock mass.....	175
<b>Figure 96:</b> SSCC of residual soil from a flysch rock mass presented by closed-form expression (68) and experimentally obtained values from direct shear tests. ....	176
<b>Figure 97:</b> Change of the void ratio and volumetric water content during the application of shear stress under 50 kPa of net vertical stress in the UVSCDS11 test. ....	178
<b>Figure 98:</b> Matric suction, horizontal displacement, the degree of saturation and volume of water inside the specimen during the a) wetting stage, and b) yielding of the specimen in the UVSCDS11 test.....	179
<b>Figure 99:</b> Change of the volumetric water content, void ratio and degree of saturation vs. horizontal displacement for the wetting part of the UVSCDS11 test. ....	180
<b>Figure 100:</b> Change of the void ratio and volumetric water content during the application of shear stress under 100 kPa of net vertical stress in the UVSCDS12 test.....	181
<b>Figure 101:</b> Initial suction measurement, consolidation, equilibration at 370 and 331 kPa of matric suction and application of shear stress vs. time for the UVSCDS12 test. ....	181

<b>Figure 102:</b> Reduction of the matric suction, horizontal displacement, degree of saturation and volume of water inside the specimen during the wetting stage vs. a) absolute duration of the test, and change of the void ratio, volumetric water content and degree of saturation vs. b) horizontal displacement in the UVSCDS11 test. ...	183
<b>Figure 103:</b> Matric suction, horizontal displacement, degree of saturation and volume of water inside the specimen during the yielding of the specimen in the UVSCDS12 test. ....	184
<b>Figure 104:</b> Stress paths from UVSCDS11 and UVSCDS12 wetting test with saturated envelope and shear strength test results obtained by using different direct shear devices.....	185
<b>Figure 105:</b> Initial and final volumetric water contents from UVSCDS11 and UVSCDS12 wetting tests plotted on derived SWRC curve in $\theta - (u_a - u_w)$ form. ....	185
<b>Figure 106:</b> Liquid water, vapor, and overall permeability coefficients with respect to soil suction for silty sand (from Fredlund et al. 2012 after Ebrahimi-Birang et al. 2004). ....	199
<b>Figure 107:</b> Estimated UHCFs for the suction range considered in performed analyses. ....	199
<b>Figure 108:</b> Back analysis for determination of critical slip surface with experimentally obtained shear strength parameters. ....	201
<b>Figure 109:</b> Initial and boundary conditions, and discretization with mixed unstructured finite element mesh for calculation of infiltration process using SEEP/W (GEO-SLOPE International, Ltd). ....	202
<b>Figure 110:</b> Measured and derived precipitation data used for determination of a flux boundary condition for seepage analysis in form of: a) ten-minute; b) hourly; and c) daily rainfall with cumulative amount of precipitation in the period from 1 September 2013 until landslide reactivation on 13 February 2014. ....	203
<b>Figure 111:</b> Water flux boundary condition used in infiltration analysis with SEEP/W in form of: a) ten-minute; b) hourly; and c) daily rainfall with cumulative amount of precipitation in the period from September 2013 until landslide activation, 13 February 2014. ....	204
<b>Figure 112:</b> Initial pore-water pressure distribution in analyzed cross-section of geotechnical profile with imposed 300 kPa of constant matric suction in the uppermost region ( $d=0.5$ m) and the initial FoS for the relevant sliding surface. ....	205

<b>Figure 113:</b> Results for initial and changing values of a) degree of saturation, and b) pore-water pressure distribution along the profile B1 during 167 days of simulation. ....	212
<b>Figure 114:</b> Pore-water pressure distributions along the cross-section of the landslide and the corresponding FoS value after a) 110; b)140; and c) 160 days of simulation. .	213
<b>Figure 115:</b> Change of shear strength components along the sliding surface due to rainfall infiltration. Starting values and decrease of a) frictional and b) strength component associated with matric suction. ....	214
<b>Figure 116:</b> Factor of safety vs. time for constant (saturated) unit weight and unit weight calculated from the SWRC- $\theta$ .....	215
<b>Figure 117:</b> Factor of safety vs. time for different $\phi b$ values. ....	216
<b>Figure 118:</b> Factor of safety vs. time for a constant (saturated) unit weight and unit weight calculated from the SWRC- $\theta$ with $\phi b = \phi'$ .....	216
<b>Figure 119:</b> Change of slope stability with time for measured 10' precipitation data applied as a flux boundary condition and artificially generated precipitation data with the same pattern as recorded precipitation and flux quantities equal to $q = q_{measured} * n$ , with $n = 0.5, 0.75, 2, 4, 8, 16$ and $32$ . ....	217
<b>Figure 120:</b> Factor of safety vs. time for constant flux boundary condition equal to $q = n * ks$ , with $n = 0.5, 0.75, 1, 2, 4, 8$ , and $16$ . ....	218
<b>Figure 121:</b> Number of days required for the slope to become unstable for different constant flux boundary conditions $q = n * ks$ , with $n = 0.5, 0.75, 1, 2, 4, 8$ , and $16$ . ..	218
<b>Figure 122:</b> Influence of different initial pore-water pressure distributions obtained for applied matric suction values of 100, 200 and 400 kPa in the uppermost region ( $d=0.5$ m): a) change of slope stability with time; b) initial pore-water pressure profile; and c) initial degree of saturation along first 5 m of depth. ....	219
<b>Figure 123:</b> Review of the convergence conditions by plotting the input UHCF and calculated permeability values for each time step of a transient simulation. ....	220





## List of tables

<b>Table 1:</b> Mean values of the basic properties of the residual soil samples used in this study (Peranić et al. 2018).....	22
<b>Table 2:</b> Natural water content determination of near-surface soil by hand-drilling using the equipment for undisturbed soil sampling (Eijkelkamp Soil&Water, Inc.).....	27
<b>Table 3:</b> Natural water content determination during machine borehole drilling at sampling pit location. ....	28
<b>Table 4:</b> Average, maximum and minimum monthly and annual precipitation amounts analyzed for the period 1958-2015, according to DHMZ data for the meteorological station Kozala (Rijeka). ....	39
<b>Table 5:</b> Surface tension of contractile skin at various temperatures (Kaye and Lany 1973). ....	51
<b>Table 6:</b> Best-fit parameters and SSR values for the Brooks and Corey (1964) and van Genuchten (1980) three-parameter equations (Peranić et al. 2018). ....	78
<b>Table 7:</b> Best-fit parameters and SSR values for the four-parameter equations: the van Genuchten (1980) and Fredlund and Xing (1994) equations (Peranić et al. 2018). ....	79
<b>Table 8:</b> Fredlund and Xing (1994) equation parameters and SSR values obtained using the Zapata (1999) and Perera (2005) SWRC correlation models (Peranić et al. 2018). ....	80
<b>Table 9:</b> Water content, the degree of saturation and void ratio for specimens tested in HYPROP device. ....	103
<b>Table 10:</b> The saturated coefficient of permeability from falling head tests performed in standard oedometer apparatus.....	104
<b>Table 11:</b> The saturated coefficient of permeability from constant head tests performed in conventional triaxial apparatus with attachments for permeability tests.....	105
<b>Table 12:</b> Common values of van Genuchten's SWRC parameters for different soil textures (sand, silt, and clay) and values of the soil investigated in this study used in Figure 61. ....	126
<b>Table 13:</b> Basic geotechnical properties and residual shear strength parameters of flysch samples with different weathering grades and obtained from various parts of the	

Rječina River Valley in previous studies by Oštrić et al. (2012) and Vivoda Prodan and Arbanas (2016).....	134
<b>Table 14:</b> Test characteristics of conventional direct shear tests performed on undisturbed and remolded specimens.....	139
<b>Table 15:</b> Test characteristics of direct shear tests performed on undisturbed specimens using the Suction Controlled Direct Shear Apparatus in the Geotechnical laboratory at the UniSa. ....	151
<b>Table 16:</b> Summary of tests performed in the UGDSBPS at the UniRi with test labels, measured initial characteristics of tested specimens and definition of applied test conditions. ....	158
<b>Table 17:</b> Conditions at failure for all direct shear tests. ....	172
<b>Table 18:</b> Determination of the apparent tensile stress and effective cohesion from the conventional direct shear test results performed on undisturbed samples.....	175
<b>Table 19:</b> Determination of the suction stress from suction-controlled direct shear test results performed on undisturbed samples.....	176
<b>Table 20:</b> LEMs available in SLOPE/W with an indication of satisfied static equations and interslice force characteristics (modified form GEOSLOPE International 2017). ....	208
<b>Table 21:</b> Material properties for slope stability analysis in SLOPE/W.....	210

## **Curriculum vitae**



## Josip Peranić

Born on 5 October 1987 in Rijeka, Croatia. He graduated from the Faculty of Civil Engineering, University of Rijeka, obtaining a master's degree in civil engineering in 2011. He enrolled in the Postgraduate doctorate study program in Civil Engineering at the Faculty of Civil Engineering, University of Rijeka. In his PhD research, he investigates the importance of the unsaturated zone on rainfall-induced landslides in flysch deposits under the mentorship of Prof. Arbanas. His research is focused primarily on studying the landslide mechanisms in saturated and unsaturated conditions by using experimental laboratory procedures, field measurements and monitoring techniques, and numerical modeling.

In 2016 and 2017 he spent a total of three months at the University of Salerno, Italy, on scientific training in the field of unsaturated soil mechanics. Under the supervision of the Prof. Cuomo, he gained knowledge and experience in numerical modeling of the water flow through unsaturated slopes and laboratory techniques for determination of soil-water retention curves and shear strength characteristics in unsaturated conditions, including the axis-translation based oedometer, direct shear, and triaxial apparatuses, standard and volumetric pressure plate extractors. He gained additional experience in using the laboratory mini-tensiometers and dew-point potentiometer through the laboratory collaboration with Assist. Prof. Maček at the Faculty of Civil and Geodetic Engineering at the University of Ljubljana, Slovenia, within the framework of the Croatian-Slovenian bilateral project "Laboratory testing and numerical modeling of landslides in flysch deposits in Croatia and Slovenia" (2016-2017).

He has been employed at the University of Rijeka, Faculty of Civil Engineering as an assistant at Geotechnical Department since March 2013 and participates as a teaching assistant in one undergraduate course (Soil and rock mechanics) and four graduate courses (Engineering rock mechanics, Foundations, Underground structures and tunnels, and Geotechnics for transportation infrastructure). In the academic years 2014/15 and 2015/2016 he participated in the undergraduate course Computer programs as well. He is a member of the Croatian Geotechnical Society (CGS), the International Society for Soil Mechanics and Geotechnical Engineering (ISSMGE), and the International Society for Rock Mechanics and Rock Engineering (ISRM). He has published a total of three journal papers and ten papers at international and national conferences. He has participated at eight international and six national scientific and professional conferences.

He participated or actively participates in the following scientific projects:

- i) Bilateral Croatian-Japanese research project “Risk Identification and Land-Use Planning for Disaster Mitigation of Landslides and Floods in Croatia,” where he participated in the following activities: maintenance of the complex monitoring system of the Grohovo Landslide, data collection and data analysis (2009-2014).
- ii) Bilateral Croatian-Slovenian research project entitled SoLiFlyD “Study of landslides in flysch deposits: sliding mechanisms and geotechnical properties for landslide modeling and landslide mitigation”, where he participated in the following activities: conduction of laboratory experiments and numerical stability analysis of the Valići Landslide (2014-2015).
- iii) Research project “Development of the landslide monitoring and early warning system for landslide hazard mitigation purposes” supported by the University of Rijeka, where he participated in the following activities: continuation of maintenance of the Grohovo Landslide monitoring system and data collection and analysis on the part of the geodetic and geotechnical monitoring system (2015-2018).
- iv) Bilateral Slovenian-Croatian research project entitled “Laboratory investigations and numerical modeling of landslides in flysch deposits in Croatia and Slovenia,” where he was involved in the following activities: field work and laboratory testing of samples from the Valići Landslide to investigate mechanical and hydraulic features of the material. Tests were conducted in two geotechnical laboratories to define water retention, permeability and compressibility characteristics of the material in saturated and unsaturated conditions (2016-2017).
- v) Research project “Rock mass analysis and instability occurrence on the contact of karst and flysch” supported by the University of Rijeka (2018-2019).
- vi) Research project “Physical modelling of landslide remediation constructions behaviour under static and seismic actions (ModLandRemSS)” supported by the Croatian Science Foundation (HRZZ) (2018-2022).

## List of publications

- Peranić J., Arbanas Ž., Foresta V.; Cuomo S., Maček M. (2018) Determination of soil water retention curve of residual soil from a flysch rock mass. In Proc. of the 7th International Conference on Unsaturated Soils (UNSAT2018), Ng, C.W.W. ; Leung, A.K. ; Chiu, A.C.F. ; Zhou, C. (ed.). Hong Kong: The Hong Kong University of Science and Technology, 2018 pp. 379-384.
- Peranić J., Arbanas Ž., Cuomo S., Maček M. (2018) Soil-Water Characteristic Curve of Residual Soil from a Flysch Rock Mass. *Geofluids*, Vol. 2018, Article ID 6297819: 15 pg. doi:10.1155/2018/6297819.
- Arbanas Ž., Mihalić Arbanas S., Vivoda Prodan M., Peranić J., Dugonjić Jovančević S., Jagodnik V. (2018) TXT-tool 2.385-1.2: Landslide Comprehensive Monitoring System: The Grohovo Landslide Case Study, Croatia. *Landslide Dynamics: ISDR-ICL Landslide Interactive Teaching Tools. Volume 1: Fundamentals, Mapping and Monitoring*, Sassa, Kyoji ; Guzzetti, Fausto ; Yamagishi, Hiromitsu ; Arbanas, Željko ; Casagli, Nicola ; McSaveney, Mauri ; Dang, Khang (ed.). Cham: Springer, 2018. pp. 465-478.
- Dugonjić Jovančević S., Arbanas Ž., Vivoda M., Peranić J., Đomlija P. (2017) Landslide hazard and risk assessment in Istria, Croatia. In: *Proceedings of the 2nd Regional Symposium on Landslides in the Adriatic-Balkan Region*, Abolmasov, B.; Marjanović, M.; Đurić, U. (ed.). Beograd: University of Belgrade, Faculty of Mining and Geology, 2017. pp. 117-121.
- Arbanas Ž., Mihalić Arbanas S., Vivoda Prodan M., Peranić J., Sečanj M., Bernat Gazibara S., Krkač M. (2017) Preliminary Investigations and Numerical Simulations of a Landslide Reactivation. *Advancing culture of living with landslides, Vol 2. Advances in Landslide Science*, Mikoš, Matjaž; Tiwari, Binod; Yin, Yueping; Sassa, Kyoji (ed.). Cham: Springer, 2017. pp. 649-657.
- Mihalić Arbanas S., Arbanas Ž., Krkač M., Bernat Gazibara S., Vivoda Prodan M., Đomlija P., Jagodnik V., Dugonjić Jovančević S., Sečanj M., Peranić J. (2017) Landslide Risk Reduction in Croatia: Scientific research in the framework of the WCoE 2014- 2017, IPL 173, IPL 184, ICL ABN. *Advancing Culture of Living with Landslides. Vol. 1 ISDR-ICL Sendai Partnership 2015-2025*, Sassa, Kyoji; Mikoš, Matjaž; Yin, Yueping (ed.). Cham: Springer, 2017. pp. 301-312.



- Arbanas Ž., Vivoda M., Mihalić Arbanas S., Peranić J., Sečanj M., Bernat S., Krkač M. (2017) Analysis of a reservoir water level impact on landslide reactivation. In: Proceedings of the 2nd Regional Symposium on Landslides in the Adriatic-Balkan Region, Abolmasov, B.; Marjanović, M.; Đurić, U. (ed.). Beograd: University of Belgrade, Faculty of Mining and Geology, 2017. pp. C1-C6.
- Dugonjić Jovančević S., Peranić J., Ružić I., Arbanas Ž. (2016) Analysis of a historical landslide in the Rječina River Valley, Croatia. *Geoenvironmental Disasters*, 3 (26). pp. 1-9. doi:10.1186/s40677-016-0061-x
- Dugonjić Jovančević S., Peranić J., Ružić I., Arbanas Ž., Kalajžić D., Benac Č. (2016) Use of Remotely Piloted Aircraft System (RPAS) in the analysis of historical landslide occurred in 1885 in the Rječina River Valley, Croatia. In: *Geophysical Research Abstracts*, Vol. 18. Wien, 2016.
- Peranić J., Zrinski T., Mujaković N. (2015) Wave equation in polar coordinates. *Zbornik radova Građevinskog fakulteta Sveučilišta u Rijeci*, XVIII: 21-32
- Zuljani D., Peranić J., Vivoda M. (2015) Parametric analysis of anchored bored pile wall as a part of landslide stabilization measures on the Grohovo road landslide, Croatia. In *Georeks IX-th conference proceedings: Geotechnical engineering design and practice*. Sofia : Faculty of Architecture, Civil Engineering and Geodesy, 2015. pp. 45-50.
- Arbanas Ž., Mihalić Arbanas S., Vivoda M., Peranić J., Dugonjić Jovančević S., Jagodnik V. (2014) Identification, monitoring and simulation of landslides in the Rječina River Valley, Croatia, *Proceedings of the SATREPS Workshop on Landslide Risk Assessment Technology*, Sassa, Kyoji; Dang, Khang Q. (eds.). Kyoto: International Consortium on Landslides. 2014. pp. 200-213.
- Benac Č., Dugonjić Jovančević S., Ružić I., Vivoda M., Peranić J. (2014) Marine erosion and slope movements: SE coast of the Krk Island, *Proceedings of 3rd World Landslides Forum: Landslide Science for a Safer Geoenvironment, Volume 3: Targeted Landslides*, Sassa, Kyoji; Canuti, Paolo ; Yin, Yueping (eds.). Beijing, 2014. Switzerland: Springer International Publishing, 2014. pp. 563-567.
- Arbanas Ž., Sassa K., Nagai O., Jagodnik V., Vivoda M., Dugonjić Jovančević S., Peranić J., Ljutić K. (2014) A landslide monitoring and early warning system using integration of GPS, TPS and conventional geotechnical monitoring methods, *Proceedings of 3rd World Landslides Forum: Landslide Science for a Safer Geoenvironment, Volume 2: Methods of Landslide Studies*, Sassa, Kyoji; Canuti, Paolo ; Yin, Yueping (eds.). Beijing, 2014. Switzerland: Springer International Publishing, 2014. pp. 631-636.

- Arbanas Ž., Jagodnik V., Ljutić K., Vivoda M., Dugonjić Jovančević S., Peranić J. (2014) Remote monitoring of a landslide using an integration of GPS, TPS and conventional geotechnical monitoring methods. In: Proceedings of the 1st Regional Symposium on Landslides in the Adriatic-Balkan Region "Landslide and Flood Hazard Assessment", Mihalić Arbanas, Snježana; Arbanas, Željko (ed.). Zagreb, : Hrvatska grupa za klizišta, 2014. pp. 39-44.
- Peranić J., Dugonjić Jovančević S., Jagodnik V., Vivoda M., Osamu N., Sassa K., Arbanas Ž. (2013) Two years observation results of the Grohovo Landslide using integrated remote monitoring. Book of Abstracts of the 4th Croatian-Japanese Project Workshop (Vlastelica, G.; Andrić, I.; Salvezani, D. eds.), Split: University of Split, Faculty of Civil Engineering, Architecture and Geodesy, 2013. pp. 21-21.
- Vivoda M., Sassa K., Arbanas Ž., Dugonjić Jovančević S., Jagodnik V., Peranić J. (2013) Shear strength properties of soil materials from the Grohovo Landslide. Book of Abstracts of the 4th Croatian-Japanese Project Workshop (Vlastelica, G. ; Andrić, I. ; Salvezani, D. eds.), Split: University of Split, Faculty of Civil Engineering, Architecture and Geodesy, 2013. pp. 22-22.